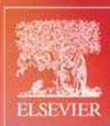

SECOND EDITION

MATERIALS SCIENCE IN MICROELECTRONICS I

THE RELATIONSHIPS BETWEEN THIN FILM PROCESSING AND STRUCTURE

E.S. MACHLIN

MATERIALS SCIENCE IN MICROELECTRONICS VOLUME 1

This page intentionally left blank

MATERIALS SCIENCE IN MICROELECTRONICS VOLUME 1

THE RELATIONSHIPS BETWEEN THIN FILM PROCESSING AND STRUCTURE

E.S. MACHLIN

ELSEVIER

AMSTERDAM • BOSTON • HEIDELBERG • LONDON • NEW YORK • OXFORD
PARIS • SAN DIEGO • SAN FRANCISCO • SINGAPORE • SYDNEY • TOKYO

Elsevier
The Boulevard, Langford Lane, Kidlington, Oxford, OX5 1GB, UK
200 Wheeler Road, Burlington, MA 01803

First published 2005

Copyright © 2005, E.S. Machlin. All rights reserved

The right of E.S. Machlin to be identified as the author of this work has been asserted in accordance with the Copyright, Designs and Patents Act 1988

No part of this publication may be reproduced in any material form (including photocopying or storing in any medium by electronic means and whether or not transiently or incidentally to some other use of this publication) without the written permission of the copyright holder except in accordance with the provisions of the Copyright, Designs and Patents Act 1988 or under the terms of a licence issued by the Copyright Licensing Agency Ltd, 90 Tottenham Court Road, London, England W1T 4LP. Applications for the copyright holder's written permission to reproduce any part of this publication should be addressed to the publisher

Permissions may be sought directly from Elsevier's Science and Technology Rights Department in Oxford, UK. Tel: (+44) (0) 1865 843830; Fax: (+44) (0) 1865 853333; E-mail: permissions@elsevier.co.uk. You may also complete your request on-line via the Elsevier homepage (http://www.elsevier.com), by selecting 'Customer Support' and then 'Obtaining Permissions'

British Library Cataloguing in Publication Data
A catalogue record for this book is available from the British Library

Library of Congress Cataloguing in Publication Data
A catalogue record for this book is available from the Library of Congress

ISBN 0080 44640 X

For information on all Elsevier publications
visit our website at www.books.elsevier.com

Typeset by Charon Tec Pvt. Ltd, Chennai, India
www.charontec.com
Printed and bound in Great Britain

Working together to grow
libraries in developing countries

www.elsevier.com | www.bookaid.org | www.sabre.org

ELSEVIER BOOK AID International Sabre Foundation

Contents

Acknowledgement xi
Foreword xiii
Preface xv
Preface to revised edition xvii

Chapter I
Deposition Parameters 1

1. Identification of deposition parameters that may affect thin film structure. 1
2. Discussion of vapor deposition parameters. 2
    2.1. Background pressure of chamber and purity of precursors. 2
    2.2. Line-of-sight travel of incident particles. 4
    2.3. Incident particle energy. 4
        2.3.1. Temperature spike. 5
            2.3.1.1. Induced by bonding alone of non-energetic particle. 5
                2.3.1.1.1. Temperature spike in film. 5
                2.3.1.1.2. Temperature spike in cluster on thermally insulating substrate. 7
            2.3.1.2. Induced by energetic incident particle. 7
        2.3.2. Penetration of surface by incident particle. 8
        2.3.3. Displacement spike. 10
        2.3.4. Momentum or pressure spike. 12
    2.4. Incident particle flux. 14
    2.5. Substrate and its cleanliness. 15
    2.6. Substrate temperature. 16
    2.7. Composition of deposit relative to target 17
    2.8. Target. 18
3. Deposition parameters for other than PVD. 18
4. Summary. 19

Chapter II
Defect Structure 23

1. Intercolumn (interfiber) “void” networks. 23
  1.1. Summary of observations concerning intercolumn “void” networks. 23
  1.2. Origin of intercolumn “void” networks. 23
  1.3. Effect of processing on void and column structure. 31
  1.4. Temperature, T_1, delineating transition between presence and absence of “void” networks. 36
  1.5. Crystalline versus amorphous structure in *zone 1*. 37
    1.5.1. Crystalline films. 37
    1.5.2. Amorphous films. 38
  1.6. Instability of “void” network. 39
  1.7. Deposition methods that eliminate the formation of “void” networks. 39
    1.7.1. Deposition processes involving energetic incident particles.. 40
2. Other defects introduced during deposition at low substrate temperature.. 43
  2.1. Point defects.. 43
    2.1.1. Vacancies and interstitials. 43
    2.1.2. Impurity atoms.. 45
    2.1.3. Point defects in amorphous films. 46
  2.2. Line defects – dislocations... 46
  2.3. Grain boundaries and stacking faults.. 47
  2.4. Three-dimensional defects. 48
3. Summary of the relations between deposition methods and defect structures. 48

Chapter III
Grain Structure 55

1. Materials science background.. 55
2. Grain morphology, texture, and size in as-deposited films. 58
  2.1. Vapor deposition onto epitaxial substrates in the absence of incident energetic particles. 58
  2.2. Vapor deposition onto non-epitaxial substrates in the absence of incident energetic particles. 60
    2.2.1. No grain boundary mobility, no adatom mobility (*zone 1a*). 60

2.2.2. Some grain boundary mobility, some adatom mobility (*zone 1b*). 62
2.2.3. Rapid grain boundary migration, rapid adatom diffusion. 70
2.2.4. Very rapid grain boundary migration, very rapid adatom diffusion. 72
2.2.5. Zone models of grain morphology for vapor deposition in chamber pressures greater than 10^{-8} Torr onto non-epitaxial substrates. 73
2.2.6. Interpretation of zone models according to present analysis. 75
2.3. Effect of anisotropic sticking coefficient. 77
2.4. Polycrystalline semiconductors on non-epitaxial substrates. 77
2.5. Conclusions regarding grain morphology, size and texture produced via vapor deposition in the absence of energetic particles. 78
3. Grain morphology, texture and size in vapor-deposited films which sense energetic (hyperthermal) particles during deposition. 79
3.1. Deposition onto epitaxial substrates. 81
3.2. Deposition onto non-epitaxial substrates. 81
3.2.1. *Zone 1aT* temperature range. 82
3.2.2. *Zone 1bT* temperature deposition. 83
3.2.3. *Zone II* deposition. 86
3.3. Summary of results on the effects of energetic particle bombardment during deposition. 88
4. Effects of post-deposition processing on grain structure. 89
4.1. Effect of post-deposition annealing. 89
4.2. Post-deposition bombardment at elevated temperature. 90

Chapter IV
Epitaxial Structures 97

1. Modes of growth in production of epilayers. 98
1.1. Modes of growth. 98
1.2. Modes of F–M epilayer growth. 99
2. Defects produced in homoepitaxial layers. 102
2.1. Point defects and their clusters. 102
2.2. Line and planar defects. 104
3. Defects in pseudomorphic films. 108
3.1. Coherent (commensurate) pseudomorphic films. 108
3.1.1. Interfacial defects. 109

3.1.2. Defects in pseudomorphic solid solutions. 110
3.2. Pseudomorphically stabilized metastable crystal structures. 114
3.3. Commensurate–discommensurate transition and misfit dislocations. 116
4. Heteroepitaxy between crystals of different symmetry, bonding class or of large misfit. 121
4.1. Metal/metal epilayer/substrate systems. 122
4.2. Metal/semiconductor epilayer/substrate systems. 124
4.3. Epitaxy at vicinal surfaces. 125
4.4. Theories of interphase interfaces. 128
4.5. Constraints on epitaxy due to symmetry. 129
5. Graphoepitaxy. 129
6. Epilogue. 132

Chapter V
Structure of Amorphous Films 141

1. Amorphous covalently bonded semiconductors. 141
1.1. Non-hydrogenated and hydrogenated Group IV elements. 141
1.1.1. α-Si and α-Si:H. 142
1.1.2. α-Ge and α-Ge:H. 156
1.1.3. α-C and α-C:H. 157
1.2. Amorphous semiconductor alloys and compounds. 159
1.2.1. α-Si,Ge:H and other alloys of α-Si. 159
1.2.2. Chalcogenides. 160
2. Amorphous metals and alloys. 160
3. Amorphous oxides. 162
3.1. Amorphous silicon oxide. 162
3.2. High dielectric constant amorphous oxides. 163
4. Amorphous ↔ crystalline transition. 163

Chapter VI
Stresses in Thin Films 173

1. Intrinsic stress. 173
1.1. Non-energetic deposition. 173
1.1.1. *Zone a* temperatures (nil mobility). 173
1.1.2. *Zone b* temperatures. 178
1.1.2.1. Origin of compressive stress. 180
1.1.3. Effect of variables other than substrate temperature. 181

1.1.3.1. Oxygen. 181
1.1.3.2. Other impurities. 182
1.2. Intrinsic stress when film surface senses energetic particles. 182
1.3. Intrinsic stress due to phase transformation. 188
1.4. Intrinsic stress due to epitaxy. 191
2. Thermal stress. 192

Chapter VII
Reaction-induced Structure 195

1. Heterogeneous reactions between thin monocrystalline layers. 195
1.1. Completely miscible layers. 195
2. Layers of immiscible components but forming intermediate compounds. 196
2.1. Epitaxial monocrystalline product phase. 196
2.2. Polycrystalline compound products. 200
3. Reactions between adatoms and substrate. 201
3.1. Silicon dioxide films. 201
4. Amorphous to crystalline transitions. 204
4.1. Silicon. 204
4.1.1. α-Si → poly-Si. 204
4.1.2. α-Si → epitaxial c-Si transition. 207
4.1.3. Solid phase epitaxy via diffusion through an intermediate phase. 211
4.1.4. Amorphous ↔ crystalline transitions during deposition. 212
4.2. Carbon. 219
4.2.1. Deposition of carbon films using ion beams. 219
4.2.2. Possible solid phase epitaxy of diamond. 222
4.3. Amorphous to crystalline transition in other materials. 223
4.3.1. Amorphous to poly-transition. 223
4.3.2. Amorphous to epitaxial silicide transition. 225
4.4. Summary of section 4. 226

Chapter VIII
Surface Structure 233

1. Surface roughness. 233
2. Surface modification for producing ordered arrays. 236

2.1. Periodic surface reconstruction pattern. 236
2.2. Periodic surface strain pattern. 237
2.3. Periodic ledge pattern. 242
2.4. Periodic surface phase pattern. 243
2.5. Periodic nanodots via kinetic control. 244
3. Processing and surface reconstruction. 247

Index. 251

Acknowledgement

James J.E. Harper read and suggested corrections to the manuscript of the first edition of this book, which have resulted in a marked improvement in readability and accuracy. However, I take responsibility for any errors and awkward sentences that may still remain, and for the choice of subject matter included and not included in this book. I am deeply grateful to Jim for having taken precious time to perform an onerous task. His having done so is, I am sure, a consequence of his dedication to the improvement of his profession, as is also exemplified by his active role in the affairs of the Materials Research Society.

This page intentionally left blank

Foreword

Materials science is the science of the relations between processing, structure, and properties of materials. The modes of forming thin films differ markedly from those used for bulk materials. Thin films are materials formed at surfaces by deposition, a process in which the surface layer is continuously submerged under a newly forming surface layer. Thus, the materials science of thin films encompasses subject matter not considered in the materials science of bulk materials. This consideration is the justification for this book. This subject matter also divides naturally into two headings: processing ↔ structure relationships and structure ↔ properties relationships. Consequently, Professor Machlin chose to write two books, one for each aspect of the materials science in thin films. The present book is the first in the series of these two books.

The structure of thin film materials considered in this book includes crystal defects (point defects, dislocations, and grain boundaries), void structure, grain structure (morphology and texture), interface structure in epitaxial films, the structure of amorphous films, and reaction-induced structure. Also, the state of stress in the thin films is known to be an important aspect of their structure, as well, and is examined in a separate chapter. In his consideration of these structures, Professor Machlin has integrated diverse observations in different fields to provide a consistent and comprehensive analysis of these structures and their origins. For example, he applies the observations on epitaxial deposition of silicon to an analysis of the structures obtained in the deposition of carbon.

Most of the thin film deposition processes and their technologies have been described in other books. However, an analysis of these processes in terms of the effects that the parameters in such processes have on the structure of the materials deposited by these processes has not been presented in prior books to the extent that they are in the present book. Indeed, this book is an essential source of knowledge for anyone involved in the deposition and use of thin films. It is my belief that what is contained in this book will help those who deposit thin films to produce more and better products, and also will help provide researchers with guides to a more rational exploration of the still unknown principles that govern the science and technology of thin film materials processing.

Professor Machlin has been uniquely prepared for the undertaking of this and the future companion book on the materials science of thin films. Along with his extensive academic experience, he has been a visiting faculty in my laboratory at the IBM T.J. Watson Research Center at Yorktown Heights, NY, where he spent a

sabbatical year and every summer from 1981 to 1991 working on thin film problems. These creative and mutually stimulating interactions were productive, had practical applications and were fun. Some of these interactions could serve as a model for academic/industrial interfacing from which mutual benefits are derived. This resource sharing certainly benefited me and I am sure it has influenced the content in this book. Indeed, I wish he had known before he came to us what he now knows after writing this book. If he had we might have succeeded in some of the more esoteric projects we undertook.

Jerome J. Cuomo
Distinguished Research Professor
Materials Science and Engineering Department
North Carolina State University

Preface

An introductory course in materials science should be an adequate preparation for understanding the concepts contained in the present book, although the more thorough is the training of the reader in physics or chemistry and materials science the greater will be her or his ability to make use of these concepts. Also, this book builds upon the textbook of my colleague, Milt Ohring, entitled **The Materials Science of Thin Films**, Academic Press, 1992, which may be used as a prerequisite text for students not familiar with the processes involved in producing thin films or with the elements of Materials Science. Similarly, concepts involving thermodynamics or kinetics may be referenced in my book **An Introduction to Aspects of Thermodynamics and Kinetics Relevant to Materials Science**, Giro Press, 1991.

I have endeavored to approach each subject in a consistent manner in relating the effect of processing on structure. The state of a thin film's surface, during the period a monolayer surface exists prior to being buried under the next monolayer being deposited, determines the structure inherited in the as-deposited thin film at the corresponding ultimate position of the monolayer in the thin film. Hence, any processing parameter that affects the state of the surface, or the kinetics of processes occurring at the surface, will affect the ultimate film structure. This processing/structure relation is unique to thin films. Consequently, I have tried to avoid discussion of reactions that occur away from the surface in the bulk of the thin film, even if such reactions may be enhanced by the presence of a high density of defects in thin films. These reactions are not unique to thin films and the theory relating to them may be found elsewhere, as, for example, in my book referenced above.

This book may be used as a text in a graduate course. Indeed, I have used much of the material in a course I taught at Columbia University and also taught to students seeking the M.S. degree at the IBM East Fishkill Facility. Teachers interested in obtaining problem sets may request them from me. Knowledge about the relations between thin film processing and structure is not a necessary condition for producing devices that function. However, such knowledge can often help to solve practical problems in thin film deposition. I hope that this book provides this knowledge and that it is useful to the reader. Many courses in Materials Science curricula are based on a study of the relation between processing and structure. The fact that the processing involved in thin film deposition is unique to this class of materials is the justification for a course offering, based on the subject matter in this book, in a Materials Science curriculum.

E.S. Machlin
Columbia University
New York, NY 10027, USA

This page intentionally left blank

Preface to revised edition

The science of thin films is not mature. Consequently, one may expect new developments over the course of several years. Some of these may change conclusions reached previously and some may reinforce such conclusions. Both types have occurred in the interim since the first edition of this book was published. The first has resulted in my having to rewrite some sections of the original book. The second type was accounted for by appendices to chapters of the original book. The latter were as brief as possible, but contained references to the latest developments that the interested reader could use to access other references on the subject. Also, a new chapter has been added on the subject of surface structure and the relation to it of processing. Much of the material in this new chapter consists of results obtained since the original edition of this book was published and is a consequence of the explosion in number of STM-related papers in this period.

This page intentionally left blank

CHAPTER I

Deposition Parameters

This chapter considers the deposition parameters common to most of the deposition methods and describes possible effects of each deposition parameter on thin film structure. Subsequent chapters will examine the various structures produced in thin films and will attempt to relate these structures to the processing variables discussed in the present chapter.

1. Identification of deposition parameters that may affect thin film structure.

Many deposition parameters may affect the structure of thin films and are common to all deposition methods. Let us attempt to develop a list of these parameters. All thin films are formed by the deposition of atoms onto a substrate. The origin of these atoms may be a vapor as in physical vapor deposition (PVD) or in chemical vapor deposition (CVD), a fluid as in electrodeposition or in liquid phase epitaxy (LPE), or a plasma.

A chamber is necessary to hold the vapor sources. The *background pressure* in an evacuated chamber affects the concentration of impurities that are incorporated in films deposited therein. Similarly, the *concentration of impurities in the vapor phase* determines the impurity content in films produced via CVD. The particles incident on a point on the substrate have kinetic energy and may have the same direction or random directions of incidence. These parameters are defined by the *mass and velocity of each of these incident particles*. Also, the *flux* of each species bombarding the film significantly affects the ultimate film structure. These parameters are equivalent to the deposition variables: *deposition rate* (of total film mass), *composition* and *inert-atom to film-atom arrival ratio*. Finally, the *substrate material, temperature, surface cleanliness, surface reconstruction (if clean), and surface smoothness* also affect the film structure. We would be remiss if we did not mention that *film thickness* varies during deposition and that it can also affect the structure of the remainder of the film yet to be deposited.

Film deposition processes other than PVD involve equivalent deposition parameters and, in addition, many other parameters unique to each deposition process. We will concentrate on the PVD parameters. (There are enough of them.) At the proper place we will consider how other deposition processes affect film

structure, e.g. in Chapter V we consider the effects of plasma assisted CVD on the structure of amorphous hydrogenated silicon films.

Mechanism maps[1] have been useful in the study of bulk materials to elucidate the relations between processing and structure. However, their usefulness in an equivalent study of thin film materials is hindered by the multidimensionality conferred by the number of deposition parameters, which we believe determines the empirical approach that dominates most thin film studies. In this book we shall attempt to illuminate the relations between film structure and processing in the language of materials science, wherever possible.

2. Discussion of vapor deposition parameters.

2.1. Background pressure of chamber and purity of precursors.

There are two distinctly different regimes of background pressure or purity of precursors. One corresponds to the condition in which no amount of surface preparation can guarantee the presence of dangling bonds at the substrate surface. In the other, it is possible to produce and maintain a substrate surface that is an unreconstructed surface and in which the dangling bonds that emanate from the surface are not terminated by impurity adatoms.

In PVD, for any background pressure greater than 10^{-8} Torr, the substrate surface will consist of chemically adsorbed layers of impurity atoms (probably oxygen) that saturate the underlying dangling bonds and prevent further primary bonding to the substrate surface. Even inert gas atom sputtering of the substrate surface just prior to deposition will not guarantee that all of the surface will consist of dangling bonds. The energy associated with the sputtering process itself can induce surface reconstruction to a more stable surface or it can produce a less stable amorphous surface. Also, seldom is the inert gas of sufficient purity to prevent reoxidation of the substrate surface during the sputtering process.

A consequence of the absence of dangling bonds at the substrate surface is that the surface may be prevented thereby from providing a template for epitaxy. There are three possible exceptions to this rule*: 1) when there can be an exchange between a surfactant type adatom that saturates a substrate surface bond with an atom of the species that is being deposited, without displacing any other atoms at or near the substrate surface; 2) when ion mixing conditions exist at the surface such that depositing atoms can join the substrate lattice at subsurface positions; 3) at an elevated substrate temperature when the buried reconstructed surface layer can break its reconstructed bonds, rearrange and rebond to the surface layer, that

* A fourth possible exception occurs under surface texture conditions applicable to grapho- or artificial epitaxy. See Ref. [19].

itself reforms the reconstructed arrangement. We shall discuss these possible exceptions in Chapter IV where epitaxial deposition is considered in detail.

When an unclean substrate surface is present at the start of deposition then deposition tends to be independent of the substrate material. In this case, if the deposition conditions produce crystalline films, rather than amorphous films, then the orientations of the initial crystal grains that form on saturated substrate surfaces are independent of the substrate material. The significance of this condition for the texture of crystalline thin films is considered in Chapter III, and for the structure of amorphous films in Chapter V.

The background pressure and the purity of precursor materials also affect the purity of the deposited thin film. This fact is well known, but bears repetition. From the kinetic theory of gases the relation between impingement rate and chamber pressure yields the following rule of thumb. *At a pressure of 10^{-6} Torr about a monolayer of gas atoms impinges every second.* (The exact relation is given in Appendix 1.) Thus, if C_o is the oxygen concentration of the chamber gas and if α is the corresponding sticking coefficient (i.e. the fraction of incident molecules that remain attached to the film), then for a deposition rate equal to $\tilde{N}$ monolayers/s, the oxygen percent concentration in the film will be given by

$$\alpha C_o P(\text{Torr})/10^{-6}\tilde{N}$$

For $\alpha = 0.1$ and $C_o = 0.1$ then even at $P = 10^{-8}$ Torr and $\tilde{N} = 100$, the oxygen concentration will equal 1 ppm. At higher background pressures and/or slower deposition rates the oxygen concentration in the film will be higher than 1 ppm and will probably affect properties adversely. For reactive film materials, such as titanium, the sticking coefficient is likely to approach unity resulting in a value of the oxygen concentration a factor 10 larger than that just estimated. Among the constituents of the evacuated chamber at a background pressure of 10^{-8} Torr are carbon dioxide, hydrogen, oxygen, nitrogen, water vapor, and various organic molecules, such as methane.

These impurities become immobile at a sufficiently low temperature and the deposition process then results in their incorporation in the solution phase. The state of their incorporation, if molecules, depends upon the degree of their dissociation upon adsorption on the film surface. Because interstitial impurities often have a low solid solubility in the thin film materials, adsorption of such species, at temperatures where the adatoms are immobile, yields highly supersaturated solid solutions. The stress induced in the lattice about an interstitial solute atom acts to pin grain boundaries and bind vacancies. Also, the presence of impurities in solution affects several film properties, such as resistivity and stress, significantly.

Summarizing, background pressure and purity of precursors affect thin film structure and properties either by controlling the deposition mode (epitaxial or not) or by controlling the soluble impurity concentration in deposited films, or both.

2.2. Line-of-sight travel of incident particles.

In line-of-sight travel of particles that deposit on a thin film, projections on the surface can shadow other parts of the film surface from the incident particles. In the absence of lateral transport of the deposited particles on the film surface, a network of voids separating fibers or columns of film material is formed in the shadowed regions. This subject is discussed in detail in Chapter II. Line-of-sight travel of atoms is prevalent in the deposition methods for which the chamber pressure is less than about 0.01 Torr. (The mean-free path between gas collisions exceeds about 1 cm at lower chamber pressure (higher vacuum).)

When all the particles incident on the film have the same direction, then it is possible to change the crystallographic texture and the orientation of columnar boundaries by changing the angle of incidence of the depositing atoms. We will consider these effects and their possible origins in greater detail in Chapters II and III.

2.3. Incident particle energy.

The average incident particle kinetic energy can vary from that corresponding to the thermal energy at evaporation (<0.5 eV) to the energy equivalent to a difference in potential between the substrate and an ion source of the incident particles. The latter is usually limited to a few hundred eV. The energy of arriving sputtered particles in typical sputtering processes at gas pressures higher than about 0.03 Torr is roughly equal to the thermal energy of the gas between target and substrate. (A treatment of thermalization is given in Ref. [2].) At lower gas pressure, where line-of-sight conditions hold, the average energy of sputtered atoms incident on the substrate can reach about 10–20 eV, while the energy of reflected neutral inert gas atoms, that also bombard the substrate, can reach much higher values. With the substrate biased negatively relative to the plasma, inert gas ions of the plasma can bombard the substrate with the bias potential, typically 50–300 eV. The average energy of particles in plasmas, such as those produced by laser evaporation or cathodic arc evaporation, is also on the order of 20 eV. Thus, the kinetic energy of incident particles, either in ion beam assisted deposition or direct ion beam deposition, ranges from about 10 eV to no more than 1000 eV.

The range of energies of incident particles in the various deposition processes is, as indicated above, in the low energy portion of the spectrum associated with particle interactions with matter. In this low energy range, among the phenomena that the incident particles can induce are: sputtering of surface atoms, insertion of the incident particles into the deposited film, local and temporal enhancement of temperature along the path of the incident particle in the film (temperature spike), production of defects (displacement spikes) and pressure or shock waves and amorphization of substrate surface. These effects can all occur

together, or separately in any combination, dependent upon the incident particle energy transferred to the film.

The production of defects requires that the bombarding particle transfer sufficient kinetic energy to the film to induce atomic displacements. In the bulk of a material, this displacement energy varies from about 10 to 50 eV. Similar displacement induced effects at the surface require only about 3/4 of the bulk displacement energy. For a head-on elastic collision between two particles, the energy transferred to the stationary particle, T, of mass m, by the incident particle, of mass m_i, and having kinetic energy, E is

$$T = 4Emm_i/(m + m_i)^2 \tag{1.1}$$

Thus, the most efficient collision for the production of defects is the one between particles having the same mass.*

In the following section, we examine, in detail, various consequences of energetic particle bombardment of films on the process of film formation and the structure of the resulting film.

2.3.1. Temperature spike.

2.3.1.1. Induced by bonding alone of non-energetic particle.

On bonding, the incident atom deposits from about one-third to the full heat of vaporization per atom, which for the average metal is about 5 eV. The bonding energy that is converted to kinetic or thermal energy depends on the number of bonds made in the adsorption step. Hence, for the usual evaporation and condensation deposition method the kinetic energy of the incident atom is negligible compared to the latent heat released in the condensation process. Both the latent heat released and the incident kinetic energy transferred to the film act to produce a temperature spike at the surface of the film. Depending on the size of the cluster acting as the substrate for the condensing atom and on the thermal contact of the cluster to its substrate, this temperature spike may or may not be sufficient to allow the cluster to approach an equilibrium configuration. Let us now consider the temperature spike that is associated with the sudden introduction of energy at a point on the surface of a film.

2.3.1.1.1. Temperature spike in film.

A hemispherical temperature spike is produced about the site at which the incident atom attaches to a sufficiently thick film already formed by condensation.

* For a solid, a fraction of the transmitted energy is dissipated in electronic excitations and the remainder in nuclear collisions. At the low range of energies in deposition the fraction dissipated in nuclear collisions equals 0.8.

We shall follow the classical analysis of Seitz and Koehler[3] to estimate the effect of this temperature spike on the surface transport of atoms in the spike and its vicinity.

There are several questions we would like to have answered. One is "What is the maximum distance from point of attachment of an adatom to the film inside of which adatoms will jump due to the thermal spike induced by the incident adatom and outside of which no adatom jumps occur?". We shall consider two answers to this question. The first is based on the work of Seitz and Koehler.[3] The second is based on the generalization of a recent molecular dynamics study.[4]

According to Seitz and Koehler[3] this maximum distance r′ outside of which no adatom jumps will occur is given by the equation

$$r' = (4/(324\pi)^{1/6})[E/Q]^{1/3}\ r_s \tag{1.2}$$

where E is the energy transferred by attachment of the incident atom to the film, Q is the activation energy for adatom diffusion and r_s is the atomic radius.

For the case of the condensation of an incident atom having thermal energy corresponding to the temperature of evaporation the value of E is about 5 eV, which is an average cohesive energy value, and corresponds to the thermal energy released when an atom condenses from the vapor state to the solid state, i.e. forms primary bonds to the film. From an empirical generalization,[5] we can take the activation energy for surface diffusion (Q) on a face-centered-cubic (fcc) metal to be given by $6.5\,kT_M$, where k is Boltzmann's constant and T_M the absolute melting temperature of the metal. (We should be aware that the experimental deviations from this rule can be appreciable, e.g. the activation energy for Ni equals $3.9\,kT_M$.) Using these values we obtain $r' = 2.6\,r_s$ for $T_M = 1000\,K$. Thus, when an adatom forms sufficient primary bonds with the film to release the full energy of sublimation, the temperature spike induced by this act of condensation will not influence the adatom to move more than an atomic spacing away from its position of attachment to the film.

Hence, at substrate temperatures where surface diffusion will not occur in the time between the deposition of successive monolayers, an adatom that originates from an evaporation source will rest in the binding potential well nearest the point of its contact with the film surface. When such deposition is onto a clean surface of a crystal it causes the epitaxial growth of the crystal, a process we will denote by the term granular epitaxy.

There are two exceptions to the rule that such deposition will be epitaxial. One is for deposition onto a film that is already amorphous (e.g. an alloy between widely disparate atomic size constituents) and the other is for deposition onto a film in which the bonding between atoms is strongly covalent. The reason for the former exception is obvious. The reason for the latter is that the directional bonding assures invariance of the bonding angle, but not of the positions of the potential

wells at the surface available for the adatoms to “fill”. (The dangling bonds of atoms having only one bond each to the surface can rotate.)

2.3.1.1.2. Temperature spike in cluster on thermally insulating substrate.

Consider a monolayer cluster of film material that has a thermal diffusivity greater than 10 times that of the substrate on which it sits. The heat released on addition of an atom to the cluster by condensation will tend to distribute through the cluster before it is conducted to the substrate. Roughly, we may relate the thermal diffusion distance in the cluster, X_C, to that in the substrate, X_S, by $(X_C/X_S)^2(t_S/t_C) = D_C/D_S = 10$. Thus, in the same time ($t_S = t_C$) it takes for heat to conduct to the substrate atom, that is just below the site of condensed atom attachment to the cluster, the heat will be conducted in the monolayer cluster a distance $(10)^{1/2}$ times larger than the spacing between the cluster and the substrate. Thus, for a monolayer close-packed cluster consisting of seven atoms, the attachment of one additional atom will suffice to raise its temperature by about $E/(8{\cdot}3k)$ or about 960°C for $E = 2\,eV$. However, this temperature pulse will last for the time it takes to begin to conduct heat to the substrate, i.e. t_S. It will decay rapidly thereafter. This time interval equals about 10 cluster atomic vibration periods and one substrate vibration period. The number of jumps that an atom of this cluster can make during this temperature pulse equals $\nu e^{-Q/kT}\tau$, where $\tau = 10/\nu$ and for a fcc metal $Q = 6.5T_M$ with $T = T_M$. By multiplying this number by the number of atoms in the cluster, 7, we obtain the result that from 2 to 3 atoms of the cluster will make a jump in the period of the condensation temperature spike. Hence, it is possible that a small cluster can change its shape during the temperature pulse induced by condensation of one atom onto the cluster.

This result is significant because it states that, even in the evaporation and condensation deposition method, at low substrate temperatures, and on substrates that have low thermal conductivity relative to the film material, the initial clusters should tend to approach their equilibrium configuration.

2.3.1.2. Induced by energetic incident particle.

In the above analysis we examined the temperature spike due to bonding. Will the temperature spikes induced in films due to energetic incident atoms have a greater effect on adatom surface diffusivity? The one-third power dependence of r' on E, indicated in equation (1.2), determines that the effect will be negligible. Even for the case of a displacement spike, when, as Seitz and Koehler argue, we should set $E = 300\,eV$, the value of r' will not exceed $10\,r_s$, i.e. the adatom on a film will not move beyond a distance corresponding to 10 atomic radii away from its point of incidence. With the knowledge that the effect an incident energetic particle has on any thermally activated process is essentially local to the point of

impact, *we may conclude that to produce a measurable effect on average adatom* ***mobility*** *the energetic particle to film atom arrival ratio must equal or exceed about unity.**

Some results of a MD study by Dodson,[4] who examined the relaxation of the energy introduced into a Si lattice by a 10 eV Si atom incident normal to the (111) surface, are shown in Figure 1.1. The significant aspect of these results relative to the calculations of Seitz and Koehler is that the temperature induced by the incident particle is less than room temperature outside the region having a radius of 7 Å about the point of impact after about 3 atomic oscillation periods subsequent to the impact. This result is to be compared with a value of r', for the same conditions, calculated from the Seitz and Koehler equation given above, given by $r' \approx 3.28\, r_s \approx 4$ Å. Thus, there is essential agreement between the modern molecular dynamics results and the classical analysis of Seitz and Koehler, insofar as they relate to the conclusions we have drawn in this section.

2.3.2. Penetration of surface by incident particle.

This subsection will examine the factors that control the penetration of incident particles that transfer less than the displacement energy in a collision with the film. There are two modes of such penetration. One is via a ring-like energy transfer that results either in sputtering of a surface atom or motion of a surface atom to adatom position, both distant from the point of incidence of colliding particle and penetration of the latter into the surface layer. The other mode is via channeling of the incident atom and its penetration to a subsurface position.

The penetration depth of incident particles striking a film in the first mode may be evaluated using sputtering theory.[6] For the low energies involved in deposition processes, the mean penetration depth, δ, is given by

$$\delta(\text{nm}) = (10 C M_f Z E_i^{2/3})/\rho_f$$

where C varies from 0.13 to 0.16 for $0.5 < M_f/M_i < 100$, E_i is the incident particle energy (keV), ρ_f the film mass density (g/cm^3), M_f the film atomic mass (amu) and $Z = [(Z_i^{2/3} + Z_f^{2/3})/Z_i Z_f]^{2/3}$. For 10 eV Si ions incident on a Si film and using $C = 0.13$, this relation predicts $\delta = 0.11$ nm, which is nearly equal to the atomic radius of a silicon atom, i.e. the incident Si atom is predicted to penetrate no further than the surface layer, if at all.

However, in one molecular dynamics simulation of this phenomenon,[7] it was found that 5–10 eV incident Si atoms could be inserted subsurface into dimers in

* This conclusion should not imply that adatom transport is not enhanced by incident energetic particles, which can induce surface displacements of adatoms, ring displacement of adatoms and near-surface enhanced vacancy concentrations that aid in the transport of adatoms.

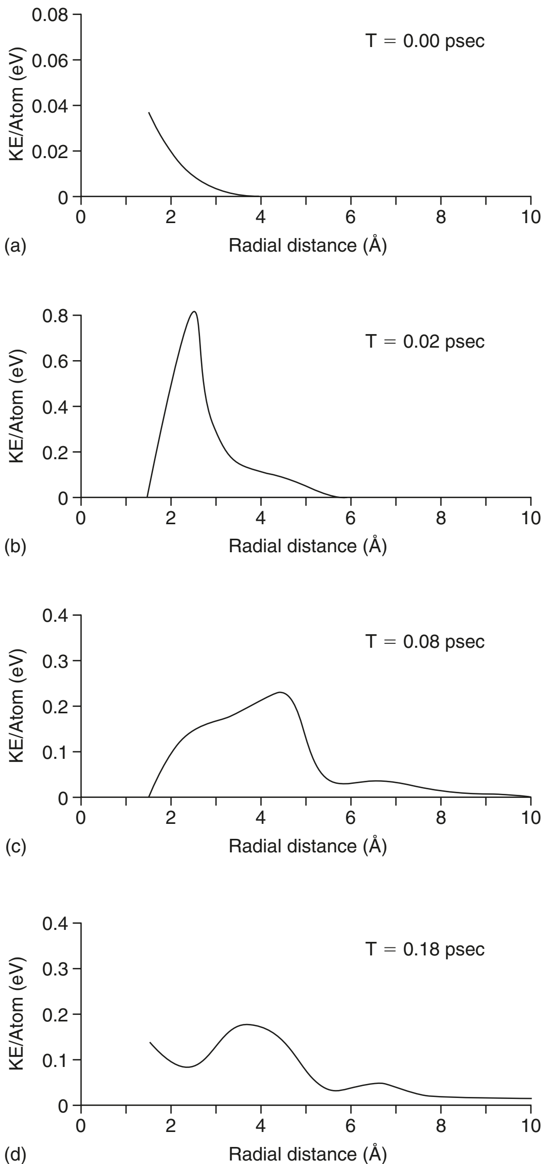

Figure 1.1. Time evolution of the average kinetic energy (KE) per atom resulting from the impact of a perpendicularly directed 10-eV silicon atom on a silicon (111) surface as a function of distance from the impact point. (a) is at t = 0, (b) is at 0.02 ps, (c) is at 0.08 ps, and (d) is at 0.18 ps. Reprinted with permission from B.W. Dodson, Phys. Rev. B36, 1068(1987). © 1987 The American Physical Society.

a (2×1) Si(100) reconstructed surface without damage to the lattice. More energetic incident Si atoms (10 eV) on the same Si surface were found, in another molecular dynamics simulation, to induce dimer breaking and to penetrate to the fourth layer ($\delta = 0.54$ nm) beneath the surface with the production of surface defects and bulk interstitials, but not vacancies.[8] In still another molecular dynamics simulation, but of the penetration of a Si(111) surface by 10 eV Si atoms at normal incidence, 70% of the incident atoms come to rest in an interstitial position between the first and second double atomic layers or substitute for an atom in the first double layer by knocking the substrate atom into an interstitial location;* the other 30% come to rest on the surface.[4] Thus, it appears likely that such low-energy penetration occurs via a channeling mode. Penetration by channeling at these low energies has not received any theoretical analysis other than the molecular dynamics simulations just mentioned. However, by noting that this phenomenon involves the insertion of an atom into an interstitial site, we may deduce that penetration under these conditions should be deeper the smaller is the diameter of the incident atom and the larger is the effective diameter of the channel that is parallel to the direction of the incident particle. Thus, it should come as no surprise that subsurface implantation of 170 eV mass-selected C^+ ions into GaAs(100) during MBE has been achieved to produce an electrically active C-doped GaAs[9], whereas large Xe^+ ions bombarding at an energy of 500 eV do not penetrate the surface of tungsten although their bombardment results in sputtering of tungsten atoms.[10]

2.3.3. Displacement spike.

When the incident particle energy that is transferred to a film atom exceeds the displacement energy, which varies from 20 to 50 eV for different materials, then displacement of lattice atoms will occur to form collision cascades involving the production of sputtered atoms, vacancies and interstitialcies and amorphous regions in some crystalline hosts.

Molecular dynamics studies,[8] as noted above, have shown that interstitials can be produced in silicon by 10 eV incident Si atoms without the concomitant production of vacancies. Thus, collision cascades are not necessary to generate interstitial type defects. However, this capability is limited to bombardment at transferred energies less than the displacement energy. For transferred energies higher than the displacement energy, interstitials and vacancies are created simultaneously by the formation of Frenkel defects, which, at low substrate temperatures, are produced only in collision cascades.

Point defects that are mobile at room temperature will move to traps, which may be vacancies, dislocations or interfaces. This motion, for sufficient fluence of

* This observation describes the microscopic process that has been termed "atomic peening", which has been proposed as a mechanism for the development of compressive intrinsic stress during deposition. We shall discuss this matter in greater detail in Chapter VI.

incident particles, can yield appreciable diffusion in the subsurface layer[11] during the deposition of these materials. Also, the range of the incident particle, corresponding to the position where defects are generated, is on the order of several atomic layers for the low-energy particles used in sputtering and ion beam assisted deposition. If some of the interstitialcies or vacancies are trapped at dislocations or grain boundaries whose half-plane or plane, respectively, are at an angle with respect to the plane of the film, then this process will lead to the development of a compressive or tensile stress, respectively, in the plane of the film. At room temperature, vacancies are much less mobile than interstitialcies in many materials. Thus, in the as-deposited state for these materials vacancies are less likely to have annihilated at traps than interstitials and more likely to reach the surface with the consequence that the intrinsic stress due to these point defects is more likely to be compressive than tensile. This possible source of intrinsic compressive stress is discussed in greater detail in Chapter VI.

While subsurface point defects are being created by energetic bombardment of the surface during deposition, monolayers of film atoms are also being added to the surface. While it is likely that a significant fraction of the interstitials created in this bombardment can reach the surface during deposition in many materials, it is worthwhile exploring whether the subsurface vacancies created in this bombardment can also reach the moving surface during deposition. This exploration is carried out in Appendix 2.

The analysis given in Appendix 2 shows that the enhanced local vibrational modes adjacent to the site at which the vacancy is generated cannot provide the excitation needed to produce the succession of vacancy jumps that will allow the subsurface vacancy to reach the surface. However, the substrate temperature is often high enough to yield vacancy diffusion velocities larger than the growth velocity. In particular, in fcc metals with absolute melting temperatures lower than about 1300°K, vacancies generated by low-energy particles will annihilate at the growth interface during deposition onto room temperature substrates. On the other hand, there are many film materials in which the vacancies generated by low-energy particle impact during growth will remain imprisoned in the film during growth. The corresponding vacancy concentration is then so high that one may expect the structure of the film to be barely stable. Indeed, it has been hypothesized that when the vacancy fraction exceeds about 0.02 then the crystal host will transform to an amorphous one.

Can the vacancies that arrive at the growth surface act to enhance adatom diffusion? There is no simple answer to this question because adatom mobility is a non-monotonic function of the surface coverage of adatoms, as revealed in the MD study of Paik and Das Sarma.[12] By decreasing surface coverage, vacancy arrival at the growth surface will increase adatom mobility at surface coverages less than 25% and at surface coverages near unity. However, at coverages between these limits the reverse effect will occur. Thus, the only likely consistent effect of energetic

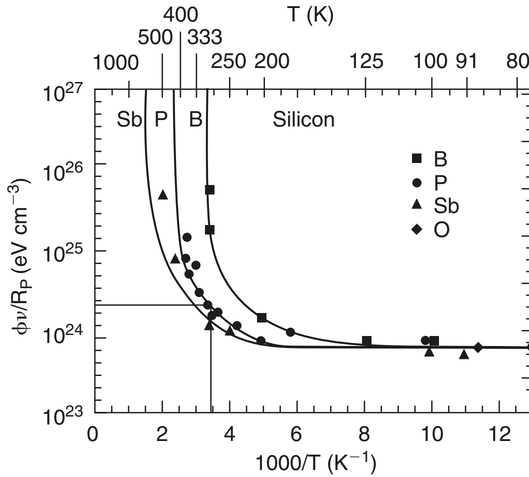

Figure 1.2. Energy density deposited in nuclear collisions required to produce a continuous amorphous layer in silicon. Reproduced with permission from F.L. Vook, in **Radiation Damage and Defects in Semiconductors**, ed. J.E. Whitehouse, The Institute of Physics, London, 1973, p. 60.

incident particles on adatom mobility is a consequence of the temperature spikes and not the displacement spikes associated with them.

The subsurface vacancies produced by low energy displacement spikes are responsible for various phenomena, many of which we will examine in detail in later chapters. One of the esoteric examples of these phenomena is suppression of three-dimensional island nucleation and the concomitant promotion of layer-by-layer growth at the expense of the Stranski–Krastonov growth mode.[13] Finally, it should be mentioned that the displacements induced by low-energy particles during deposition can reduce the transition temperature delineating the deposition of amorphous and crystalline films[14] (i.e. promote the formation of crystalline films at the expense of amorphous films) and, as shown in Figure 1.2, can produce an amorphous layer in crystalline silicon.[15] Various consequences of these phenomena are discussed in Chapters V and VII including the effect of the incident beam energy and flux on the amorphization of substrates desired for epitaxial deposition.

2.3.4. Momentum or pressure spike.

A 10 eV Si atom incident on a Si lattice will produce a shock wave, which we will call a pressure spike. (The velocity of the incident Si atom exceeds the sound velocity in solid Si at and above the incident kinetic energy of 10 eV.)

It has been claimed that the combination of a pressure and temperature (P–T) spike might induce a transformation of the film material in the spike to a crystal structure that is stable in some regime of the P–T spike history, e.g. stabilize the diamond structure of carbon at the expense of the graphite structure. It is highly unlikely for this process to occur via the normal nucleation and growth mode of transformation, because the temperature spike lasts too short a time period to allow the number of jumps needed to produce a nucleus of the new phase and to allow an already present nucleus to grow by one atomic layer.

The only transformation that a pressure spike can induce is a diffusionless transformation or a transformation that does not require individual atomic jumps between adjacent sites. For example, a barely stable configuration of atoms might be destabilized by a pressure wave passing through it and thereby induced to assume a more stable configuration. The suggestion was made in a previous subsection that a supersaturation of vacancies can bring about such a barely stable state. A recent three-dimensional MD computer simulation provides evidence that supports this possibility.[16] Recrystallization may be the product of a diffusionless transformation induced in barely stable, vacancy supersaturated materials subject to ion bombardment. We shall explore this possible phenomenon in Chapter III.

Momentum transfer also can lead to forward sputtering via a series of primary and recoil collisions, which may result in the displacement of atoms in the film from their equilibrium positions into interstitial positions. Theoretical treatment of this effect (see Ref. [17] for a review of the theory) suggests that the compressive intrinsic stress induced by the excess interstitial sited atoms should scale as the square root of the particle energy. This functional dependence of the compressive stress on particle energy has been found by various investigators. We will delve into this phenomenon in greater detail in Chapter VI.

Analysis of intrinsic stress indicates that a correlating parameter for momentum controlled effects is the normalized momentum, $2\varphi(ME)^{1/2}$, where φ is the ratio of bombarding ion flux to depositing atom flux, and M and E are the mass and energy, respectively, of the bombarding particles. On the other hand, as is suggested by the ordinate in Figure 1.2, another correlating parameter is the energy density dissipated in nuclear collisions, $\varphi \nu E N_v[4MM_f/(M + M_f)^2]$, where ν is the fraction of the transmitted energy dissipated in nuclear collisions (0.8 for low-energy particles used in ion deposition or assisted deposition), M_f is the atomic mass of the film material, N_v is the number of atoms per unit volume of film. The latter correlating parameter, in deposition processes that expose the film or substrate surface to energetic particles during deposition, determines whether the film or substrate surface will be amorphous when either the film or substrate is a covalently bonded element. In particular, for the case of Figure 1.2, a silicon surface will be amorphized in silicon ion deposition at room temperature when the incident ion energy is 41 eV/ion. There exists evidence in the literature that many practitioners of deposition are unaware of this constraint.

2.4. Incident particle flux.

The deposition rates of most of the vapor deposition processes fall in the range 0.1–100 monolayers/sec. Epitaxial deposition processes use rates at the lower end of this range, whereas the higher end is used to achieve economical throughput of the coated product. The deposition rate can affect the structure of the resulting film. At low substrate temperatures, the higher the rate, the higher is the concentration of defects in the as-deposited film. At high substrate temperatures, these deposition-induced defects act to enhance the driving force for grain boundary migration and grain coalescence, processes that act to remove these defects, and hence to yield, paradoxically, films having the lowest defect content.

For processes in which the film is subjected to fluxes of both film and inert gas atoms, the film's structure is also likely to be a function of the ratio of the two fluxes. Indeed, as shown in Figure 1.2 this ratio can determine whether the film will be amorphous or crystalline under certain deposition conditions. Also, the internal stress developed in the as-deposited film is a sensitive function of this ratio. We will explore this and other structural phenomena affected by the inert gas/film atom arrival ratio in several subsequent chapters.

Deposition rate determines the time between the deposition of successive monolayers and thereby affects the limiting temperature between various zones of behavior. We shall discuss this relation in the next chapter for the case of the transition temperature between the region where intercolumnar void networks are formed in films and the region where they do not exist. Deposition rate also affects the transition between step migration limited epitaxial deposition and deposition that produces RHEED oscillations. This subject is discussed in Chapter IV. We will find other examples of the effect of deposition rate on various transition temperatures in the following chapters. In all cases deposition rate, $\tilde{N}$, and transition temperature, T^*, are related through the following equation

$$\tilde{N}e^{Q/kT^*} = \text{constant}.$$

According to the classical theory of nucleation and for most deposition rates and substrate temperatures, the equivalent supersaturation is sufficient to yield a critical nucleus volume consisting of one atom. Thus, for most of the deposition conditions likely to be met in practice, the process of nucleation can be disregarded. The rate of film thickening in low temperature deposition is independent of the nucleation rate. Indeed, the rate of film growth for thermal beams equals the impingement rate less the reevaporation rate and the latter is negligible at low substrate temperatures. The grain size of the initial layer deposited on non-epitaxial substrates, on which adatoms are highly mobile, may, in principle, be deduced from the atomistic theory of nucleation. However, in practice, this grain size is

often determined by surface defect concentration. Thus, we will not devote space to a consideration of nucleation, which is adequately treated elsewhere.[18]

The reevaporation rate varies with orientation of the crystal surface and may thereby determine the crystallographic texture of thick films, when deposition conditions allow the reevaporation rate to be non-zero. Also, the texture of thin films may be affected by the impingement rate. We shall consider these matters in detail in Chapter III. The deposition rate also affects the resulting impurity content of the deposited film. High deposition rates can minimize the impurity concentration and their structural effects. We shall discuss one such effect in Chapter III.

2.5. Substrate and its cleanliness.

Very seldom are thin films used as free-floating films. They are usually intimately connected to the substrate on which they are deposited. Thus, a thin film is in reality a system consisting of the thin film itself and its substrate. We know that the substrate is the source of most of the stresses sensed by the film. It is possible that the substrate affects many of the other properties of the film as well, e.g. the dielectric constant of the substrate affects the speed with which electrical signals move along thin film conductors. Thus, the choice of a substrate material is not unconstrained. It may be chosen to minimize thermal stresses in the film. It may be a material that needs to have its surface properties modified by a thin film coating. These are only two examples of the many conditions governing choice of a substrate material.

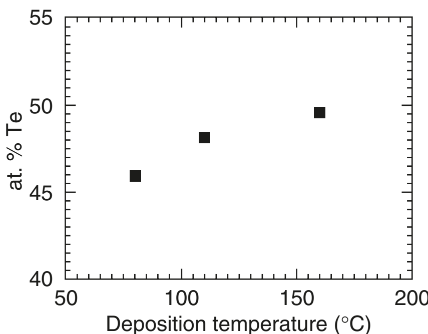

Figure 1.3. Effect of substrate temperature at a constant fluence upon film composition in laser ablation of PbTe. Reprinted with permission from A. Jaquot et al., Appl. Phys. A69, 5613(1999), Figure 2. © 1999 Springer.

We note here that monocrystalline films can be produced on a substrate by a process that does not involve epitaxy. The term epitaxy in the literature is misused. *We reserve the term epitaxy to denote a consistent crystallographic relationship between the* ***crystal lattices*** *of the film and substrate.* It is possible to form a monocrystalline film on an atomically smooth amorphous substrate. In the latter case, obviously, there is no such relationship and the substrate did not influence the production of the monocrystalline film. However, when there is a consistent epitaxial

relationship between film and substrate, then the existence of a substrate influence on the production of that relationship must be concluded. (The presence of a fiber texture* in the film does not denote an epitaxial relationship between substrate and film!) The effect of the substrate on the texture of the film stems from the tendency of the film-substrate system to minimize its total free energy. There is one exception where other than thermodynamic effects govern the epitaxial relation. Geometry, via the phenomenon of graphoepitaxy,[19] can influence the epitaxial relationship assumed by films. These concepts are discussed in greater detail in Chapters III and IV.

The presence of an intermediate layer of material between an ultra-clean surface of the substrate and the film must modify the influence of the substrate on the epitaxial relationship between film and substrate, if any, that results. Since, for an unclean surface, this intermediate layer is uncontrolled in composition and amount, it is highly unlikely that a consistent epitaxial relationship can be produced in film deposition on it.

Ultra-high vacuum (10^{-10}Torr) is necessary to maintain surfaces ultra clean for time periods in the order of an hour. Thus, most epitaxial depositions are carried out under ultra-high vacuum conditions. However, this is not to say that epitaxial deposition cannot be produced under poorer vacuum conditions. Ion beam deposition onto unclean substrates can produce epitaxial relationships between film and substrate at low temperature by allowing the incident particles to come to rest in lattice positions below the substrate surface. Higher temperature deposition where coalescence of mobile clusters can occur also can produce epitaxial relationships between film and “unclean” substrate. There appears to be a fundamental difference between the mode of forming the epitaxial relationship on ultra-clean surfaces at low temperature and the mode of forming them on unclean substrates at high temperature. We will explore these differences in Chapter IV.

At low temperature the initial clusters that deposit onto a substrate do not have sufficient mobility to coalesce and approach the equilibrium state of a monocrystalline layer. However, atoms in individual clusters do have sufficient mobility to allow the cluster to approach a metastable state. The nature of this metastable state is conditioned by the cleanliness of the substrate surface.

2.6. Substrate temperature.

The substrate temperature is the deposition parameter that probably has the greatest effect on the structure of the deposited thin film. For this reason, in the

* A fiber texture is defined by parallel orientation between a crystallographic plane in the grains of the film and the substrate plane. All possible rotations of the grains about the axis normal to this crystallographic plane (and the substrate plane) can take place, i.e. azimuthal directions in the film are undefined.

following chapters we will consider the effects of the other deposition parameters in different regimes of temperature. This procedure will facilitate the separation of the effects of the various deposition parameters, some of which can exert opposite effects on the behavior of a structural parameter in the different temperature regimes. The temperatures delineating the different regimes are defined in terms of the motion of various species required to produce observable effects. Such species may be adatoms, grain boundaries, excess vacancies, or bulk atoms. For example, in Appendix 2, the substrate temperature delineating the regimes in which excess vacancies will or will not be incorporated into thermal beam deposited films is calculated.

2.7. Composition of deposit relative to target.

Of all the modes of physical vapor deposition (PVD), laser ablation is the preferred one to use to attempt to produce a film concentration that is the same as that of the target. Hence, in this subsection attention will be paid to the deposition parameters associated with this task. Some of the possible sources of deviation of film composition from target composition are: different sticking coefficients of components, different resputtering rates of components, preferential ablation of components, different angular distribution of components in plume due to different mass and/or different charge, preferential backscattering from plume onto target. The latter process has been shown to be involved in the deviation of substrate composition from that of the average composition of the target in deposition of Si–Ge alloy.[21] Fluence affects the degree of backscattering and also the differential evaporation of components from the target surface. The larger the fluence the greater is the effect.[22] For components having a high vapor pressure the substrate temperature can affect the composition, as illustrated in Figure 1.3.[23] In this example, Te is the more volatile element. Often, in the circumstance of a large difference in vapor pressure of the components, the fluence will also affect the final composition of the film for various possible reasons including differential backscattering. An example is given in Figure 1.4. In such cases, where two deposition parameters affect the film composition, it is then possible to modify the deposition conditions to achieve congruent deposition (same composition of film as that of target).

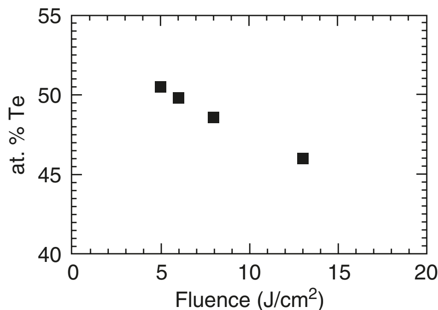

Figure 1.4. Effect of fluence at constant substrate temperature on film composition in laser ablation of PbTe. Reprinted with permission from A. Jaquot et al., Appl. Phys. A69, 5613(1999), Figure 2. © 1999 Springer.

2.8. Target.

Last, but not least, we need to be aware that aspects of the target may affect film structure and properties. One is the gas content of the target. If the target is not vacuum melted and cast then the gas content in it may cause splattering in any deposition process that raises the temperature of the target, such as laser ablation, and lead to the incorporation of frozen droplets of particles in the film. Another, is the manufactured form of the target, sintered or cast, which may yield inhomogeneities that affect the vapor composition produced from the target and the gas content in the target.

3. Deposition parameters for other than PVD.

In no other deposition process than a PVD process are the deposition parameters and their effects on structure and properties known as well as they are known for the PVD process. This fact accounts for the extended discussion devoted to these PVD parameters in the foregoing and the brevity of the discussion relating to the deposition parameters for other deposition processes that follows.

Electrodeposition, high-pressure (i.e. >0.1 Torr) CVD and LPE have in common the existence of a potential gradient ahead of the growing film surface. In electrodeposition, this gradient is an electropotential gradient. In CVD and LPE it is a chemical potential gradient, or a temperature gradient, or both. The gradient in electrodeposition can be tuned during deposition. Such tuning is much more difficult to accomplish in the other processes.

Diffusion of the film-atom-containing species occurs as a consequence of these gradients. In such processes, the controlling mechanism of growth is either the diffusion process or the interface reaction process involving incorporation of the adatom species into the film structure.[20] If the diffusion process controls, then growth is subject to morphological instability, which produces dendrites or the equivalent. One of the main functions of addition agents to electrolytic baths is to hinder growth by adsorption at growth sites, such as kinks along surface ledges. Such adsorption decreases the mobility associated with the interface reaction process, makes it the controlling process, and thereby removes the morphological instability. Denser and smoother films can be produced under interface reaction control conditions than under diffusion control conditions.

Electrodeposition has developed as an empirical discipline for most of its history. Only recently, with the application of electrodeposition to high-technology products, has an attempt been made to understand the effect of deposition parameters on film structure and consequent properties. It has been found that the deposition parameters that affect structure sensitively, and that are absent in vapor deposition, are the nature and composition of addition agents to the electrolyte. Such addition agents are usually organic. They can affect film stress, grain size,

texture, and void structure. Other deposition parameters, such as the presence of a high chemical potential for the introduction of hydrogen into the film, current density and overvoltage, have also been found to influence film structure.

In CVD diffusion control may occur only when the chamber pressure is above about 10 mTorr and a laminar layer can develop at the film surface. As noted above, this condition leads to morphological instability and produces a columnar or dendritic film structure. When the chamber pressure is less than about 10 mTorr then the morphology depends upon whether or not the incident particle sticks to the film where it impinges upon the film. If indeed the incident particle does stick upon impingement then deposition proceeds as in PVD. At low temperatures shadowing leads to the production of a columnar structure and intercolumnar void networks, as discussed in Chapter II. If there is an impediment to instant bonding upon impingement, and if a layer of the reactants can build up via van der Waals attraction to the film surface and via transverse diffusion, then the deposition conditions correspond to CVD with morphological stability, i.e. a planar film surface and an isotropic film structure.

Since about 1995 the growth in computer power has made it possible to simulate electrodeposition and CVD processes to the extent that many simulations are able to reproduce experimental results. Such simulations enable process control and often provide information concerning the process origins of structural characteristics of deposited films. There are several commercial simulation software packages as well as research oriented simulation software.[24]

4. Summary.

Table 1.1 lists the parameters that affect the structure of thin films in PVD.

Table 1.1.

Deposition parameters	Structure or phenomenon affected
Background pressure	Epitaxial or non-epitaxial deposition Impurity content in films
Parallel incidence	Columnar boundary orientation Texture
Incident particle energy	Defect, grain and crystal structures
Normalized momentum	All structures, intrinsic stress
Deposition rate	Transition temperatures, all structures
Film atom/inert gas atom flux ratio	All structures
Substrate surface nature	Epitaxial or non-epitaxial deposition
Substrate temperature	All structures, composition
Fluence (in laser ablation)	Composition

References

1. H.F. Frost and M.F. Ashby, **Deformation-Mechanism Maps**, Pergamon, Oxford, 1982.
2. R.E. Somekh, J. Vac. Sci. Technol. A2 (3), 1285(1984).
3. F. Seitz and J.S. Koehler, in **Solid State Physics**, Vol. 2, eds. F. Seitz and D. Turnbull, Academic Press, Inc., New York, 1956.
4. B.W. Dodson. Phys. Rev. B36, 1068(1987).
5. E.S. Machlin, **An Introduction to Aspects of Thermodynamics and Kinetics Relevant to Materials Science**, Giro Press, Croton-on-Hudson, NY, 1991.
6. J.A. Davies, MRS Bulletin XVII, (6), 26(1992). See also C. Carter and D.G. Armour, Thin Solid Films 80, 13(1981); E.V. Kornelsen, Can. J. Phys. 42, 364(1964).
7. B.J. Garrison, M.T. Miller and D.W. Brenner, Chem. Phys. Lett. 146, 553(1988).
8. M. Kitabatake, P. Fons and J.E. Greene, Mat. Res. Soc. Symp. Proc. 157, 259(1990).
9. T. Iida, Y. Makita, S. Winter, S. Kimura, Y. Tsai, Y. Kawasumi, P. Fons, A. Yamada, H. Shibata, A. Obara, S. Niki, S.-I. Uekusa and T. Tsukamoto, Mat. Res. Soc. Symp. Proc. 316, 1029(1994).
10. P. Bedrossian and T. Klitsner, Phys. Rev. B44, 13783(1991).
11. T.D. Andreadis, M. Rosen, M.I. Haftel and J.A. Sprague, Mat. Res. Soc. Symp. Proc. 202, 283(1991).
12. S.-M. Paik and S. Das Sarma, Surf. Sci. 208, L53 and L61(1989).
13. C.H. Choi, R. Ai and S.A. Barnett, Phys. Rev. Lett. 67, 2826(1991).
14. H. Windischmann, J.M. Cavese, R.W. Collins, R.D. Harris and J. Gonzalez-Hernandez, Mat. Res. Soc. Symp. Proc. 47, 187(1985).
15. F.L. Vook, in **Radiation Damage and Defects in Semiconductors**, ed. J.E. Whitehouse, The Institute of Physics, London, 1973, p. 60.
16. C.M. Gilmore and J.A. Sprague, Phys. Rev. B44, 8950(1991).
17. H. Windischmann, CRC Crit. Rev. Sol. State Mater. Sci. 17, 547(1992).
18. J.A. Venables, G.D.T. Spiller and M. Hanbuchen, Rep. Prog. Phys. 47, 399(1984).
19. M.W. Geis, D.C. Flanders, H.I. Smith, D.A. Antoniadis, J. Vac. Sci. Tech. 16, 1640(1979).
20. See Ref. [5], p. 269.
21. C.B. Arnold and M.J. Aziz, Appl. Phys. A69, S23(1999).
22. F. Claeyssens, A. Cheesman, S.J. Henley and M.N.R. Arnold, J. Appl. Phys. 92, 6886(2002).
23. A. Jacquot, B. Lenoir, M.O. Boffoué and A. Dauscher, Appl. Phys. A69, S613(1999).
24. Among the many examples are Flux-Expert (www.simulog.fr), Phoenics-CVD (www.simuserve.com), Chemkin (www.reactordesign.com), Ansys (www.ansys.com).

Appendix 1

The kinetic theory of gases (e.g. see L.I. Maissel and M.H. Francombe, **An Introduction to Thin Films**, Gordon and Breach Science Publishers, NY, 1973) provides the following relation between the impingement rate, $\tilde{N}$ in monolayers/s, and the gas pressure, P in Torr:

$$\tilde{N} = Pa/(2\pi mkT)^{1/2} = 3.513 \cdot 10^{22}\ aP/(MT)^{1/2}$$

where a is the surface area (in cm^2) covered by the impinging particle, M is the molar mass of the impinging particle (in g), and T is the absolute temperature. For O_2, $a \approx 16.2 \cdot 10^{-16} cm^2$, $M = 32$ g and taking $T = 300$ K yields $\tilde{N} = 0.58 \cdot 10^6 P$. Thus, when P is about $2 \cdot 10^{-6}$ Torr, then the impingement rate corresponds to about 1 monolayer/s.

Appendix 2

There are two temperature regimes experienced by the subsurface vacancies. One involves the temperature spike developed coincidentally at the point where the vacancy is generated. The other corresponds to the average substrate temperature.

The number of jumps that the vacancy can make in the zone of the temperature spike has been calculated by Seitz and Koehler[A1] and equals $0.093\rho(E/Q)^{2/3}$. The value of ρ is the ratio of the atomic vibration frequency and the frequency with which the translational energy of the moving atom is transferred from atom to atom. This ratio was assumed by Seitz and Koehler to be close to unity and this assumption has been verified in the molecular dynamic simulation of Dodson.[A2]

For a vacancy to diffuse from the third surface layer to the surface in a random process, the number of jumps it must make must equal or exceed 4. With $Q = 8.5kT_M$ and $T_M = 1500$ K, then E must exceed 312 eV for the displacement spike-generated vacancies to be able to annihilate at the surface during the temperature spike associated with the displacement spike. However, it is unlikely that more than 50 eV is transferred to the lattice at the point where the displacement spike generates a single vacancy in the collision cascade. Thus, it is unlikely that the temperature spike contributes to the annihilation of the displacement spike-induced vacancies.

To evaluate whether the substrate temperature is high enough to allow the subsurface-generated vacancies to diffuse to the surface and annihilate during growth we make use of the Nernst–Einstein relation, $V = FD/kT$, where F is the driving force and D the diffusivity for the diffusing species. In the case where vacancies generated by displacement spikes are the diffusing species, we may set $F = kT\ln(X_V/X_{Ve})/(2d_{hkl})$, where X_V is the atom fraction of vacancies at the depth corresponding to the range ($2d_{hkl}$) of the energetic incident particles and X_{Ve} is the vacancy atom fraction corresponding to thermodynamic equilibrium conditions. Also, d_{hkl} is the interplanar spacing with (hkl) being the indices of the surface plane.

We may estimate X_V from the assumption that the distribution of vacancies generated by impacts is a normal one and that the inert atom to film atom arrival ratio is unity. In this case $X_V = 0.4$. The equilibrium concentration is given by $X_{Ve} = e^{-W/kT}$, where W is the work to form a vacancy at a particular lattice site. For fcc metals, $W \approx 0.5(\pm 0.1)Q$ where $Q = 17kT_M$. Now $V = \tilde{N}d$. Also, $D = D_0 e^{-(Q-W)/kT}$, where $D_0 = 10^{-5} m^2/s$. We choose the substrate temperature to be room temperature, $\tilde{N} = 10/s$, $d_{hkl} = 10^{-10}$ m and solve the Nernst–Einstein relation for the corresponding value of T_M. The result is 1300 K. This result is not sensitive to the value estimated for the vacancy concentration. A reduction in this concentration by a factor of 10 results in a reduction of T by less than 15 K. According to this result, fcc metals with melting points less than 1300 K will be able to annihilate the displacement-induced vacancies during deposition at the growth surface, whereas for higher melting point metals such annihilation will not be able to occur.

A1. F. Seitz and J.S. Koehler, in **Solid State Physics**, Vol. 2, eds. F. Seitz and D. Turnbull, Academic Press, Inc., New York, 1956.

A2. B.W. Dodson. Phys. Rev. B36, 1068(1987).

CHAPTER II

Defect Structure

1. Intercolumn (interfiber) "void" networks.

1.1. Summary of observations concerning intercolumn "void" networks.

Thin films grown under the conditions of low-adatom mobility ($T < 0.25T_M$), incident particle energy less than about 1 eV, and with a unidirectional flux of impinging atoms develop a fibrous or columnar structure in which the intercolumn space is less dense than that in the intracolumn space.[1] This region of lower density has been described as a "void" network,[2] although the shape of the "voids" is more ribbon-like[3] than "void-like". The columns or fibers abut, but not perfectly. They may be either crystalline[4] or amorphous.[5] It has been stated that there are five different scales of void networks and associated columns; the smaller ones are contained within the larger ones, and the size of the largest one is dependent on the film thickness.[6] The angle made by the fibers with the film normal, β is often related to the angle of incidence of the impinging atoms, α by $2 \tan\beta = \tan\alpha$ the tangent "law".[7] However, this "rule" is not always obeyed.[8] The interfiber spacing is a function of the substrate[9] and the substrate temperature.[10] The void network disappears above a critical temperature, T_1.[1] Let us consider first the origin of the intercolumnar voids and then the relationships between processing and the void network.

1.2. Origin of intercolumn "void" networks.

Numerous computer simulations have been performed to study the phenomenon of intercolumn "void" networks.[11,51–59] One such simulation,[52] with incident direction normal to the substrate, concluded that from the similar variation of density and surface roughness, with substrate temperature and incident energy, the void production depends upon surface roughness and shadowing effects. Because asperities, the aspect of surface roughness providing a measurable quantity, do not produce shadows then some other aspect of surface roughness must be involved. Overhangs that have no material just beneath them do shadow under this circumstance. However, overhangs do not contribute to the surface roughness that is measured. The extent of the overhangs does correlate to the surface roughness in that

the larger the roughness wavelength and amplitude, the longer the overhang may be and the larger may be the void produced by shadowing of such an overhang. Thus, the question arises as to the origin of the surface roughness produced by deposition.

Assuming an atomically smooth substrate plane and a low substrate temperature, film growth first proceeds by the formation of clusters of atoms or islands. When incident atoms stick where they hit the cluster diameter is controlled by probability considerations. In particular, when the probability of an incident atom arriving on top of a cluster (growth in height) is the same as that of arriving at a point on the edge of the cluster (growth in diameter), the average diameter of a cluster will be defined. As discussed in Appendix 1 this concept leads to a minimum diameter of about 3.5 nm. This value is about the minimum grain size measured in deposited films as revealed in Figure 3.2. At larger cluster diameters, at these low temperatures, the probability of the cluster growing in height is higher than that of growing in diameter. Here then is the origin of the initial surface roughness. As the substrate temperature increases, because of surface diffusion, the probability of an atom reaching a cluster edge increases relative to that of arriving on top of a cluster, i.e. atoms near to the cluster edge on the substrate surface may diffuse to the edge but not to the top of the cluster. Hence, with increasing substrate temperature one may expect the surface roughness wavelength (the inverse of the population density of clusters) to increase. Even if the probability of forming an overhang in a well of a rough surface were independent of roughness wavelength, the diameter of the average void produced by overhang shadowing, in a plane parallel to that of the substrate, will increase with roughness wavelength. This expectation is supported by the rough graphical simulation of two surface roughness waves of different wavelength in Figure 2.1. It is also supported by the simulation results shown in Figure 2.2a and b. However, another effect of increasing

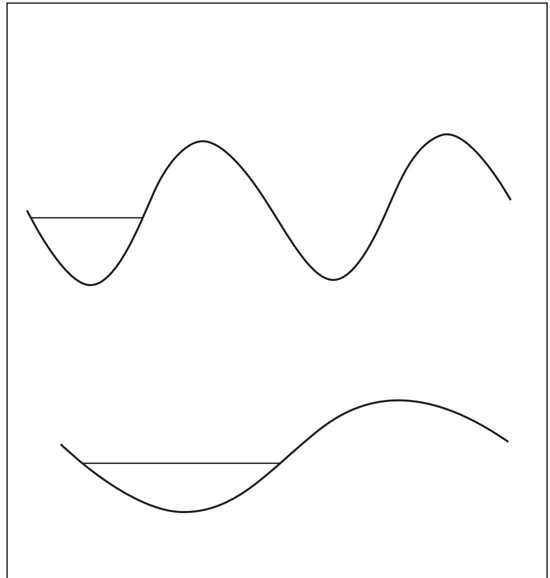

Figure 2.1. Idealized roughness (intersection of hills and valleys with plane normal to substrate surface) revealing diameter of average void under overhang (horizontal line).

the substrate temperature is to decrease the amplitude of the surface roughness as shown in Figure 2.3, an effect that overcomes the effect of substrate temperature on the wavelength of the surface roughness. Hence, the net effect of an increase in substrate temperature is to cause an initial increase in the diameter of voids in the film plane, then voids disappear entirely at a sufficiently high substrate temperature.

Columns grow in height upon the clusters formed on the substrate. On a monocrystalline substrate the intercolumnar surface is the loci of voids produced by shadowing of overhangs. On an amorphous or polycrystalline surface the columns may be either amorphous or crystalline depending upon the material deposited and the deposition conditions. Crystalline columns grow in height by granular epitaxial deposition. Figure 2.4 shows a one-layer thick slice normal to the film produced in a three-dimensional Monte Carlo simulation at low substrate temperature revealing the columnar grains that survive the shadowing effect and those that do not.

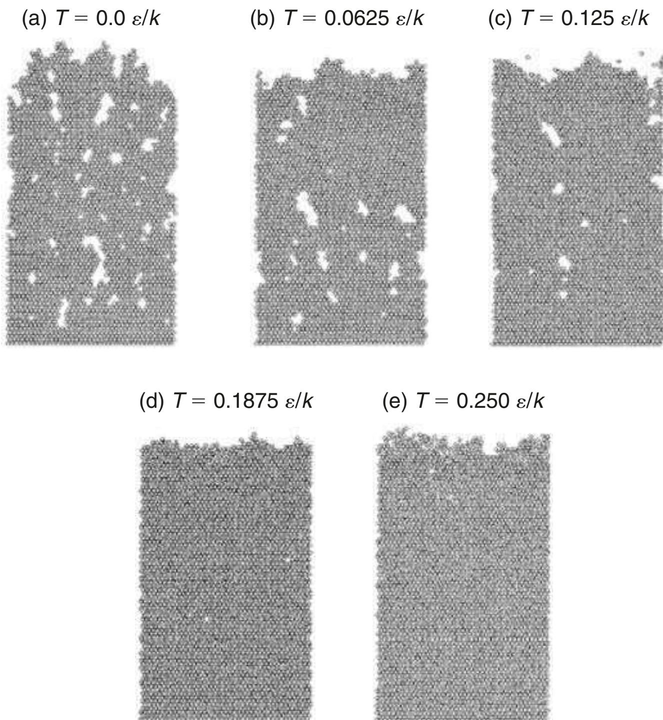

Figure 2.2. Sequential snapshots from a kinetic Monte Carlo simulation of deposition at normal incidence of a hypothermal beam of atoms with substrate temperatures as shown increasing from (a) to (e). Reproduced with permission from J. Appl. Phys. 79, 1448(1996).

The shadowing effect becomes much more pronounced when the incident beam of atoms is at an oblique angle with respect to the film normal. Now voids develop not because of overhangs in the intercolumnar space but because of shadowing by the asperities of the columns (clusters) themselves. The original edition of this book contained a rough analysis of the differential probabilities of atoms sticking on the "windward" and "leeward" sides of clusters in an attempt to provide an explanation for the so-called tangent law: $2\tan\beta = \tan\alpha$ where β is the angle made by the fibers with the film normal and α is the angle made by the incident beam with the film normal. The assumptions of this analysis were not realistic (more applicable to a two-dimensional mode of deposition along a line). Hence, it is not repeated here. Other analytic attempts have not been much more successful.[49] Figure 2.5 shows that the tangent law functions adequately for α values less than 60°, but not for higher values and better than at least one of the deduced analytic relations. A possible reason for this difficulty is that analytical attempts are based on one or two-dimensional models. The difference between the predictions of models involving different dimensions is illustrated by comparison of Figures 2.2 and 2.4. The former is a product of a two-dimensional molecular dynamics (MD) simulation and the latter is a result of a three-dimensional MC simulation for nearly identical deposition conditions. It appears that shadowing is much more effective in producing intercolumnar voids in three dimensions than in two dimensions for incident atoms normal to the substrate.

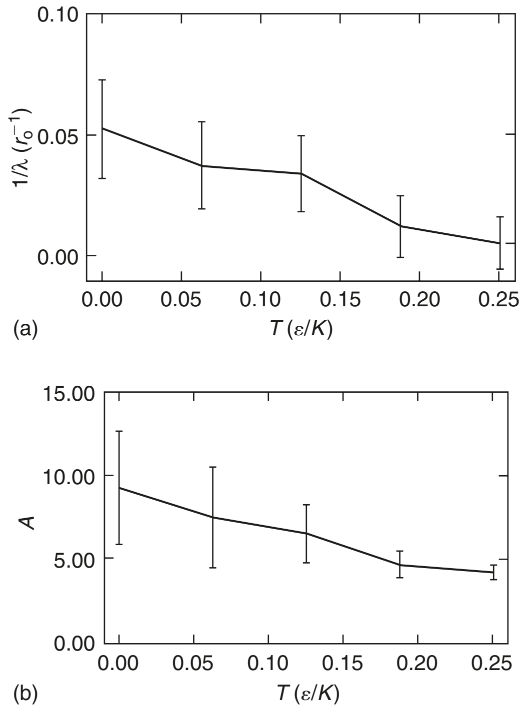

Figure 2.3. Wave number (a) and amplitude (b) of film surface roughness versus substrate temperature as deduced in a kinetic MC simulation. Reproduced with permission from J. Appl. Phys. 79, 1448(1996).

Dirks and Leamy[11] have suggested an explanation for the "tangent" law, which is neither convincing nor rigorous. It is based on an assumed effect of atomic

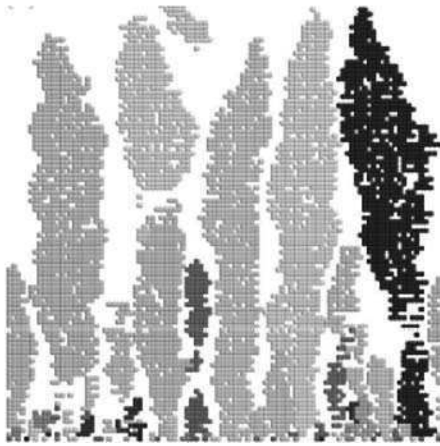

Figure 2.4. One-layer thick slice through polycrystalline film produced at low temperature in a three-dimensional MC simulation. Reproduced with permission from Tech. Proc. of the 1999 Intl. Conf. on Modeling and Simulation of Microsystems. Nano Science & Technology Institute, p. 467 (ISBN 0-9666135-4-6).

shadowing on the “leeward” angle of a column and is reproduced verbatim in Appendix 2, where an equivalent derivation is given to show the shortcomings in this suggestion for the origin of the tangent law. Others[49] have suggested that the column angle is determined by the weighted average of the flux incident upon a differential area rdγ normal to a radial vector at an angle γ with respect to the film normal, drawn from an origin that is at the midpoint of the column width, with the limits of the angle γ determined by “windward” and “leeward” shadowing. In the opinion of this writer, the agreement between the relation deduced from this concept is worse than that produced by the tangent law.

Nieuwenhuizen and Haanstra[7] and Leamy and Dirks[3] collected the most convincing experimental evidence for the tangent rule, which is reproduced in Figure 2.5. The theoretical values deduced in Ref. [49b] are represented by open squares. As shown, the tangent law gives better agreement than the latter theory for incident angles smaller than about 60° and yields poorer values only at 80°. Despite that apparent agreement between the tangent law and experiment revealed in Figure 2.5, there is still some doubt as to its universal applicability. In particular for a given incident angle, the column angle was found to be a function of pressure[8] and substrate temperature.[14]

Most theories for the origin of the tangent rule are based on the concept of shadowing. However, the tangent rule is obeyed in many cases when the mode of deposition is via sputtering rather than evaporation. When the gas pressure exceeds about 0.03 Torr, as discussed in Chapter I, the atom directions are more nearly random than unidirectional. How can shadowing contribute to the tangent law in this case? One possible answer to this question is that a shadowing effect arises from the fact that a site on the side of a column “sees” only a small solid angle of free space. A site on top of a column can “see” unobstructed views for a solid angle of about 2π, whereas a site on the side of the column has a much more restricted view of the “open sky” from its position. The latter source of shadowing has been explored by Karunasiri et al.[15]

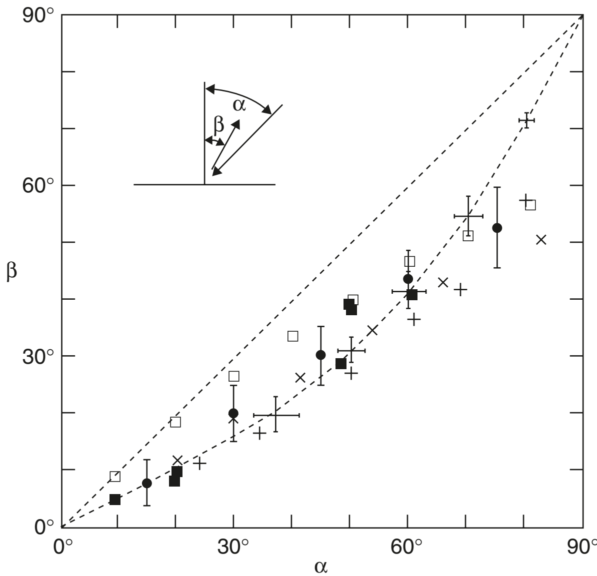

Figure 2.5. The column angle as a function of the incident angle for crystalline and amorphous materials. The dotted line represents the tangent law.[3,7] The open squares represent the theoretical values of Ref. [49b]. The other points are experimental values.

Ramanlal and Sander[46] have shown that if the tangent law is assumed as an axiom, then it can be shown that ballistic aggregation onto one seed leads to the growth of a fanlike column with the angle defining the fan's extremities equal to 19.5° as a maximum. Thus, a column tends to grow in width as well as in length. Simulation-based examples of the fanlike mode of column growth are shown in Figure 2.6. The columnar mode of growth apparent in Figure 2.4 contrasts sharply with the fanlike mode shown in Figure 2.6. One potential cause for this difference suggested by Dirks and Leamy is that the former involves local relaxation after an incident particle contacts the film, whereas the latter does not.* An analysis of the analytic proposals put forth to explain the tangent law is given in Appendix 2. However, as noted in the conclusion of this analysis, we still do not understand what controls the direction of growth of the "leeward" side of the tree and the mean growth direction. Fortunately, the production of columns in computer simulations of deposition provides hope that one day this understanding will emerge.

There does not appear to be any mention in the literature of the fact that the ballistic aggregation models are not wholly consistent with the growth

* Space is subdivided in this simulation into a matrix of square boxes. An atom that impinges into a box, which is a neighbor to an occupied box, is captured in this box.

Figure 2.6. Results of a spatially correlated ballistic deposition using a two-dimensional lattice model. A tree of sites connected by the growth process is identified by filled lattice sites. Reprinted with permission from P. Meakin, Phys. Rev. A41, 983(1990). © 1990 The American Physical Society.

conditions operating during the formation of intercolumn "void" networks in the following sense. For most, if not all, of the microscopic studies of the intercolumnar "void" networks in various materials, the substrate material was such as to provide appreciable adatom mobility, under growth conditions where the self adatom mobility is nil. Under these conditions, the intercolumn spacing is determined by the intercluster spacing achieved by deposition on the substrate. The latter is usually determined by the surface density of defects that bind and immobilize the clusters and, in the case where such defects are scarce, by nucleation considerations.

Most of the substrates used in studies of the intercolumnar void network were either oxidized surfaces, alkali halides, or organic films. Adatoms bond poorly to such substrates and consequently the adatom mobility is very high. For example, the activation energy for gold adatom diffusion on a clean NaCl substrate is 0.16 eV,[16] whereas that for gold on gold is 0.91 eV.[17] Not only is there adatom diffusion on these substrates, but for many of the cases where intercolumn "voids" are produced there is also cluster mobility. These clusters will begin to grow normal to the substrate plane when the number of sites on clusters for adatoms exceeds the number remaining on the substrate. Thereafter, shadowing will occur to produce voids between neighboring clusters.

Whether or not a multitude of columns will form on a given cluster depends upon the adatom mobility on the cluster relative to the rate of deposition and the intercolumn spacing. The same considerations, with the intercluster spacing replacing the intercolumn spacing, determine whether or not an intercluster "void" network will propagate during growth. Let us consider these concepts in greater detail at this point.

Typical values of cluster densities produced by slow evaporation (0.01 monolayers/s) onto alkali halide substrates at room temperature equal about $10^{11}/cm^2$. This number corresponds to an intercluster spacing of about 30 nm. However, much higher cluster densities have been measured and analysis[16] indicates that the cluster density should increase as the 2/3 power of the rate of deposition. Thus, the measured column diameters ranging from about 4–15 nm in very thin films are consistent with the hypothesis that clusters or islands, produced by adatom collision during diffusion on substrates, represent the origin of the columns.

The experimental evidence supports the proposition that the substrate affects the column diameter and determines the absence or appearance of columns and void networks. In particular the structure of substrate surfaces is transmitted through the film to the film surface;[18] anisotropic distribution of preferential sticking sites on the substrate is revealed by a corresponding anisotropic distribution of columns;[20] the column diameter produced in very thin films is a function of the substrate and its treatment;[18,20] and the column diameter in α-Ge films deposited on an amorphous, structureless substrate at 200°C to 20 nm thickness, with continued deposition at −100°C, is the same as for continuous deposition at 200°C and much larger than for initial and continued deposition at −100°C.[10] The latter observation indicates that the temperature dependence of the column diameter is not growth determined. Rather, it is a function of the process that determines the intercluster spacing on the substrate. This observation does not support the expectation of Leamy and Dirks[3] that the column diameter will be determined by the supply of adatoms diffusing to the intercolumn space during the growth stage. The observed temperature dependence of the column diameters[10] is consistent with the temperature dependence, deduced from the atomistic theory of nucleation,[19] of the cluster diameter at a stage close to coalescence.

Messier et al.[6] have recently studied the range of structure from nano- to macro-scale structures and have concluded that there are five different void-column combinations, with the smaller ones present within the larger ones. The larger scale void-column structures begin to appear as the film thickness increases. According to Messier et al. the five characteristic column sizes are: 1–3, 5–20, 20–40, 50–200, and 200–400 nm. The corresponding film thickness at which these columns begin to appear are >0, 5, 50, 500, and 5000 nm, respectively. The scale of the voids in each group is roughly one-tenth of the average column diameter for that group. Small angle neutron scattering measurements confirm that columns

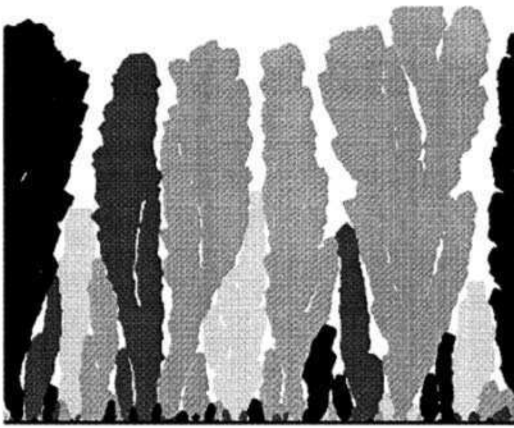

Figure 2.7. Showing the result of deposition at 10,000 μm/min in a three-dimensional MC model. The shades of darkness represent different crystal orientations. Reproduced with permission from H. Huang and G.H. Gilmer, J. Computer-Aided Materials Design 6, 117(1999).

6 nm in diameter exist in 20 nm thick films of α-Si:H.[21] However, it has been reported that the density increases with film thickness and speculated that this result is a consequence of the closing up of intercolumnar space.[28] Figure 2.7 may help one to understand some of the above observations. This figure is a snapshot of the film deposited in a three-dimensional MC model at a temperature and deposition rate where some adatom diffusion may occur without the closing up of the voids. The average column and void diameters increase with thickness in this figure.

1.3. Effect of processing on void and column structure.

Among the processing variables that are known to affect void and column structure are substrate temperature, incident particle energy, direction and degree of collimation, deposition rate, and adhesion to substrate. Among the structural parameters usually measured or observed are density, surface roughness, microstructure, texture, and internal stress. We postpone consideration of the effects of processing on texture and internal stress and consider processing effects on the other structural parameters.

First we may note that there is a general agreement that increasing substrate temperature increases density (mainly by removing voids or intercolumnar space, as illustrated in Figure 2.2). Figure 2.8 provides an indirect measure of the effect of temperature on density in that, as substrate temperature increases so does the adatom diffusivity; and this figure shows the effect of increasing adatom diffusivity on density for two different textures and for an incident angle of 60° relative to the film normal. The main physical effect of increasing temperature is to increase the diffusion length of adatoms prior to their burial under the arriving flux of atoms. Thus, diffusing adatoms arrive at and fill-in the intercolumnar voids with increasing efficiency as substrate temperature increases. Another effect of increasing substrate temperature is to increase the mobility of grain boundaries, which

brings about columnar diameter increases and decreases, and concomitant changes in texture; but these occur mainly above the temperature at which intercolumnar voids are eliminated. The latter effects will be discussed in later chapters. From the effect of substrate temperature on the diffusion length we may deduce that an increase in deposition rate corresponds to a decrease in substrate temperature. This relation is illustrated by a comparison of Figures 2.7 and 2.9 which show films of the same thickness, but which were deposited at 10,000 and 1,000 μm/min, respectively. The main effects revealed in this comparison are that the individual columns show a denser internal packing and smoother surfaces with the development of facets and a change in texture with decreasing deposition rate. This result indicates that the diffusion length in the smaller deposition rate film is still not long enough to fill up the intercolumnar space but is sufficient to smoothen the surfaces and remove internal voids of the columns and bias the growth of columns. In this simulation study the incident atoms obeyed a cosine law in their angles of incidence. The effect of the incidence direction is significant in the biasing of the column growth rates and in the formation of texture as will be discussed in a later chapter.

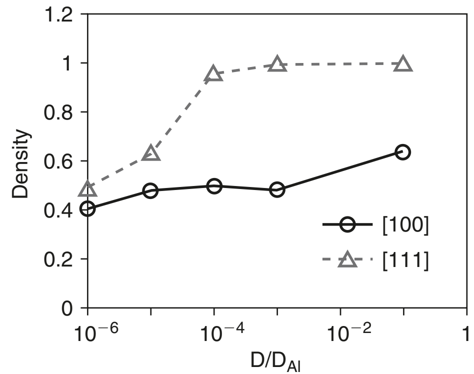

Figure 2.8. As measured in a three-dimensional MC simulation. Reproduced with permission from J. Dalla Torre et al., Proc. MRS Symp. L, Spring Meeting, 1999.

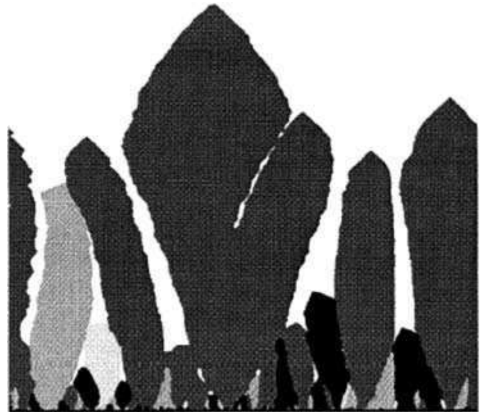

Figure 2.9. Showing the result of deposition at 1000 μm/min in a three-dimensional MC model. The shades of darkness represent the same crystal orientations shown in Figure 2.7. Reproduced with permission from H. Huang and G.H. Gilmer, J. Computer-Aided Materials Design 6, 117(1999).

Increase in substrate temperature also decreases the surface roughness (as already noted in Figure 2.3) although the development of facets can over a

short range of temperature bring about an increase of roughness before the further increase in substrate temperature decreases the surface roughness.

The effect of deposition angle upon the density of the film produced in an MD simulation of deposition at temperatures below T_1 has been investigated by Dong, Smith, and Srolovitz.[53] Their results shown in Figure 2.10 pictorially demonstrate that density decreases drastically with increase in the angle of deposition relative to the film normal. These authors also showed for temperature still below T_1 that increases in substrate temperature and incident particle energy result in an increase in the density, fewer and smaller voids, and smoother surfaces. Similar results were obtained in a three-dimensional MC simulation by Dalla Torre et al.[56] Their results are shown in Figure 2.11 where the results are quantified. This effect of angle between beam and film normal has been used to achieve various film products for a variety of applications. For example, nanorods are produced using this technique.[57] Figure 2.12 shows orthogonal views of Si nanorods obliquely deposited onto a template consisting of W pillars arranged on square lattice points. Another application relating to thermal conductivity systematically alters the direction of the beam during deposition to produce zigzag columns. One such array is shown in Figure 2.13. It is also possible to produce helical shaped rods in oblique deposition

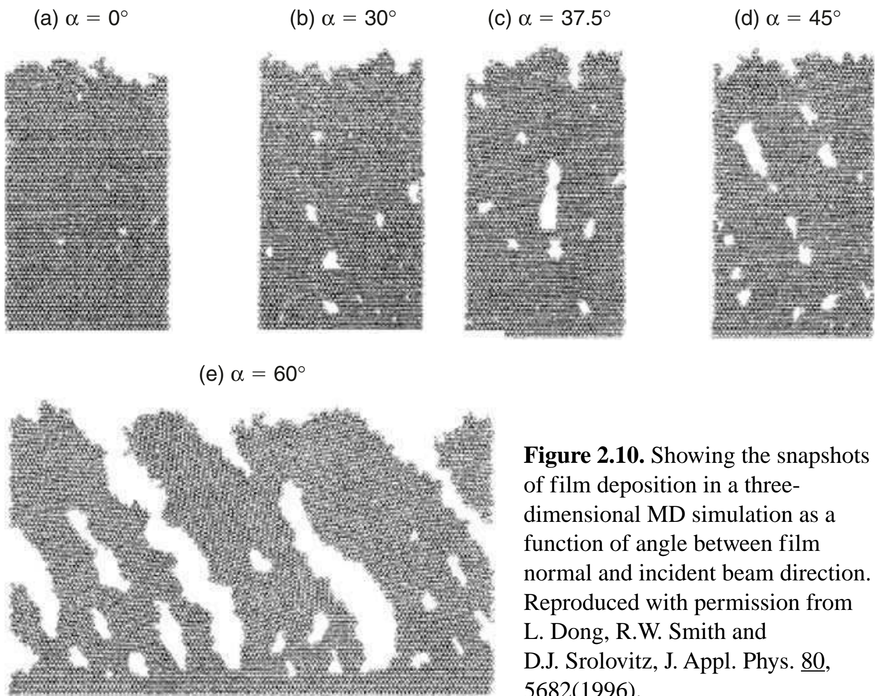

Figure 2.10. Showing the snapshots of film deposition in a three-dimensional MD simulation as a function of angle between film normal and incident beam direction. Reproduced with permission from L. Dong, R.W. Smith and D.J. Srolovitz, J. Appl. Phys. 80, 5682(1996).

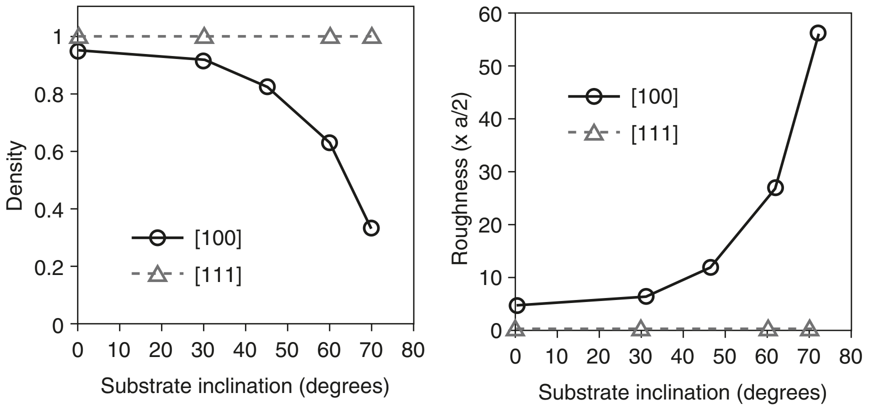

Figure 2.11. Measured in a three-dimensional MC simulation showing density and surface roughness as a function of substrate inclination (angle between substrate normal and incident beam direction). Reproduced with permission from J. Dalla Torre et al., Proc. MRS Symp. L, Spring Meeting, 1999.

with a rotating substrate. Indeed, in both of the preceding examples the substrate rotated.

The previous discussion concentrated on the formation of the intercolumn "void" network via physical vapor deposition (PVD) processes. The equivalent of this network can be produced by morphological instability in other deposition processes, such as chemical vapor deposition (CVD) and electroplating. In the latter processes, the morphological instability produces dendrites and tends to occur when growth of the deposit is diffusion limited, with the diffusion occurring ahead of the growing interface through a potential gradient. If surface reaction kinetics limits the growth rate of the deposit then growth occurs under morphologically stable conditions and dendrites are not produced. Instead, the film surface is smooth.[24] However, commercial reasons provide a barrier to the use of the regime of surface reaction limited kinetics. It is still possible to find conditions in the diffusion limited regime where, although a planar growth front is not produced, the instability leading to dendritic growth can be

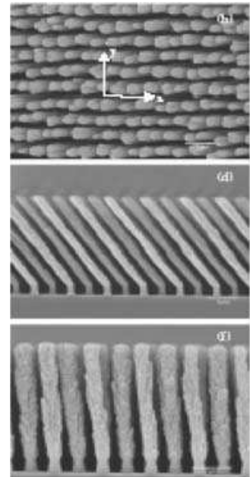

Figure 2.12. Orthogonal views of nanorods produced in oblique deposition. Reproduced with permission from D.-X. Ye et al., Nanotechnology 15, 817 (2004) (Institute of Physics).

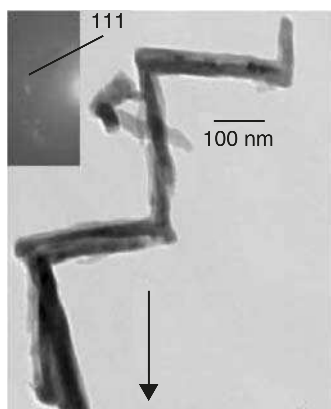

Figure 2.13. A zigzag rod produced in oblique deposition. Reproduced with permission from B. Djurfors et al., MRS Symp. Proc. 749, W5.4.1(2003).

forestalled during the deposition. CVD growth under these conditions has been explored theoretically by Bales et al.[25] The growth front in this case consists of parabolic segments separated by narrow cusps. The latter authors contend that the Eden model,[26] which has been proposed as a description of growth for CVD and other processes, neglects an effect that does not allow the growth interface to approach a planar interface asymptotically in this growth regime. Computer simulation models of diffusion-limited growth, denoted *diffusion-limited aggregation models*, have been developed by Meakin.[27]

Despite the longer history of electroplating and CVD relative to PVD, the degree of characterization of the resulting films is much less. It is difficult to provide evidence regarding the presence or absence of void networks in films deposited by these processes. Also, because the mode of growth in electroplating is sensitive to surface active impurities, it is difficult to develop a universal model that relates the defect structure to the mode of growth.

The presence of tensile stress in the plane of the deposited film, at the substrate temperature, has been ascribed, at least for electroplated films, to the tendency for adjacent crystallites to coalesce, i.e. move towards each other.[29] This tendency to coalesce is resisted by the substrate to which the film adheres and thereby induces tensile stress in the film. These adjacent crystallites could not move toward each other if there were no space between them. From this deduction we may conclude that if the coalescence process did not occur uniformly over all the side faces of the crystallites then there would still remain void pockets at the locally uncoalesced areas. If these crystallites were columnar in shape then these voids would form a network of voids. Despite this analysis, the author is not aware of any experimental studies on electroplated films, similar to those performed on physically vapor-deposited films, that directly reveal intercolumnar "void" networks.

The desire to produce smooth surfaces usually constrains CVD to be carried out under or near to surface reaction limited growth conditions. Thus, if there is ready lateral transport of the adatom containing species it should be possible to deposit such films without the production of columns or an intercolumnar "void" network.

1.4. Temperature, T_1, delineating transition between presence and absence of "void" networks.

Movchan and Demchishin,[1] in their structure zone model (SZM), were the first to define a substrate transition temperature that separates the temperature regime where void-free films are deposited from that in which the deposited films contain voids. They denoted the temperature regime in which voids were produced in thin films as *zone 1*, and the next highest temperature zone, in which the films were free of voids, as *zone 2*. The transition temperature between these two zones was denoted T_1. Movchan and Demchishin[1] recognized that T_1 is related to some critical value of adatom mobility. The question is: "What critical value of adatom mobility determines T_1?"

The answer to the question posed above is that T_1 is determined by the temperature above which the rate of filling-in of voids by adatom diffusion equals the rate of production of these voids. Muller,[13] using a two-dimensional computer simulation of void production and an Monte Carlo type calculation to govern adatom jumping to neighboring sites, found a transition temperature at which the packing density increased from about 0.7 to 1, which was a function of the deposition rate.

It is possible to estimate the Critical temperature, T_1, from the condition that the diffusion distance,[24] $X = (4D\Delta t)^{1/2}$, exceeds some multiple of the void network width (i.e. the separation between columns), where Δt is the time interval between deposition of successive monolayers. We will assume that most of the density decrement due to voids is associated with the columns having a diameter in the order of 20 nm or less. (This assumption is equivalent to the assumption that the void networks associated with larger diameter columns in thicker films will not form if the void network corresponding to the 20 nm column group are filled-in.) Also, we will assume that the multiple of the intercolumn void ribbon thickness required to supply it is unity, so that, with the knowledge that the intercolumn void thickness equals about one-tenth the column diameter, we obtain $X = 1$ nm. Now $D = D_o \cdot e^{-Q/kT}$. For metals and for adatom diffusion, $D_o = 10^{-7}$ m^2/s and $Q = 6.5kT_M$.[24,30] Also, $\Delta t = n_o\Omega/R$, where n_o is the number of atoms per unit area in a monolayer of atoms on the surface, Ω is the atomic volume and R is the deposition rate. For $R = 25$ nm/s and $n_o = 10^{19}/m^2$, the above relations yield $T_1/T_M = 0.3$. This result is about that found experimentally by Movchan and Demchishin[1] for metals corresponding to the n_o value chosen and deposited at the R value chosen. Table 2.1 lists some representative values of T_1 for the two values of R.

The effect of deposition rate suggested by the above relation and Table 2.1 is sometimes not obeyed experimentally. In particular, it has been found that increasing the deposition rate leads to the densification of, and the elimination of, the void network in nickel and palladium films deposited at room temperature.[31] A possible explanation of this contrary result is that the concentration of codeposited impurity atoms decreases as the deposition rate increases and may thereby eliminate an

Table 2.1. Zone transition temperature

Metal	Temperature (°C)	
R(nm/s) =	**100**	**0.01**
Ag	112	−5
Al	18	−70
Au*	214	68
Cu	149	21
Ni*	94	−26
Pt*	228	67

* Values based on experimental adatom diffusion activation.

inhibiting effect of surface situated impurity atoms on surface diffusion of the metal adatoms. This inhibiting action of oxygen on adatom diffusion is likely to be present in the deposition of Al films and probably accounts for the observation of intercolumnar voids in Al films deposited at room temperature and above when according to Table 2.1 the substrate temperature should be above T_1. With the current ability to evaporate in ultra-high vacuum chambers it would be useful to evaluate the effects suggested by Table 2.1 in the absence of such impurities. It is already known that monocrystalline films of nickel and platinum can be deposited at substrate temperatures between 20°C and 100°C onto clean single crystal substrates at deposition rates less than 1 nm/s.[32,33] It is not known if void networks develop in these metal films when the deposition rate exceeds a limit.

1.5. Crystalline versus amorphous structure in *zone 1*.

Whether a crystalline structure or an amorphous one is obtained in a *zone 1* condensed film depends upon the type of material being deposited. Metals produce polycrystalline films, whereas covalently bonded materials, such as silicon, and many alloys and compounds deposit as amorphous films.

1.5.1. Crystalline films.

The mechanism of forming crystals in *zone 1* is not known. It has been suggested that the crystals form by an athermal process from some unknown type of higher free-energy precursor.[34] It is impossible in the *zone 1* temperature range for a crystal on the order of 10 nm diameter to be produced by any process involving the activated addition of atoms, one at a time, to a cluster that is in good thermal contact with the substrate. However, as argued in Chapter I, for a cluster that is not in good thermal contact with the substrate, or on a low thermal conductivity substrate, the heat of condensation can provide the energy for sufficient adatom diffusion to produce a crystalline array from an amorphous array, for small clusters. At these low temperatures the supersaturation ratio is so high that the critical nucleus consists of one atom. Hence, it is reasonable that small crystalline clusters will continue to grow as crystals. However, whether the initial cluster is amorphous and transforms athermally into a crystal or whether it is initially crystalline is not really known.

Once a cluster is crystalline it can continue to grow by the process of granular epitaxy, i.e. a process in which the impinging atoms fall into the nearest

potential well adjacent to their points of impact and continue the growth of the substrate crystal. This statement is certainly valid for metallic elements. However, it is not valid for semiconductors and compounds. In the latter case, the adatom mobility must be sufficient to move the adatom several interatomic distances to arrive at the potential well consistent with a stable crystalline array. Because too little is known about the adatom mobility on compounds, it is not possible at this time to predict whether a given compound will deposit as a crystalline or as an amorphous film at a given substrate temperature. Indeed, there exists a transition substrate temperature above, which compounds deposit to form crystalline films and below which these films are amorphous.

1.5.2. Amorphous films.

The formation of amorphous structure in covalently bonded materials deposited in the *zone 1* range of substrate temperatures is understandable. The production of a metal crystal in a deposition process, at temperatures below which surface reconstruction can occur spontaneously, requires that an incident atom move only to the nearest empty lattice site; a fraction of an interatomic distance away, without any barrier to that motion. The production of a covalently bonded crystal requires either the rotation of bonded atoms about some bond to satisfy the crystal symmetry, or the making and breaking of a bent bond, or both. All these processes must involve appreciable energy barriers. The positions of potential wells in the plane above the surface of a metallic crystal are well determined and fixed. Those above the surface of a covalent crystal are not necessarily well determined. (Rotation about the bond of a singly bonded atom can occur to randomize the position of the dangling bonds.) Thus, incident atoms will form those covalent bonds, that their nearest neighbors, at the moment of contact of the incident atom, allow. These bonds are much more likely to produce an amorphous solid than a crystalline one. Another reason that has been proposed for the production of amorphous solids in covalently bonded material is that the surface diffusivity is much smaller at a given homologous temperature for covalently bonded materials than for metals. However, a crystalline metal will be produced even for conditions where the incident atom will not diffuse on the surface (i.e. will not move from its point of incidence by more than a fraction of an interatomic distance). Thus, there is reason to doubt the latter proposal.

Some amorphous alloys involve components that differ significantly in atom size. A solid solution of such components will not have long-range correlations between atom positions. Whether crystal diffraction patterns can be obtained from such a solid solution depends on the longest dimension over which such correlations exist, and this dimension is related to the difference in atom size between components. Other factors are involved in the competition between crystalline and amorphous structures for alloys. One such factor is thermodynamic in origin. If

the amorphous solid alloy has a more negative free energy than that of the crystalline alloy of the same composition, then it is stable relative to the latter and, given no kinetic barriers to its formation, will exist at the expense of the same composition crystalline alloy.

Thus, the *zone 1* range of temperature associated with the production of columns of material separated by voids is unrelated to the crystalline or amorphous nature of the material being deposited, as evidenced by the production of these columns in crystalline metals and amorphous semiconductors.

1.6. Instability of “void” network.

There is a lack of knowledge concerning the stability of the void network in as-deposited films. The fact that leads one to question this stability is the existence of an intrinsic tensile stress in most films deposited from vapors having the thermal spectrum of energies. Such intrinsic tensile stress in as-deposited films can arise only by a decrease in length of the film in the film plane that occurs during the deposition process, while it is bonded to the substrate. The most obvious origin of a decrement in film length is the onset of bonding across intercolumnar voids subsequent to their formation. At temperatures in the *zone 1* regime such bonding cannot be due to adatoms migrating or vacancy diffusion. In Chapter VI we show that for voids thinner than about 1.7 Å, the bounding surfaces of the void will be attracted to each other with sufficient force to bond together. Also, for thin (<20 Å) and long (>200 Å) columns, long wave transverse oscillations of thermal origin may bring the opposite surfaces of some voids (<3 atom layers thick) near enough to bond together.

In a three-dimensional MD simulation of deposition at a substrate temperature slightly higher than T_1 it was found that whenever overhangs developed above voids during the deposition, these overhangs became unstable and collapsed into the voids.[35] The onset of instability for these overhangs may be the arrival of an atom having an energy in the high segment of the thermal spectrum of energies. The process of developing overhangs, which is made apparent in this simulation, may, for thin voids, lead to the onset of bonding and thereby to the formation of a continuous bridge joining the walls of the thin void. The act of pulling together the walls of the void and bonding them together via the bridge should simultaneously induce a tensile stress in the columns that the bridge connects.

1.7. Deposition methods that eliminate the formation of “void” networks.

“From the discussion of the mechanisms of formation of the column-“void” network morphology it is possible to deduce that the production of this

morphology can be avoided either by having energetic particles irradiate the film surface during deposition or by preventing island formation during the initial deposition onto the substrate or by promoting lateral transport of the attaching species prior to attachment to the film.

1.7.1. Deposition processes involving energetic incident particles.

In sputtering under conditions such that the substrate is held at a negative bias relative to the floating potential of the plasma, and in ion beam deposition, the kinetic energy of the particles that condense to form the deposit is increased to above the thermal range. In ion beam assisted deposition, as well as bias sputtering, the film/vapor substrate is bombarded by energetic inert gas atoms during the deposition process. At temperatures below T_1 the effect of low energy incident particle bombardment is to transfer momentum to the lattice of the film and thereby induce several processes. Among these possible processes are the initiation of an elastic pressure wave that propagates into the lattice from the point of impact, phonon and electron excitations, atomic displacements, break-up of surface reconstructed atom arrangements by insertion of the energetic incident atom into the arrangement to produce the bulk lattice array in place of the reconstructed arrangement,[36–38] collapse of barely metastable atom configurations,[35] forward sputtering of void overhang atoms,[39,40] collision cascades and backward sputtering,[41] and the enhancement of activated processes due to induced thermal spikes.[12]

As noted in Chapter I the deposition parameter that correlates to the structure of the bombarded film is the normalized momentum, $2\varphi\sqrt{ME}$, where φ is the ratio of the energetic particle flux to the flux of the condensing atoms, M is the atomic mass of the bombarding particle and E its energy. We noted in Chapter I that at low values of the normalized momentum, the first effect of the bombarding particles on the structure is the production of interstitial sited atoms, without the concomitant production of vacancies. Depending upon the material and substrate temperature the interstitial atoms may or may not be mobile. If they are mobile they migrate to sinks, which may be voids, grain boundaries, dislocations, and the film surface. The forward transmission of momentum along a close-packed row of atoms, which is responsible for the formation of the interstitial sited atoms, also can produce forward sputtered atoms that exit an overhang and enter a void or can act to destabilize the overhang and drive it into the void. At somewhat higher values of the normalized momentum, vacant sites are produced along with the interstitial sites via the production of Frenkel defects in displacement spikes. Also, lattice disorder is produced along the path of the displacement spike. The reordering that occurs under the influence of the concomitant thermal spike and the subsequent diffusion of point defects may bring about a recrystallization of the grain structure. Finally, at higher values of the normalized momentum,

an initially crystalline lattice can be converted to an amorphous structure by the disordering associated with the displacement spike when overlap of these spikes takes place.

In the present section we are interested in the possible effects of energetic incident atoms on the void structure. There have been several MD simulations that describe the latter effect. One that is instructive yielded the results shown in Figure 2.14. This simulation[42] was two-dimensional and hence some of the voids shown may not appear in a three-dimensional simulation. Nevertheless, the qualitative trends indicated are likely to be valid. These trends are the disappearance of voids as the incident particle energy increases; the concomitant increase in film density and a cyclic dependence of the grain boundary population with increase in the incident particle energy. No interstitial sited atoms are found in this simulation. However, their absence may be due to their rapid diffusion to sinks. Interstitials have been found in MD simulations of low energy self-bombardment of silicon.[50] (The simulation corresponding to Figure 2.14 used a Lennard-Jones potential fitted to parameters pertaining to nickel.)

The first two trends were also observed by Müller,[13] although the third trend was not observed in his MD simulation. A three-dimensional MD simulation of ion beam assisted deposition[22] found that the effect of the ion beam is restricted at any time to a limited depth beneath the film surface. Hence, to accomplish full densification, the ion-beam-to-deposited-atom arrival ratio must be adjusted to an optimum value for a given beam energy, i.e. there is an optimum value of the normalized momentum for complete densification. Increasing the beam energy enhances its effectiveness in collapsing voids. Further, it was found that the diffusion of residual interstitialcies produced by the ion bombardment is important to the densification process. Interstitialcies have high mobility in metals and can diffuse readily in the *zone 1* temperature range, whereas vacancies generally cannot, even under the influence of ion bombardment induced thermal spikes.[12, 47] Thus, at low substrate temperatures, a significant fraction of vacancies produced in metals by the ion beam bombardment that are not annihilated by combination with interstitialcies, or by diffusion to vacancy sinks, such as the growth surface, or grain boundaries, remain in the lattice.

This section would not be complete without the reminder that it is not always desired to remove the intercolumnar “void” network. For example, copper films can be projection patterned* in a low partial pressure of chlorine when the intercolumnar “void” network is present and cannot be projection patterned when it is absent; etching of films containing intercolumnar “void” networks is used to form surfaces that absorb radiation efficiently; the magnetic properties of some films can be favorably affected by the presence of the separated columns, etc.

* Projection patterning involves pulse illumination of sufficient intensity through a mask so that the illuminated portion of the high vapor pressure layer on the surface of the film is ablated.

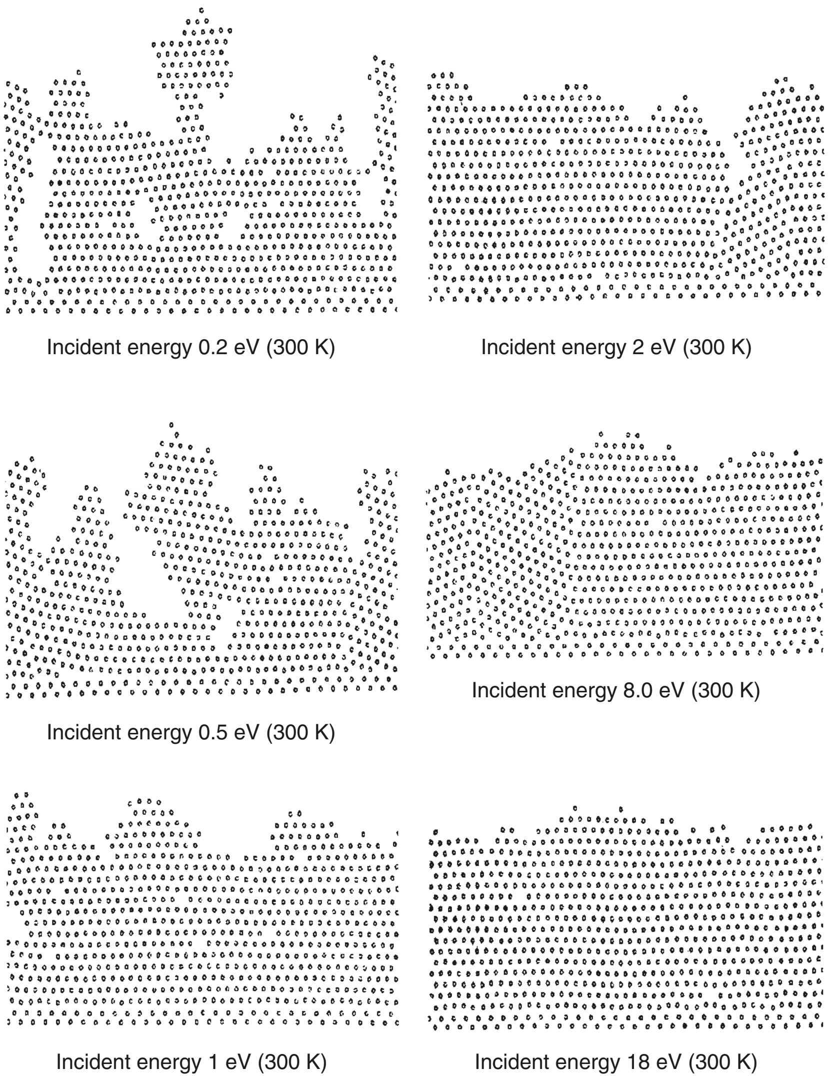

Figure 2.14. Two-dimensional MD simulation of deposition onto (100) surface showing effect of incident particle energy.[42]

Other possible applications involve: a) porous silicon films that have been deposited to produce α-Si, etched, and then recrystallized at a low temperature to produce films that can emit light; b) porous films, that provide a low Young's modulus in the film plane as a consequence of the easy bending of thin columns, to act as substrates

and allow the deposition thereon of stress-free films; porous films which, through control of the effective minimum diameter of the interconnected pores via etching, can act as tunable molecular sieves. Hence, an attempt to understand and thereby control the mode of formation of the intercolumnar void network and related column morphology may have practical consequences.

2. Other defects introduced during deposition at low substrate temperature.

2.1. Point defects.

2.1.1. Vacancies and interstitials.

In addition to voids, vacancies in excess of the equilibrium concentration are incorporated in films produced by most deposition processes at substrate temperatures lower than another transition temperature, which will be called T_V. The latter temperature is defined by the condition that the excess vacancies in the penultimate monolayer reach the surface layer by diffusion just as the latter is covered by the next monolayer. Thus, to determine T_V we make use of the Nernst–Einstein relation given in Appendix 2 of Chapter I, where we set $T = T_V$ and solve for the deposition rate R as a function of T_V/T_M. The results are given in Table 2.2, and these are based on the arbitrary assumption that the activation energy for vacancy jump from the penultimate surface layer to the surface equals one-fourth that for self diffusion. This approximation is rough and values can deviate by 20% from the assumed value. The corresponding uncertainty in the R values is a factor of about 100. Vacancies are believed to have much higher mobility in semiconductors than in metals of the same melting point and thus are less likely to be incorporated during deposition in the former than in the latter class of materials.

Table 2.2. Corresponding values of deposition rate and critical temperature ratio

T_V/T_M	0.1	0.125	0.15
Deposition rate, R (nm/s)	0.0014	5.4	1312

For substrate temperatures less than T_V, vacancies in supersaturated concentrations are incorporated into the lattices of crystalline films grown by any of the deposition processes. It has been reported[43] that the vacancy concentration introduced by condensation of thermally induced vapors is 1 at%. Subsequent annealing above T_V will allow these vacancies to diffuse to sinks in the drive to reduce the free energy of the film. Such sinks may be voids, grain boundaries, free surface and edge dislocations. This process has been observed in gold films at room

temperature,[43] where voids were prominent vacancy sinks and the films were produced by evaporation and condensation.*

At substrate temperatures less than T_V ion bombarded films are likely to contain vacancy concentrations much higher than that produced by deposition alone. The concentration reached may be so high as to make the film structure barely stable or even liquid-like, especially for high incident particle energy and ion atom arrival ratio. It has been suggested in this and the previous chapter that this vacancy-induced instability may be responsible, in part, for the effect of ion bombardment in removing intercolumnar voids, and for the production of crystalline grains in an amorphous matrix, where in the absence of ion bombardment only an amorphous film is obtained. It may also be responsible for the recrystallization of already deposited grains in the course of deposition. This phenomenon is exhibited in the MD simulation of ion beam deposition graphically described in Figure 2.14. In a more recent MD simulation[58] using an embedded atom potential for the interaction between Ni atoms the result shown in Figure 2.15 was obtained which appears to contradict the above expectation based on Figure 2.14. However, the range of energy considered in these two simulations differ.** We shall comment further on this possible process in the next chapter. The writer is not aware of any systematic experimental studies relating to the vacancy concentrations induced by hyperthermal beams.

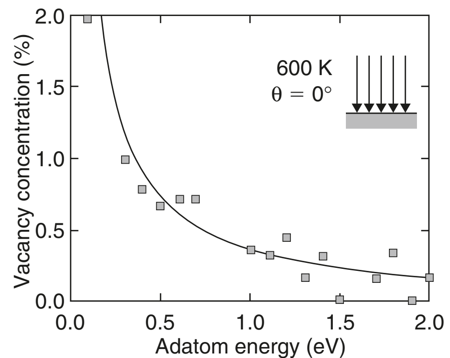

Figure 2.15. Vacancy concentration versus adatom energy achieved in an MD simulation. Reproduced with permission from X.W. Zhou et al., Acta Mater, 45, 1513(1997).

A positron annihilation study[59] of electroplated Cu, deposited and annealed, revealed the formation of vacancy clusters in the lattice upon annealing. This behavior is in agreement with the observations noted above by other means by Lloyd and Nakahara[43] for PVD Au films. Since grain boundary migration was observed to occur in the Cu study in the annealing process that revealed vacancy clustering and since vacancies would be expected to annihilate at grain boundaries

* A more recent investigation, using synchrotron X-ray reflectivity, determined the vacancy concentration deposited into films at low temperatures. A figure from that paper is reproduced in Appendix 3. Their results suggest that the estimates of T_V in Table 2.2 are too low by about 30–50°C.

** The results of these studies may not differ if one counts the vacancies in pores in Figure 2.14 (i.e. the density of the solid submitted to the 2 eV beam in Figure 2.14 is certainly greater than for the 0.2 eV thermal beam deposit).

a question arises as to the origin of this result. One possible answer is provided by a study of hydrogen incorporation into electroplated films.[60] From thermal desorption experiments Fukai et al. concluded that "a large number of vacancy-hydrogen clusters are incorporated in the process of electrodeposition". Effectively, hydrogen stabilizes the vacancy clusters despite the passage of grain boundaries through them.

It does not seem likely that interstitials are incorporated into films during deposition from thermally induced vapors. However, they are introduced into films subject to energetic particle bombardment during deposition, even at as low an energy as 10 eV for self-bombardment, as noted in Chapter I. There will be a T_I, corresponding to T_V below which these interstitials will be frozen-in. The T_I values for metals are much below the corresponding T_V values. Hence, it is unlikely that individual interstitials survive in the as-deposited films of metals. Rather, clusters of interstitials that give rise to dislocation loops are the most likely product in such as-deposited films. The T_I values are believed to exceed the T_V values in semiconductors and, hence, interstitials are more likely to survive in as-deposited semiconductors subject to particle bombardment during deposition. Depending upon the substrate temperature relative to T_I, these interstitials may or may not form clusters. This subject is considered in much more detail in Chapter VI, since such interstitials are responsible for intrinsic compressive stress in as-deposited films subject to particle bombardment during deposition.

2.1.2. Impurity atoms.

Among the other point defects that are often incorporated into films during their growth, in all the deposition methods, are gaseous impurity atoms from the environment adjacent to the growth interface. Prominent among this type are oxygen, water vapor, and carbon derived from organic vapors. This subject has been discussed in detail in Chapter I. We reiterate this matter at this point because these impurities can and often do affect film structure and properties.

Deposition processes that involve inert gas bombardment of the film during growth insert another point defect, inert gas atoms, into the films. The mobility of the inert gas atoms in the *zone 1* temperature range is high. However, they can be trapped at vacancies and they can be self-trapped by the spontaneous formation of Frenkel defects. A significant concentration (1–5%) of inert gas atoms in the film is produced in these deposition processes.

Gaseous impurities thus introduced into the film during its deposition can exert various effects on the defect structure. One is to impede grain boundary and dislocation migration. Another is to bind point defects, an effect that increases the temperature required for annealing out of the point defects. Except for excess vacancies, these point defects require annealing temperatures higher than $0.5\,T_M$ for their removal from the film or for their precipitation. The most significant effects of the incorporation of oxygen into the film during its growth in a deposition

process arise from the tendency of the oxygen to remain on the film surface and thereby to control surface sensitive processes, such as nucleation, and the ability to grow an epitaxial film.

2.1.3. Point defects in amorphous films.

Point defects are also produced in amorphous films during their deposition. Among such defects in covalently bonded solids are dangling bonds, strained bonds, bonds of different types (i.e. sp^2 instead of sp^3), atoms that contain other than 4 bonds, bond angles that depart from the tetrahedral bond angle of 109.47°, interstitial atoms, voids and impurities. The role played by inert ion bombardment during deposition of covalently bonded amorphous films is relatively unknown, although it is known that the defect content is greatly influenced by the method of deposition. Most studies have been concentrated on the use of hydrogen in plasmas to effect saturation of dangling bonds during deposition. Very few studies have been carried out of the effect of deposition method, in the absence of hydrogen, on the point defect content of the resulting amorphous films. Indirect evidence from studies of amorphous diamond-like films suggests that concurrent ion bombardment during deposition can have opposing effects on the point defect content. By breaking covalent bonds, an energetic inert gas atom impact increases the point defect content. However, if sufficient bonds are broken so as to make the structure unstable and transform to a more stable structure, the total point defect concentration can be decreased. We will consider the deposition of amorphous films and their resulting structure in greater detail in Chapter V.

2.2. Line defects – dislocations.

The grain size of films deposited at low substrate temperatures is on the order of 10 nm, which corresponds to the density of dislocations in heavily cold-worked materials and to slightly more than the measured densities in gold films formed in the *zone 2* temperature range.[44] These films have nearly all their dislocations located in the grain boundaries. Most of the dislocations introduced into monocrystalline films appear at the stage when the voids formed between coalescing islands begin to sinter out. The dislocations produced initially are mostly the threading type, which run through the film from substrate interface to film surface. At higher substrate temperatures, in the *zone 3* temperature range, grain boundary migration occurs during deposition and the resulting dislocation density in the grains is on the order of that found in well-annealed bulk materials, i.e. about $10^6/cm^2$. Monocrystalline films contain both misfit dislocations adjacent to the interface with the substrate and threading dislocations. We will discuss these dislocations in detail in Chapter IV when we consider epitaxial deposition. Dislocations are also produced in energetic deposition processes that induce atom displacements, as

illustrated in Figure 2.14 (see left-hand side of the figure corresponding to 8 eV). The absence of dislocations in the figure corresponding to 18 eV in Figure 2.14 suggests that dislocation production is not a necessary consequence of displacement processes during deposition, but that it may occur sometimes. Indeed, a study of the dislocation content of TiN films produced by magnetron sputtering under negative bias conditions showed that there were two opposing tendencies controlling the dislocation density.[48] The dislocation density was found to first decrease with increasing bias voltage and then to increase with further increase in this voltage. At a substrate temperature of 550°C the dislocation density at zero bias was $5 \cdot 10^{12}/\text{cm}^2$. The initial decrease in dislocation density was believed to be due to either the enhancement of adatom mobilities that acted to prevent the formation of vacancies or to the annealing out of vacancies so as to maintain the vacancy concentration below that necessary to nucleate dislocation loops. At bias voltages higher than that corresponding to the minimum dislocation density, it is believed that dislocation loops are formed by the annihilation of the vacancies in supersaturation. Other explanations are also possible for the same observations.

2.3. Grain boundaries and stacking faults.

Grain boundaries are significant defects in films deposited at low substrate temperatures in that they have significant effects on various properties. As mentioned in the previous section, the as-deposited grain size is on the order of 10 nm. Thus, an appreciable fraction of the atoms in these films is at grain boundaries. The grain size increases with increasing substrate temperature or with post deposition annealing at elevated temperature. Also, there is an equivalent population of stacking faults in the grains of these films. The latter arise because all the potential wells on many crystal surfaces do not belong to the same stacking sequence. For example, on the (111) face of a face-centered-cubic (fcc) crystal, there are two sets of potential wells for the adatoms to occupy. One set continues the ABCABC … stacking of (111) planes in this crystal structure. The other set, if occupied, develops a stacking fault in this sequence. Unless deposition proceeds by the spreading out of only one cluster, based on only one of these two sets of potential wells, to occupy fully the entire surface of the substrate grain, then stacking faults will be developed during growth. Thus, there is a greater propensity for stacking faults to exist in films formed by deposition at low substrate temperatures than in bulk materials. Not only are there stacking fault interfaces as planar defects within grains, but there are twin boundaries and anti-phase boundaries (in compounds) as well. The stacking faults and twin boundaries tend to lie along the film plane.

These planar defects can be introduced not only as intrinsic defects during growth or deposition, but can also be nucleated by impurities or inclusions extrinsically.

2.4. Three-dimensional defects.

Isolated voids represent the most common volume defect present in thin films.[43] They are produced either as a consequence of the incomplete coalescence of islands at a temperature near to the transition temperature T_1, or as the consequence of condensation of the excess vacancies incorporated during deposition of the films. Voids produced during bias sputtering, or ion beam assisted depositions are likely to contain inert gas atoms. On post deposition annealing, vacant voids in fcc metals should disappear at temperatures greater than about $0.33T_M$ for voids that intersect grain boundaries, and about $0.65T_M$ for voids that do not intersect grain boundaries. The temperature at which voids containing inert gas atoms disappear depends on the binding energy of the inert gas atoms to the void. Usually this temperature increases in the sequence from helium to krypton.

As indicated above, one of the ways of eliminating undesired defects is to anneal subsequent to deposition. However, the trend in integrated circuit manufacturing is towards miniaturization of all components. The decrease in scale also requires a decrease in the maximum temperature experienced by the integrated circuit. Hence, there is a need for deposition and processing methods that will not require subsequent annealing to remove harmful defects. This need represents a challenge to creative materials scientists.

Voids are not the only three-dimensional type defect. In brittle films cracks may be produced by tensile stress developed either on deposition or during thermal cycling. Control of stress in thin films is thus an important objective in thin film deposition. Thin film stress can also lead to spalling of the thin film away from the substrate. This subject will be considered in detail in a later chapter. Also, three-dimensional arrays of twins and stacking faults are nucleated extrinsically in impure materials during deposition, usually at inclusions or precipitates.

3. Summary of the relations between deposition methods and defect structures.

Summarizing, *intercolumnar "void" networks are produced when the deposition conditions maintain incident particle energies less than that required to displace atoms in the film from their binding sites and when the substrate temperature is too low to allow for adatom diffusion. The columns form when the probability of attachment of an adatom on the surface of a cluster exceeds that on the surface of the substrate. The latter probability is diminished by the effect of "atomic" shadowing of the substrate by the cluster. The columns make an angle β with the substrate normal that obeys the tangent rule, $\tan\alpha = 2\tan\beta$, where α is the angle the incident flux makes with the substrate normal. Ballistic aggregation*

develops a tree from a single cluster on a substrate. The mode of evolution of a column from a tree is unknown. Evidence exists for five different scales of intercolumnar "void" networks that form successively and increase monotonically in size as the film thickness increases. The origin of these different scales, other than the original and smallest one, is unknown. There is a critical temperature above which adatom diffusivity is sufficient during deposition to provide atoms to fill-in the voids and thereby to produce void-free films. Intercolumnar "void" networks can be developed in amorphous, as well as, crystalline films.

Columns and "void" networks do not form when the growth surface is subject to particle bombardment of sufficient energy and flux, as may be achieved in low pressure bias sputtering and in ion beam assisted deposition.

When the substrate temperature is less than a critical temperature, T_V or T_I, vacancies and interstitials, respectively, that are generated during deposition cannot annihilate at the growth surface during deposition. Vacancies are generated in every deposition process at these low substrate temperatures. The remanent vacancy concentration after such deposition is on the order of 1 atom% for evaporation and condensation. The remanent concentration after other deposition modes is not known, but may be higher for modes that produce displacement spikes. Sufficiently high vacancy concentrations formed by displacement spikes during deposition may destabilize the deposited structure and lead to transformation to more stable structures. Interstitials are also introduced as a consequence of energetic particle bombardment during deposition and their diffusion to various sinks leads to significant effects.

Bombardment during deposition by inert gas (or impurity) atoms leads to the incorporation of an appreciable inert gas atom (or impurity) concentration in films. Dislocations, stacking faults, twin boundaries and grain boundaries are among the other imperfections that may be introduced during deposition. An additional spectrum of defects may be introduced into amorphous films during deposition.

References

1. B.A. Movchan and A.V. Demchishin, Fiz. Met. Metalloved. 28, 653(1969).
2. N.G. Nakhodkin and A.I. Shaldervan, Thin Solid Films 10, 109(1972).
3. A.G. Dirks and H.J. Leamy, J. App. Phys. 49, 3430(1978).
4. N.G. Nakhodkin and A.I. Shaldervan, Sov. Phys.-Sol. State 13, 1627(1972).
5. A.I. Shaldervan and N.G. Nakhodkin, Sov. Phys.-Sol. State 11, 2773(1970).
6. R. Messier, A.P. Giri and R.A. Roy, J. Vac. Sci. Technol. A2, 500(1984).
7. J.M. Nieuwenhuizen and H.B. Haanstra, Philips Tech. Rev. 27, 87(1966).
8. K. Okamoto, T. Hashimoto, K. Hara, M. Kamiya and H. Fujiwara, Thin Solid Films 129, 299(1985).
9. J.C. Knights, J. Non-Cryst. Sol. 35/36, 159(1980).
10. A. Barna, P.B. Barna, Z. Bode, J.F. Pocza, I. Pazsgai and G. Radnoczi, in **Amorphous and Liquid Semiconductors**, eds. J. Stuke and W. Brenig, Taylor and Francis, London, 1974, p. 109.

11. D.J. Henderson, M.H. Brodsky and P. Chaudhari, Appl. Phys. Lett. 25, 64(1974); A.G. Dirks and H.J. Leamy, Thin Solid Films 47, 219(1977); S. Kim and D.J. Henderson, Thin Solid Films 47, 155(1977); H.J. Leamy, G.H. Gilmer and A.G. Dirks, in **Current Topics in Materials Science**, ed. E. Kaldis, North Holland, Amsterdam, 1980, Vol. 6; T.D. Andreadis, M. Rosen, M.I. Haftel and J.A. Sprague, MRS Symp. Proc. 202, 283(1991); K. Muller, Phys. Rev. B35, 7906(1987); P. Meakin, CRC Crit. Rev. Sol. State Mater. Sci. 13, 143(1987); P. Ramanlal and L.M. Sander, Phys. Rev. Lett. 54, 1828(1985).
12. K.-H. Muller, J. Vac. Sci. Technol. A4, 184(1986).
13. K.-H. Muller, J. App. Phys. 58, 2573(1985).
14. T. Hashimoto, K. Okamoto, K. Hara, M. Kamiya and H. Fujiwara, Thin Solid Films 91, 145(1982).
15. R.P.U. Karunasiri, R. Bruisma and J. Rudnick, Phys. Rev. Lett. 62, 788(1989).
16. B.F. Usher and J.L. Robins, Thin Solid Films 90, 15(1982).
17. T.-S. Liu and Y.-W. Chung, Surf. Sci. 207, 539(1988).
18. See Ref. [9].
19. J.A. Venables, G.D.T. Spiller and M. Hanbucken, Rep. Prog. Phys. 47, 399(1984).
20. W. Fuhs, H.-J. Hesse and K.H. Langer, in **Amorphous and Liquid Semiconductors**, eds. J. Stuke and W. Brenig, Taylor and Francis, 1974, p. 79.
21. A.J. Leadbetter, A.A.M. Rashid, R.M. Richardson, A.F. Wright and J.C. Knights, Sol. State Commun. 33, 973(1980).
22. T.D. Andreadis, M. Rosen, M.I. Haftel and J.A. Sprague, MRS Symp. Proc. 202, 283(1991).
23. T.M. Donovan, W.E. Spicer, J.M. Bennett and E.S. Ashley, Phys. Rev. B2, 397(1970).
24. E.S. Machlin, **An Introduction to Aspects of Thermodynamics and Kinetics Relevant to Materials Science**, Giro Press, Croton-on-Hudson, NY, 1991.
25. G.S. Bales, A.C. Redfield and A. Zangwill, Phys. Rev. Lett. 62, 776(1989).
26. M. Kardar, G. Parisi and Y.-C. Zhang, Phys. Rev. Lett. 56, 889(1986).
27. P. Meakin, CRC Crit. Rev. in Sol. State Mater. Sci. 13, 143(1987).
28. H.K. Pulker, **Coatings on Glass**, Elsevier, Amsterdam, 1984, pp. 331, 356.
29. K. Sheppard and R. Weil, MRS Symp. Proc. 47, 127(1985).
30. G. Ehrlich, Ann. Rev. Phys. Chem. 31, 603(1980).
31. R.H. Wade and J. Silcox. Appl. Phys. Lett. 8, 7(1966); Phys. Stat. Sol. 19, 63(1967).
32. C.-A. Chang, Surf. Sci. 245 (1991).
33. C.H. Lee, R.F.C. Farrow, B.D. Hermsmeier, R.F. Marks, W.R. Bennett, C.J. Lin, E.E. Marineri, P.D. Kirchner and C.J. Chien, J. Magnet. Magnet. Mat. 93, 592(1991).
34. H.T.G. Hentzell, B. Andersson and S.-E. Karlsson, Acta Metall. 31, 2103(1983).
35. C.M. Gilmore and J.A. Sprague, Phys. Rev. B44, 8950(1991).
36. E.T. Gawlinski and J.D. Gunton, Phys. Rev. B36, 4774(1987).
37. J. Lampinen, R.M. Nieminen and K. Kaski, Surf. Sci. 203, 201(1988).
38. D.W. Brenner and B.J. Garrison, Surf. Sci. 198, 151(1988).
39. B.W. Dodson, Phys. Rev. B36, 1068(1987).
40. A.M. Mazzone, Nucl. Instrum. Meth. B33, 776(1988).
41. B.J. Garrison, N. Winograd, D.M. Deaven, C.T. Reimann, D.Y. Lo, T.A. Tombrello, D.E. Harrison and M.H. Shapiro, Phys. Rev. B37, 7197(1988); D.Y. Lo, T.A. Tombrello, M.H. Shapiro, B.J. Garrison, N. Winograd and D.E. Harrison, J. Vac. Sci.

Tech. A6, 708(1988); M.M. Jakes and D.E. Harrison, Phys. Rev. Lett. 55, 1782(1985); C.-C. Chang, N. Winograd and B.J. Garrison, Surf. Sci. 202, 309(1988).
42. C.C. Fang, Department of Mechanical Engineering, Columbia University, unpublished research.
43. J.R. Lloyd and S. Nakahara. J. App. Phys. 48, 5092(1978).
44. D. Pashley, **Thin Films**, ASM, Metals Park, Ohio, 1964, p. 68.
45. P. Meakin, Phys. Rev. A41, 983(1990).
46. P. Ramanlal and L.M. Sander, Phys. Rev. Lett. 54, 1828(1985).
47. Ref. [12] studied the effect of thermal spikes alone on the structure of vapor deposited columns (displacement spikes were excluded). A count of the vacancy concentration in columns showed that the vacancy concentration was reduced by no more than one-half at the highest ion-atom arrival ratio of unity.
48. L. Hultman, U. Helmarsson, S. A. Barnett, J.-E. Sundgren and J.E. Greene, J. Appl. Phys. 61, 552(1986).
49. a) R. Fiedler and G. Schirmer, Thin Solid Films 167, 281(1988); b) R.N. Tait, T. Smy and M.J. Brett, Thin Solid Films 226, 196(1993).
50. M. Kitabatake, P. Fons and J.E. Greene, MRS Symp. Proc. 157, 259(1990).
51. P. Smilauer, M.R. Wilby and D.D. Vvedensky, Phys. Rev. B47, 4119(1993); B48, 4968(1993); J. Salik, J. Appl. Phys. 57, 3017(1985).
52. R.W. Smith and D.J. Srolovitz, J. Appl. Phys. 79, 1448(1996).
53. L. Dong, R.W. Smith and D.J. Srolovitz, J. Appl. Phys. 80, 5682(1996).
54. J. Emiliano Rubio et al., J. Appl. Phys. 94, 163(2003).
55. H. Huang and G.H. Gilmer, J. Computer-Aided Mater. Design 6, 117(1999).
56. J. Dalla Torre et al., MRS Symp. Proc. Spring Meeting 1999, Session L (preprint on Internet).
57. D.-X. Ye et al., Nanotechnology 15, 817(2004).
58. X.W. Zhou, R.A. Johnson and H.N.G. Wadley, Acta Mater. 45, 1513(1997).
59. A. Uedono, T. Suzuki and T. Nakamura, J. Appl. Phys. 95, 913(2004).
60. Y. Fukai et al., J. Alloy. Comp. 356–357, 270(2003).

Appendix 1

We will first calculate an approximate value for the cluster size in a two-dimensional lattice at which the probability of adding an adatom to the top of a cluster exceeds that of adding it to the substrate. Suppose there are N total lattice sites per unit area and M adatom clusters per unit area, each cluster containing m atoms. Suppose the shape of the cluster is that of an equilateral triangle. Then the probability of adding an adatom to a cluster to cause it to grow in area will equal that of forming a new cluster on top of a cluster when the number of atoms in the cluster is 36. The probability of adding an adatom onto the area outside of the clusters and their immediate perimeter of adatoms equals that of adding an atom on top of a cluster when N equals $2 \cdot 10^{15}/cm^2$. This yields an average grain diameter of about 3.5 nm, which is about the smallest grain size found in Figure 3.2 at homologous temperature below about 0.12. Thus, it is reasonable to deduce that for deposition onto non-epitaxial substrates at homologous temperature below 0.12 the minimum grain size will be about 3.5 nm the value corresponding to the condition that the probability of an adatom

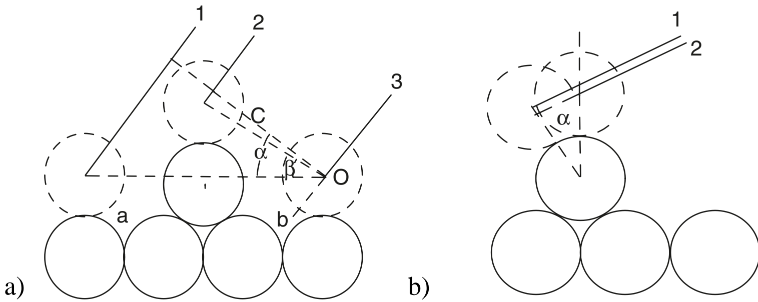

Figure 2.A1.

depositing on a cluster is equal to the probability of the adatom initiating a new cluster on the substrate.

Appendix 2

We desire to derive the angle β which the "leeward" side of the column makes as deposition proceeds. We will follow the lead of Dirks and Leamy[11] to assume that planar layers are added one-by-one on top of a column. They argue that "Because a given point in the layer can only be either occupied or unoccupied, the thickness of the continuum model layer can be thought of as being proportional to the probability that the layer is occupied at the point under consideration. The mean location of the position where the layer terminates is therefore that for which the continuum model thickness is one-half. If successive layers (of thickness t) are deposited on the step … and if each is terminated at the mean location a distance $(t/2)\tan\alpha$ from the end of the preceding layer, a columnar void results. The void orientation β is given by $\tan\beta = (t/2)(\tan\alpha)/t = (1/2)\tan\alpha$." It must be admitted that this derivation lacks clarity. Further we will show that it is not correct. We divide the column width into units $(t/2)\tan\alpha$ wide, where t is the thickness of the atomic layer and α is the angle that the incident atoms make with the film normal. Consider three such sequential units, A, B and C just adjacent to the "leeward" edge of the column, as shown in Figure 2.A2. The probability of the incoming atom defining the terminating edge of a continuous "atomic" layer having its "leeward" edge fall into unit A is equal to that for this edge to fall into unit B, if both units and unit C are unoccupied. If the incident atom's left edge falls in unit A, the average horizontal position of the left edge will be $(t/4)\tan\alpha$ to the "windward" side of the "leeward" column edge. On the other hand, if the incident atom's left edge falls within unit B, then the average horizontal displacement to the "windward" side of the "leeward" column edge will be $(3t/4)\tan\alpha$. It should be noted that if the incident atom's left edge falls anywhere in units A and B then succeeding incident atoms cannot deposit on top of the column to the "leeward" side of it. Further, once the first atom deposits with its left edge anywheres in units A and B further deposition occurs only on the "windward" side of it to complete the deposition of one atomic layer with vacant defects in it at various positions. Now the average horizontal displacement to the "windward" direction of the "leeward" edge of the average atomic layer relative to that of the one below equals

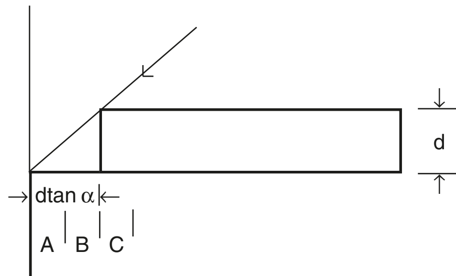

Figure 2.A2. Illustrating geometry basic to Dirks and Leamy's derivation of tangent law.

$$(1/2)[(t/4)\tan\alpha + (3t/4)\tan\alpha] = (t/2)\tan\alpha.$$

Thus, the average angle β made by the "leeward" edge with the vertical axis is:

$$\tan\beta = \frac{(t/2)\tan\alpha}{t} \quad \text{or } 2\tan\beta = \tan\alpha.$$

and it would appear that we have proven Dirks and Leamy's derivation of the tangent law. However, note that the above depends upon unit C being unoccupied prior to occupation of units A and B. However, the probability of C being occupied first is equal to that for either A or B. If it is occupied then there is still a possibility that unit A can be occupied subsequently while unit B cannot. In this case, the mean position of the terminating edge of the average atomic layer is not at $(t/2)\tan\alpha$ to the "windward" side of the terminating edge of the underlayer, but is less than this value, and, in particular, at $(9t/24)\tan\alpha$. Thus, Dirks and Leamy's assertion about the mean terminating position of an atomic layer is wrong.

Appendix 3

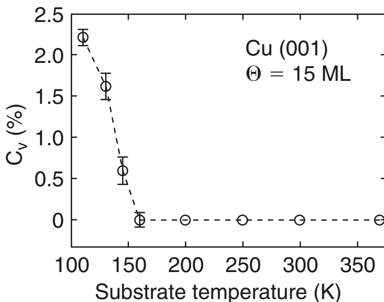

Figure 2.A3. Vacancy concentration in as-deposited Cu as measured by synchrotron X-ray reflectivity. Reproduced with permission from C.E. Botez et al., MRS Symp. Proc. 749, W8.1.1(2003).

This page intentionally left blank

CHAPTER III

Grain Structure

Three aspects of grain structure affect properties of thin films: crystallographic texture, grain morphology, and grain size. For example, control of thin film magnetic properties requires control of the film texture; resistance to electromigration damage is affected by both grain morphology and size.

It is important at the outset to recognize the need to distinguish between two types of film deposition in studying the grain structure of thin films. One class involves deposition in the absence of energetic particle bombardment and the other in its presence. It is further necessary to distinguish between films deposited on epitaxial substrates from those deposited on non-epitaxial substrates. Films deposited on the former substrates have a relation defining a crystallographic plane in the film that is parallel to a crystallographic plane in the substrate and defining parallel directions in these planes. A non-epitaxial substrate is one that does not produce such epitaxy.

Grain morphology has been studied to a greater extent than texture and mechanisms have been suggested to account for the observed morphology. We shall evaluate these mechanisms. The study of crystallographic texture in thin films has not led to a coherent proposal for the origin of the observed textures and an attempt will be made to fill this lacuna in our understanding.

The most extensive study of all these aspects of thin film grain structure has been carried out on films deposited in the absence of energetic particle bombardment. Thus, we will first consider this body of work and use it to determine the effect of other methods of deposition on grain structure.

1. Materials science background.

There are several concepts, which belong to the realms of materials science and thin films, whose understanding will help us to comprehend many aspects of grain structure in thin films.[1] First among these are the concepts associated with the modes of film growth during deposition. When there is sufficient adatom mobility to allow for configurations to approach their equilibrium state, then local interfacial and volume equilibria conditions govern these modes of growth. Thus, on substrates where the contact angle, θ, between deposit and substrate materials is zero (see Figure 3.1), the deposit will tend to form monatomic layers successively during deposition. This kind of deposition process is called the Frank–van der Merwe or layer-by-layer growth mode. If the relative interfacial energies, according to equation (3.1),

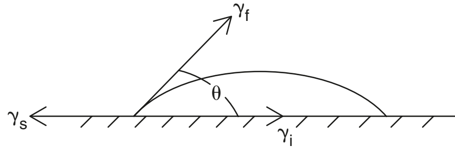

Figure 3.1. Illustrating parameters that determine local interfacial equilibrium at the junction where island of film material meets substrate. The γ values are the specific free energies of the substrate, film and film-substrate interfaces denoted by subscripts s, f, and i, respectively.

$$\gamma_s = \gamma_i + \gamma_f \cos\theta \tag{3.1}$$

where the parameters are defined in Figure 3.1 yield a finite positive contact angle, θ, then deposition follows what is called the Volmer–Weber or island growth mode. If the contact angle is zero and the deposit is elastically stressed from its bulk equilibrium lattice parameters, then deposition follows the layer-by-layer mode up to some critical thickness, and the island mode above this thickness. This deposition path is called the Stranski–Krastonov (S–K) growth mode.

The relative bonding of the deposit to the substrate and to itself controls the contact angle. Strong substrate–deposit bonding relative to the bonding between deposit atoms alone leads to the layer-by-layer or S–K modes and reversal of this relation yields the island mode. Thus, the state of the substrate surface is one significant parameter that should affect grain morphology, size and, texture. It is a sensitive function of the vacuum level. Hence, the chamber pressure is expected to be a parameter that may affect grain structure materially.

If the adatom diffusivity becomes sufficiently low, then the mode of growth is controlled by kinetic rather than thermodynamic considerations. Indeed, under slow adatom diffusion elevated clusters will form even when the contact angle is zero merely as a consequence of random probability statistics governing the point of attachment of an adatom to the substrate. Thus, another significant parameter for grain structure is the adatom diffusivity, which itself is a function of the substrate temperature and the bonding between the adatom and its substrate. Since this bonding changes with crystal orientation of the substrate surface, adatom diffusivity is also a function of this parameter.

Once grains are formed, the grain morphology may be affected by the mobility of the boundaries between these grains. Grain boundary mobility is a function of the substrate temperature, the presence of dissolved impurities or impurities adsorbed along these boundaries, and the type of grain boundary. Only a few parts per million of impurities can decrease the mobility of most grain boundaries by orders of magnitude. Also, grain boundary mobility can vary by orders of magnitude between different grain boundaries. Since the properties of only a few grain

boundaries have been characterized, it is not possible to predict the behavior of specific boundaries. The velocity of boundary migration is affected not only by the grain boundary mobility, but it also depends on the effective "driving force". This "driving force" can arise because of the difference in specific surface-free energy between adjacent grains or because of a difference in bulk-free energy between adjacent grains.*

Finally, because thin films grow by deposition of atoms, one at a time, which ultimately occupy potential wells on the surface of their substrate, it should be recognized that certain crystal faces on substrates, such as {111} surfaces on face centered cubic (fcc) metals, may contain alternate sites of potential wells that can lead to the formation of twins if adjacent islands are formed by occupation of both sets of sites.[2]

Let us consider all the concepts in greater detail in order to aid a better understanding of these factors that determine grain structure. Suppose the substrate is amorphous, or contains an adsorbed film of impurities and provides weak bonds to the adatoms. Such a substrate is likely to induce an island mode of growth and there is not likely to be any crystallographic relationship between the orientations of the island, if crystalline, and the substrate, i.e. the islands are not epitaxial with the substrate. *This type of substrate will be called non-epitaxial.*

The adatom diffusion distance on non-epitaxial substrates is usually much larger than on a substrate composed of the adatom species. We may distinguish two temperature regimes on non-epitaxial substrates. In the lowest-temperature regime, the island mobility is too small to allow for island migration and/or rotation. In the highest-temperature regime, the mobility is sufficiently high so that when island coalescence occurs island rotation and grain boundary migration can yield monocrystalline films. The temperature that distinguishes between these two regimes is called the epitaxial temperature for the non-epitaxial substrate–film system. A corollary concept is that above this epitaxial temperature any activation energy barriers that tend to impede the approach of the system to its lowest free energy state are easily surmounted or have disappeared.

The use of the term epitaxial in this context may be misleading because, in fact, the monocrystalline film produced may not have a crystallographic relationship to the substrate. Its use really signifies the formation of a monocrystalline film. The resulting film may or may not have a crystallographic relationship with respect to the substrate and this relationship, if it occurs, usually does not result from any influence of the surface atoms of the substrate on the orientation of the film. Rather, the relationship is induced by indirect effects of the substrate, such as the effect of cleavage steps to attract islands and orient linear sections of the latter parallel to the cleavage steps.[3]

* A grain boundary moves because atoms at the grain boundary jump from positions of higher free energy to positions of lower free energy. There is a gradient in free energy across the grain boundary corresponding to this free energy difference. This gradient varies in magnitude and direction along the grain boundary, but has the same sense, everywhere, in the direction normal to the grain boundary.

Let us consider the lowest temperature regime corresponding to the condition where the self-adatom diffusion distance is less than an interatomic spacing and deposition is onto a non-epitaxial substrate. Usually the surface of the latter will not be atomically smooth so that the orientations of the individual vapor-deposited crystalline islands will obey a random distribution. If the non-epitaxial substrate surface is atomically smooth, then there will be a tendency for these islands to develop orientations corresponding to a fiber texture. An atomically smooth surface is likely to exist only on the cleavage surface of a single crystal between cleavage steps, in the absence of surface adsorbed molecules. Thus, except for the latter type of substrate, vapor deposition onto non-epitaxial substrates at very low temperatures should result in thin films having random grain orientation in the layer closest to the substrate.

We may estimate the critical temperatures below which both adatom diffusion and grain boundary migration is negligible in fcc metals. The former critical temperature will be higher than the latter because during deposition the time period during which adatom diffusion can occur is that between the deposition of successive monolayers of atoms, whereas that for the latter is the period between the start of deposition and observation of the grain size in the completed film (providing that the temperature is invariant during this period). We may estimate the critical homologous temperatures for fcc metals using the relation

$$X^2 = 4D\tau \tag{3.2}$$

where $X \approx 0.1$ nm, $D = 10^{-7} \cdot e^{-6.5T^*/T}$ m^2/s, where T* is the melting point temperature in (°K) and T the actual temperature while τ the time period will be taken to equal about 3600 s for grain boundary migration and to $n_o\Omega/R$ for adatom diffusion, where n_o is the number of atoms per unit area ($\approx$10/nm^2), Ω is the atomic volume (0.02 nm^3) and R is the deposition rate (nm/s). We obtain for the case of adatom diffusion that $T/T^* \approx 0.21$ (for R = 1 nm/s) and for that of grain boundary migration $T/T^* \approx 0.17$. We shall use this information in our analysis that follows.

2. Grain morphology, texture, and size in as-deposited films.

2.1. Vapor deposition onto epitaxial substrates in the absence of incident energetic* particles.

Recently, experiments involving vapor deposition onto epitaxial substrates at chamber pressures, deposition rates, and substrate temperatures normally

* The term “energetic” is used to define energies higher than the thermal energy of evaporated particles.

used to produce films on non-epitaxial substrates have been performed which act *to limit the spectrum of possible mechanisms affecting the grain size, morphology and texture of polycrystalline films deposited on non-epitaxial substrates*. Let us now consider these experiments and their consequences.

In these experiments due to Chang,[4] the chamber pressure was about $2–3 \cdot 10^{-7}$ Torr, the deposition rate was 1 nm/s, and the substrate temperature was room temperature. The substrate was a Si(100) wafer, which had been surface treated to leave the surface Si atoms terminated by a hydrogen bond (thereby protecting the surface from oxidation) and which provided an unreconstructed surface. In all the experiments, a thin layer of copper was deposited by e-beam evaporation onto the substrate to produce a Cu(100) surface. The latter was used as a substrate, without breaking the vacuum, for deposition by e-beam evaporation of all the other metal films subsequently deposited. The latter included the following list: Ni, Co, Rh, Ir, Pd, Au, Ag, Pt, Al, Fe, Cr, V, Mo, and W. In all cases, deposition was epitaxial with the substrate, and growth in thickness was self-epitaxial, i.e. by granular epitaxy.

These results prove, at substrate temperatures as low as $0.08T_M$ (W), *that nucleation of new grains on the surface of growing grains and the claimed production of an equiaxed grain structure*[5] *does not occur, at least at the chamber pressure of* $2–3 \cdot 10^{-7}$ *Torr and a deposition rate of 1 nm/s!* Hence, at low substrate temperatures at which adatom diffusion is nil, at chamber pressures that impinge impurities onto the growing surface, and at fairly rapid deposition rates, condensation of metal vapor extends the orientations of the grains formed on the substrate in the thickness direction of the film, i.e. deposition produces columnar grains via self-epitaxy. This process of self-epitaxy has also been called granular epitaxy. It is believed that this important conclusion is also applicable to the deposition of other materials that result in crystalline films.

Under conditions of a clean substrate and environment, and strong bonding between film and substrate atoms, but where perfect epitaxy is not possible (i.e. there is a large lattice mismatch) two results have been obtained. At very low temperature, the film formed is a randomly oriented polycrystalline film.[6] (In this case the film thickness, 15 nm, equals the grain size.) At intermediate temperatures textures are obtained that are same in the layer closest to the substrate as in the thicker layers.[7] These results may be interpreted to mean that at the low temperatures at which there is no mobility of either adatoms, grain boundaries, or point defects, the orientation of the clusters is determined by the statistics of condensation onto a mismatched, but clean, substrate (i.e. the clusters are randomly oriented). At temperatures where adatom or grain boundary mobility exists, the local interfacial equilibrium between cluster and substrate can be approached, and this equilibrium state determines the crystal orientation of the cluster relative to the substrate and, via granular epitaxy, the film texture and morphology. When the difference in the interface energy between different cluster orientations overwhelms the corresponding difference in the surface energy, then the lowest cluster/substrate interface energy controls the cluster

orientation and film texture. The present circumstances correspond to this condition. These circumstances do not exist when film to substrate bonding is weak.

2.2. Vapor deposition onto non-epitaxial substrates in the absence of incident energetic particles.

For all the regimes considered in this section the interface between the film and the substrate exerts a negligible effect on the driving force for either grain boundary migration or island rotation contrary to the conclusion applicable to the previous section.

2.2.1. No grain boundary mobility, no adatom mobility (*zone 1a*).*

The constraints of no grain boundary mobility and no adatom mobility require the homologous temperature to be low (for fcc metals $\leqslant 0.15$ and for body centered cubic (bcc) metals $\leqslant 0.1$).

The conditions defining this section normally lead to the production of amorphous films for covalently bonded materials[8] and for many alloys that consist of components having markedly different atomic diameters.[9] However, for relatively pure metals and many polar compounds, crystalline films are formed under the same conditions.

When the diffusion distance is on the order of an interatomic distance there can be hardly any progress of the system towards the state of equilibrium (interface or bulk). However, adatoms on the substrate, when sufficiently close to each other, are drawn together to occupy minima in the potential wells they experience and to this extent do make progress towards the state of lowest free energy. For relatively pure metals, in so doing, they form two-dimensional crystalline arrays as a consequence of the non-directional bonding between such atoms. These two-dimensional arrays or clusters become the substrates for the columns produced, via the process of granular epitaxy, by subsequent deposition. The lateral dimension of these two-dimensional crystalline clusters, under the condition of zero mobility of adatoms on the substrate, should be determined by the relation which equates the area on the substrate surface within which adatoms will be drawn to clusters to the area outside these zones not occupied by adatoms or clusters of same. Roughly, this relation predicts a lateral grain (column) diameter equal to about 3 atomic diameters or about 1 nm, if it is assumed that the interatomic force between adatoms drops precipitously beyond a spacing between their centers exceeding 2 atomic diameters, which is consistent with most interatomic potentials developed for metals. However, even at room temperature, and when adatom mobility on the *surface of the deposit* is zero, the mobility of adatoms on *non-epitaxial substrates* is not likely to be zero. (The weaker

* The adatom mobility refers to the mobility on the surface of the deposit material.

the bonding of the adatom to the substrate the lower is the activation energy for an adatom jump on the substrate and the higher is its mobility.) It follows that the lateral dimension of two-dimensional crystalline clusters is then determined by the processes considered in the atomistic theory of nucleation[10] at the stage close to coalescence.

Thus, for relatively pure metals, for the conditions applicable to this subsection, the deposited film will consist of crystalline columns separated by voids. These columns need not be straight columns, but can take the form of tree-like dendrites, as illustrated in Figure 2.6, which is a computer simulation produced by a particular ballistic deposition model.[11] Indeed, the grains produced by deposition under the stated conditions cannot be equiaxed since renucleation cannot occur (see Section 2.1 of this chapter) and since granular epitaxy is the mode of growth of these grains. The lateral dimension of these columns will vary from about 1 nm to about 20 nm and may increase with the film thickness. There is one caveat to the above conclusion, which is that the intrinsic tensile stress developed in the films may trigger barely unstable atom arrangements to rearrange to more stable ones and in this manner, develop what may appear to be equiaxed grains. However, equiaxed grains have not been observed for conditions applicable to this subsection, whereas columnar grains have been detected.

So much for the morphology and grain size. Now we address the problem of what we should expect for the film texture. Normally, the grains formed on non-epitaxial substrates under the constraints defining this subsection would be expected to have a random orientation in the layer adjacent to the substrate. Although this author has not been able to discover any investigation that sheds light on this subject for the conditions under consideration it is possible to infer from the results of deposition under slightly less restrictive conditions that this expectation is very likely to be validated by experiment, once it is performed.

Some measurements of texture in films formed under the conditions applicable to this subsection reveal a weak texture and this observation is not inconsistent with the possibility that the thin layer adjacent to the substrate has a random texture. In particular, 88.5 nm thick gold films deposited onto glass at 80°K (homologous temperature of 0.06) exhibit a weak <111> texture.[12a] Also, copper films similarly deposited exhibit a weak <111> texture.[12b] However, 15 nm thick films of Mo and W deposited at a rate of 0.1–0.3 nm/min in an UHV system reveal a random texture with a 20 nm lateral grain size at homologous temperatures <0.13 and 0.15, respectively.[6] If adatoms and grain boundaries do not move at these low homologous temperatures, and if texture develops as the films thicken, as appears to be the case, then these observations suggest that either there may be a greater tendency for certain planes to develop shadowing overhangs than other crystallographic planes or at the grain

* This concept, which is championed by D.A. Smith and A. Ibrahim in MRS Symp. Proc. 317, 401(1994), is inconsistent with the lack of such an effect in Chang's work.[4]

boundary abutment between two grains at the film surface adatoms will join the grain having the lower surface energy plane exposed thereby leading to the transverse growth of this grain at the expense of the neighboring grain, or both.

It may be significant that the texture first found to develop under these conditions of zero mobility corresponds to the crystallographic plane that has the lowest value of the surface energy. We shall comment further on this possible correlation in a subsequent subsection.

2.2.2. Some grain boundary mobility, some adatom mobility (*zone 1b*).

The homologous temperature being considered in this subsection is somewhat higher than the upper limit given in the previous subsection. We estimate the homologous temperature limits for this subsection are 0.15 and 0.25 for a deposition rate in the order of 1 nm/s, at least for fcc metals. Other classes of materials have their corresponding homologous temperature limits for *zone 1b*. For these conditions, what then may be expected for the morphology, size, and texture of the grains produced by thermal energy vapor deposition?

Insofar as the adatom diffusion distance is still smaller than the lateral dimension of the columns considered in the previous subsection, it is reasonable to expect that the morphology found will be similar to that of the previous subsection, i.e. columns separated by voids. The lateral grain size may be expected to be somewhat larger than for the previous subsection in that this dimension is probably determined by cluster formation dynamics on non-epitaxial substrates, and in the latter the cluster size increases with increasing substrate temperature. Let us examine selected experimental results to obtain a consistent model for the texture(s) that may be expected to form in this regime of temperature.

Wong et al.[13] found that thin films (50 nm thick) of Au deposited onto amorphous SiO_2 substrates at room temperature (homologous temperature equal to 0.22) underwent secondary recrystallization with time held at room temperature to produce <111> oriented grains that were several μm in lateral diameter surrounded by grains having the as-deposited grain size of about 20–50 nm. (At the end of deposition, the secondary grain size was about 800 nm.) *In the layer closest to the substrate the film had a random texture prior to secondary recrystallization.** Further, no grain growth occurred in the grains that have the random orientation and that are not consumed by the secondary grains, although their grain size, as observed on the surface, was proportional to the film thickness.

The process of secondary recrystallization requires that the boundaries between the randomly oriented grains be immobile while those between the growing grains and their neighbors be mobile. Apparently, intercolumnar voids are the

* This observation negates the possibility that in this case texture is controlled by the orientation of the nuclei. See Appendix 2.

agents preventing grain boundaries from moving. For most of the grain boundaries the driving force due to their curvature tending to make them move equals the pinning force due to the voids. The boundaries surrounding the <111> oriented grains move because the extra driving force due to the difference in surface energy between the <111> oriented grains and their neighbors allows these boundaries to overcome the resistance to their motion due to the voids. Since the as-deposited grains at the film surface have a diameter equal to about the film thickness, then the rate at which the <111> oriented grains grow is given by

$$\frac{dr}{dt} = M \frac{2\Delta\sigma}{h}$$

where r is the diameter of the <111> oriented grains, $\Delta\sigma$ is the average difference in surface energy between the <111> oriented grains and their neighboring grains, and M is the average grain boundary mobility. (The driving force due to the curvature is just balanced by the resisting force due to the voids.) In the above relation we assume implicitly that the difference in grain/substrate interface energy equals that for the grain/vacuo interface energy.

With this knowledge we can now understand an observation due to Grovenor et al.[5] that is shown in Figure 3.2. According to these observations a bimodal grain size appears in vapor-deposited metal films equal to or thicker than 100 nm at homologous substrate temperatures higher than 0.15 without growth of the smaller grains until a homologous temperature of about 0.25 is reached.* The large grains develop a grain size of about 250 nm at the latter temperature. These are just the results expected if secondary recrystallization had occurred for all these metals in the homologous temperature regime between 0.15 and 0.25, i.e. a bimodal

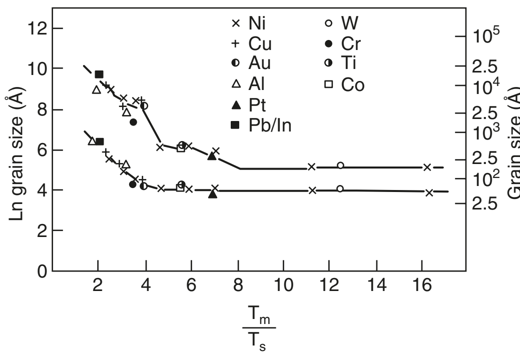

Figure 3.2. A plot of grain size variation with homologous substrate temperature for thin films of 10 different metals. Reproduced with permission from C.R.M. Grovenor, H.T.G. Hentzell and D.A. Smith, Acta Met. 32, 773(1984).

* The temperature independence of grain size below a homologous temperature of about 0.12 deserves comment, which is provided in Appendix 3.

grain size distribution with no growth of the smallest grains and explosive growth for some of the larger grains.

The maximum grain size found in the work of Grovenor et al. is much smaller than that reported by Wong et al. for the same homologous temperature. In fact, it is surprising that there is not a larger scatter in the size of the largest grains for ten different metals in Figure 3.2. A possible explanation of these results is that the large grain size is impurity limited. All the data of Grovenor et al. were obtained in one apparatus while that of Wong et al. in another. In support of this suggestion, Grovenor et al. found that the average grain size in films deposited at a homologous temperature of 0.33 was smaller in films deposited under “relatively contaminated conditions” as compared to those deposited in “clean conditions”.

The significance of the observation that the smallest grains did not grow until above the homologous temperature of 0.25 is likely to be that above this temperature the intercolumnar void network disappears, as noted in Chapter 2; i.e. intercolumnar voids are no longer present to pin grain boundary motion. Thus, above the homologous temperature of 0.25, grain growth is normal – secondary recrystallization cannot occur.

Despite the seeming simplicity of the principle governing the initial fiber texture applicable to the constraints of this subsection – that secondary recrystallization, driven by a difference in the energies of surface planes, develops the fiber texture corresponding to a film surface having the lowest free energy, it has been found that other textures develop with increasing film thickness.

By using a technique sensitive to the texture at the film surface, Wilman and his collaborators[14] were able to detect texture changes with increasing film thickness in copper, silver and gold films. For copper and gold the homologous temperature was 0.22, whereas for silver it was 0.24. Other investigators generally have used X-ray diffraction to evaluate the texture. The latter technique measures the average texture and would not reveal changes in texture until film thicknesses larger than those revealed by the electron diffraction measurements.

The textures found by Kakati and Wilman[14] for Au films are indicated in Figure 3.3. As shown, the orientation of grains in the layer closest to the non-epitaxial substrate is invariably random. Whereas, the texture developed in the next layer corresponds to having the crystallographic plane with the lowest surface energy parallel to the substrate surface. The same results have been found for copper and silver films. These are just the results expected if the mode of texture development is via surface energy difference driven secondary recrystallization.

However, Figure 3.3 shows that additional textures develop in thicker films. The explanation given by Wilman and his collaborators for these textures is as follows. The tendency to approach local surface equilibrium will promote, with film thickening, the appearance of low surface energy facets in the <111> oriented grains. (One may question why facets should appear in an atomically smooth surface. An answer may be that the substrates used by these investigators – polished

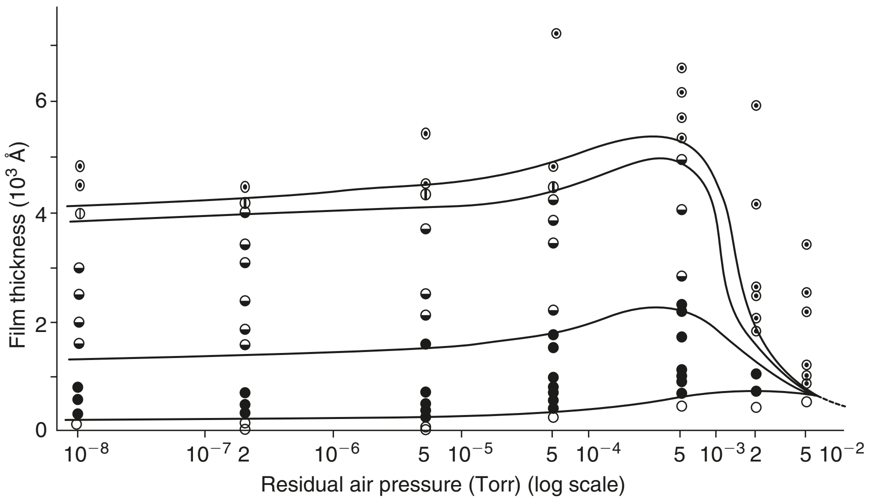

Figure 3.3. Electron diffraction observations of crystal orientation in the surface region of gold films condensed at about 30 Å/s on polished stainless steel at room temperature: open circles, random orientation; filled circles, {111} orientation; half-filled circles, {111} + {111} twinning; vertical line in circles, {111} + {211}; dotted circles, {211}. Reproduced with permission from K.K. Kakati and H. Wilman, J. Phys. D6, (1973).

stainless steel and glass slides – are not atomically smooth.) If there are two different sets of potential wells for adatoms on these low surface energy planes, then there is a possibility to develop primary and secondary twins during deposition. This development does not require grain boundary migration and can occur merely as a consequence of the deposition process itself.

With continued deposition to increase the thickness of such films evidence was found for the presence of both primary and secondary twins. At film thicknesses in the field denoted by {111} + {111} twinning, they observed that there were grains that had the {115} plane parallel to the substrate plane. They interpreted this result to be a consequence of primary twinning on a surface facet of a (111) oriented grain. The meaning of the term "primary twinning" is defined by Figure 3.4b, which shows it to correspond to a rotation about the <111> axis of any {111} facet of the (111) oriented grain by 180°. As shown, primary twinning yields a {115} plane to be parallel to the substrate surface. Primary twinning occurs when during deposition onto different areas of a single {111} surface plane two different sets of potential wells (denoted by B and C) are occupied so that to one side of a <110> axis in the {111} plane the {111} plane stackings are in the order ABCABC … and on the other side of this axis the stacking is in the order ACBACB. … These stacking sequences can be produced by the deposition process alone.

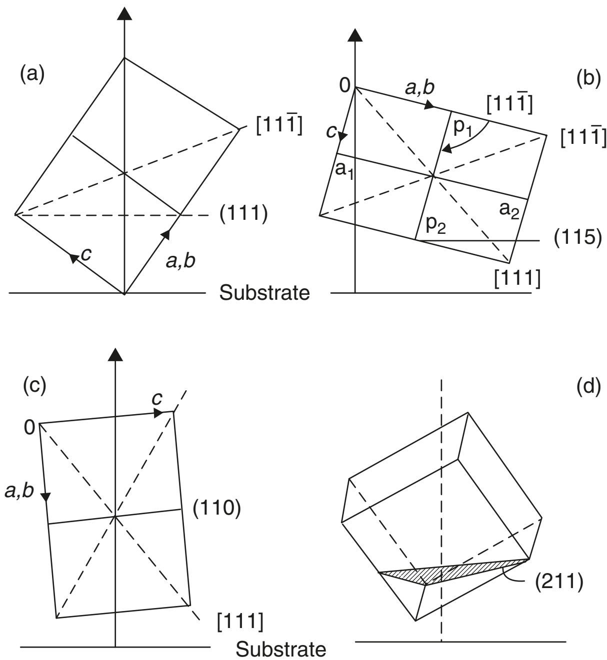

Figure 3.4. Side view of cubic unit cells of (a) a (111) oriented crystal; (b) [111] rotation twin of (a); (c) and (d) secondary twins of (b), near to {110} and {211} orientations. Reproduced with permission from P.K. Dutta and H. Wilman, J. Phys. D3, 839(1970).

Secondary twinning on a particular {111} facet of the primary twin can yield a {112} plane parallel to the substrate surface as illustrated in Figure 3.4(d) and, in fact, grains at the surface having such orientation were found by Kakati and Wilman in much thicker gold films, as shown in Figure 3.3.

The other possible orientation that can be produced via secondary twinning, {110} (illustrated in Figure 3.4(c)), was also found by them in silver films. Thus, there is a film thickness dependence of the texture that may be related to the incidence of primary and secondary twinning that may take place. The atmosphere had a much larger effect for Ag and Cu than for Au on the onset thickness of the apparent twinning responsible for the changes in texture. This result was believed to be due to the greater tendency for surface adsorption of gas molecules onto the former materials than onto gold. Evidently, the surface adsorbed species presumably enhance the tendency to produce multiple twinning during deposition. More direct evidence for twinning during deposition of these metals has been found by others.[30]

Thus, in the work of Wilman and his collaborators the surface planes are still the planes of lowest surface energy and the different textures they found result from

deposition-induced twinning on these planes. It should be mentioned that Wilman et al. believed that the presence of the observed {111} surface planes in their work was a consequence of a kinetic factor, according to which the close-packed planes, on which the adatom diffusivity is highest, extend laterally at a higher rate than any other crystallographic plane and thus win the species survival contest that occurs during deposition. This concept, however, cannot account for the results shown in Figure 3.2, whereas surface energy difference driven secondary recrystallization can.

One may speculate as to why the onset of multiple twinning depends on thickness. As noted above, the development of surface facets during an attempt to minimize the surface energy requires that a sufficient surface roughness exists at some point in the deposition process. One possible source of this surface roughness stems from the fact that, for the homologous temperature range we are considering, the surface diffusion distance is smaller than the distance between growth-induced singularities due to shadowing of the incoming flux of atoms. In this case, according to Tang et al.,[45] the surface consists of paraboloidal cusps between cusp singularities. The height of these cusps depends on many factors, but when it is controlled by statistical noise in the deposition current then it will increase with film thickness beyond some critical thickness. Indeed, their treatment of this problem provides a possible explanation of the fact that multiple twinning is not always observed, or at least reported, for the same metals considered by Wilman and his collaborators and at the same film thicknesses. An experimental evaluation of this possibility may be fruitful in view of its many ramifications.

A more direct effect of film thickness on texture has been found in other studies. Vook and Witt[12b] were the first to note that Cu films thicker than 6000 Å, deposited in a chamber having a background pressure of $2 \cdot 10^{-9}$ Torr onto a glass substrate held at 80 K at a deposition rate of 0.1 nm/s were able to change texture from <111> to <100> (and others) upon subsequent heating to room temperature or to develop a stronger <111> texture in films thinner than 6000 Å. These observations suggest that grain growth, in the thicker films and under the constraints of this subsection, may be driven by other than a difference in surface energies, since the <100> surface has a higher energy than the <111> surface of copper. In fact, Vook and Witt found an inverse correlation between the strength of texture components and the elastic strain energy* stored in the grains having these texture components. From this observation it is a small step to infer that the driving force for the change in texture was a difference in elastic energy stored in the grains having these different textures.

Stress can be developed in the film plane during deposition due to densification of the film in the present homologous temperature range. Indeed, it is well

* The difference in elastic strain energy between differently oriented grains is a consequence of the orientation dependence of the elastic moduli, since the intrinsic stress is confined to the film plane and zero normal to the film plane.

known that evaporated films generally exhibit an intrinsic tensile stress after such deposition, which has been ascribed to the production of grain boundaries at the expense of free surfaces,[16] a process that tends to contract the film, and to the presence of very thin isolated voids and vacancies, which tend to collapse inwards due to attractive forces between opposing surfaces.[17] (This subject is treated in much greater detail in Chapter VI.) This tendency to contract is prevented by the constraint imposed by the substrate and a tensile stress thus develops in the film. The elastic modulus is crystal orientation dependent and hence, the elastic strain energy, for a given strain, will be correspondingly crystal orientation dependent.

Under the constraints of this subsection the first layer adjacent to the substrate should have a random texture and grain boundaries should be able to migrate during deposition until they are pinned by the intercolumnar voids. With increasing thickness the texture corresponding to the lowest surface energy should form by the process of grains having this orientation grow at the expense of grains that have different orientation. Above a critical film thickness, h*, when the decrease in elastic strain energy in the film exceeds the increase in the surface energy due to a change in texture, then the preferred texture will correspond to the orientation of the grains having the lowest strain energy.* This change is accomplished by the growth of grains having the low strain energy orientation at the expense of neighbors having higher strain energy orientations. The film thickness, h*, above which elastic strain energy will control the texture is given by

$$\Delta g = 2\Delta\sigma/h^* \qquad (3.3)$$

where Δg is the average difference in elastic strain energy stored in the grains of different orientation, $\Delta\sigma$ is the average difference in the specific energy of the exposed surfaces of these grains. The maximum homogeneous elastic stress stored in any grain is the yield strength. Using this value to estimate a value for Δg and known values for the surface energies it is possible to calculate a corresponding value for h*. This calculation is performed in detail in Appendix 1.

Gittis and Dobrev[18] have studied the transition between the <111> texture and the <100> texture in silver. Figure 3.5 is taken from their paper and shows that the transition from <111> to <100> at 300°K begins to occur at about a 2 μm film thickness and reaches a maximum at about a 5 μm film thickness. The value of h* deduced in Appendix 1 from the above equation for their conditions is about 3 μm, which is in agreement with the transition thickness measured by these authors. Implied in the above explanation for the <100> texture is that this texture should disappear above a temperature at which stress relaxation is rapid. Gittis and Dobrev[18] do find that the <111> texture replaces the <100> above about 673°K.

* J.A. Florel, R. Carel and C.V. Thompson, MRS Symp. Proc. 317, 419(1994). This work proposes the same interpretation for the {111}/{100} texture transition.

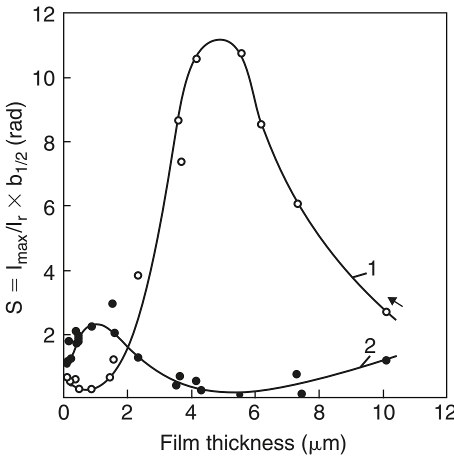

Figure 3.5. Thickness dependence of the texture in silver films deposited onto glass at 300°K and a deposition rate of 200 nm/s: curve 1, <100> orientation; curve 2, <111> orientation. Reproduced with permission from A. Gittis and D. Dobrev, Thin Solid Films 130, 335(1985).

Figure 3.5 indicates that the intensity of the <100> texture begins to decrease as the film thickness increases above 5 μm. Although the reason for this behavior is not known it may be speculated that this trend occurs because the difference in bulk strain energy between differently oriented grains begins to disappear. One possible reason for the latter trend is the onset of plastic yielding* with increasing thickness and grain size with the consequence that the excess energy per unit volume associated with the dislocations begins to exceed the stored elastic strain energy in the absence of these dislocations. (Observations of the intrinsic stress and dislocation density as a function of film thickness and deposition rate would be useful in the evaluation of some of the above proposed explanations and mechanisms. In particular, the results would bear upon not only the validity of the proposed explanation for the <100> texture and its dependences, but also upon the origin of the intrinsic stress.)

A similar result was found by Vook and Witt[12b] for copper as noted above, where their value for h* is about 6000 Å, which is also in fair agreement with that obtained from the above equation. (See Appendix 1 for details of these calculations.)

As just noted, the difference in intrinsic elastic stress and the difference in surface energy may not be the only factors controlling the texture. Another may be a difference in the energy associated with the different defect contents of adjoining grains. Indeed, if the latter is larger in magnitude than the other two differences then it may control the texture.

There are several observations which at first glance appear to be in disagreement with the models for texture described above. One of these observations is that when the Ag films were deposited at a rate of 5 nm/s at room temperature the texture was found to be independent of the film thickness up to a thickness of about 10 μm.[18] One possible answer is that at this deposition rate-homologous temperature

* Yield strength decreases with increase in grain size.

combination, the intrinsic stress level developed in the film is so small that the value of h* is much larger than the thickness of the thickest film deposited. There are at least two possible reasons for a lower intrinsic stress in Ag at a low deposition rate (R) than found at high R. The homologous temperature corresponding to room temperature for Ag is 0.24, which is close to both T_V and T_1. Either the vacancy concentration incorporated on deposition of Ag at room temperature and low R is much smaller than at high R or fewer intercrystalline voids are produced at low R than at high R, or both. (Again we are missing the experimental evidence to evaluate these suggestions.)

The other observation that appears to be in contradiction to our present explanation for the <100> texture is that the transition line between the zones of <111> and <100> textures in a map of deposition rate versus absolute temperature for films having an approximately invariant thickness appears to follow an Arrhenius relation with an activation energy of 0.21 eV for Ag.[46] However, if we refer to equation (3.3), we can obtain an explanation for this observation of Grantscharova.[46] Since $\Delta\sigma$ is roughly insensitive to temperature and by the experiment h* is maintained constant, then Δg and the internal stress also must be independent of temperature. Now if the magnitude of the intrinsic stress is proportional to the fraction of void area consisting of voids less than 3 vacancy layers thick (see Chapter VI), then it seems reasonable to assume that the intrinsic stress will be inversely proportional to the number of atoms transported to the intercrystalline void volume by surface diffusion, N*, for a given film thickness. Now N* should be proportional to the surface diffusivity and inversely proportional to the deposition rate. Hence, at constant N* we obtain that at the transition line, the deposition rate should be proportional to the surface diffusivity, which is qualitatively the relation found to hold experimentally by Grantscharova, with a value of the activation energy close to that for adatom diffusion. Thus, the observations which appear to disagree with our models for the origin of the various textures need not be in disagreement at all.

Summarizing the results of this section, *the evidence suggests that secondary recrystallization, driven by a difference in surface energy, yields a bimodal grain size distribution, with the large grains having the texture corresponding to the surface orientation of lowest free energy. Fluctuations which lead to surface roughness in the* zone 1b *temperature range may be responsible for the development of low-energy surface facets and consequent multiple twinning and associated textures. In thick films, the difference in stored elastic energy between neighboring grains can overcome the driving force due to the difference in surface energy and lead to a concomitant change in fiber texture. In all cases, columnar grains are formed due to granular epitaxy.*

2.2.3. Rapid grain boundary migration, rapid adatom diffusion.

In the regime of the present subsection, it is expected that the homologous substrate temperature varies between about 0.3 and about 0.5 and that the

background pressure in the vacuum chamber is less than about 10^{-7} Torr. These conditions assure that there are no intercrystalline voids to pin grain boundary migration, that the concentration of excess vacancies left in the lattice after deposition is negligible although their diffusion to and annihilation at grain boundaries can enhance the grain boundary mobility during deposition. Also, in the present section of the kinetics spectrum, grain boundary migration through clusters, and cluster rotation during cluster coalescence, can occur so as to increase the population of grains that have the lowest energy surface parallel to the substrate surface *in the first continuous layer formed adjacent to the substrate*.

Those grains having surfaces with the lowest energy parallel to the substrate surface will grow at the expense of their neighboring grains, that have higher energy surfaces exposed, by grain boundary migration, and will extend in the film thickness direction, in the form of columnar grains, by granular epitaxy. Thus, in this kinetic regime films will be produced that have columnar grains with a texture corresponding to a film surface of lowest energy. The intensity of this texture will be expected to be higher than obtained in the lower temperature regime. Also, the lateral width of the columns will correspond approximately to the spacing between the grains in the first continuous layer adjacent to the substrate that have this low surface energy orientation, i.e. further lateral grain growth will occur at a much slower rate because the tilt boundaries (the boundaries between grains having the same fiber texture) have low energy and the excess vacancies that would enhance their mobility exist only adjacent to the surface during deposition, i.e. the homologous temperature is too low to generate sufficient excess vacancies thermally.

Because differences in elastic strain energy or defect populations between grains are small in this regime of homologous temperature such differences should not contribute to the development of a texture.

It should be recognized that the impurity content captured by the film during deposition can shift the homologous temperatures defining the transition between these subsections either by affecting the rate of adatom diffusion or grain boundary diffusion. Also, these transition temperatures can be shifted by deposition rate variations. For example, an increase in deposition rate should result in an increase in the transition temperature defining the transition between subsections 2.2.2 and 2.2.3, i.e. raise the homologous transition temperature above 0.25. The latter effect is believed to be present in the experiments of Gittis and Dobrev[18] who found that the <100> texture was present in thick Ag films at deposition rates greater than 100 nm/s up to a homologous temperature of 0.38, above which the <111> texture was dominant.

When there is sufficient cluster mobility and cluster rotational mobility on non-epitaxial substrates it is possible to produce a monocrystalline film in the first continuous layer to form on the substrate, which on further deposition yields thicker monocrystalline films by self-epitaxy. The homologous temperature above which such monocrystalline films are produced, known as the “epitaxial temperature”,

lies at the top of the range associated with the present subsection.* The texture of this monocrystalline film is expected to correspond to the film surface having the lowest energy.

2.2.4. Very rapid grain boundary migration, very rapid adatom diffusion.

The homologous temperature range corresponding to the present subsection is that above about 0.5. In all of the kinetic phase space occupied by the sectors described in the previous subsections, the driving force for the approach to equilibrium was either the difference in surface energy or the difference in excess bulk-free energy. In the present case, when the films are very thin the driving force for the approach to equilibrium is the difference in surface energy between adjacent grains. The high grain boundary mobility allows the film to develop the surface energy driven fiber texture when very thin. As the film becomes thicker during deposition, further grain growth is driven by the excess energy associated with the tilt grain boundaries between adjacent grains, already having the lowest energy surface parallel to the substrate surface. The latter growth corresponds to the phenomenon of normal grain growth that has been investigated intensively in the materials science of bulk materials. Not that the latter driving force does not exist also in the kinetic regime of the previous subsection, but the mobilities required to produce an observable effect due to this driving force are inadequate there.

The grain morphology produced in vapor deposition under the conditions of the present subsection is expected to be columnar, but with the lateral diameter of the columnar grains being larger than the thickness of the film. Further, the expected texture is that corresponding to a film surface having the lowest energy.

In summary, we have shown, in the discussion encompassed in the above subsections of 2.2, that in all of the kinetic regimes, except the one in which bulk-free energy differences between adjacent grains can develop during deposition and grain boundaries can migrate, the surface of the film is made up of facets that have the lowest specific surface-free energy. The texture of the film is not unique when twins can be deposited on this surface. In the absence of twins, the texture or the pole of the surface plane is that corresponding to the lowest surface-free energy. It is only on epitaxial substrates that the grain orientation will be controlled by that of the substrate. In the kinetic regime where bulk-free energy difference can exert an effect on texture, the effect can only take place when this driving force for grain boundary migration exceeds the counter driving force due to the difference in surface-free energy. Since the latter decreases and the former increases with film thickness then there will be a critical film thickness above which the former reigns and below which the latter reigns. Further, in all regimes of homologous temperature the

* An alternate explanation for the epitaxial temperature and texture based on nucleation concepts is considered in Appendix 2.

grain morphology is columnar. The lateral grain size is on the order of 20 nm in the regimes of subsections 2.2.1 and 2.2.2, except for the grains that undergo secondary recrystallization in the latter regime. This lateral grain size increases with the homologous substrate temperature until in the regime of subsection 2.2.4 it can exceed the film thickness.

2.2.5. Zone models of grain morphology for vapor deposition in chamber pressures greater than 10^{-8} Torr onto non-epitaxial substrates.

Figure 3.6 illustrates schematically the grain morphology classification of Movchan and Demchishin.[19] The columns in *zone 1*, as noted in the previous chapter, either are crystalline or are amorphous. The crystalline columns in *zone 1* may or may not be monocrystalline. They contain defects, such as low angle and twin boundaries, dislocations, vacancies, etc. The columns in *zone II* are monocrystalline, separated by grain boundaries, rather than the spongy, porous network, found in *zone I*, and are freer of defects than those in *zone I*. The grains in *zone III*, according to the Movchan–Demchisin scheme, are equiaxed. However, as shown later by Grovenor et al.,[5] the lateral grain size usually exceeds the film thickness so that the grains are not really equiaxed, but are columnar.

Subsequent to this classification of the grain morphology, Grovenor et al.[5] deduced a different classification based on a systematic study of metallic films. They found that the grains, in films deposited on substrates at $T < 0.15T_M$, ranged from about 5 to 20 nm in diameter, are equiaxed, and can be smaller than the fiber or column diameter. However, later one of the authors[20] modified this description by replacing the term "equiaxed" with the phrase "columns of slightly misoriented crystallites". The preponderance of evidence argues against the possibility that differently oriented

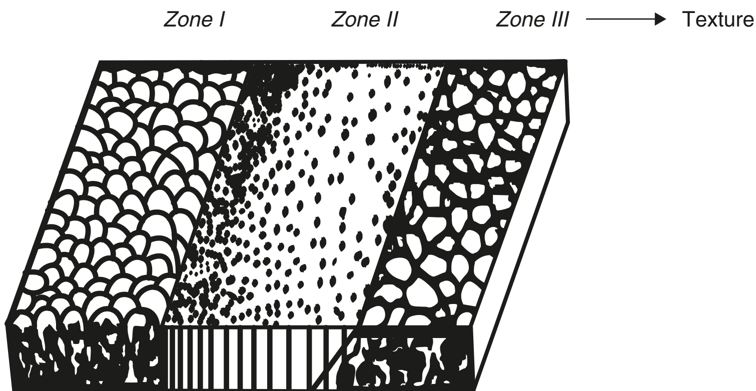

Figure 3.6. Structure zone model according to Movchan and Demchishin.[19]

grains form on top of grains of the same metal during deposition. Indeed, this evidence supports the proposition that deposition and grain growth along the thickness direction occurs by granular epitaxy. Grovenor et al. denoted this temperature zone as *zone a*.

They observed that for $0.15T_M < T < 0.3T_M$ the grain size distribution is bimodal with the difference in diameter between the largest and smallest grains increasing with substrate temperature (see Figure 3.2). Also, the diameter of the smallest grains remained constant and equal to the size found in the *zone a* structure. The diameters of the largest grains found at substrate temperature near to the upper temperature limit of this zone approach 500 nm in films 100 nm thick and greater than 3 μm in films 10 μm thick. These grain sizes are about a factor 10 larger than the characteristic column sizes for these film thicknesses. Grovenor et al. denoted this temperature regime as *zone b*. It corresponds to the same temperature regime previously denoted as *zone T* by Thornton.[21]

At homologous temperatures (T/T_M) higher than 0.3 the grains are columnar with the columnar diameter increasing with film thickness, but remaining smaller than the latter up to a homologous temperature of 0.5. The description by Grovenor et al.[5] of this regime is similar to that of Movchan and Demchishin[19] with the addition that activation energy measurements, determined from plots of log column diameter versus reciprocal absolute temperature, yield values equal to about one-half of that for self-diffusion or slightly less than this value. The latter result suggests that grain boundary migration in this zone is limited by the rate at which deposition-generated vacancies diffuse to the grain boundaries. This temperature regime denoted *zone II* by Movchan and Demchishin was denoted by Grovenor et al. as *zone c*.

It is interesting that Srolovitz et al.[47] proposed a model for columnar grain growth in *zone II* that yields results found not in *zone II* but in *zone 1b*. In particular, their Monte Carlo simulations revealed the bimodal grain size distribution found in *zone 1b* and the onset of secondary recrystallization, also characteristic of *zone 1b*. Their results disagree with experiment in the morphology of the distribution of the secondary and primary grains. In the model, the secondary grains are produced by the deposition process itself, whereas in practice they appear to occur because of grain boundary migration. These two different modes lead to two different distributions of the two types of grains. The probability that grain boundary migration is involved follows from the fact that it is observed in films deposited at *zone a* temperatures that are subsequently heated into the *zone 1b* range.

Above an homologous temperature of 0.5, measured activation energy values from log column diameter versus reciprocal temperature approximately equal the activation energy for self-diffusion.[22] In addition, Grovenor et al. point out that the grains in the zone above $T/T_M = 0.5$ are not equiaxed, as Movchan and Demchishin claim, but are columnar. However, in the latter zone, the ratio of column diameter to

film thickness exceeds unity. This temperature regime above $T = 0.5T_M$ has been denoted *zone III* by Movchan and Demchishin. Grovenor et al., however, denote both *zones II* and *III* as *zone c* to indicate a common origin. Inexplicably, they ignore the fact, also reported in their paper, that the activation energies in *zones II* and *III* differ markedly. This fact suggests strongly that two different mechanisms are rate controlling in these two temperature regimes. We have therefore used Grovenor et al.'s *zones a* and *b* (our 1a and 1b) and Movchan and Demchishin's *zones II and III* as the basis for the homologous temperature regimes described in Subsections 2.2.1–2.2.4.

The new contributions of Grovenor et al. to the zone classification of grain morphology are that the grain size distribution in *zone b* is bimodal and that the columnar grains in *zone III* have an aspect ratio of lateral dimension to length greater than unity.

In the following subsection we will reinterpret the zone models according to the arguments we have already presented in subsections 2.2.1–2.2.4.

2.2.6. Interpretation of zone models according to present analysis.

First, we may note that the zone models are not universal in their application. They are obviously limited to deposition at chamber pressures greater than about 10^{-8} Torr and onto non-epitaxial substrates. For these constraints, then *zone 1a* behavior corresponds to the behavior described in Subsection 2.2.1. It should be recalled that the zone models are models of grain morphology and not texture. Thus, according to the present analysis the texture should be random with a weak admixture of the texture corresponding to exposure of the lowest energy surface orientation.

The grain morphology corresponding to *zone 1b* is produced by the conditions described in subsection 2.2.2. The textures produced in this zone depend upon the film thickness. As noted in subsection 2.2.2 bulk-free energy differences between adjacent grains can develop, which in sufficiently thick films can exceed the surface-free energy differences between these grains. The fiber textures developed depend upon which of these factors drives grain boundary migration. In fcc metals the former driving force leads to a <100> texture and the latter to a <111> texture.

As noted in subsection 2.2.2 the bimodal grain size is produced by the process of secondary recrystallization, and the latter occurs because the network of intercolumnar voids acts to restrict the migration of all except those grains which either have a surface of the lowest specific-free energy or have the lowest bulk-free energy. Because most of the grain boundaries are immobile in this substrate temperature regime the layer closest to the substrate has a random texture.

Zone II behavior corresponds to that described in subsection 2.2.3. Here, voids do not form and, consequently, secondary recrystallization cannot occur. In very

thin films the grain boundary mobility becomes sufficient so that curvature driven grain boundary migration can occur. Also, in these very thin films grain growth driven by the difference in surface energies occurs at a much higher rate due to the much larger driving force thus yielding a fiber texture corresponding to the surface of lowest energy. The lateral grain size is limited to the average distance between the grains having the ultimate fiber texture in the film layer closest to the substrate, but is usually smaller than this distance and is rate limited by the supply of excess vacancies furnished from the surface during deposition. Further lateral grain growth in thicker films does not occur because the supply of deposition produced vacancies is limited to the near-surface region and because both the driving force due to the curvature of the resulting tilt boundaries and their mobility is too low. The resulting grain morphology is columnar with a lateral grain size less than the film thickness. The temperature is too high in *zone II* to allow differences in bulk-free energy due to elastic stresses to develop between adjacent grains. The ultimate fiber texture in thick films is also that corresponding to the film surface having the lowest specific-free energy.

Finally, *zone III* corresponds to that described in subsection 2.2.4, where it is shown that still higher mobilities lead to lateral grain growth of the grains having the ultimate fiber texture corresponding to a film surface having the lowest specific-free energy and a closer approach to the state of thermodynamic equilibrium than is achieved in *zone II*. The activation energy is that for grain growth in the absence of excess vacancies.

We have summarized our modified zone description in Figure 3.7, where in *zone 1a* the grains are fibrous and wavy with a fiber diameter ranging from 5 to 20 nm. In *zone 1b* there is a bimodal grain structure with the fine grains fibrous, of the same diameter as in *zone 1a*, but perhaps less wavy, while the large grains are columnar. In both *zones 1a* and *1b* there exist voids between the fibers that form a continuous network extending through the thickness of the film. In *zone 2* the grains are columnar with diameter less than the film thickness. In *zone 3* the grains are columnar with diameter larger than the film thickness.

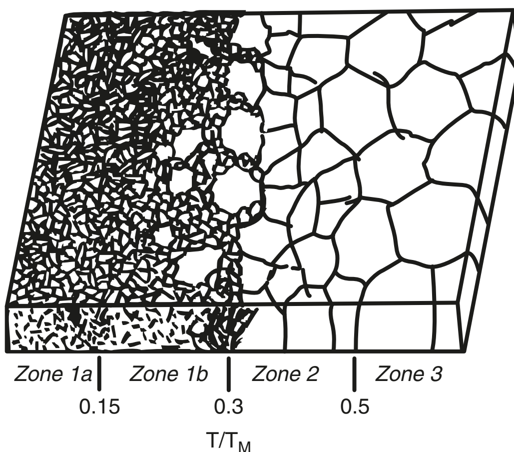

Figure 3.7. Modified zone diagram.

2.3. Effect of anisotropic sticking coefficient.

In all of the work considered above, the sticking coefficient on all surfaces is assumed to have a value close to unity. This assumption is valid for metallically bonded materials. However, it is not necessarily valid for layered materials where the bonding between specific planes is mainly of the van der Waals type. These materials are usually composed of layers, such that the bonding between layers consists of weak, secondary type bonds, whereas the bonding within the individual layers is made up of the strong, covalent type bonds. An example of such a material is MoS_2, which consists of a stacking of S–Mo–S layers, each parallel to (001) of the hexagonal crystal structure, with van der Waals bonding between the S atoms of adjacent layers. The (001) plane has the least surface energy and because of the saturated bonding in each layer this surface also has a very low sticking coefficient. Any plane normal to (001) will have the highest density of dangling bonds and, consequently, a near-unity sticking coefficient. Under these circumstances, grains with c axes parallel to the substrate plane will grow faster than those with c axes perpendicular to the substrate. Thus, after some period of deposition, the film surface will be devoid of grains having the lowest surface energy[40] and neither secondary recrystallization nor normal grain growth can then occur to produce a film having the lowest surface free energy. (See Appendix 4 for additional anisotropic effects.)

2.4. Polycrystalline semiconductors on non-epitaxial substrates.

The discussion that follows is confined to semiconductors where the impurity concentration is sufficiently low as to have no effect on the texture of the polycrystalline film. Such films are produced either by deposition in an ultra-high vacuum or by high-rate chemical vapor deposition (CVD). Most such films are produced via CVD. There are two ways to form polycrystals in elemental semiconductors: anneal an amorphous film or deposit above the amorphous→crystalline transition temperature. The former method produces equiaxed grains of random texture. The latter produces columnar grains. The texture of the columnar grains varies with pressure of the reactant gas and with substrate temperature. For silicon produced by CVD, at low pressures, the {110} texture predominates in the temperature range between 600°C and 650°C, the {100} between 650°C and 710°C, and the {110} again predominates above 710°C. At atmospheric pressure the {110} is the strongest texture component between 710°C and 850°C, whereas the {111} is strongest above 810°C.[53a,b] A further evaluation of the effect of silane pressure showed that for substrate temperatures between 550°C and 700°C, a random texture is obtained for silane pressures less than $2 \cdot 10^{-4}$ Torr, the {100} texture is

found between $2 \cdot 10^{-4}$ and 1 Torr, while the {110} texture is found for pressures exceeding 1 Torr.[53c] Now the surface orientation which is believed to have the lowest surface energy in Si is {111}.[58] Thus, the observations of the {110} and {100} textures require other explanations. The grains having the {110} texture contain a high density of twins and stacking faults. No satisfactory explanation for the latter two textures has been given as yet. The fact that the texture varies with silane pressure at a constant substrate temperature suggests that the orientation of the surface plane may affect both the forward and backward reaction rates occurring at the surface differently with increasing silane pressure and thus lead to relative growth rates of these two textures that reverses with silane pressure. Incidentally, the latter explanation is equivalent to the statement that the sticking coefficient is anisotropic. This author is not aware of any texture measurements in poly-Si films produced by UHV-PVD.

2.5. Conclusions regarding grain morphology, size and texture produced via vapor deposition in the absence of energetic particles.

On epitaxial substrates, and even when perfect matching of the crystal lattices of film and substrate does not exist, the low substrate-film interface energy generally dictates the orientation of the clusters and of the subsequent film that grows on the substrate. However, there is no evidence that, on non-epitaxial substrates that the texture of the film is the same as that of the clusters that first form on the substrate. To the contrary, texture appears to arise in the subsequent layers rather than in the layer closest to the substrate, *i.e. texture is not determined by nucleation.*

For non-epitaxial substrates there are the following additional conclusions:

1. The mode of extension of crystalline grains in the thickness direction during deposition is self- or granular epitaxy. Renucleation of grains on the clean surface of a film during deposition does not occur.

2. The zone models of grain morphology apply only to deposition onto non-epitaxial substrates.

3. The fiber textures assumed by films during physical vapor deposition are determined by thermodynamic considerations in the presence of some mobility either of adatoms or of grain boundaries except when the sticking coefficient is anisotropic.

4. Grain morphology is fibrous or columnar which is a consequence of the phenomenon of granular epitaxy. The bimodal morphology observed in zone b is a consequence of secondary recrystallization.

5. Grain size in thin films is determined by kinetic factors which also act to determine the transition temperatures between the four zones of homologous temperatures.

3. Grain morphology, texture and size in vapor-deposited films which sense energetic (hyperthermal) particles during deposition.

Incident hyperthermal atoms during deposition can produce displacement spikes and forward and backward sputtering. We shall in the following distinguish between the effects of displacement spikes and sputtering on the grain structure of deposited films. First to be considered are the effects of displacement spikes.

Displacement spikes can yield a liquid-like structure similar to that shown in Figure 3.8, which is produced by a collision cascade. The liquid-like region illustrated in Figure 3.8 is unstable. At some point during bombardment and deposition, at the low homologous temperatures associated with *zone a* the shear modulus of such material will approach zero and a cooperative transformation to a more stable structure can occur, i.e. an incident particle can trigger a solid→liquid→metastable solid transformation sequence that may result in a crystalline grain having a random orientation, i.e. recrystallization.

At higher substrate temperatures relaxation processes can occur during deposition that act to remove defects. Among these are diffusion of interstitials to vacancies and other sinks, diffusion of vacancies to vacancy sinks and collapse of disordered

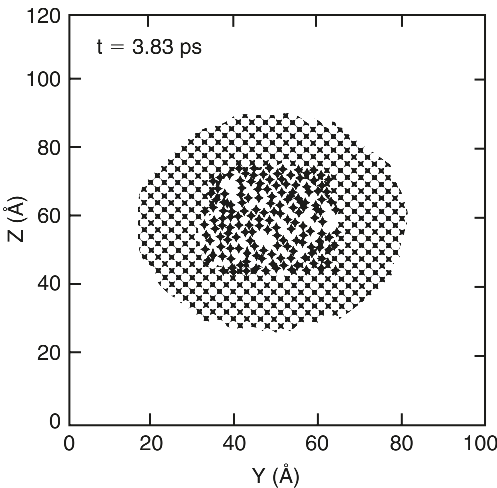

Figure 3.8. A schematic illustration of a two-dimensional section through a collision cascade at 3.83 ps after the event. Reproduced with permission from M. Lu, J.H. Judy and J.M. Sivertsen, IEEE Trans. Magn. 26, 1581(1990). © 1990 IEEE.

atom arrays to form new crystalline grains of different orientations. In Appendix 2 of Chapter I it was shown that displacement-induced vacancies (and interstitials) can diffuse out of the exposed surface of the film during deposition at room temperature, for metals that have melting points lower than 1300°K. However, it is also possible that a fraction of the displacement-generated vacancies can collide during diffusion and form vacancy clusters, which themselves can collapse to form dislocation loops. Segments of these dislocations can align to form tilt and twist boundaries, which, in turn, yield misoriented grains.

Forward sputtering acts to eliminate voids between grains and columns. As noted in Section 2 above, voids act to pin grain boundary migration and thus satisfy one of the necessary conditions for secondary recrystallization found in *zone 1b*. Hence, it may be expected that, contrary to the case for thermal beams, secondary recrystallization will not occur and bimodal grain sizes will not be observed in films deposited using hyperthermal* beams.

Another possible effect of incident particle bombardment during deposition relates to alteration of the substrate surface. Appropriate particle bombardment can clean the substrate surface so as to convert it from a non-epitaxial substrate to an epitaxial type substrate for suitable film materials. If the conditions for formation of an epitaxial relationship are satisfied then particle bombardment that cleans the substrate surface can allow the production of a grain structure that corresponds to such epitaxy, i.e. an epitaxial monocrystalline film can be formed on a monocrystalline substrate. Already clean substrate surfaces can be altered by particle bombardment so as to enhance the density of sites for nucleation of clusters and thereby yield a film having smaller grain size than obtained by evaporation alone for film–substrate combinations that do not form epitaxial relationships. However, appropriate particle bombardment can also lead to the elimination of small clusters by sputtering and dissociation and thereby yield an enhancement in grain size, i.e. an enhancement of the process of Ostwald ripening. Sufficient particle bombardment can even produce amorphous surfaces.

Another possible effect of incident particle bombardment is enhancement of processes, such as adatom diffusion and grain boundary migration, which may possibly affect the homologous temperatures defining the zone boundaries.

From the above introduction we can understand that prediction of the effect of a specific particle bombardment in some particular deposition is very difficult, if not impossible at this time. Much research is needed to characterize the effects of the various energetic particle bombardment and deposition parameters on the grain structure. In the following we offer a review of studies aimed at elucidating such effects.

* Hyperthermal beams are defined in this book to be beams that contain particles having energies exceeding thermal energies, i.e. energies that can vary from about 1eV to 1000eV.

3.1. Deposition onto epitaxial substrates.

Jona[24] found it possible to sputter clean aluminum surfaces to the point where it was possible to obtain epitaxial deposition of aluminum on these surfaces. It is interesting to consider the cleaning treatment in detail to obtain an estimate of what is necessary to achieve the required cleanliness. The penultimate treatment of the Al substrate surface subsequent to metallographic polishing was an electropolish which left an oxide film estimated to be about 300–400 Å thick. This film was then sputtered away in a conventional radio frequency (RF) sputtering apparatus at 7 mTorr of argon (the substrate was the target in this apparatus). On transfer to the deposition chamber it had an estimated "natural" oxide film thickness of about 15–20 Å. The deposition chamber had a background pressure of $2–5 \cdot 10^{-10}$ Torr. The final cleaning in the latter chamber consisted of four to five sequences of argon ion-bombardment (400–500 eV, 2 μA/cm^2) for 30 min followed by annealing in vacuo at 400–450°C for about 1 h. LEED patterns indicated no improvement after the third such treatment. (It is not known what role the annealing treatment contributed to the cleaning, although it certainly smoothened the surface and removed lattice defects generated by the ion bombardment.) Thus, we can estimate that a fluence of $6.8 \cdot 10^{16}$/cm^2 of 400 eV argon atoms is necessary to sputter away an oxide layer about 15–20 Å thick. Roughly, given the uncertainties, these data indicate a sputtering yield of about unity. Jona then found it possible to deposit Al epitaxially, on the Al surfaces cleaned as described above, in situ in the UHV apparatus. However, Jona's experiment was carried out in a UHV apparatus, which would not introduce any oxygen to the substrate surface during or after the argon ion bombardment. Hence, fluence is not the critical parameter in an ordinary vacuum system. In the latter type of system the cleaning flux must exceed the contamination flux by a sufficient amount, over the cleaning time before deposition begins, to sputter away the oxide layer on the substrate surface.

Cleaning the substrate surface is not the only effect that energetic particles have in the promotion of epitaxial deposition. However, consideration of these effects is postponed until the next chapter, which explores the gamut of epitaxial deposition.

3.2. Deposition onto non-epitaxial substrates.

Thornton[21] in his review of the grain structures produced in films deposited via magnetron sputtering replaced *zone 1* with a *zone T* for films subjected to hyperthermal beams. In *zone T* the grains were fibrous and the grain boundaries were not voided. The temperature range encompassed by *zone T* depended upon the gas pressure in the deposition chamber. For the case of negligible gas pressure (i.e. negligible thermalization of the incident particles) the temperature range of *zone T* equaled that of *zone 1* for deposition from thermal vapors. We shall in the following

subdivide *zone T* into *1aT* and *1bT*, using the T character to denote that the grain structure in these zones corresponds to films deposited using hyperthermal beams.

3.2.1. *Zone 1aT* temperature range.

The above analysis suggests that in the *zone 1aT* temperature range the particle bombardment of sufficient energy during deposition will yield a refined grain structure consisting of randomly oriented, equiaxed grains. On the other hand, a particle bombardment that favors the sputtering of surface situated atoms over the development of displacement spikes may well accomplish the development of a strong texture due to the difference in sputtering yield between differently oriented surface planes of crystalline grains.

Sputtered Ti coatings deposited at liquid nitrogen temperature were found to have a <110> texture.[25] Moreover, they had the high-temperature beta (bcc) phase structure, rather than the stable alpha hexagonal closed packed (hcp) structure. The latter observation is an interesting result and has been interpreted as an illustration of Ostwald's rule.[26] (This interesting result deserves further investigation in view of the fact that the conditions relating to the energetic particle bombardment were not defined in this study.) The {110} surface has the lowest energy in the bcc structure.

Bland et al.[27] found it possible to disrupt the columnar structure and produce fine-grained structures in RF sputtered Cr and W at homologous substrate temperatures of 0.14 and 0.08, respectively, at which temperatures excess vacancies should be immobile in these films. However, in order to accomplish this feat they had to raise the negative bias to 500 V. At smaller absolute values of the bias voltage the columnar structure was not disrupted. Unfortunately, no mention was made of texture observations, although X-ray diffraction data were obtained from these films. Much smaller bias (30 eV) was found to be required in the deposition of amorphous Si to remove the intercolumnar void network.[51] Thus, results of Bland et al. indicate that a critical energy input (per deposited atom?) may be needed to achieve athermal recrystallization of the columnar grain morphology.

Thornton[25] found that sputtered Cr deposited onto glass and stainless steel substrates cooled by liquid nitrogen (homologous temperature of 0.04) and at a rate of about 1 nm/s yielded a <110> texture in the absence of bias potential. A similar result was obtained by Patten and McClanahan[28] who observed that Cr sputtered onto a Cu target held at 15°C (homologous temperature equal to 0.14) at a rate of 6 nm/s with negative bias voltages not exceeding 75 V yielded a <110> texture and a columnar structure. Also, Lu et al.[29] found a <110> texture for Cr films produced by sputtering onto glass with the extent of the <110> texture increasing as bias voltage varied from 0 to −175 volts. The columnar grain diameter averaged at 57 nm.

Copper films sputter deposited at 80 K (T/T = 0.06) at a rate of 8–11 nm/s exhibited a columnar structure and a <111> texture, which after recrystallization at room temperature changed to a <100> texture.[30]

From the above facts and from the knowledge that deposition in the absence of displacement spikes in this zone of homologous temperature produces at most only a weak fiber texture (see subsection 2.2.1) we may deduce the following conclusions:

1. Energetic bombardment with particle energies less than about 500 eV enhances the mobilities that control the approach to the equilibrium state, thereby allowing the film to develop the fiber texture corresponding to the film surface having the lowest specific-free energy even at homologous temperatures smaller than 0.15 and to achieve somewhat larger grain size than is produced in films condensed from thermal vapors. The morphology remains columnar.

2. Athermal recrystallization may be achieved when a critical energy input (per deposited atom?) is exceeded. However, see Appendix 5.

3.2.2. *Zone 1bT* temperature deposition.

It was found by Sundgren et al.[31] that a negative bias of 700 V had to be applied before the columnar structure of reactively sputtered TiN could be changed to an equiaxed structure at a total gas pressure of 5 mTorr and a homologous temperature of 0.24. The effect of increasing bias below this critical value simply caused the grain size to increase initially and then to decrease above about 200 V negative bias. The grain size remained constant at about 30 nm above 700 V negative bias. Further, it can be deduced from the data that the ion current required to eliminate the columnar structure is just about equivalent to the deposition rate in units of particles/s. This result supports the deduction made in the previous subsection that energetic incident particles will not induce recrystallization until the incident particle energy exceeds about 500 eV.* Incidentally, the production of an equiaxed grain morphology of 30 nm grain size from a columnar grain morphology of lateral grain size equal to about 30 nm before recrystallization requires that there be an excess bulk-free energy to supply the additional interface free energy. The latter corresponds to an excess vacancy concentration of about 0.001 above the equilibrium concentration. Given a production of about five vacancies for each incident 500 eV argon ion it seems reasonable to conclude that the excess bulk-free energy required to produce the new grain boundary area could be provided by the excess vacancies alone.

Patten et al.[32] found that in Kr sputter deposition of Cu at a homologous substrate temperature of 0.22 the film texture changed from $<111>$ to $<100>$ as the substrate bias changed from -25 to -75 V and changed back to $<111>$ when the deposition rate was decreased from 10 nm/s to below 2.3 nm/s at the latter bias. At a homologous substrate temperature of 0.2, at a rate of 2–50 nm/s, Cu sputtered onto glass and stainless steel substrates in a hollow cathode apparatus yielded

* However, see Appendix 5, where a contradictory observation is discussed.

a <111> texture when the argon pressure was 0. 1 mTorr and a <110> texture when this pressure was 3 mTorr. However, in an apparatus containing a post-cathode and at the higher argon pressure a <111> texture was obtained at the same homologous substrate temperature.[25] Both of the latter results were obtained in the absence of an applied bias potential. Dahlgren[30] found that Cu films sputter deposited at a homologous substrate temperature of 0.21 at a negative bias of 75 V had a columnar grain morphology with a lateral grain size equal to about 70 nm.

Ziemann and Kay[33] found that the peak in the <111> fiber texture intensity for Pd in Kr at 1 m Torr relative to that for <100> as a function of the energy delivered per arriving Pd atom correlated with a sharp decrease in lattice parameter in its approach to the bulk value. This result is consistent with the explanation provided in the previous section for this fiber texture in fcc metals, i.e. the tendency to produce the <111> texture in fcc metals on non-epitaxial substrates is driven by the difference in specific surface-free energy. The driving force to produce the <100> fiber texture, according to our previous analysis, is the difference in bulk-free energy between adjacent grains, which becomes small as the bulk elastic strain (the difference between film and bulk lattice parameters) becomes small. Thus, it seems that the explanations for the fiber textures found in films condensed from thermal sources are consistent with observations of fiber textures in films subject to energetic bombardment during deposition, with the caveat that because of the particle bombardment additional effects on the fiber texture may also exist.

Another aspect of Ziemann and Kay's work may be significant in that they point out that the parameter that governs the texture is not the particle energy or bias potential but the energy delivered per depositing atom, i.e. it is both the bias potential or particle energy and the ratio of ion flux to depositing atom flux that independently affect the texture. We shall remark on this relationship in the next paragraph.

Kant et al.[34] found that a 1500 eV Ar atom bombardment of a nickel film during deposition at a homologous substrate temperature of about 0.17 yielded a peak in the <111> texture intensity at about an ion/atom arrival ratio of 0.02. The existence of a peak in the <111> texture population as a function of ion/atom arrival ratio for ion energies exceeding about 500 eV and a corresponding peak in this fiber texture population at a given arrival ratio as the incident particle energy increases is a common occurrence. The initial increase in the <111> fiber texture is due to the enhanced mobility the incident energetic particles provide to the columnar grain boundaries, probably as a consequence of an enhanced flow of vacancies to these boundaries, thereby allowing the conversion of a larger fraction of the volume to this texture during the deposition. The subsequent decrease in this fiber texture and the production of a more random texture is due to the recrystallization induced by the injection of sufficient energy per deposited atom.

Westwood[35] found that in the absence of bias that thin Pt films, deposited by sputtering in argon at a homologous substrate temperature of 0.21, exhibited a random

texture and a low film density (14 g/cm^3) when the pressure of the argon was 140 mTorr and a <111> texture and high film density (21.4 g/cm^3) when this pressure was 10 mTorr. These observations are consistent with the interpretation that voids in the film prevent grain boundary migration at the high argon pressure, whereas at the low argon pressure there is sufficient particle bombardment to remove some of these voids and thereby allow secondary recrystallization under the surface energy difference driving force to produce the <111> texture.

Mattox and Kominiak[36] found that a negative bias potential exceeding 500 V was necessary to recrystallize Ta at a homologous substrate temperature of 0.18 and thereby produce a fine grain size varying from 6 to 20 nm diameter with the absence of a columnar morphology.

Duan and Artman[37] found a random texture for RF diode sputtered Cr in Ar at 10 mTorr, at a homologous temperature of 0.22, using a glass substrate and in a thin film of 40 nm thickness. As negative bias increased an increasing <100> texture was found. Further, at a homologous substrate temperature of 0.31 (at the *zone b* to *zone 2* transition) the texture was a strong <100> . For thicker Cr films (170 nm) Duan et al.[38] found that the texture was random at homologous substrate temperatures ≤ 0.18 and strongly <100> above a homologous temperature of 0.22. Above the latter substrate temperature there was an increase in the <110> texture relative to <100> with increasing thickness of the film.

Non-cubic films tend to yield the low-energy surface as the fiber texture in thin films. For example, on amorphous substrates the c axis of ZnO was found to be perpendicular to the substrate surface.[39] However, in layered materials, as noted above for evaporated and condensed films, a highly anisotropic sticking coefficient can develop to bring about a change in this rule. For example, in the first 7 nm adjacent to the substrate, films of MoS_2 deposited at 300°C (homologous temperature = 0.39) have the c axis perpendicular to the substrate surface, whereas beyond this film thickness the texture is such that the c axis is parallel to this surface.[40] A similar result is found for the high-temperature superconducting films of YBaCuO, provided that the substrate temperature is between 480 and 530°C.[41]

As mentioned in the introduction to this section, one of the additional parameters that may affect texture of vapor-deposited films in the presence of incident energetic particles during deposition is the possible influence of a dependence of the sputtering rate on crystal orientation. Snouse and Haughney[42] have shown that the sputter yield is orientation dependent. In particular, they found that the sputter yield for argon ion energies less than about 1000 eV incident on copper increased in the following order: {110} << {100} < {111}. The very low value for the sputter yield from a {110} surface for normal incidence occurs because channeling of incident particles occurs most readily along the <110> axis for the fcc structure. Whetten et al.[43] found a marked decrease in the sputter yield when incident particles were within about 5° of the <110> axis for diamond. Finally, the

differential sputter yield was found to be responsible for the azimuthal preferred orientation developed in Nb films at a ion/atom arrival ratio of about unity and argon ion energy of about 200 eV.[44] The azimuthal orientation corresponded to orientations which have the {110} plane parallel to the glancing ion beam direction. Thus, for fcc films, with a sufficient ion/atom arrival ratio of normal incident energetic particles, the differential sputter yield should bring about a <110> fiber texture. Indeed, as noted above, Thornton[25] observed the <110> fiber texture in copper. Dobrev[57] observed it in Ag bombarded by 10 keV Ar^+.

Summarizing, in the *zone 1bT* temperature regime, we find that:

*1. As in zone 1aT, to achieve recrystallization and elimination of the columnar grain structure it appears necessary for the incident particle energy/deposited atom to exceed a critical value.**

2. At lower incident particle energies/deposited atom the columnar diameter varies non-monotonically with a monotonic increase in particle energy.

3. Most of the textures that appear are those produced in the tendency for the film to approach the lowest free energy configuration.

4. Texture may be altered from that corresponding to the lowest free energy when the film is subject to sufficient particle bombardment to sputter atoms from the film surface and the sputter yield is strongly anisotropic or when the surface of least energy is sufficiently saturated (bondwise) as to yield a low value of the sticking coefficient on this surface.

5. The morphology remains columnar or fibrous and the columnar grain diameter monomodal at incident energies per deposited atom insufficient to induce recrystallization.

3.2.3. *Zone II* deposition.

In deformed bulk fcc metals recrystallization begins above about a homologous temperature of 0.3, which suggests the possibility that recrystallization might also take place in thin films during deposition if the energetic particle bombardment is sufficient to induce the generation of dislocations. Figure 3.9 demonstrates that dislocations are indeed generated at a homologous temperature of 0.24 in silver and their number approaches the density observed in deformed metals. Hence, it should come as no surprise to find evidence for recrystallization in films subjected to energetic particle bombardment in this temperature regime. For example, "more than one layer of overlapping grains, in contrast with the columnar grain structure of evaporated films" is reported by Roberts and Dobson[48] in magnetron sputter-deposited Al films at a deposition homologous temperature of 0.32. These

* R. Mitra et al.[60] report a critical bias voltage that differs from those reported in the text. They found also that in thick films the initial columnar grains are succeeded by equiaxed grains at a distance of between 0.2 and 0.4 mm from the film–substrate interface in the absence of bias. This phenomenon is discussed further in Appendix 5.

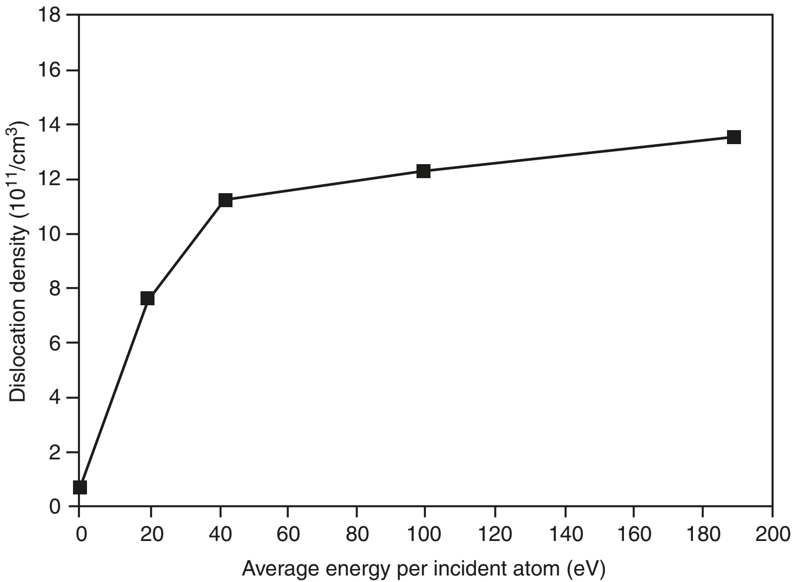

Figure 3.9. Dislocation density in Ag films deposited near room temperature as a function of average energy deposited per atom. Reproduced with permission from S.M. Rossnagel and J.J. Cuomo, Thin Solid Films 171, 143(1989).

films exhibited a random texture with a grain size of 150 nm. The film thickness was 500 nm. Selvaraj et al.[49] found similar evidence for thermally induced recrystallization in Al films deposited at the same homologous temperature. Additional evidence consistent with the assertion that recrystallization occurs during deposition is found in the work of Yapsir et al.,[50] who found that with increasing ion energy or ion/neutral atom ratio the <111> fiber texture first increases to a maximum and then decreases sharply to produce a nearly random texture in a partially ionized beam (PIB) deposition of Al at the same homologous temperature as the previous studies. Their results are very similar to those obtained by Kant et al.[34] who used Argon ion bombardment during the deposition of Ni at a homologous substrate temperature of 0.17. The former found the peak in the <111> intensity to occur at an ion/atom ratio of about 0.01 for a 2 kV bias voltage whereas the latter found it to occur at an ion/atom ratio of about 0.02 at a bias voltage of 1.5 kV. The similarity of these results brings into question the assertion that the recrystallization is thermally induced above the homologous temperature of 0.3. Indeed, a bombardment-induced recrystallization probably occurs in the work of Yapsir et al. However, these investigators also found that increasing substrate temperature reduced the bias potential corresponding to the disappearance of the <111> texture.

Hence, after all has been considered, it appears that there may well be a thermal contribution to the onset of the recrystallization process.

Additional systematic research designed to shed light on the subject of bombardment-induced recrystallization during deposition is needed before firm conclusions can be drawn. In particular, microscopic and other evidence is needed to demonstrate unequivocally that the grain morphology becomes equiaxed, rather than columnar beyond a critical impact energy per deposited atom. Also, a knowledge of the recrystallized grain size, if recrystallization occurs, as a function of deposition parameters would be helpful. Further, it may be useful to know the dependence of the critical impact energy per deposited atom on the substrate temperature. One can conceive the possibility of using this knowledge to devise a technique to produce a monocrystalline film on an amorphous substrate, for example.

Summarizing, in the *zone II* temperature range *the possibly new effect of energetic particle bombardment during deposition, not found in the lower-temperature zones, is that of thermal recrystallization of a bombardment-induced dislocation (and other defects) rich matrix.*

3.3. Summary of results on the effects of energetic particle bombardment during deposition.

1. Suitable energetic particle bombardment can facilitate epitaxial deposition onto epitaxial substrates by providing a clean, nascent substrate surface.

2. Energetic particle bombardment during deposition at values of the particle energy per deposited atom less than a critical value acts primarily to enhance surface and grain boundary mobility to produce the grain structure normally found in the absence of particle bombardment, but at higher substrate temperatures, and with the absence of a bimodal grain size.

3. Energetic particle bombardment during deposition at values above a critical energy per deposited atom radically changes the texture and morphology of the grains in much the way that recrystallization would change these properties. In zone 1aT *and* 1bT *temperature ranges this recrystallization probably occurs as a displacive, non-diffusive, transition. In* zone II*, recrystallization may also occur, as in bulk materials, via a diffusive transition of a matrix having a high value of stored energy due to defects induced by particle bombardment.*

4. Under particle bombardment conditions that yield a significant difference in the sputtering yield between grains at the surface of the deposited film, selective sputtering during deposition can affect the texture to yield an orientation corresponding to that of the minimum sputtering yield. These conditions are not ordinarily attained during the low energy bombardment processes normally used during deposition.

4. Effects of post-deposition processing on grain structure.

4.1. Effect of post-deposition annealing.

In addition to the effect of time at temperature on grain structure, post-deposition annealing, by involving a change in temperature from the substrate temperature to the annealing temperature, imposes a biaxial strain in the plane of the film. Depending upon the magnitude of the annealing temperature this strain involves a concomitant film stress or a plastic deformation of the film. With this knowledge it becomes possible to predict the effect of a post-deposition anneal on the grain structure. For simple metals, the grain structure should be qualitatively the same as found for the same deposition temperature with the exception that the grain size will be larger and the texture more developed. Further, in the temperature regime below $0.5T_M$, where elastic stresses can reach significant levels because the yield strength remains high, the texture corresponding to the minimum elastic strain energy will develop sooner in thinner films.

An examination of the literature confirms the expectations raised in the above paragraph. For example, Vook and Witt[12] found that copper films, which, when deposited at 80°K had a mild <111> texture and about a 100 nm grain size, after annealing to room temperature had a mild to strong <100> texture and a grain size varying from 0.05 to 0.1 mm, except in very thin films ($\leqslant$300 nm). Similarly, Thompson[59] reports that annealing a Ag film deposited at 77°K and having a (111) texture changes that texture to (100) due to the thermal stress developed on raising the temperature to 400°C (the grain growth temperature).

When the annealing temperature is high enough so that the yield strength is small (at temperatures higher than $0.5T_M$) then the tendency to minimize the surface energy controls the texture, as was found to be the case for as-deposited films. For example, Roberts and Dobson[48] and others have found that post-deposition annealing in this temperature range produces a strong <111> texture and a log-normal distribution of the grain sizes for Al films either deposited or annealed above $0.5T_M$.

We may remark here that in recent work of Thompson and his collaborators there is an implication that secondary recrystallization will perforce occur once a stagnant columnar grain structure develops, in which the grain sizes are log-normally distributed. (See p. 259 in Thompson's review article on grain growth in thin films,[52] items 3 and 4 in the list of the general features of grain growth in pure thin films.) We believe this comment is not applicable to the secondary recrystallization that occurs in films deposited in the absence of energetic particles in the *zone b* temperature range. The basis for this belief is discussed below.

The primary origin of the stagnant grain structure, according to Thompson, is the presence of grain boundary grooves at the intersection of grain boundaries with

the film surface. However, as first emphasized by Grovenor et al.,[5] abnormal grain size distributions, characteristic of secondary grain growth, first appear in metal films at $0.15T_M$ and then disappear above $0.3T_M$. As we noted in a previous section, the coincidence of the latter temperature with the transition temperature between *zone I* and *II* behavior, at which grain boundary void networks disappear, strongly supports the concept that below $0.3T_M$ grain boundaries are immobilized by voids. Further, the surface diffusivity in copper, evaluated from thermal grooving experiments,[56] is too low to be able to produce thermal grooves at temperatures below $0.3T_M$. Hence, grain boundary grooves cannot be responsible for grain boundary immobilization below $0.3T_M$ in copper and other fcc metals. Thus, the secondary recrystallization that has been observed in as-deposited films in the *zone b* temperature range is not due to the prior formation of stagnant grains via a thermal grooving effect.

However, above $0.3T_M$ it is entirely possible and likely that grain boundary grooves develop during deposition in the absence of energetic particle bombardment. In this case, it would be possible for the secondary recrystallization mechanism suggested by Thompson to take place during deposition. However, it appears that in the as-deposited films the grain size distribution is log normal and the texture corresponds to the lowest energy film surface. Thus, if the Thompson secondary recrystallization mechanism were to operate in *zone II*, it would have to go to completion before the temperature of the as-deposited film was decreased to room temperature. It is apparent that much more experimentation is needed to delineate the regimes and their associated mechanisms in a mechanism map for as-deposited, as well as post-annealed grain structures.

4.2. Post-deposition bombardment at elevated temperature.

A sufficient fluence of high-energy inert gas or self-ions can also result in the growth of grains[54] at temperatures below those required for grain growth via thermal annealing. The mechanism responsible for this ion bombardment-induced grain growth is not known at this writing. Originally, it was believed due to the effect of ion bombardment-induced point defects enhancing the grain boundary mobility. However, this view was shown to be inadequate because it predicted a linear dependence of the grain boundary mobility on the energy deposited in elastic collisions, whereas it was subsequently shown by many others that this dependence is quadratic. An alternate explanation based on thermal spike enhanced local temperature at the grain boundary was proposed.[55] It is too early at this writing to know if the thermal spike model satisfies its undoubted testing that will occur with the passage of time.

References

1. E.S. Machlin, **An Introduction to Aspects of Thermodynamics and Kinetics Relevant to Materials Science**, Giro Press, Croton-on-Hudson, NY, 1991, p. 247.

2. C.S. Barrett, **Structure of Metals**, 2nd edn., McGraw-Hill, NY, 1952, p. 327.
3. D.A. Smith, J.T. Wetzell and A.R. Taranko, MRS Symp. Proc. 37, 77(1985).
4. C.-A. Chang, a) Phys. Rev. B42, 11946(1990);. b) Appl. Phys. Lett. 57, 297(1990); J. Vac. Sci. Tech. A8, 3779(1990); Surf. Sci. Lett. 237, L417, L421(1990); J. Vac. Sci. Tech. A9, 98(1991); J. Appl. Phys. 68, 5893(1990); Phys. Rev. B42, 11946(1990).
5. C.R.M. Grovenor, H.T.G. Hentzell and D.A. Smith, Acta Metall. 32, 773(1984).
6. J. Bloch, M. Heiblum and Y. Komem, Appl. Phys. Lett. 46, 1092(1985).
7. M. Eizenberg, A. Segmuller, M. Heiblum and D.A. Smith, J. Appl. Phys. 62, 466(1987).
8. H.-J. Gossman, MRS Symp. Proc. 94, 53(1987).
9. H.S. Chen, H.J. Leamy and C.E. Miller, Ann. Rev. Mater. Sci. 10, 363(1980).
10. J.A. Venables, G.D.T. Spiller and M. Hanbrucken, Rep. Prog Phys. 47, 399(1984).
11. P. Meakin, Phys. Rev. A41, 983(1990).
12. R.W. Vook and F. Witt, J. Vac. Sci. Tech. 2, a) 243(1965); b) 49(1965).
13. C.C. Wong, H.I. Smith and C.V. Thompson, Appl. Phys. Lett. 48, 335(1986).
14. K.K. Kakati and H. Wilman, J. Phys. D6, 1307(1973).
15. H. Norenberg and H.-G. Neumann, Thin Solid Films 198, 241(1991).
16. R.W. Hoffman, Thin Solid Films 34, 185(1976).
17. C. Fang, Ph.D. Dissertation, Columbia University, 1992.
18. A. Gittis and D. Dobrev, Thin Solid Films 130, 335(1985).
19. B.A. Movchan and A.V. Demchishin, Fiz. Met. Metalloved. 28, 653(1969).
20. D.A. Smith, MRS Symp. Proc. 122, 3(1988).
21. J.A. Thornton, Ann. Rev. Mater. Sci. 7, 239(1977).
22. B.A. Movchan, A.V. Demchishin and L.D. Kooluck, J. Vac. Sci. Tech. 11, 869(1974).
23. W.L. Brown and A. Ourmazd, MRS Bulletin XVII, 6, 30(1992).
24. F. Jona, J. Phys. Chem. Solid. 28, 2155(1967).
25. J.A. Thornton, J. Vac. Sci. Tech. 11, 666(1974).
26. W. Ostwald, Z. Phys. Chem. 22, 289(1897).
27. R.D. Bland, G.J. Kominiak and D.M. Mattox, J. Vac. Sci. Tech. 11, 671(1974).
28. J.W. Patten and E.D. McClanahan, J. Appl. Phys. 43, 4811(1972).
29. M. Lu, J.H. Judy and J.M. Sivertsen, IEEE Trans. Magn. 26, 1581(1990).
30. S.D. Dahlgren, J. Vac. Sci. Tech. 11, 832(1974).
31. J.-E. Sundgren, B.O. Johansson, H.T.G. Hentzell and S.E. Karlsson, Thin Solid Films 105, 385(1983).
32. J.W. Patten, E.D. McClanahan and J.W. Johnston, J. Appl. Phys. 42, 4371(1971).
33. P. Ziemann and E. Kay, J. Vac. Sci. Tech. A1, 512(1983).
34. R.A. Kant, G.P. Chambers and B.D. Sartwell, MRS Symp. Proc. 157, 67(1990).
35. W.D. Westwood, J. Vac. Sci. Tech. 11, 466(1974).
36. D.J. Mattox and G.J. Kominiak, J. Vac. Sci. Tech. 9, 528(1972).
37. S.L. Duan and J.O. Artman, IEEE Trans Magn. 25, 3884(1989).
38. S.L. Duan, J.O. Artman, B. Wang and D.E. Laughlin, IEEE Trans. Magn. 26, 1587(1990).
39. H.W. Lehman and R. Widner, J. Appl. Phys. 44, 3868(1973).
40. J. Moser, H. Liao and F. Levy, J. Phys. D, Appl. Phys. 23, 624(1990).
41. S. Wu, K.-W. Ng, J.D. Robertson and R.J. Jacob, J. Appl. Phys. 72, 5337(1992).
42. T.W. Snouse and L.C. Haughney, J. Appl. Phys. 37, 700(1966).
43. T.J. Whetten, A.A. Armstead, T.A. Grzybowski and A.L. Ruoff, J. Vac. Sci. Tech. A2, 477(1984).

44. L.S. Yu, J.M.E. Harper, J.J. Cuomo and D.A. Smith, Appl. Phys. Lett. 47, 932(1985).
45. C. Tang, S. Alexander and R. Bruinsma, Phys. Rev. Lett. 64, 772(1990).
46. E. Grantscharova, Thin Solid Films 224, 28(1993).
47. D.J. Srolovitz, A. Mazor and B.G. Bukiet, J. Vac. Sci. Tech. A6, 2371(1988).
48. S. Roberts and P.J. Dobson, Thin Solid Films 135, 137(1986).
49. R. Selvaraj, S.-N. Yang, J.F. McDonald and T.-M. Lu, Proc IEEE VLSI Multilevel Interconn. Conf. (Electron Device Society, NY, 1987), p. 440.
50. A.S. Yapsir, L. You, T.-M. Lu and M. Madden, J. Mater. Res. 4, 343(1989).
51. R.C. Ross and R. Messier, J. Appl. Phys. 52, 5329(1981).
52. C.V. Thompson, Ann. Rev. Mater. Sci. 20, 245(1990).
53. a) T.I. Kamins and T.R. Cass, Thin Solid Films 16, 147(1973); b)T.I. Kamins, J. Electrochem. Soc. 127, 686(1980); c) P. Joubert, B. Loisel, Y. Chouan and L. Haji, J. Electrochem. Soc. 134, 2541(1987).
54. H.A. Atwater, C.V. Thompson and H.I. Smith, J. Appl. Phys. 64, 2337(1988).
55. D.E. Alexander and G.S. Was, Mat. Res. Soc. Symp. Proc. 202, 205(1991); Phys. Rev. B47, 2983(1993).
56. N.A. Gjostein in **Metal Surfaces** (American Society for Metals, Metals Park, Ohio, 1963) p. 136.
57. D. Dobrev, Thin Solid Films 92, 41(1982).
58. H.A. Atwater, C.V. Thompson and H.I. Smith, J. Mater. Res. 3, 1232(1988).
59. C.V. Thompson, MRS Symp. Proc. 280, 307(1993).
60. R. Mitra, R.A. Hoffman, A. Madan and J.R. Weertman, J. Mater. Res. 16, 1010(2001).

Appendix 1

To obtain a value for the thickness h* in the following equation, we must evaluate the other parameters that appear in it.

$$\Delta g = 2\Delta\sigma/h^*$$

The elastic strain energy difference, Δg, may be evaluated using the following relation

$$\Delta g = (1 - v)({}_1t^2/E_1 - {}_2t^2/E_2)$$

where ν is Poisson's ratio, ${}_it$ is a principal stress in the ith film plane, and E_i is the mean elastic modulus for a direction in the ith film plane. We assume that Poisson's ratio is isotropic, that the substrate is rigid and that the bulk dilation in the film responsible for the production of film stress is isotropic (independent of direction in each grain of the film and the same for each grain in the film). Let us further assume, in order to obtain a maximum value for Δg that this value of the strain causes the maximum value that any principal stress can assume to equal the yield strength. For these assumptions, ${}_1t = Y$ and ${}_2t = {}_1t^*E_2/E_1$. Substituting in the above relation for Δg we obtain

$$\Delta g = (1 - v)(1 - E_2/E_1)(Y^2/E_1)$$

Using $\nu = 0.3$, and the following values for thin film Ag: $E_2/E_1 = 0.376$, $Y/E_1 = 0.0014$, $Y = 1.0 \cdot 10^9 \, erg/cm^3$, and $\Delta\sigma = 100 \, erg/cm^2$, we obtain $h^* = 3 \mu m$. For thin film Cu the thin film values are: $E_2/E_1 = 0.35$, $Y/E_1 = 0.0013$, $Y = 2.56 \cdot 10^9 \, erg/cm^3$ and $\Delta\sigma = 100 \, ergs/cm^2$, we obtain $h^* = 1.3 \mu m$. These values should be accurate to a factor of about 3 since the uncertainty in the surface energy difference is on this order. (Yield strength values for thin films were taken from M.F. Doerner, D.S. Gardner and W.D. Nix, J. Mater. Res. 1, 845(1986) and S.L. Lehoczky, J. Appl. Phys. 49, 5479(1978). The former gave a value for an Al film and the latter for both Al and Cu films. The value for Ag was taken to be the average of that for Al and Cu.)

Appendix 2

The nucleation theory of Rhodin and Walton[A1] as an explanation for the epitaxial temperature and texture has been given credence in a recent text.[A2] This explanation suggests that the epitaxial temperature is defined by the transition between nucleation with a critical cluster size of one atom and that with critical cluster sizes slightly larger, i.e. two and three. The texture is associated with the critical cluster size. The critical cluster of two atoms yields the {111} texture while that of three atoms yields the {100} texture. The data used to substantiate this explanation involves plots of the logarithm of deposition rate versus reciprocal temperature, in which it is shown that a straight line separates the region of polycrystalline films from that of monocrystalline films and that the activation energy associated with this boundary line yields values in reasonable agreement with those expected from the theory. Despite the attraction of such an apparently elegant solution to the problems of the origins of texture and the deposition of monocrystalline films, one must be skeptical in view of several facts. First, there is a difference between a film having a fiber texture and a monocrystalline film, i.e. the former has a rotational degree of freedom about the fiber axis whereas the latter does not. The theory does not explain the transition between texture and monocrystallinity. Further, the theory is inconsistent with the observations that show that during the deposition process a fiber texture can develop in the later deposited fraction of the film thickness over the initially deposited polycrystalline layer.[A3] Thus, the proposed nucleation origin of texture cannot be a general mechanism for texture. Finally, there is no reason known to this writer why a two-atom critical cluster necessarily produces a {111} oriented three-atom nucleus and why a three-atom critical cluster must necessarily have an arrangement of the atoms (one that produces the square orientation associated with the {100} oriented nucleus) different from that for a three-atom nucleus promoted to this state by the addition of one atom to a two-atom critical cluster (a triangular arrangement associated with the {111} orientation). A more reasonable explanation for the existence of one crystal orientation common to different isolated islands, which is the experimental inspiration for the nucleation theory of texture, that has been observed in experiments[A4] concerning nucleation of metals on alkali halides, mica, and similar non-epitaxial substrates is graphoepitaxy-induced orientation of such islands via the pattern of cleavage striations and ledges on such substrate surfaces. In the latter case, the observed epitaxial temperature corresponds to the required mobility for metal atom clusters to migrate and rotate on the substrate surface.

A1. T.N. Rhodin and D. Walton in **Single Crystal Films**, eds. M.H. Francombe and H. Sato, Pergamon, Oxford, 1964, p. 31.
A2. M. Ohring, **The Materials Science of Thin Films**, Academic Press, Inc., San Diego, CA, 1992, p. 205.
A3. K.K. Kakati and H. Wilman, J. Phys. D6, 1307(1973)
A4. H. Poppa, in **Epitaxial Growth**, ed. J.W. Matthews, Academic Press, NY, 1975, p. 248.

Appendix 3

The temperature independence of the average grain size for films deposited on non-epitaxial substrates below a homologous temperature of 0.12, shown in Figure 3.2, indicates that this grain size is not a function of nucleation and surface diffusion. Rather, the grain size is more likely determined by the concept considered in Appendix 1 of Chapter II.

Appendix 4

Texture has several origins. In section 2.2.2 of this chapter it was proposed that one origin of the <111> texture in sufficiently thin films is secondary recrystallization in which the grains with lowest surface energy have the least free energy. In thicker films and at temperatures that allow grain boundary migration the text suggests that another driving force, the minimization of the strain energy associated with film stress, controls. These suggestions still seem valid in that there are no observations that contradict the hypothesis when no other factors override. Odd textures not corresponding to those obeying the above two driving forces may arise. For example, hyperthermal beam collimation and grain orientations that allow channeling to occur in some of the grains may bring about a texture of the grain orientations for which channeling is maximized. Either channeling minimizes sputtering of these grains during deposition or minimizes the energy due to defects generated by the hyperthermal beam so that the driving force for grain boundary migration is into the grains having higher defect content. The latter actions bring about the (110) texture in fcc films.[A5]

A5. L. Dong and D.J. Srolovitz, J. Appl. Phys. 84, 5261(1998).

Appendix 5

Mitra et al.[A6] observed equiaxed grains in thick Ni films above the initially deposited and grown columnar grains for room temperature, magnetron-deposited nickel. This observation implies that nucleation and growth of grains can occur. This implication has been accepted in the text for the case where hyperthermal incident beams with energy higher than 500 eV are present. It is unlikely that the energy of the magnetron beam in the absence of bias was this much high in experiments of Mitra et al. Hence, their observations do not concur with those described in this chapter. The transition from columnar to equiaxed occurred with increasing thickness, decreasing deposition rate on room temperature deposition and the onset of 100 volts negative bias. An explanation of the difference in conditions responsible for the formation of equiaxed grains between those cited in the text and Mitra et al. has not yet

been given. However, one speculation is that the critical bias voltage above which equiaxed grains are nucleated depends upon the ion/atom arrival ratio which, as noted in section 3.2.2, is a parameter that affects the texture. The change in texture observed by Mitra et al. upon formation of the equiaxed grains from a strong <111> texture in the columnar films to a weakened <111> and strengthened <100> texture in the equiaxed grain films may be a key to the explanation. The <100> texture in fcc metals is believed, as noted in the text, to stem from the driving force toward a lower free energy corresponding to a decrease in the strain energy due to the intrinsic tensile stress developed in these films. Thus, the minimum hyperthermal beam energy required to bring about recrystallization may depend on the level of the intrinsic tensile stress, which in the films of Mitra et al. are at the level of 1 GPa, the level of the yield strength of Ni. These concepts suggest that recrystallization in depositing films depends upon the same factors determining the onset of recrystallization in cold-worked metals: the existence of sufficient stored excess energy (dislocation tangles, etc.) and sufficient probability of activating the recrystallization process (local temperature, time). Thus, the critical hyperthermal beam energy needed to induce recrystallization during deposition may vary with deposition conditions, material being deposited, etc. It is surprising that equiaxed grains were found in room temperature deposition of Ni in the absence of bias in thick films upon a thinner columnar grain base. However, there are still reflected neutral argon atoms with incident hyperthermal energy incident upon the growing film at zero bias. Since recrystallization during thermal deposition has never been found it appears that these hyperthermal atoms may be the activating triggers of recrystallization at room temperature in a sufficiently thick Ni film in the experiments of Mitra et al. That said, another explanation of the results found by Mitra et al. is as follows.

As noted in the text, Kakati and Wilman found that when other {111} facets develop in (111) oriented columnar grains then secondary twinning can occur during deposition to yield what appears to be equiaxed grains. Such secondary twins can give rise to multiple twinning orientations (and the appearance of equiaxed grains) leading to a diminution in the <111> texture and the growth of <100>, <110>, and random textures with increase in thickness. In a recent study of texture formation in electroplated Cu[A7] this sequence of events was verified via X-ray pole figure analysis. Evidence was found for multiple twinned grains in as-deposited samples, such grains corresponding to about 20% of the volume. The formation of twins on {111} facets does not require recrystallization in the normal sense of this term. Such twins can be produced directly by deposition, as noted in the text in section 2.2.2 of this chapter. It seems reasonable then that multiple twinning can occur in the deposition of Ni in the experiments of Mitra et al. These authors do report that "The grains tend to possess twin relationships in many cases, or have low-angle boundaries between them". Unfortunately, Mitra et al. did not carry out the requisite X-ray analysis to evaluate the presence of multiple twinning. Thus, which of the above two explanations for their observation of equiaxed grains at low to zero bias voltage is valid is not known.

A6. R. Mitra, R.A. Hoffman, A. Madan and J.R. Weertman, J. Mater. Res. 16, 1010(2001).
A7. M.T. Perez-Prado and J.J. Vlassak, Scripta Mater. 47, 817(2002).

CHAPTER IV

Epitaxial Structures

Epitaxy was defined by Royer[1] as the oriented growth of one substance on the crystal surface of another substance. At this writing this definition belongs to what is called heteroepitaxy. The oriented growth of a substance on the crystal surface of the same substance is now called homoepitaxy. In the previous chapter we called the process of extending the grain structure by deposition, without the formation of grain boundaries between the deposit and the substrate, granular epitaxy. The latter is a form of homoepitaxial deposition.

The defects contained in epitaxial monocrystalline films are the main subject matter of epitaxial structure. These defects are produced in the deposition process. Also, there are unique epitaxial structures, such as superlattices involving alternate sets of atomic planes of different species, vertically integrated circuits and quantum wells, wires, and boxes. These unique geometric arrangements or epitaxial units also have their associated defects, which are mainly of interfacial origin.

An exploration of the factors controlling the different modes of epitaxial deposition is carried out in Section 1. Section 2 considers defects and their origins in homoepitaxial films grown layer-by-layer.

Heteroepitaxial films may involve small or large misfits between the lattice parameters of the unit cells of film and substrate. In the former case, as the film thickens during deposition the first few monatomic layers tend to grow pseudomorphically, adjusting the unit cell dimensions of the film to that of the substrate in their common coherent interface. There are a variety of pseudomorphic films. The crystal structure of these films may be the bulk stable structure or a bulk metastable one. The latter is said to be pseudomorphically stabilized. These films are usually elastically strained. Alloy films can be pseudomorphically stabilized as supersaturated solutions. With film thickening the film/substrate system can become more stable thermodynamically by destroying the coherent interface and developing a discommensurate one through the production of misfit dislocations or via a phase transformation. These subjects and the defects unique to these films are considered in Section 3.

Heteroepitaxy is found to occur also when the misfit between unit cells of epilayer and substrate, having the same symmetry, is large or when these unit cells have different symmetry. Possible principles controlling these relationships are explored in Section 4 for metal/metal and metal/semiconductor interfaces.

In 1975, when the now classic book edited by Matthews entitled *Epitaxial Growth*[2] appeared, the concepts then current concerning epitaxy were obtained

from studies of heteroepitaxial deposition onto crystal surfaces formed by cleavage of single crystals, such as alkali halides and mica, for the most part. What was not known at that time and is known now is that the type of epitaxy studied in this way, for the great majority of these studies, belongs to the class called graphoepitaxy or artificial epitaxy. The crystallographic relations between film and substrate in these studies are independent of any bonding that exists across the film–substrate interface, but are entirely dependent on features, such as cleavage steps, that exist on the surface of the substrate. The lack of rules concerning epitaxy that arose from these studies on cleavage surfaces of non-metallic crystals can now be understood in terms of this insight concerning the origin of this epitaxy – that these examples of epitaxy are manifestations of graphoepitaxy. We shall therefore consider the structure of films produced via this mode in Section 5 of this chapter on graphoepitaxy.

1. Modes of growth in production of epilayers.

1.1. Modes of growth.

The three modes of growth have been discussed in a previous section. Here we are interested in the possible effects of these modes of growth on the structure of epilayers. The production of pseudomorphic epilayers and useful device structures is facilitated by the absence of mobile dislocations in the epilayer/substrate system. Dislocations, twins and stacking faults are readily incorporated into the epilayer at the interfaces of impinging islands.[2a] Hence, the island and Stranski–Krastonov (S–K) modes of growth are avoided in the deposition of epilayers. A necessary condition to avoid island growth on a substrate is for the quantity $S = (\gamma_s - \gamma_e - \gamma_i)$ to be greater than zero, where γ_s is the substrate–vacuum surface energy, γ_e is that of the epilayer and γ_i is the substrate–epilayer interface energy. However, as noted by Grabow and Gilmer,[3] at thermodynamic equilibrium the Frank–van der Merwe (F–M) or layer-by-layer growth mode is limited to the case where there is zero misfit between the epilayer unit cell and the substrate unit cell. Any misfit strain destabilizes the F–M mode. In practice, fortunately, this limitation is often avoided. One explanation for this observation is that the production of islands in S–K growth requires nucleation.[4] Another is that the production of islands on a flat film, as in S–K growth, requires the film to become unstable with respect to periodic perturbations in film thickness.[5] The latter mode of instability can occur more readily than the first-order transition corresponding to nucleation, as in the analogous spinodal decomposition mode of a metastable solid solution. Bruinsma and Zangwill[5] have shown that flat films are morphologically stable during growth up to film thicknesses equal to the critical thickness at which the homogeneously strained pseudomorphic film has a higher free energy than one containing some

misfit dislocations. We consider the latter subject later in this chapter. Incidentally, if the island or S–K modes of growth are observed then we may conclude that the film thickness has exceeded the critical thickness, as defined above. However, if these modes are not observed then we may not make the inverse conclusion that the film thickness is less than the critical thickness. The film thickness may exceed the critical thickness as a consequence of activation energy barriers to the motion or nucleation of dislocations, which are significant in semiconductor materials. Let us now consider some techniques used to promote F–M growth at the expense of the other modes.

Surfactants have been used to reverse the inequality $S < 0$, to make S exceed 0. For example, it has been found that the growth of Ge on a Si substrate can be changed from the island mode to the F–M mode by use of Sb as a surfactant.[6] The mode of growth on ionic compounds may be affected by alteration of the surface composition as by electron beam exposure. A result of this exposure may be a decrease in the substrate/epilayer interface energy, sufficient to make the sign of S change from negative to a positive value. It is believed that this result occurred in the experiments of Kanemaru et al.[7] who found it possible to prevent the island mode of growth of Ge on CaF_2 by exposing the surface of the latter to an electron beam. It has been found possible to suppress island nucleation during the S–K mode of growth of GaAs on Si(100) by impinging a low-energy (28 eV), high-flux ($\approx$0.4 mA/cm^2) of Argon on the growing surface during MBE.[8] The mechanism for the latter result is not known. However, one mechanism for the beneficial effect of a surfactant on defects associated with an epilayer has been deduced from ingenious observations.[78]

1.2. Modes of F–M epilayer growth.

It is believed that there is a critical temperature above which epitaxial deposition occurs via the migration of terrace steps without the nucleation of adatom clusters on the terraces. Given a knowledge of the distance between adjacent steps, as can be estimated from the off-axis misorientation of the substrate surface, equating this distance to the diffusion length, X, and using the relation $X^2 \approx (\pi^2/4)D\tau$, a critical value of the surface diffusivity D can be evaluated corresponding to a critical diffusion time τ, that is defined by the condition that an adatom not collide with another adatom during its diffusion from point of incidence to the nearest ledge. This condition is expressed by the relation

$$1 = \tilde{N}^*KX\tau/a$$

where $\tilde{N}$ is the deposition rate in monolayers/s, a is the lattice parameter of the cubic unit cell and K equals 4 for the diamond cubic structure and $\sqrt{2}$ for the face-centered-cubic (fcc) structure. Substituting, yields

$$D = (4K/\pi^2)\tilde{N}X^3/a$$

Flynn[9] pointed out that the maximum value of X is about 10^{-5} cm. Hence at a deposition rate of about 1 monolayer/s D will equal about 3×10^{-8} cm^2/s. To be safe Flynn[9] chose the minimum limiting D value to equal 10^{-7} cm^2/s for terrace ledge migration to be the mode of growth and then used this concept to prepare a figure equivalent to Figure 4.1 to define the critical temperature for onset of the step flow mode of deposition. Our figure differs from his quantitatively, but not qualitatively, to refine the plot to include the dependence of the surface diffusivity on the surface orientation.

Just below the critical temperature for onset of step flow, deposition is believed to occur via the nucleation of two-dimensional adatom clusters and two-dimensional growth of these clusters. The result of this mode of growth is that planar regions alternate between being planar and rough on an atomic scale. This mode of deposition gives rise to oscillations in the RHEED pattern from such film surfaces during deposition. The lower critical diffusivity for RHEED oscillations

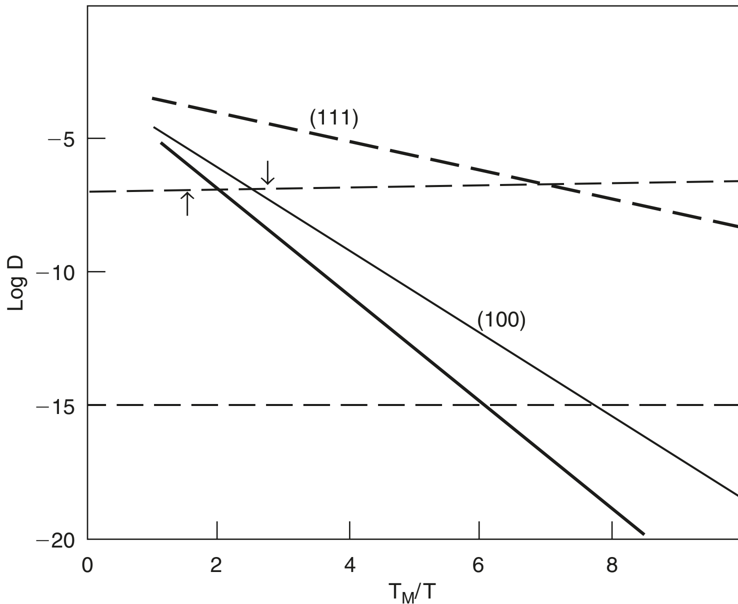

Figure 4.1. Surface diffusion coefficients for metals (light lines) and semiconductors (dark line). The lowest diffusivity for RHEED oscillations is about 10^{-15} cm^2/s, as shown by the lower horizontal dashed line. These oscillations disappear above a surface diffusivity of about 10^{-7} cm^2/s (the upper dashed horizontal line), when ledge migration becomes the growth mode. See text for significance of arrows.

may be estimated from the previous relation for the diffusion length setting it equal to a diffusion jump length and setting the allowed time for diffusion equal to $1/\tilde{N}$ to obtain $D = 10^{-15}$ for $\tilde{N} = 1$ monolayer/s. The corresponding critical temperatures are shown in Figure 4.1. This estimate is obviously rough. A more rigorous evaluation of the critical temperature below which three-dimensional island growth will occur must consider both the size of the two-dimensional adatom clusters as a function of temperature and the adatom diffusion distance as a function of temperature. By equating these two lengths we would then obtain a relation defining the lower critical temperature for RHEED oscillations. Unfortunately, we do not have values for the parameters in this relation so that a more rigorous evaluation of this critical temperature is not justified at this time.

Below this lower critical temperature deposition proceeds so as not to produce planar facets on the film surface, i.e. the surface is rough with island heights greater than one monolayer. Since the diffusion distance is now no more than an interatomic spacing the temperature is in the range where shadowing can lead to the development of voids.

Above the upper critical temperature for RHEED oscillations growth proceeds by terrace ledge migration. For this mode to occur without volume diffusion this critical temperature must be smaller than the freezing-in temperature for volume diffusion. The latter temperature for metals, as Flynn has estimated it,[9] equals about $3T_M/8$, whereas for semiconductors it equals about $0.64T_M$. The former temperature is indicated by a downward pointing arrow and the latter by an upward pointing one in Figure 4.1. The conclusion drawn from comparison of these data is that bulk diffusion occurs along with ledge migration on (001) metal surfaces, whereas ledge migration on semiconductor and (111) metal surfaces can occur in the absence of bulk diffusion.

Superlattices have been produced in both the terrace ledge migration and RHEED oscillatory regimes. The known effects of deposition in each regime on epitaxial structure are discussed in the following sections. One-dimensional structures can be produced in both regimes by suitable sequencing of alternate compositions in deposition onto vicinal surfaces with small tilt angles from a low index orientation. The architecture produced by this mode of deposition has been termed a tilted superlattice (TSL).[10] The epitaxial structure of TSLs is discussed in Section 3.

The brief discussion given above of the modes of epitaxial deposition ignores many details involved in the deposition process: the nature of the surface reconstructions on terraces, steps and kinks along these steps; the mode of diffusion of adatoms on terraces (channel steered walk or random walk); the mode of attachment of adatoms to steps; the mobility of adatoms and their clusters; the mode of attachment of adatoms to clusters; the mode of production of three-dimensional islands; the effect of low energy bombardment during deposition on the growth modes; the exchange of adatoms with subsurface atoms; the tendency for adatoms of one species to segregate at the surface, etc. All these aspects of epitaxial deposition

are the subject of current research. Their known effects on the structure of epitaxial films will be discussed at the appropriate places in the remainder of this chapter.

2. Defects produced in homoepitaxial layers.

2.1. Point defects and their clusters.

An implication of the terrace ledge migration (step flow) growth mode is that it occurs in such a way that no excess vacancies are introduced into the lattice of the growing film. Conversely, it seems reasonable to expect that excess vacancies will be incorporated into the film in the oscillatory mode of producing planar ledges on the film surface. Indeed, Roland and Gilmer[11] have found that adatoms do exchange with subsurface atoms in their molecular dynamic (MD) simulation of homoepitaxial growth in the RHEED regime. Such vacancies in the penultimate surface planes have the possibility of diffusing to the film surface before the latter is covered during deposition. This problem was treated in Chapter II, where it was found that the critical temperature for the freezing-in of subsurface vacancies in fcc metals equals about $0.12T_M$. The lower critical temperature for RHEED oscillations in metals is about $0.125T_M$ whereas the upper critical temperature is about $0.375T_M$. Thus, it appears unlikely that excess vacancies are frozen-in during the epitaxial deposition of fcc metals at substrate temperatures in the RHEED oscillation regime.

The vacancy migration activation energy is not well established for semiconductors. Some investigators[12] believe that it is high enough to immobilize vacancies. However, values measured by Watkins[13] and assigned to the vacancy migration energy equal about 0.4 eV for Si. Further, a recent molecular dynamic simulation[14] provides a value of about 0.4 eV for the migration energy of a neutral vacancy, and values for the migration energy of a self-interstitial that agree with values obtained independently by another MD simulation,[15] and for the activation energy for diffusion that is in agreement with experiment. Hence, it appears likely that excess vacancies are not frozen-in above room temperature in either Si or Ge. For there to be a reasonable chance to form less mobile divacancies, the probability of a two vacancy collision must be high. Given that the number of jumps that deposition formed vacancies make in their walk to the surface probably is no greater than about 10 then the concentration of deposition-induced vacancies must exceed 0.1 for divacancies to be formed by collision. All the evidence from scanning tunneling microscopy (STM) and MD simulations suggest that the concentration of deposition generated subsurface vacancies is much smaller than 0.1. Hence, vacancies, divacancies and other defects due to the condensation of vacancies are not likely to exist in epitaxial elemental semiconductor films, except perhaps in films subject to energetic bombardment during deposition.

The possibility that vacancies can be bound to traps, such as solute atoms, or satisfy thermodynamic stability requirements, suggests that vacancies can be present in both semiconductor alloy and compound epilayers.[16]

The evidence this writer has discovered concerning the concentration of deposition-induced vacancies relates to metal films. One is due to the work of Lloyd and Nakahara[17] referred to in section 2.1.1 where it was shown that excess vacancies captured during low energy deposition of gold at room temperature diffused to sinks, such as voids, in subsequent annealing at room temperature. This work also reports estimates of the deposition-induced vacancy concentration in metal films deposited at room temperature from thermally induced vapors, which yield the value of 1% as the best value. The other in Appendix 3 of Chapter II reveals that vacancies in Cu must be deposited below 150 K to be frozen-in during deposition.

An MD simulation of the effect of 10 eV Si^+ incident on Si(001)2 $\times$ 1 performed by Kitabatake et al.[15] found hexagonal and split interstitials to be introduced into the lattice and the activation energy necessary for their removal from the lattice by diffusion to the surface to vary from 0.92 eV (hexagonal) to 1.48 eV (split, in the fourth layer beneath the surface). A rough calculation shows that such defects will be frozen-in at deposition temperatures below 85°C (hexagonal) and 300°C (split). Although the former is not, the latter is, an attainable deposition temperature for energetic, particle assisted, epitaxial deposition. Hence, it is possible that split interstitials may exist in such deposition of Si. No vacancies were found in this simulation in agreement with the tentative conclusion made above.*

Hsu et al.[18] have found dislocation loops in remote plasma chemical vapor deposition (RPCVD) of Si(100) at temperatures lower than 300°C at a power level having a plasma potential of 50 V and a plasma density of $10^8/cm^3$, but not at a lower power level input to the plasma. They stated their belief that these loops were due to collapsed vacancy platelets. However, these loops may have had an interstitial origin since no evidence was presented to distinguish between the two origins. Unfortunately, no estimate was given of the ion/atom flux ratio to provide an estimate of the bombardment induced vacancy concentration at a distance below the surface corresponding to the range of the energetic ions. No dislocation loops have been observed in Si homoepitaxially deposited at substrate temperatures above about 450°C with or without low-energy ion bombardment during deposition.[18] Since the probability of immobile divacancy formation is independent of the temperature it seems that the observed dislocation loops are more likely to be a consequence of interstitial condensation. Stacking fault tetrahedra in P^+ ion implanted Si originating from vacancy condensation have been reported[19]

* 20 eV Si ion-assisted deposition on Si(100) at 460°C resulted in a point defect density of $10^{13}/cm^3$. Such deposition at other temperatures but less than 550°C or on Si(111) resulted in higher point defect densities. However, above 550°C point defect density was less than minimum observable limit on (100) deposition.[118] See Appendix 1 for fuller description of these results.

along with the remark that "this (fault) is the only vacancy type defect reported in silicon". In this case, vacancy annihilation at the surface is unlikely due to the long range of the incident ions and this observation does not confirm the presence of deposition or low-energy bombardment-induced vacancies in Si.

Kohyama and Takeda[20] and others have observed {113} planar defects that are believed to originate from the condensation of bombardment-induced self-interstitials.[21] Although it has been claimed that the {113} defects form at C atom traps in the Si lattice Kohyama and Takeda[20] show that it is possible for these defects to form in pure Si.

For still lower substrate temperatures, voids that may be interconnected can be expected to form under the influence of the phenomenon of shadowing. In Chapter II it was shown that these voids were believed to be associated with inter-columnar boundaries. Long layer like "voids" have been found in a three-dimensional MD simulation of the low temperature deposition of nickel.[22] Also, columnar growth, with column widths of 20 nm, has been detected in the room temperature formation of Co–Pd multilayers in epitaxial deposition,[23] but not yet been reported in homoepitaxial deposition. Further, there exists indirect evidence for interconnected void-like space in experiments involving the room temperature heteroepitaxial deposition of Rh on a Ag substrate. These two metals are immiscible. Nevertheless, after this bilayer was heated to 400°K Ag was found on top of the Rh layer.[24] There is a great need for further research in this area to characterize the structure of homoepitaxial metal films formed on a substrate to which the film atoms bond strongly, at temperatures below the T_1 of Movchan and Demchishin (see Chapter II) and in ultra high vacuum chambers ($<10^{-10}$ Torr).

2.2. Line and planar defects.

Impurities, unclean areas on the substrate surface, and dislocations in the substrate that intersect the substrate surface and have a component of their Burger's vectors normal to the surface greatly facilitate the production of stacking faults and other defects in the non-energetic, homoepitaxial deposition of semiconductors and metals. This subject is discussed in detail in many reviews,[33] is the subject of an ongoing series of publications[34] and will not be considered here. Low-energy deposition of Si^+ ions can yield defects[118] as already noted in MD simulations. Dislocation loops have been observed at the end of the range of high energy ion-bombarded Si due to the condensation of interstitials. The presence of impurities makes this process more likely. Also, it is important to note that stacking faults that originate from impurities or unclean substrate surfaces appear for any surface orientation.

In the first edition of this book it was conjectured that the origin of the stacking faults in deposition onto clean and defect-free (111) or equivalent

plane* is the existence of two sets of sites at which adatoms sense local minima in the potential energy. One set of these sites corresponds to the normal stacking of (111) planes for the crystal structure. The other set of sites corresponds to the stacking of similar planes of atoms but one for a different crystal structure (e.g. hexagonal-close-packed (hcp) stacking versus fcc stacking of close-packed planes of metals). Although the energy associated with these two sets of sites are not the same, still the difference in this energy is small enough to not make one set so favored that all adatoms on the (111) surface always occupy this set of sites. Although this conjecture seems not to have been accepted in the literature, just before this revision was written a paper appeared[119] that provides the first evidence for its validity.

This "proof" is based on the agreement between experiment and a quantitative theory governing the formation of the intrinsic adatom clusters in positions of stacking faults, in the absence of adjustable parameters.[119] These observations consist of STM measurements of the ratio of the number of fault adatom islands to non-fault islands with the island identification determined by the orientation of the islands' perimeter. This ratio was measured as a function of deposition temperature and incident flux of Ir atoms. The identification method was verified by supplemental measurements of the tunneling STM tip currents through such islands and the different heights of such islands above the substrate.[120] The reader is referred to the original paper[119] for a detailed explanation of the theoretical models used to evaluate the numbers of stacking fault islands and non-fault islands. The figure that compares theory and experiment is given in Appendix 2 along with a brief description of the theory.

For a full appreciation of the concept governing the observation of fault islands in this experimental setup the reader is referred to the original article. Suffice it to say that kinetic considerations govern the appearance of the fault islands as is apparent from the dependence of this probability of observation on temperature and rate of deposition and that at each deposition temperature island clusters smaller than a critical size are mobile while those larger than this size are not mobile. Further, from the agreement between theory and experiment it is reasonable to conclude that fault islands are produced during MBE deposition onto (111) planes by occupation of the set of sites corresponding to a stacking fault in the fcc lattice in the absence of catalysts (e.g. impurities, defects) tending to direct such occupation. It is apparent from Figure 3.A2 in Appendix 2 that there is a deposition temperature above which fault islands do not appear during deposition and, hence, stacking faults will not be produced via this homogeneous nucleation procedure above this transition deposition temperature (a homologous temperature of 0.23 in Figure 3.A2). This writer believes that such homogeneous nucleation of stacking

* By equivalent is meant any plane that contains more than one set of minimum potential energy sites for adatoms, each set corresponding to a different stacking sequence of the atoms in the adatom plane relative to the surface plane.

faults during deposition onto (111) and basal planes exists not only for fcc and hcp metals, but also for semiconductors with the diamond cubic, sphalerite and wurtzite structures. This is not to say that other origins for stacking fault production do not exist. However, the homogeneous nucleation origin of stacking faults is universal to the crystal structures that satisfy its requirements, whereas the heterogeneous nucleation, extrinsic origin is specific to the particular deposition situation (i.e. impurities present, defects in the substrate, hyperthermal beams forming defects, etc.) and is not necessarily limited to deposition onto a (111) or (00.1) basal plane.

Given the above knowledge let us now consider the literature. Clean deposition onto Cu(111) at and above a homologous temperature of 0.21 did not reveal adatom islands in fault sites.[121] However, this homologous temperature is at the tail end of the probability distribution shown in Figure 3.A2 where the ratio of fault island population to non-fault island population is 0.02. Fault islands were found in this study on terraces of (111) planes slightly off the normal to the film plane. The authors attributed their formation to strain along the terraces between the steps. These observations do not invalidate the theory of homogeneous nucleation of the fault islands proposed in Ref. [119].

In normal MBE deposition of homoepitaxial Si onto substrates that do not have dislocation intersections at the substrate surface, stacking faults are not found in films deposited at temperatures above about 700°. In MBE deposition onto Si(100) no stacking faults are found even in films deposited at much lower temperatures (100°C).[28] However, deposition onto Si(111) at lower deposition temperatures (i.e. less than about 450°C (homologous temperature of 0.43)) but above the temperature at which amorphous films are formed (homologous temperature of 0.34) results in the formation of stacking faults and extended defects.[27] The transition temperature below which stacking faults are produced and above which stacking fault free films are deposited seems to be a function of deposition rate. The slower is this rate the lower is this transition temperature. Although this homologous temperature is higher than that for metals noted above (0.23) the behavior described is the same as that described for metals.

Recent belief is that these faults stem from the 7×7 reconstruction on Si(111) for which one-half the unit cell consists of a stacking fault which can be inherited by the bulk during growth. However, the observations of intrinsic stacking fault formation on (111) in diamond and GaAs, which have different reconstruction patterns as noted below, place this conjecture in doubt. Further, argument against this conjecture follows from the data given in Gossmann[39] and Weir et al.[27] concerning the reordering of surface reconstructions. These reorderings take place at about 100°C lower than the transition temperature between amorphous and epitaxial deposition for both the {100} and {111} surfaces of Si. Reordering of the surface reconstruction allows the deposition to reproduce the substrate crystal lattice, i.e. when the adatom becomes subsurface the reordering of the reconstruction causes this adatom to end up on a bulk crystal lattice site.

Stacking faults and twins are ubiquitous in the homoepitaxial CVD of {111}diamond, but are absent in such deposition of {001}diamond.[29] As already noted, stacking faults that originate from impurities or unclean substrate surfaces appear for any surface orientation. Hence, it is likely that the defects observed in the {111}diamond CVD arise from an intrinsic source during deposition. Using the homologous temperature corresponding to the freezing-in temperature calculated above for Si (0.43) we obtain that the corresponding freezing-in temperature for stacking faults in diamond is predicted to be about 1564°C, i.e. this is a hypothetical temperature because graphite is produced above about 1200°C in this deposition process. The much larger temperature window in which these faults are observable in diamond compared to Si is a consequence of the much lower homologous temperature for the amorphous to crystalline transition in diamond, as compared to Si, i.e. about 0.25 versus 0.34. Finally, it should be mentioned that the reconstruction pattern of C(111) in the diamond structure is 2×1 and not 7×7.[122]

Stacking faults and twins have been observed also in the homoepitaxial deposition of GaAs($\bar{1}\bar{1}\bar{1}$) at a substrate temperature of 500°C[30] and 565°C,[31a,b] but not in the equivalent deposition onto GaAs(100).[32] Further, it has been reported that the twin density is significantly reduced on deposition onto GaAs($\bar{1}\bar{1}\bar{1}$) when the deposition temperature is above 600°C.[30,31b] The transition between step migration and RHEED oscillation deposition modes occurs between 550 and 600°C for GaAs. Further, the reconstructions of the GaAs(111) do not include the 7×7 but do include the 2×2 and $\sqrt{19} \times \sqrt{19}$.[123] That stacking faults and twins are formed in the RHEED oscillatory temperature regime on a GaAs($\bar{1}\bar{1}\bar{1}$) surface, but not in the step flow regime, and that deposition on GaAs(001) in the RHEED oscillatory regime does not produce these defects are facts that are consistent with the hypothesis that these defects are produced by growth faults emanating from differently oriented clusters on a given ($\bar{1}\bar{1}\bar{1}$) terrace.

It is apparent that much remains to be done before the origin of intrinsic stacking faults is securely established. Among the questions that need answers are: why is the homologous transition temperature separating stacking fault deposition from stacking fault-free deposition different for semiconductors and metals? how do the parameters that affect the probability of stacking fault nucleation vary between (111) surfaces that are ledge free and (111) surfaces between steps? will deposition at homologous temperatures much below 0.23 on Cu(111) and other metal(111) surfaces yield stacking fault island clusters, as required by the theory?

After the coverage during deposition approaches unity so that fcc and hcp clusters contact then a self-healing process occurs in which the fcc clusters grow at the expense of the hcp clusters.[124] For sufficiently high deposition temperatures this self-healing process can lead to the removal of nearly all the hcp clusters during deposition. Those stacking faults that are not removed during deposition may be removed by higher temperature annealing. Studies of the removal of twins and stacking faults from bulk metals[38] suggest that this process occurs at rates equivalent to that

associated with grain boundary migration. If this turns out to be a valid suggestion then the lowest homologous temperature for the annealing-out of any stacking faults and twins produced in homoepitaxial deposition would be between 0.15 and 0.25, i.e. in the neighborhood of the temperature above which fault clusters do not form on deposition.

3. Defects in pseudomorphic films.

3.1. Coherent (commensurate) pseudomorphic films.

In the small misfit class we can expect the unit cell structure in the crystal planes of film and substrate that adjoin the common interface to be the same or that for the film to be deformable to the unit cell structure of the substrate. Further, the lattice parameters of the epilayer unit cell and substrate unit cell will be the same initially, as film deposition proceeds from the thinnest layer. The film having this characteristic is called pseudomorphic. It has a coherent (commensurate) interface with the substrate. The principle that governs deposition at this stage was first enunciated by Frank and van der Merwe.[40] It is that thermodynamics controls to produce the equilibrium, minimum free energy, configuration of the substrate/film system. (The statement that the pseudomorphic film/substrate system is in its lowest free energy configuration at film thicknesses less than the critical thickness is not strictly true because it neglects a modifying restriction. The latter is that the temperature is low enough that atomic diffusion cannot occur.) Since any non-zero misfit introduces strain energy into the pseudomorphic film, which increases with increase in the thickness of the film, whereas the interface energy between a non-strained film and substrate is independent of the film thickness, it is apparent that there will be a critical thickness below which the pseudomorphically strained film configuration will have the lower free energy, but above it the strain-relaxed film, separated from the substrate by a discommensurate interface having excess energy, will have the lower free energy. We shall consider the commensurate–discommensurate transition in a later subsection.

There are two classes of pseudomorphic films. One consists of stable crystal structures that may or may not be strained. Metastable phases, which also may or may not be elastically strained, comprise the second class.

What types of defects can develop in these films in addition to those found or expected in homoepitaxial films? One type of defect in pseudomorphic superlattice films consists of a diffuseness of the interface between layers, or rows, or between the substrate and the adjacent layer. Another type of defect in solid solutions involves deviation from the desired atom distribution in the solid solution layers. Usually this desired distribution is a random one. A third type of defect

relates to the distribution of elastic strain in each layer. Usually the desired distribution is to have the elastic strain the same throughout a given layer. In this case, static or dynamic perturbations that may cause the strain to have a non-uniform distribution are undesired defects. Finally, it is usually desired for the interfaces to be strictly planar and then any deviation from such planarity must also be considered to be a defect.

3.1.1. Interfacial defects.

An observation of Rowland and Gilmer,[11] who performed an MD simulation study of atom dynamics during deposition, is significant to note at this point. They found that adatom exchange with vacant sites in the first two subsurface layers contributed to the "observed" adatom diffusivity in the RHEED oscillation deposition regime. This observation suggests that there is sufficient mobility at interfaces between pseudomorphic films and substrates deposited in the RHEED oscillation temperature regime, when they are within three monolayers of the surface, to produce diffuse interfaces should the free energy decrease thereby. There are at least three possible reasons for the free energy to decrease in the transition from a sharp to a diffuse interface. One is if this process increases the entropy of mixing negative contribution to the free energy more than any positive increase due to the enthalpy of mixing. Another is a decrease in the enthalpy due to a decrease in the interface stress on atom interchange across interfaces.[41] The third is a decrease in the free energy due to Gibbs adsorption when the interface is within three monolayers of the surface.

Evidence for mixing that yields diffuse interfaces as a consequence of the third driving force has been found by Matsuhata et al.[42] They found that intermixing occurred at Ge/Si interfaces when Si was the overlayer, but did not occur when Si was the underlayer. It was stated that this intermixing was occasioned by the tendency for Ge to occupy surface sites due to its lower surface energy as compared to Si. This statement is probably correct in that the free energy would be increased by exchange of a surface Ge atom on a Si sublayer with a Si atom even though this exchange would lower the free energy per unit volume of the Si layer, because the free energy of the system would be increased by replacement of the surface Ge atom by a Si atom. This interfacial mixing defect is also likely to occur in the terrace migration growth regime above the upper critical temperature for RHEED oscillations. There is a small temperature window in this regime where bulk diffusion will not occur in semiconductor systems. Matsuhata et al.[42] observed that these Si/Ge superlattices were not homogeneously strained. Similar effects possibly due to intermixing at the interfaces of different composition layers have also been reported in the InAlAs/InP system.[43] Another manifestation of interface mixing has been found by Tromp et al.,[41] who suggested that decrease in the interface

stress by atom interchange at the interface acts to drive such interchange. Evidence has also been found for mixing at compound semiconductor interfaces via scanning tunnelling spectroscopy.[44] The driving force for this mixing is not known, but it may involve a combination of all three listed above. Defects at the interfaces of tilt superlattices will be more significant than in planar superlattices because of the much higher ratio of interface area to volume of the superlattice rod morphology.

Another interfacial defect may occur in multilayers, whether they are pseudomorphic or not. This defect is that of interface roughness. One obvious source of this roughness is due to the deposition temperature being in zone 1 as described in Chapter 2 and Table 2.1.

3.1.2. Defects in pseudomorphic solid solutions.

The use of a substrate producing a coherent interface with a metastable solid solution and lattice parameter matched to it will stabilize the latter if the decrement in interface energy associated with the stable phase mixture on this substrate exceeds the increment in the volume free energy.[47,66] However, if the composition and substrate temperature are within the spinodal limits then spinodal decomposition may occur. Also, the critical temperature for the miscibility gap may be higher in thin films than in bulk due to the loss of the coherency stress component normal to the film plane for spinodal wavelengths exceeding the film thickness. Evidence for spinodal decomposition in such films has been found by many investigators.[45] For example, InGaAs and InGaAsP solid solutions decompose spinodally via adatom diffusion during deposition onto an InP substrate. These solutions are metastable with respect to phase separation,[46] and are above the miscibility gap critical temperature for spinodal decomposition in bulk samples,[47] but not necessarily in thin films. An extended discussion of the bases for calculation of phase diagrams in ternary and quaternary semiconductor systems is given in Stringfellow's book.[47] The theory of spinodal decomposition in thin films has been considered by Bruinsma and Zangwill.[64]

Evidence for *composition fluctuations in the presumably stable solid solution range of compositions* in these semiconductor alloys which have positive enthalpies of mixing has been deduced by Cherng et al.[48] They found that the half-width of a low temperature photoluminescence peak induced in these alloys, normalized by the composition dependence of the band gap, correlated with the ratio of the miscibility gap critical temperature to the growth temperature. In particular, as shown in Figure 4.2, the closer is the deposition temperature to the miscibility gap critical temperature (from above) the broader is the normalized PL half-width. Such composition fluctuations have been studied by Warren,[49] who developed the X-ray diffuse scattering technique of measuring short-range order in solutions, and his students[50] since the 1950s in metallic solid solutions. A caveat, however, to the

conclusion that these fluctuations are in the stable composition range follows from the discussion in the preceding paragraph.

No indications of either spinodal decomposition or clustering have been found in $Si_{1-X}Ge_X$ solid solution thin films to date. The driving force for clustering, the positive enthalpy of mixing, at X = 0.5 is calculated to equal 0.013 eV/atom using the delta lattice parameter model.[51] This force is about one-half of that found to produce spinodal decomposition in InGaAs. The critical temperature for the $Si_{1-X}Ge_X$ solid solution should then be about one-half of that for InGaAs and if the deposition temperature is the same for both systems then according to Figure 4.2 no clustering or spinodal decomposition would be observed in the former solid solutions.

Long-range ordering has been observed in InGaAsP[52] and SiGe[53] solid solutions deposited on (100) substrate surfaces yielding CuPt type {111} arrangements. The similarity between the ordering in these two systems does not seem to have been remarked upon before. The explanation for the ordering seems to be the same for the two solid solutions. In particular, the formation of surface dimers leads to the production of regions of alternate sites subject to tension and compression,[54] as illustrated schematically in Figure 4.3. The local free energy would be lowered

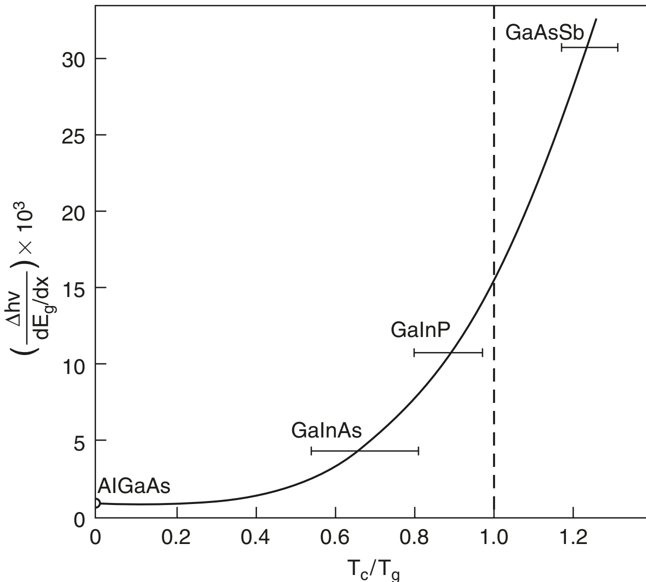

Figure 4.2. Photoluminescence line half-width normalized by the composition dependence of the band gap, dE_g/dx, versus critical temperature divided by the growth temperature for several alloys grown lattice-matched to the appropriate substrates. Reprinted with permission from M.J. Cherng, R.M. Cohen and G. B. Stringfellow, J. Elect. Mater. 13, 799(1984).

when these sites are occupied by atoms that are bigger and smaller, respectively, than by random occupation of these sites. Hence, there is a bias for these sites to be occupied in the suggested ordered fashion. Such occupation leads to selective occupation of the {111} plane that contains the <110> direction that is normal to the direction of the dimer row, e.g. suppose the dimer row is oriented parallel to [$\bar{1}$10] and the surface normal is [001], then the plane containing mainly one type species only will be ($\bar{1}$11). In SiGe we have alternate Si and Ge ($\bar{1}$11) planes. In InGaAsP these planes are alternately In, As, Ga and P. These long-range ordered solutions are not the thermodynamically stable solutions for the semiconductor alloys. Rather, they are metastable because the substrate temperature is too low to allow for bulk diffusion, whereas in the RHEED oscillatory regime diffusive interchange can occur between the surface and the next two subsurface layers allowing for the thermodynamically biased siting of the several species. This thermodynamic bias has its origin in the local stresses introduced by dimerization of the {100} surface in these semiconductors. In the absence of such dimerization (i.e.

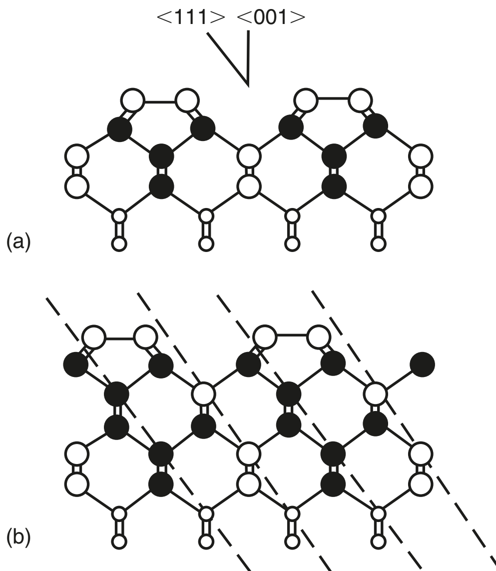

Figure 4.3. (a) Cross-section of the (100) 2 × 1 surface, projected onto a (110) plane. Surface dimers are at the top. Large solid circles correspond to sites under compressive stress and large open circles to sites under tensile stress. (Dimer sites are also shown as large open circles.) (b) After growth of one double layer showing CuPt ordering along (111) planes. Figure is for growth of SiGe. For InAsGaP insert anion planes at position of dashed lines. In the latter case the larger cations and anions fill the tension regions and the smaller ones the compressive region.

for a 1×1 surface) no long-range ordering takes place. Indeed, the calculated enthalpy of the ordered bulk phase is higher than that of the random disordered bulk phase.[55] Incidentally, spinodal decomposition may occur simultaneously with the long-range order and thereby enhance the resistance to degradation of the optical properties of these solutions.[56]

Other variants of ordered structures, which are more stable than the random solid solutions, have been observed. In particular, evidence for the presence of the $L1_0$ (CuAu)[57] and the $E1_1$ (chalcopyrite)[57] in equiatomic III–V pseudobinary alloys has been published. Also, at the $GaAs_{0.25}Sb_{0.75}$ composition the ordered array of $L1_3$ has been found[57] with GaSb and a 50/50 mixture of GaAs and GaAs/GaSb forming alternate monolayers along the <100> directions. For $GaAs_{0.5}Sb_{0.5}$ the $L1_2$ structure was found.[58] In all cases, the ordering is brought about not by diffusion in the bulk, but at the surface during deposition.

For all the defects considered above the diffusion length for the adatoms required to produce them was small, in the order of the spinodal wavelength or smaller. However, when the driving force for adatom migration is large and the mobility is also large, it should be possible to accomplish phase separation as a surface process during deposition of the film. This was shown by Adams et al.[59] who produced such phase separation in films of Al-Ge into fcc Al and dc Ge at a substrate temperature where volume diffusion was nil. Atzmon et al.[60a] noted that this process is analogous to the process of eutectoid decomposition of a metastable solid solution via diffusion along the interface between the product eutectoid and the parent metastable solid solution, originally suggested by Turnbull[60b] and treated theoretically by Cahn.[60c] In the present case, the film is the product and the as-deposited randomly distributed adatom layer is the parent.

In the above we have considered only semiconductor pseudomorphic materials. However, pseudomorphic metallic and insulating materials are also of interest. In particular, the production of three-dimensional integrated circuits requires the epitaxial deposition of conductor (usually metallic) and insulating materials on semiconductor material and vice versa. Thus, there has been a recent spate of activity in this field.[61] Practically nothing has been published concerning the defect structure in such films. However, it is possible to use our knowledge base to surmise the defects likely to be found in these films. In particular, pseudomorphic films should contain the same faults found in homoepitaxial films of the same materials. Further, films deposited in the temperature range where RHEED oscillations occur should contain diffuse interfaces and misfit dislocations should appear in metal films just above the critical thickness, but much above the critical thickness in insulating films.

We should remark upon a phenomenon that can affect the formation of a pseudomorphic film and even prevent it when superficial analysis would lead to a prediction that the pseudomorphic film would be formed. The phenomonon is the production of a compound between the adatoms and the substrate material which

forms a thin interlayer separating the substrate from the remainder of the deposit. A case in point is the deposition of Pd on GaAs(100). The lattice parameter of fcc Pd is 3.8902. The lattice parameter of GaAs is 5.653, which when divided by $\sqrt{2}$ equals 3.997. Thus, there is a 2.7% misfit for (100)[100]Pd/(001)[$1\bar{1}0$]GaAs. However, what is formed on deposition of Pd onto GaAs at a substrate temperature less than 80°C is a 9 nm thick layer of a Pd_XGaAs compound.[62] Despite the fact that the adatom diffusion length for Pd on Pd is 0.4 nm at $\tilde{N} = 1$ monolayer/s, Pd and/or GaAs seem to have diffused an appreciably longer distance during the deposition period. One possible explanation for this result is that the heat released on contact of a Pd atom with GaAs is sufficient to raise the temperature locally to allow for interdiffusion of these species in a process that tends to lower the free energy, another is that Pd may be a fast interstitial diffuser in GaAs and Pd_XGaAs and the production of a pseudomorphic epilayer of Pd on GaAs(100) would require deposition and observation at a suitable temperature. Pseudomorphic films are required for Schottky contacts to minimize interface defect states. Hence, the above considerations suggest that it is desirable to use phase mixtures that are thermodynamically stable as metal/semiconductor contact materials.

In the present subsection we have considered the defects formed in pseudomorphic solid solutions. However, the same defects would form in these solid solutions on deposition in the RHEED oscillatory regime even if the film is not pseudomorphic with the substrate. These defects are not affected by the commensurateness of the film/substrate interface.

A consequence of either spinodal decomposition or non-uniform distribution of constituents along an interface is the presence of local (non-uniform) elastic strains in the film. Evidence for such strains has been reported in many of the papers cited in this section. These strains can be detrimental or beneficial to properties, dependent on the application.

Summarizing, we have found that the *adatom mobility that exists in the RHEED oscillatory temperature regime brings about redistribution of constituents under the influence of various driving forces. This redistribution of constituents produces diffuse interfaces, clustering of solute, spinodal decomposition, metastable long-range order, phase separation and non-uniform strain in pseudomorphic films.*

3.2. Pseudomorphically stabilized metastable crystal structures.

In this section we investigate the pseudomorphic stabilization of metastable crystal structures. As an example, the stable crystal structure of Ni is fcc. Yet it has been found possible to produce thin films of body-centered-cubic (bcc) Ni by deposition onto (001)Fe(bcc).[63] The number of papers concerned with the pseudomorphic stabilization of metastable structures has begun to increase at an accelerating

rate since 1990. Scientists have become aware of the possibility of synthesizing new materials with useful properties that this process confers. The theory of pseudomorphic stabilization is simple. By providing a metastable film/substrate interface with no excess energy, the free energy of a thin metastable film/substrate system can be less than that for the stable film/substrate system, because the excess energy of the latter interface exceeds the difference in bulk energy between the two crystal structures of the film material. Since the latter increases with film thickness there will be a critical thickness at which there will be a driving force to convert the metastable structure to a more stable structure or mixture of phases. The theory governing this transition has been considered in detail by Bruinsma and Zangwill.[64]

All the defects present in homoepitaxial and heteroepitaxial films and discussed above are also expected to be present in pseudomorphically stabilized films. Since defects may be sites for heterogeneous nucleation of the stable structure their absence from metastable pseudomorphic films is necessary to prolong the metastability beyond the thermodynamically defined critical thickness. We will consider such critical thicknesses for elastically strained films in the next section. Let us now consider critical thicknesses for various possible transitions from metastable to more stable structures.

The simplest phase transition is from one crystal structure to another without a change in composition. Even for a supersaturated alloy, this transition to a metastable phase of the same composition, but intermediate in stability between the starting phase and the thermodynamically stable mixture of phases, may be the fastest route along the path to a more stable system. For this case and the assumption that the substrate and starting pseudomorphic metastable film are perfectly lattice matched (i.e. zero strain energy in the film) the critical thickness below which the pseudomorphic film/substrate system will be in their thermodynamically stable state is given by

$$h^* = [(\gamma_\alpha - \gamma_\beta) + (\gamma_{\alpha/S} - \gamma_{\beta/S})]/\Delta G_{\beta\to\alpha}$$

where α and β denote the product and parent phases, respectively, $\Delta G_{\beta\to\alpha}$ is the free energy difference per unit volume between parent and product phases, γ_i are the surface energies and $\gamma_{i/S}$ are the film/substrate interface energies. Obviously, the parameters in this equation depend on the film and substrate materials and orientations. Nevertheless, it is possible to obtain a rough estimate for h*, based on the approximations that $\gamma_\alpha \approx \gamma_\beta$ and $\gamma_{\beta/S} \approx 0$. Since $\gamma_{\alpha/S}$ is in the order of a grain boundary energy, i.e. $\gamma_{\alpha/S} \approx 0.5\,J/m^2$, we find that the pseudomorphic metastable film/substrate system will become thermodynamically unstable when for film thicknesses of 100 and 1000 Å the $\Delta G_{\beta\to\alpha}$ values exceed 50 and $5\,J/cm^3$, respectively. These values limit the possible candidates for metastable structures that may be pseudomorphically stabilized in useful thicknesses of films.

Pseudomorphically stabilized metal films have been explored recently because it has been possible to develop unusual properties in them. For example,

perpendicular magnetic anisotropy with a square hysteresis loop has been developed in very thin fcc Fe films[65] at room temperature. Since these films are quite thin (<7 monolayers on (100)Cu and <3 monolayers on (111)Au) the diffuseness of the interfaces of such films can exert a significant effect on this property. This effect has yet to be explored. Incidentally, the smaller critical thickness for fcc Fe on Au as compared to fcc Fe on Cu is a consequence of the greater difference in lattice parameter for the former combination which acts to induce more strain energy into the former pseudomorphic film, i.e. inside the square brackets in the above equation for h* there should be a term to account for the strain energy of the pseudomorphic film.

In addition to the transition to the stable structure, pseudomorphically stabilized films may also be subject simultaneously to phase separation. For example, the α-$Sn_{1-X}Ge_X$ system was considered as a candidate metastable system for pseudomorphic stabilization[66] because calculations had revealed that compositions in the range $0.25 < X < 0.75$ should yield direct band gap semiconductors. These investigators found that phase separation occurred for $X > 0.1$ into α-Sn and Ge, but not for smaller X. According to the calculations of these investigators this dividing composition corresponds to a driving force for phase separation of about 0.06 eV/atom, which is higher than the value of 0.03 eV/atom found to produce spinodal decomposition in the InGaAs metastable solid solution reported in section 3.1.2. Since the driving force increases with X up to $X = 0.5$ it seems unlikely that under conditions of adatom mobility applicable for $X < 0.1$ that decomposition during deposition can be prevented for $0.1 < X < 0.9$. Thus, if the desired α-$Sn_{1-X}Ge_X$ solution is to be obtained in the desired composition range some way of depositing a crystalline covalently bonded film in the absence of adatom mobility will need to be used. Incidentally, despite the instability with respect to phase separation noted in this system, the metastable crystal structure was pseudomorphically stabilized for many of the conditions investigated by these authors.[66] Further, others[126] have found means of pseudomorphically stabilizing SnGe for $X_{Sn} < 0.26$ and also pure Sn[127] in the diamond cubic structure.

Pseudomorphic stabilization of metastable phases may also be achieved in A/B type multilayers (i.e. in A/B multilayers there is only one type of interface – that between the A/B layers). Thompson et al.[125] have used classical thermodynamics as outlined in the equation above to devise a bilayer phase diagram for this system and have explored this phase diagram for the Nb/Zr system.

3.3. Commensurate–discommensurate transition and misfit dislocations.

The transition thickness between the regime where the film is coherent with the substrate and that where this coherence is no longer perfect (the interface

contains an array of misfit dislocations) or does not exist, the commensurate–discommensurate transition, is governed not by thermodynamics, but by kinetic considerations. Either efficient misfit dislocations that lie and have Burgers vector in the interface plane, or inefficient misfit dislocation segments that lie in and have a component of their Burgers vector lying out of the interface plane, or both, are nucleated at the commensurate–discommensurate transition. The inefficient misfit dislocation segments are connected to threading dislocations that intersect the film surface. Both types form to decrease the misfit strain [{a(substrate) − a(film)}/a(film)], where “a” is the unstrained lattice parameter in the film. The ease of nucleation of such dislocations in metals allows the transition thickness to approximate that predicted by thermodynamics. However, the difficulty of such nucleation in semiconductors causes the observed transition thickness to be much larger than that predicted by thermodynamics.

There are two different configuration states that misfit dislocations can approach. One is the thermodynamic stable state and the other is a metastable state that is kinetically reachable in thin films. The former endpoint has been treated by van der Merwe[68] while the latter by Matthews and Blakeslee.[69] The former considers efficient misfit dislocations and the latter inefficient ones.

All misfit dislocations act to reduce the total free energy of the pseudomorphic film/substrate system above the transition epilayer thickness. As mentioned previously, for a given epilayer elastic strain, the corresponding strain energy per unit area increases with film thickness. Misfit dislocations act to reduce the elastic strain in the film and thereby reduce the elastic strain energy. However, each dislocation has an excess energy itself and the total free energy per unit area increases with increase in the density of the misfit dislocations. Since the latter is proportional to the decrement between the misfit strain and the film’s elastic strain the equilibrium state can be obtained by minimizing the total free energy with respect to the elastic strain. The critical film thickness corresponding to this thermodynamic equilibrium state is then obtained by setting the elastic strain equal to the misfit strain in the resulting equation (i.e. at this condition there are no misfit dislocations in the film).

Misfit dislocations can be nucleated in a variety of ways. The reaction path involving the smallest barrier to nucleation and glide or climb will determine the type of misfit dislocations that are produced for a given film/substrate material system. Most heteroepitaxial films involving small misfit are relatively strongly bonded to their substrates. In this case, growth proceeds initially via the layer-by-layer mode before switching to the island mode. In the latter mode, a network of efficient misfit dislocations is left behind upon the initial coalescence of the island bases.[70] If the islands are thick before base coalescence, and if there is any misorientation of the islands, then further coalescence can lead to the generation of a high dislocation density at the island junctions. If the island thickness normal to the substrate is smaller than the critical thickness then the residual misfit strain in

the film when the latter thickness is reached may be large enough to drive threading dislocations into and through the epilayer. If the growth mode is layer-by-layer until the critical thickness is reached then the residual strain is sufficient to generate and move misfit dislocations into the epilayer. At low enough temperatures, the dislocation motion will be by glide. Misfit dislocation generation and glide will occur until the residual stress driving the dislocations equals the frictional stress opposing the dislocation motion yielding what is called the constrained equilibrium endpoint.[71] At high enough temperature, dislocation motion via glide or climb continues with time, as an activated process, until the thermodynamic equilibrium state is attained.

It is important to consider the possible time dependence of the misfit strain relaxation process for semiconductor structures. One such model of the time dependence[72] leads to the stability diagram illustrated in Figure 4.4, which separates the regime in which coherent (commensurate) films are deposited from that in which misfit dislocations are generated during the normal time of an MBE mode of film deposition for the case of SiGe on a Si(100) substrate. In this figure,

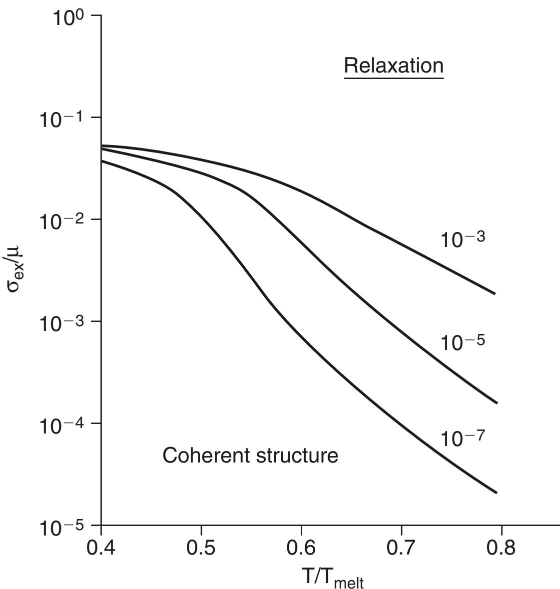

Figure 4.4. Strained-layer stability diagram for SiGe/Si(001). Relaxation is dominated by lattice-resistance-limited dislocation glide mechanisms. Structures having points lying below the 10^{-7} contour will be free of misfit dislocations. Reproduced with permission from B.W. Dodson and J.Y. Tsao, Ann. Rev. Mater. Sci. 19, 419(1989). © 1989 Annual Reviews Inc.

the excess stress σ is the difference between the stress arising from the misfit strain and the stress that corresponds to the array of misfit dislocations that would be generated by the misfit strain. The variable μ is the shear modulus. The numbers on the curves correspond to the reduction of strain by relaxation. This relaxation proceeds initially by an increase in the density of misfit dislocations by multiplication from some undetermined background source density according to this model.

There have been many reviews[73] describing misfit dislocation arrays in various materials. We shall limit our discussion of them to the illustration of several types of misfit dislocations. A micrograph showing a distribution of efficient misfit dislocations is given in Figure 4.5.

For the case of SiGe/(001)Si it is found that at the typical growth temperature of about 500°C, no misfit dislocations are introduced for lattice misfit less than 1.8% in the absence of substrate dislocations, inclusions, oxygen and other impurities.[74] When the lattice misfit exceeds this value half-loops of dislocations can be generated at the surface to produce misfit segments in the substrate/film interface with attached threading segments that intersect the surface. Such misfit dislocation segments terminating in threading dislocations that emanate from the plane of the figure are shown in Figure 4.6.

Because dislocations are traps for electrons they are not desired in the active regions of semiconductors. Hence, schemes have been developed to prevent threading dislocation generation, or to prevent their motion into active areas of the

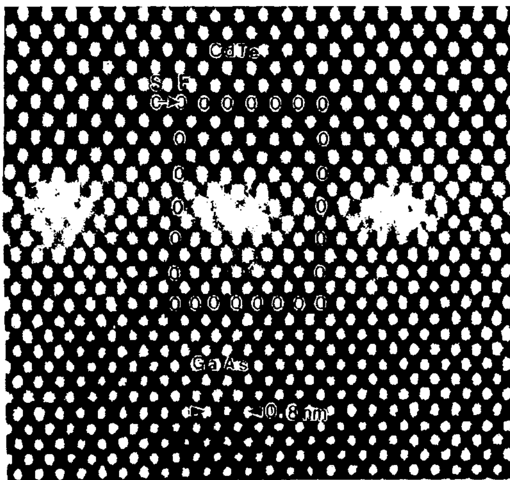

Figure 4.5. Lattice image of CdTe epilayer on GaAs substrate illustrating Burgers circuit around a Lomer efficient misfit dislocation. Reproduced with permission from A.F. Schwartzman and R. Sinclair, J. Elect. Mater. 20, 805(1991).

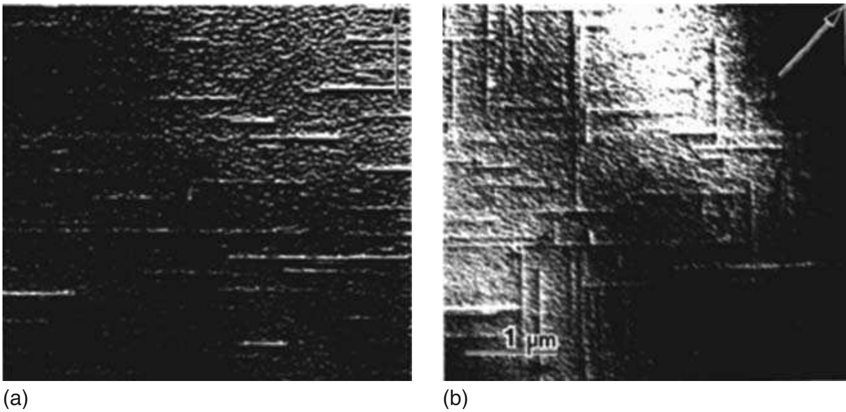

Figure 4.6. Short misfit dislocation segments after the onset of surface nucleation in GeSi/Si(001); change in contrast with diffraction conditions illustrates the edge character of the dislocations ((a) g = 220; (b) g = 400). Reproduced with permission from J. Washburn, E.P. Kvam and Z. Liliental-Weber, J. Elect. Mater. 20, 155(1991).

epilayers, or to remove them. Appropriate substrate patterning can decrease the density of misfit dislocations appreciably, either by limiting the lengthwise growth of any misfit dislocations that may happen to nucleate, or by decreasing the actual strain per unit volume of mesa for a given misfit,[75] or by both. Superlattice layers[76] and lattice parameter gradient buffer layers[77] have also been used as threading dislocation filters. It has been found that surfactant mediated epitaxial growth can produce defect-free epilayers, except at the film/substrate interface, under appropriate conditions where normally the films would contain threading dislocations throughout.[78] The latter is accomplished as a consequence of the surfactant acting to change the growth mode from Stranski–Krastonov to layer-by-layer so as to alter the type of misfit dislocations from efficient to inefficient and by modifying the latter mode so that the first misfit dislocations consist of partial dislocations that glide from the film surface to the film/substrate interface leaving behind stacking faults that thread through the epilayer. But these stacking faults act as heterogeneous nucleation sites for the generation of complementary partial dislocations that act to annihilate the initial partials to the extent of leaving full, but split, dislocations at the film/substrate interface only. Low-energy ion beams have been used to change growth from the island mode to the layer-by-layer mode with a consequent reduction in epilayer dislocation density.[8] Off-axis substrate orientations have also been proposed to reduce threading dislocation density.[79] There seems to be no limit to the ingenuity devoted to achieve a desired commercial objective. Fortunately, there also has been a concomitant gain in fundamental understanding of these phenomena over the years.

4. Heteroepitaxy between crystals of different symmetry, bonding class or of large misfit.

The interface structure formed when there is a change of symmetry between substrate and epilayer crystal structures or when the misfit is large (>10%) has been the subject of recent intensive study. One hypothesis governing the structure of the interface is that it represents the configuration of least free energy for the constraints that may exist. It has not yet been possible to determine the validity of this proposal. Neither is it easy to use to predict the nature of the interface and epitaxial relationship between epilayer and substrate. Other hypotheses have been proposed, which are not necessarily in contradiction to the one just given, such as that of Zur and McGill,[80] which, based on an O-lattice type of construction at the interface, proposes that epitaxy should be expected when the density of coincident sites is high enough.

One of the factors that affects epitaxy is the relative bonding between epilayer and substrate atoms as compared to that between epilayer atoms themselves. If the interface has weak bonding relative to the epilayer then it becomes energetically favorable for the epitaxy to involve the presence of interface dislocations. On the other hand strong interface bonding relative to that in the epilayer implies that the more stable situation may involve a pseudomorphic, but elastically strained epilayer. Indeed, these same considerations, in the case of small misfit, determine whether misfit dislocations will be of the efficient kind or the inefficient kind, respectively.

It is worth considering at this point the possible effects of bonding type at the interface on epitaxy. Metallic bonding is non-directional and is driven by the interaction between the valence electrons and the ion cores, which attempts to increase the valence electron density, i.e. decrease the specific volume. The interface is a region of excess volume. Hence, atoms at the interface in metallic bonding seek to occupy sites that result in a decrease in the interface's excess volume. With this brief background we can understand why the interface between metals will tend to have a high coincidence of O-lattice sites. The latter types of sites are at the minima of periodic potential wells on a substrate surface. A rigid epilayer having a high density of O-lattice coincident sites with the substrate at their interface will produce an interface having a smaller excess volume and consequently a smaller excess energy than one having a low density of such coincident sites. This concept is illustrated in Figure 4.7 using a one-dimensional model of the interface. We will see in the succeeding subsection that this drive to decrease the excess volume of the interface determines the epitaxial relation when the interface bonds are metallic.

Covalent bonds are directional. Thus, the positions of adatoms on substrates are no longer determined by the tendency to decrease the excess volume at the interface. Rather, they are determined by the hybridization of the interface covalent bonds that yields the minimum energy. At this writing there does not appear to be

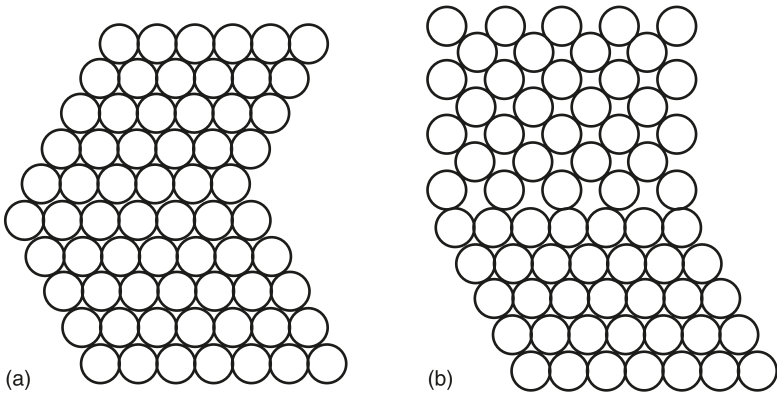

Figure 4.7. Illustrating the change in excess volume at interface between (a) coincident lattice site density equal to lattice site planar density in interface and (b) coincident lattice site density equal to zero.

any rule applicable to all such interfaces. From the calculations of Batra[81] it is known that the interface bonds between some metallic and covalent materials are the covalent type.

4.1. Metal/metal epilayer/substrate systems.

van der Merwe[82] has shown, based on a rigid lattice model and a periodic substrate potential, for a (110) bcc substrate and a (111) fcc or a (0001) hcp epilayer, that the calculated interface energy exhibits minima at the Nishiyama–Wassermann (N–W) $\{[\bar{2}11]_{fcc}//[\bar{1}10]_{bcc}$ or $[0\bar{1}1]_{fcc}//[001]_{bcc}\}$ and the Kurdjumov–Sachs (K–S) $\{[1\bar{1}0]_{fcc}//[1\bar{1}1]_{bcc}\}$ orientation relations and only at these relations, for certain values of the atomic radius ratio of epilayer to substrate materials. The significance of these results, since the N–W and K–S are common orientation relations found between parent and product in the fcc→bcc transformation, is that they support the hypothesis that the interface between heterostructures tends to be one that minimizes the free energy of the system. Further, these minima in the interface energy occur at the atomic radius ratio that yields the same spacing between atoms along the rows defined by the respective relations. The geometric arrangement at the interface for these ideal relations consists of n epilayer atomic rows in the same distance as m substrate rows, with the atom spacings along the rows being the same. The epilayer rows lie in troughs between substrate atom rows and if the misfit along one of the rows is accounted for by misfit dislocations (in a non-rigid, elastically strainable epilayer) then the atoms between the

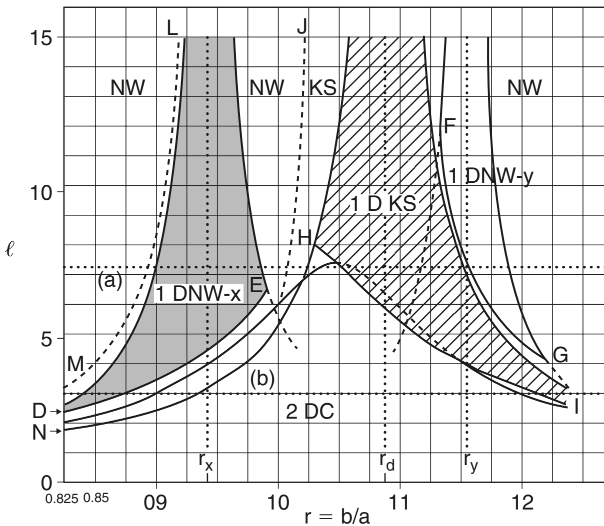

Figure 4.8. Stability ranges for pseudomorphic (2 DC), 1 D coherency in N–W and K–S orientations of homogeneously strained (111) monolayers on (110) bcc substrates. The ordinate increases with the ratio of the strength of the bonds between epilayer atom relative to that for interface bonds between substrate and epilayer atoms. The abscissa is the ratio of atomic radius of epilayer atom to substrate atom. Reproduced with permission from E. Bauer and J.H. van der Merwe, Phys. Rev. B33, 3657(1986).

dislocations and outside their cores are situated along coincident lattice sites at the bottoms of the troughs.

van der Merwe and collaborators[83] have calculated the effects of allowing for homogeneous strains on complete coherence of an epimonolayer and substrate, and for misfit dislocations. The results for these calculations are complicated because they depend upon the relative bonding between epilayer and substrate as compared to bonding within the epilayer. A stability diagram so calculated is shown in Figure 4.8. In this figure the letter D represents the word, “dimensional”. Hence, 1D means one-dimensional. As shown, there is a region where a pseudomorphic monolayer is the most stable configuration. This region occurs where the interface bonds are strong relative to the bonds in the epilayer (i.e. in the two DC region). This is not an unrealistic result because multilayer assemblies, or strained layer superlattices, can be deposited with only a few monolayers in each epilayer.

Many observations of metal epilayers on metal substrates agree with the specific predictions made by van der Merwe and with the more general consideration based on minimization of the excess volume and excess interface energy. In particular, for deposition under ultra clean conditions and at substrate temperatures

where alloy formation does not occur, the N–W orientation has been found for a monolayer of Be on W,[84] for a thick epilayer of Cu on Nb[85] and other systems, such as Nb and Ta on Au,[86] having the atomic radius ratio, r, between 0.894 and 0.963 (the latter is that for Pd on Nb[87]), for Pd on W[84] ($r = 1.004$), for Pd on Mo[88] ($r = 1.009$) and for $r > 1.162$, such as Fe on Ag,[89] Fe on Au[65] and rare earth metals on Mo.[90] Epilayer examples that exhibit the K–S relationship with substrates are sparse. Those systems that have been reported (Cr on Cu(111),[86] Fe on Cu(111),[65b] thick Fe on Ni(111)[91]) also exhibit N–W orientations as well. The inverse N–W relation has also been found for metal on metal systems. This orientation relation is defined as $(110)_{bcc}//(100)_{fcc}$ and $[\bar{1}11]_{bcc}//[011]_{fcc}$. Cr on Cu and W on Ni[86] exhibit this relation, which has a similar geometric description for the atom configuration at the interface as that given for the N–W and K–S relations. The other metal on metal relation that this writer has found is one that exhibits almost perfect coincidence of lattice sites at the interface – (100)[011]Cr//9(100)[001]Au[86] and a similar one for Fe on Ag.[92] In summary, *the near totality of examples of metal/metal epitaxial relationships correspond to the class where the density of coincident sites is maximized, the excess interface volume is minimized and, consequently, the interface energy is minimized.*

4.2. Metal/semiconductor epilayer/substrate systems.

The rule we have just summarized in the previous subsection for metal/metal epilayer/substrate systems does not appear to apply to metal/semiconductor systems. For example, consider the cases of Al/Si and Ag/Si. Al and Ag have the same structure and nearly the same lattice parameter (4.049 and 4.0856, respectively). Thus, if geometric factors alone were to control the epitaxy, they should yield the same epitaxial relationships with the same substrate. However, Ag forms the following epitaxial relation on Si(100):[93] Ag(111)<110>//Si(100) <011>, while Al forms Al(011)[100]//Si(001)[110].[94] On Si(111) they also form different sets of epitaxial relations with one set in common (i.e. Ag(111)<110>// Si(111)<110> and Ag(111)<110>//Si(111)<114>:[93] Al(111)<110>//Si(111) <110> and Al(100) <110>//Si(111)<110>).[95] Thus, it is apparent that geometric factors alone do not determine the epitaxial relations assumed by metal/semiconductor epilayer/substrate systems. Directional bonding, due to the different hybridizations formed between a given semiconductor surface and different metal adatoms and vice versa may play the other significant role in determining epitaxy between metals and semiconductors if the bonding calculations of Batra[81] represent reality.

Geometry must affect the epitaxy of metal/semiconductor systems because experiment validates the predictions of a rigid lattice model using a periodic potential for the effect of the substrate surface on the energy of a rigid adatom monolayer.[94]

In particular, this model predicts two relative orientations at which an Al(011) plane will have minimum energy on a Si(100) substrate: Al[100]//Si[011] and Al[100] 18.9° from Si[011]. These epitaxial relations were confirmed experimentally, as was the prediction that the former is more stable than the latter.

Lattice imaging of the interface formed between Al(111) and Si(111) shows that the interface is stepped, and the terraces between steps have a fair density of broken bonds in a periodic array (one every four Al atoms in a <110> direction), although the remainder of the bonds along the terrace may be coherent[95] (i.e. the interface along the terrace is discommensurate). For such cases of large misfit (i.e. 33%) it has been suggested that the ultimate epitaxial relation assumed in a thick film may be determined by that with the least excess energy associated with the misfit dislocations. It will not be a simple matter to develop predictions for epitaxial relations between metals and semiconductors. The geometric relations applicable to metal/metal systems can only provide potential epitaxial relationships, which may or may not satisfy bonding requirements in the other classes of heteroepitaxial systems.

One approach towards obtaining a desired epitaxial orientation of a particular metal on a particular semiconductor substrate has involved a combination of a phenomenological approach with that involving a principle. In particular, it has been noted that the epitaxial relation that results depends upon substrate surface reconstruction and temperature. Hence, for a given substrate, a list of epitaxial relations has been developed from experiment for various metals. Then, if it is desired to produce a particular epitaxial relation for a given metal not in the list, use is made of the list to choose another metal which can act simultaneously as a substrate for the given metal and an epilayer of the semiconductor substrate to produce the desired epitaxial relation of the given metal to the semiconductor substrate. This technique has been termed the “template” method.[96]

4.3. Epitaxy at vicinal surfaces.

Tilting a Si(100) substrate surface a few degrees off the low index plane serves the objective of eliminating inversion domain boundaries by converting monoatomic steps to diatomic steps. This result has inspired the testing of the effect of substrate misorientation on the epitaxy of other systems sometimes with good results and other times with bad results.[97] We shall investigate in some detail the potential of a good result.

Hall et al.[98] appear to have been the first to recognize that elastic strain, in a precipitate within a solid phase, induced by misfit strain is reduced at interfaces consisting of structural ledges. It is but a step to extend this concept to epilayers, which was carried out by van der Merwe and Shiflet.[99] The dislocation character of interfacial steps has been considered by Pond[100] in a series of papers.

Using a rigid lattice model, a periodic potential for the interaction of an adatom (or interfacial atom) with the surface of the substrate, Shiflet and van der Merwe[101] calculated the energy of the interface between a fcc(111) oriented crystal and a bcc(110) oriented crystal as a function of the atomic radius ratio of fcc/bcc materials and as a function of azimuthal misorientation from the Nishiyama–Wasserman orientation relation $[\bar{2}11]_{fcc}//[\bar{1}10]_{bcc}$, and for 4M + 1 by 4N + 1 atomic rows in the interface. They found two orientations that yielded sharp minima in the interface energy (i.e. the N–W and Kurdjumov–Sachs ($[1\bar{1}0]_{fcc}//[11\bar{1}1]_{bcc}$). Further, the N–W orientation was favored for an atomic radius ratio of unity and exhibited two minimum energy stepped interfaces one with steps normal to $[\bar{1}10]_{bcc}$ and the other with steps normal to $[001]_{bcc}$. The K–S orientation relation is favored for a radius ratio (fcc/bcc) of 32/27. They further calculated the energy difference between a stepped interface and a planar interface, now allowing for elastic strain and under the assumptions of a Poisson's ratio of 1/3 for epilayer, substrate and interface material and equal values of shear moduli for the former two materials, and 1/3 and 1/10 of this value for the interface region along the N–W or K–S directions and normal to these directions, respectively. They found that the stepped interface is energetically preferred to the planar one at radius ratio values less than about unity for this particular epilayer–substrate combination.

The following simple analysis, which neglects the energy associated with the short-range strain in the epilayer at steps along the substrate surface, demonstrates how long-range strain energy in the epilayer can be eliminated. Suppose that n atomic rows in the epilayer match m atomic rows in the substrate along a planar interface, where $nd_e > md_s$ and $d_{e,s}$ are the distances between rows for epilayer and substrate, respectively. Rotation by an angle α will now allow this matching to occur with a much smaller strain because the length along the tilted substrate that corresponds to m atomic rows along the terraces now becomes $md_s \sec\alpha$. For complete absence of long-range strain in the epilayer the following relation must hold

$$nd_e = md_s \sec \alpha$$

There is an additional constraint for long-range strain in the epilayer to be absent, which is that

$$ld_i = nd_e \sin \alpha$$

where l, m, and n are integers and d_i is the spacing between atomic planes of the substrate along the direction normal to the terrace plane.

Dodson et al.[79] have suggested the first relation above with $n = m$. On the other hand, if we set $l = 1$, and $n = m \pm 1$ we then allow for one tilt misfit

dislocation of Burgers vector equal to d_i and one misfit dislocation of Burgers vector equal to d_e for each terrace step to obtain a set of relations for m and α. The result is

$$\cos\alpha = (d_s/d_e)[m/(m \pm 1)]$$

$$\sin\alpha = (d_i/d_e)/(m \pm 1)$$

Applying the above relations to the case of GaAs on a Si(100) substrate we find no solution for the Dodson et al. case of $n = m$, whereas setting $n = m - 1$ yields a tilt angle of 3.35° about <110> to produce an epilayer having zero long-range strain. Yet observation[117] of the epilayer tilt angle for a vicinal surface having about a 3.7° tilt about <110> yields the result, 0.2°. How can this result be explained? The answer is that deposition does not occur to yield the interface structure described in Figure 4.9a, which corresponds to the model used above. Rather, bonding between the epilayer and substrate along the terraces introduces short-range stresses that tend to produce slip in the epilayer along planes that coincide with the steps and a consequent reverse rotation of the epilayer segments between steps, but not all the way to the horizontal, as illustrated in Figure 4.9b. The state corresponding to the latter figure is that described by the geometric model of Aindow and Pond.[102] It is apparent that for the former model (corresponding to Figure 4.9a) to work in practice it is necessary for the substrate to be elastically soft with respect to the epilayer or for bonding at the interface to be weak.

A system that supports the general argument presented above consists of rare earth metals as epilayers on (211) bcc transition metal substrate surfaces.[103] In this system the first monolayers that form are pseudomorphic with the substrate, have the $(10\bar{1}2)$ hcp plane parallel to the (211) bcc plane, and are strained. Upon

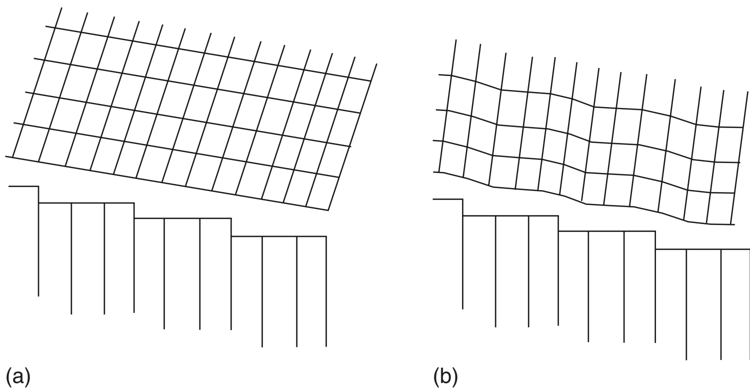

Figure 4.9. Schematic illustrating stress-free epilayer (a) and stressed epilayer (b).

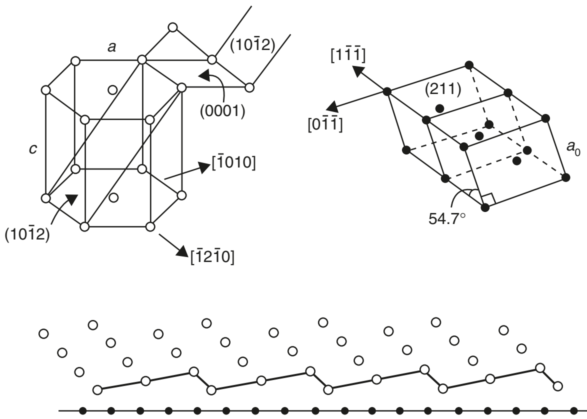

Figure 4.10. Geometry of rare earth hcp epilayer on bcc transition metal substrate. Reproduced with permission from R. Du and C.P. Flynn, J. Phys. Condens. Matter 2, 1335(1990).

growth in thickness dislocations are generated between every second basal plane with slip in the [$\bar{1}$010] direction, partial unbonding across the interface at the intersection of every other basal plane with the interface, and with a consequent rotation of the epilayer with the latter described by the previous relations, but applicable to the geometry described above and in Figure 4.10. The epitaxial relation shown in the figure is that after slip of every other basal plane and rotation of the epilayer. The rotation is opposite to the sense described in going from Figure 4.9a to 4.9b. Effectively, the slip process has produced a stepped (10$\bar{1}$2) surface that matches the (211) bcc surface at every 4th <110> atom row spacing along the latter surface. In this case the predicted angles are observed for five rare earth metals on three different bcc metal substrates. One facet of this system that may be useful in a search for other tilt systems that can produce long-range stress-free epilayers is that m and n are small, i.e. 4 versus 2. In the case of the GaAs/Si(100) system the step free terrace length is 54 adjacent [002] rows. The bonding strength across the interface along the terrace may have been exceeded in the former case and not in the latter case. Perhaps, minimization of the across interface bonding between steps may hinder the formation of a coherent interface and promote one corresponding to that of the desired long-range stress-free epilayer directly on deposition of the first monolayer.

4.4. Theories of interphase interfaces.

Because direct calculations for the energy of an interphase interface is difficult (appropriate interatomic potentials between different elements have not yet

been developed), a variety of theories has arisen all of which propose explicitly or implicitly to provide a recipe for discovering the interface between two phases having the minimum energy. All of these theories neglect the influence of bonding type at the interface and to this extent we know that they cannot be general theories applicable to all materials. These theories fall into several categories: matching models and invariant line and plane models. Also, within such categories there are subcategories of models. Descriptions of these models is outside the scope of this section and the interested reader is referred to the original articles[115] and several reviews.[116]

4.5. Constraints on epitaxy due to symmetry.

Consider the case where the substrate plane and parallel film plane do not have the same symmetry and there is matching of atoms along one characteristic direction in each of film and substrate. If the substrate plane has higher symmetry than the film plane parallel to it then it will not be possible to produce a single crystal film on the substrate. This rule can be understood using the following example. Suppose the film plane has no rotational symmetry (i.e. 1-fold rotational symmetry) while the substrate plane has 4-fold rotational symmetry. Then the direction in the film plane that matches a direction in the substrate plane has four orientations in which it matches the latter. But since the film plane has only 1-fold rotational symmetry there are then four azimuthal orientations of film grains which can deposit onto the substrate with equal probability. Suppose the symmetries were reversed. In this case there are four equivalent directions in the film plane that can orient parallel to one direction in the substrate plane. But the 4-fold rotational symmetry in the film plane yields the same azimuthal crystal orientation, or a single crystal film. Stated briefly, to produce a single crystal film the point symmetry group of the substrate surface must be a subgroup of that of the film growth plane.

5. Graphoepitaxy.

Graphoepitaxy or "artificial epitaxy" refers to the case where epitaxial relationships exist between epilayer and substrate in the absence of primary bonding between these surfaces. The extreme case of such graphoepitaxy occurs when the substrate is covered by a thin amorphous layer, yet the epilayer over the amorphous layer exhibits an epitaxial relationship with the underlying substrate crystal. How can such a relationship be explained?

Most cases of graphoepitaxy occur when there is weak bonding between epilayer and substrate. In this case, growth occurs via the island mode. Although it has not been mentioned as yet, such islands tend to grow with faceted surfaces to

minimize their free energy, because the surface energy is usually anisotropic and has minima parallel to low index planes. Most substrate surfaces are not ideally planar. Rather they consist of terraces and surface steps. The steps are usually along low index directions. If the substrate surface plane has 3-fold rotational symmetry then the steps will mimic this rotational symmetry and there will be step intersections where the angles between steps are either 60° or 120°. Similarly, on substrate surfaces having either 2- or 4-fold rotational symmetry, the angle between intersecting steps will be 90°. Heterogeneous nucleation of the islands will occur preferentially at the step intersections on the substrate. The angles between steps determine whether the islands that nucleate there have the corresponding rotational symmetry. Thus, if the steps on a substrate surface are reproduced on the surface of an amorphous overlayer, then the islands of the epilayer that either nucleate at, or migrate to and align along step intersections and stay there will have a preferential orientation. If deposition is carried out such that these islands determine the orientation of the resulting monocrystalline epilayer then graphoepitaxy of the epilayer on an amorphous substrate will have been achieved.

It is one thing to provide a possible explanation for a phenomenon. It is another thing to provide a proof that the explanation is Nature's mode for production of the phenomenon. However, the phenomenon can be reproduced by following the explanation's recipe as shown by a variety of examples.[104–106]

Although it is not possible to prove that any particular case of deposition of a monocrystalline film onto a substrate when the bonding between substrate and epilayer is weak represents an example of graphoepitaxy, it seems very reasonable to conclude that graphoepitaxy is likely to be responsible for any epitaxy that exists when the density of coincident sites is low at the interface between epilayer and substrate. There are numerous examples of epitaxy in the presence of large misfit.[107] Among these are Cr, Fe, Co, Ni and Cu on NaCl,[107] many alkali halide films on other alkali halide substrates[108] and many, many others. It is interesting that these cases of epitaxy have been produced under poor vacuum conditions when the surface of the substrate is covered with at least a monolayer of adsorbed gas and other impurities. Further, often the same epitaxy is observed when the substrate surfaces are clean. A monolayer of adsorbed gas is usually sufficient to prevent pseudomorphic contact between epilayer and substrate.

For many cases of epitaxy it has been discovered that the ultimate epitaxial relationship is not that for the original clusters deposited on the substrate, but is a consequence of coalescence of migrating clusters to a new relationship.[109] This observation does not support the concept that this form of epitaxy is a consequence of bonding between substrate and epilayer. On the other hand, it could easily be a consequence of graphoepitaxy. Further, support for the anti-bonding origin of epitaxy between weakly bonded substrate and epilayer is the existence of an epitaxial temperature, above which monocrystalline layers could be formed and below which polycrystalline layers are formed. In the strong bonding regime and for clean substrate

surfaces, monocrystalline layers are easily formed at and below room temperature. A graphoepitaxial origin for the epitaxial temperature is reasonable inasmuch as the translational and rotational mobility of clusters increases with temperature while those clusters aligned along surface ledges are not likely to rotate as easily.

Given all of the above facts it is surprising that no scientist in this field recognized that the origin of most of the epitaxial relationships did not involve bonding between epilayer and substrate. Indeed, in Pashley's historical review of epitaxy in the 1975 book *Epitaxial Growth* edited by J.W. Matthews in discussing Distler et al.'s[110] 1968 observations of oriented nuclei on amorphous carbon overlayers on cleaned rock salt surfaces, he states "These results are interpreted in terms of the effect of long-range forces . . .". This statement reveals that at least up to that moment the thought that epitaxy could arise from other than a bonding relation between substrate and epilayer did not occur to anyone.

Graphoepitaxy[104] or artificial epitaxy, the production of epitaxially aligned monocrystalline films, involved the alignment by patterned substrates of faceted crystals floating on a liquid layer[105,106,111] and deposition onto these aligned thin crystals to produce the desired epitaxial monocrystalline film. It was not until 1985[112] that the possibility that most of the epitaxial studies prior to 1975 consisted of studies of graphoepitaxy was indirectly suggested. The aligning function of surface steps and the ability of clusters to migrate and rotate on weakly bonding substrates were recognized as possible crucial contributions of graphoepitaxy to the production of epitaxial films in these studies.

With the proliferation of MBE deposition apparati and UHV deposition equipment in the 1980s it has become possible to deposit at low substrate temperatures onto in situ cleaved alkali halide surfaces and to achieve atomic bonding between such substrates and epilayers, and thereby to produce bonding epitaxial relations rather than graphoepitaxial relations.[113] However, because of the relatively weak interface bonding (high interface energy) and relatively low substrate surface energy, the mode of growth for metal and semiconductor layers is usually the island mode.

Let us now consider the defects likely to be present in films produced via deposition and graphoepitaxy, i.e. graphoepitaxial deposition. The main feature of the process of graphoepitaxial deposition that differs from the deposition processes that produce epitaxial films based on strong bonding between substrate and epilayer is that the film in the former case is formed by coalescence of islands. It is known that island coalescence introduces a high density of dislocations due to the misorientation, albeit small, between the adjacent islands.[114] Thus, it is unlikely that active devices can be produced in semiconductor films formed via graphoepitaxial deposition. Metal and insulator epitaxial films produced via graphoepitaxial techniques cannot be used as substrates for active semiconductor devices because the dislocations they contain that intersect the interface will grow into the epilayer producing threading dislocations therein, unless these layers are separated by a buffer layer that acts to pinch off the threading dislocations and reduce their density

in the overlayer. Thus, it is unlikely that graphoepitaxial deposition will be a useful technique in the production of integrated circuits. However, it may be a useful technique to produce surface layers of ferroelectric, piezoelectric, pyroelectric, magnetic, and superconducting materials which have properties that are not degraded by the presence of dislocations.

6. Epilogue.

We have not endeavored to provide an encyclopedic review of epitaxy in this chapter. Indeed, we have not discussed other modes of epitaxy, such as solid phase epitaxy. Further, we have not discussed the effect of hyperthermal beams during deposition on the production of an epitaxial film. A discussion of both these topics is deferred until Chapter VII. However, we have attempted to discuss the significant aspects of epitaxy produced by deposition from the vapor phase that are of interest to the materials scientist and, in particular, the resulting defect structure. Further, we have attempted to describe the factors that affect the production of epitaxy when there is large misfit between epilayer and substrate. Since this is a science in development undoubtedly there will be future discoveries that will answer many of the questions that arise in the present chapter.

References

1. L. Royer, Bull. Soc. Fr. Mineral. Crist. 51, 7(1928).
2. J.W. Mathews (ed.), **Epitaxial Growth**, Academic Press, NY, 1975; a) Vol. II, p. 447.
3. M.H. Grabow and G.H. Gilmer, in **Semiconductor-Based Heterostructures: Interfacial Structure and Stability**, eds. M.L. Green, et al., The Metallurgical Society, Warrendale, PA, 1986, p. 3.
4. M.H. Grabow and G.H. Gilmer, in **Layered Structures and Epitaxy**, eds. J.M. Gibson et al., MRS Symp. Proc. 56, 1986, p. 13.
5. R. Bruinsma and A. Zangwill, Europhys. Lett. 4, 729(1987).
6. H.J. Osten, E. Bugiel and J. Klatt, Appl. Phys. Lett. 61, 1918(1992).
7. S. Kanemaru, H. Ishiwara and S. Furukawa, in **Initial Stages of Epitaxial Growth**, eds. R. Hull et al., MRS Symp. Proc. 94, 1987, p. 71.
8. C.-H. Choi, R. Ai and S.A. Barnett, Phys. Rev. Lett. 67, 2826(1991).
9. C.P. Flynn, J. Phys. F: Met. Phys. 18, L195(1988).
10. P.S. Peercy, MRS Symp. Proc. 160, 3(1990).
11. C. Roland and G.H. Gilmer, Phys. Rev. B46, 13428(1992).
12. N. Herbots, O.C. Hellman and O. Vancauwenberghe, MRS Symp. Proc. 236, 287(1992).
13. G.D. Watkins, J. Phys. Soc. Jap. 18(Suppl. II), 22(1963); G.D. Watkins and J.R. Troxell, Phys. Rev. Lett. 44, 593(1980).
14. C.G. Morgan-Pond, J. Elect. Mat. 20, 399(1991).
15. M. Kitabatake, P. Fons and J.E. Greene, MRS Symp. Proc. 157, 259(1990).

16. T.Y. Tan and U. Gosele, MRS Symp. Proc. 144, 221(1989).
17. J.R. Lloyd and S. Nakahara, MRS Symp. Proc. 10, 289(1982).
18. T. Hsu, B. Anthony, L. Breaux, R. Qian, S. Banerjee, A. Tasch, C. Magee and W. Harrington, J. Elect. Mat. 19, 1043(1990).
19. J. van Lunduyt, A. De Veirman, J. Vanhellemont and H. Bender, Inst. Phys. Conf. Ser. No 100, Sect. 1, 1(1989).
20. M. Kohyama and S. Takeda, Phys. Rev. B46, 12305(1992).
21. W.K. Wu and J. Washburn, J. Appl. Phys. 48, 3742(1977).
22. T.D. Andreadis, M. Rosen, M.I. Haftel and J.A. Sprague, MRS Symp. Proc. 202, 283(1991).
23. A.E.M. De Veirman, F. Hakkens, W. Coene and F.J.A. Den Broeder, MRS Symp. Proc. 263, 119(1992).
24. P.J. Schmitz, W.Y. Leung, G.W. Graham and P.A. Thiel, Vacuum 41, 1411(1990).
25. W.A. Fisher and J.A. Amick, J. Electrochem. Soc. 113, 1054(1966).
26. A. George and J. Rabier, Rev. Phys. Appl. 22, 1941(1987).
27. B.E. Weir, B.S. Freer, R.L. Hedrick, D.J. Eaglesham, G.H. Gilmer, J. Bevk and L.C. Feldman, Appl. Phys. Lett. 59, 204(1991).
28. D.J. Eaglesham, H.J. Gossman and M. Cerullo, Phys. Rev. Lett. 65, 1227(1990).
29. M. Geis, MRS Symp. Proc. 162, 15(1990); R.E. Clausing, L. Heatherly, E.D. Specht and K.L. More, in **New Diamond Science and Technology**, eds. R. Messier et al., MRS, Pittsburgh, PA, 1991, p. 575; S. Matsumoto and Y. Matsui, J. Mater. Sci. 18, 1785(1983); B.E. Williams, J.T. Glass, R.F. Davis and K. Kobashi, J. Cryst. Growth. 99, 1168(1990); J. Narayan, J. Mater. Sci. 5, 2414(1990); Z.L. Wang, J. Bentley, R.E. Clausing, L. Heatherly.
30. J.E. Angelo, J.W. Hoehn, A.M. Dabiran, P.I. Cohen and W.W. Gerberich, MRS Symp. Proc. 263, 175(1992).
31. a) K.C. Rajkumar, P. Chen and A. Madhukar, J. Appl. Phys. 69, 2219(1991); b) T. Hayakawa, M. Morishima and S. Chen, Appl. Phys. Lett. 59, 3321(1991).
32. M. Kanenska, Z. Liliental-Weber, E.R. Weber, T. George, J.B. Kortright, F.W. Smith, B.Y. Tsaur and A.R. Calawa, Appl. Phys. Lett. 54, 1881(1989).
33. See Ref. [2a]; G.B. Stringfellow, Rep. Prog. Phys. 45, 469(1982); **Defects in Silicon: Processing in Semiconducting Materials and Related Technologies**, eds. S. Mahajan and L.C. Kimerling, Pergamon Press, Oxford, 1992, p. 78; or see M. Ohring, **The Materials Science of Thin Films**, Academic Press, 1992, p. 319.
34. Defects in Semiconductors.
35. R.W. Vook and F. Witt, J. Vac. Sci. Tech. 2, 49,243(1965).
36. A.E.M. De Vierman, F. Hakkens, W. Coene and F.J.A. Den Broeder, MRS Symp. Proc. 263, 119(1992).
37. C.M. Gilmore and J.A. Sprague, Phys. Rev. B44, 8950(1991).
38. M.J. Stowell, in **Epitaxial Growth**, ed. J.W. Matthews, Academic Press, 1975, p. 468.
39. H.-J. Gossman, MRS Symp. Proc. 94, 53(1987).
40. F.C. Frank and J.H. van der Merwe, Proc. Roy. Soc. London 198, 217(1949).
41. R.M. Tromp, A.W.D. van der Gon and M.C. Reuter, Phys. Rev. Lett. 68, 2313(1992).
42. H. Matsuhata, K. Miki, K. Sakamoto and S. Yoshida, Phys. Rev. B47, 10474(1993).
43. B.B. Bennett, J.A. del Alamo, MRS Symp. Proc. 240, 153(1992).
44. H.W.M. Salemink and O. Albrektsen, Phys. Rev. B47, 16044(1993).

45. S.N.G. Chu, S. Nakahara, K.E. Strege and W.D. Johnston Jr, J. Appl. Phys. 57, 4610(1985); S. Mahajan, B.V. Dutt, H. Temkin, R.J. Cava and W.A. Bonner, J. Cryst. Growth 68, 589(1984); M.M.J. Treacy, J.M. Gibson and A. Howie, Phil. Mag. A51, 389(1985).
46. K. Onabe, NEC Research and Development 72, 1(1984).
47. G.B. Stringfellow, **Organic Vapor-Phase Epitaxy: Theory and Practise**, Academic Press, 1989, p. 95.
48. M.J. Cherng, R.M. Cohen and G.B. Stringfellow, J. Elect. Mat. 13, 799(1984).
49. See B.E. Warren and B.L. Averbach, in **Modern Research Techniques in Physical Metallurgy**, American Society for Metals, Cleveland, OH, 1953, p. 95 for early review. Also, B.E. Warren, **X-Ray Diffraction**, Addison-Wesley, Reading, MA, 1969.
50. B. Borie and C.J. Sparks, Acta Cryst. A27, 195(1971); J.M Cowley, **Diffraction Physics**, 2nd edn. North Holland, Amsterdam, 1981; L.H. Schwartz and J.B. Cohen, **Diffraction from Materials**, Academic Press, 1977.
51. Ref. [47], p. 65.
52. M.A. Shahid and S. Mahajan, Phys. Rev. B38, 1344(1988).
53. V.P. Kesan, F.K. LeGoues and S.S. Iyer, Phys. Rev. B46, 1576(1992).
54. P.C. Kelires and J. Tersoff, Phys. Rev. Lett. 63, 1164(1989).
55. J.E. Bernard, L.G. Ferreira, W.-H. Wei and A. Zunger, Phys. Rev. B38, 6339(1988).
56. S. Mahajan, M.A. Shahid and D.E. Laughlin, Inst. Phys. Conf. Ser. 100, 143(1989).
57. H.R. Jen, M.J. Cherng and G.B. Stringfellow, Appl. Phys. Lett. 48, 1603(1986); H.R. Jen, M.J. Cherng, M.J. Jou and G.B. Stringfellow, in **Ternary and Multinary Compounds**, eds. S.K. Deb and A. Zunger, Materials Research Society, Pittsburgh, 1987; Inst. Phys. Conf. Ser. 83, 159(1987).
58. Y.E. Ihm, N. Otsuka, J. Klem and H. Morkoc, App. Phys. Lett. 51, 2013(1987).
59. C.D. Adams, M. Atzmon, Y.-T. Cheng and D.J. Srolovitz, J. Mater. Res. 7, 653(1992).
60. a) M. Atzmon, D.A. Kessler and D.J. Srolovitz, J. Appl. Phys. 72, 442(1992); b) D. Turnbull, Acta Met. 3, 55(1955); c) J.W. Cahn, Acta Metall. 7, 18(1959); 9, 795(1961); Trans. AIME 242, 166(1968).
61. Among the insulators that have been epitaxially deposited are the fluorites, such as CaF_2, MgO and ZrO_2.
62. T. Sands, K.M. Yu, S.K. Cheung and V.G. Keramidas, in **Semiconductor-Based Heterostructures: Interfacial Structure and Stability**, eds. M.L. Green et al., The Metallurgical Society, Warrendale, PA, 1986, p. 397.
63. B. Heinrich, A.S. Arrott, J.F. Cochran, S.T. Purcell, K.S. Urquhart, N. Alberding and C. Liu, in **Thin Film Growth Techniques for Low-Dimensional Structures**, eds. R.F.C. Farrow et al., NATO ASI Series B: Physics 163, Plenum Press, NY, 1986, p. 521.
64. R. Bruinsma and A. Zangwill, J. Phys. 47, 2055(1986).
65. a) B. Voigtlander, G. Meyer and N.M. Amer, Surf. Sci. Lett. 255, L529(1991); b) M.T. Kief and W.F. Egelhoff Jr, Phys. Rev. B47, 10785(1993).
66. E.A. Fitzgerald, P.E. Freeland, M.T. Asom, W.P. Lowe, R.A. Macharrie, Jr, B.E. Weir, A.R. Kortan, F.A. Thiel, Y.-H. Xie, A.M. Sergent, S.L. Cooper, G.A. Thomas and L.C. Kimerling, J. Elect. Mat. 20, 489(1991).
67. Ref. [11], p. 13437.
68. J.H. van der Merwe, J. Appl. Phys. 34, 117(1963).

69. J.W. Matthews and A.E. Blakeslee, J. Cryst. Growth 27, 118(1974); 29, 273(1975); 32, 265(1976).
70. R. Vincent, Phil. Mag. 19, 1127(1969); W.A. Jesser and J.H. van der Merwe, Surf. Sci. 31, 229(1972).
71. B.A. Fox and W.A. Jesser, J. Appl. Phys. 68, 2801(1990).
72. B.W. Dodson and J.Y. Tsao, Ann. Rev. Mater. Sci. 19, 419(1989).
73. For example, see J.W. Matthews, in **Epitaxial Growth**, eds. J.W. Matthews, Academic Press, NY, 1975, p. 560; **Microscopy of Semiconducting Materials** 1989, Inst. Phys. Conf. Ser. 100; MRS Symp. Proc 160; J. Elect. Mat. 20, (1991).
74. J. Washburn, E.P. Kvam and Z. Liliental-Weber, J. Elect. Mat. 20, 155(1991).
75. E.A. Fitzgerald, Y.-H. Xie, J. Michel, P.E. Freeland and B.E. Weir, MRS Symp. Proc. 160, 59(1990).
76. See Ref. [69]; S. Sharan, J. Narayan and J.C.C. Fan, MRS Symp. Proc. 160, 375(1990); T. Soga, T. Imori, M. Umeno and S. Hattori, Jpn. J. Appl. Phys. 26(5), L536(1987).
77. M. Umeno, S. Sakai, M. Takeyasu and T. Soga, in **Semiconductor-Based Heterostructures: Interfacial Structure and Stability**, The Metallurgical Society, Warrendale, PA, 1986, p. 207.
78. M. Horn-van Hoegen, F.K. LeGoues, M. Copel, M.C. Reuter and R.M. Tromp, Phys. Rev. Lett. 67, 1130(1991).
79. B.W. Dodson, D.R. Myers, A.K. Datye, V.S. Kaushik, D.L. Kendall and B. Martinez-Tovar, Phys. Rev. Lett. 61, 2681(1988).
80. A. Zur and T.C. McGill, J. Appl. Phys. 55, 378(1984).
81. I.P. Batra, J. Vac. Sci. Tech. B2, 427(1984).
82. J.H. van der Merwe, Phil. Mag. A45, 145(1982).
83. Ref. [82], p. 159; J.H. van der Merwe, Thin Solid Films. 74, 129(1980); L.C.A. Stoop and J.H. van der Merwe, Thin Solid Films 91, 257(1982); 94, 341(1982); 98, 65(1982); L.C.A. Stoops, Thin Solid Films. 94, 353(1982).
84. E. Bauer, Appl. Surf. Sci. 11/12, 479(1982).
85. E. Bauer and J.H. van der Merwe, Phys. Rev. B33, 3657(1986).
86. D.A. Smith, A. Segmuller and A.R. Taranko, MRS Symp. Proc. 94, 127(1987).
87. M. Sagurton, M. Strongin, F. Jona and J. Colbert, Phys. Rev. B28, 4075(1983).
88. C. Park, E. Bauer and H. Poppa, Surf. Sci. 154, 371(1985).
89. H.C. Snyman and G.H. Olsen, J. Appl. Phys. 44, 889(1973); Acta Met. 21, 769(1973).
90. E. Bauer, in **The Chemical Physics of Solid Surfaces and Heterogeneous Catalysis**, eds. D.A. King and D.P. Woodruff, Elsevier, Amsterdam, 1984, Vol. IIIB, p. 1; also Ref. [89].
91. N.M. Jennett, D.J. Dingley and Y. Ando, MRS Symp. Proc. 160, 183(1990).
92. S. Nahm, L. Salamanca-Riba, B.T. Jonker and G.A. Prinz, MRS Symp. Proc. 160, 209(1990).
93. F.K. LeGoues, M. Liehr and M. Renier, MRS Symp. Proc. 94, 121(1987).
94. F.J. Lamelas, M.-T. Tang, K. Evans-Lutterodt, P.H. Fuoss and W.L. Brown, Phys. Rev. B46, 15570(1992).
95. F.K. LeGoues, W. Krakow and P.S. Ho, Phil. Mag. A53, 833(1986).
96. T. Sands, J.P. Harbison, C.J. Palmstrøm, R. Ramesh and V.G. Keramidas, MRS Symp. Proc. 221, 271(1991).

97. T. Minemura, J. Asano, K. Tsutsui and S. Furukawa, MRS Symp. Proc. 160, 521(1990).
98. M.G. Hall, H.I. Aaronson and K.R. Kinsman, Surf. Sci. 31, 257(1972).
99. J.H. van der Merwe, S. Afr. J. Phys. 9, 55(1985); G.J. Shiflet, M.W.H. Braun and J.H. van der Merwe, S. Afr. J. Sci. 84, 653(1988); J.H. van der Merwe, G.J. Shiflet and P.M. Stoop, Met. Trans. 22A, 1165(1991).
100. R.C. Pond, **Dislocations and the Properties of Real Materials** Institute of Metals, London, 1985; **Dislocations in Solids**, Vol. 8, ed. F.R.N. Nabarro, North-Holland, Amsterdam, 1989, p. 1.
101. G.J. Shiflet and J.H. van der Merwe, J. Elect. Mat. 20, 785(1991).
102. M. Aindow and R.C. Pond, Phil. Mag. A63, 667(1991).
103. R. Du and C.P. Flynn, J. Phys. Condens. Matter, 2, 1335(1990).
104. M.W. Geis, D.C. Flanders and H.I. Smith, J. Vac. Sci. Tech. 16, 1640(1979); Appl. Phys. Lett. 35, 71(1979).
105. H.I. Smith, M.W. Geis, C.V. Thompson and H.A. Atwater, J. Cryst. Growth 63, 527(1983); I. Klykov, R.N. Sheftel and N.N. Sheftel, in **Protessy Realnogo Kristalloobrazovaniya**, eds. N. Belov and N.N. Sheftel, Nauka, Moscow, 1977, p. 144.
106. E.I. Givargizov, **Oriented Crystallization on Amorphous Substrates**, Plenum Press, NY, 1991.
107. E. Gruenbaum, in **Epitaxial Growth**, ed. J.W. Matthews, Academic Press, NY, 1975, p. 611.
108. L.G. Schulz, Acta Cryst. 4, 483, 487(1951); 5, 130(1952).
109. A. Masson, J.J. Metois and R. Kern, in **Advances in Epitaxy and Endotaxy**, eds. V. Ruth and H.G. Schneider, V.E.B. Deutscher Verlag fur Grundstoffindustrie, Leipzig, Chapter 2.2; J.J. Metois, M. Gauch, A. Masson and R. Kern, Surf. Sci. 30, 43(1972), Thin Solid Films 11, 205(1972).
110. G.I. Distler, S.A. Kobzareva, Proc. Int. Congr Electron Microsc., 6th, Kyoto, 1966, p. 493. Maruzen, Tokyo; G.I. Distler, S.A. Kobzareva and Y.M. Gerasimov, J. Cryst. Growth 2, 45(1968); G.I. Distler, Y.M. Gerasimov, S.A. Kobzareva, V.V. Moskin and L.A. Shenyavskaya, Proc. Eur. Reg. Conf. Electron Microsc., 4th, Rome, 1968, p. 517. Tipographia Poliglotta Vaticana, Rome.
111. M.W. Geis, H.I. Smith, B.Y. Tsaur, J.C.C. Fan, D.J. Silversmith and R.W. Mountain, J. Electrochem. Soc. 129, 2812 (1982).
112. D.A. Smith, J.T. Wetzel and H.T. Taranko, MRS Symp. Proc. 37, 77(1985).
113. J. Mattson, M.B. Brodsky, J. Ketterson and H. You, MRS Symp. Proc. 160, 231(1990).
114. M.J. Stowell, in **Epitaxial Growth**, II, Academic Press, NY, 1975, p. 444.
115. W. Bollman, **Crystalline Defects and Crystalline Interfaces**, Springer, Berlin, 1970; G.B. Olson and M. Cohen, Acta Met. 27, 1907(1979); M.S. Wechsler, D.S. Lieberman and T.A. Read, Trans. Metall. Soc. AIME 197, 1503(1953); U. Dahmen, in **Encyclopedia of Physical Science and Technology**, Vol. 10, Academic Press, NY, 1987, p. 319; See Ref. [98]; T. Zheleva, K. Jagannadham and J. Narayan, J. Appl. Phys. 75, 860(1994).
116. D.A. Smith and R.C. Pond, Int. Metall. Rev. 205, 61(1976); R.W. Balluffi, A. Brokman and A.H. King, Acta Met. 30, 1453(1982); D.A. Smith and G.J. Shiflet, Mater. Sci. Eng. 86, 67(1987); H. Gleiter, in **Physical Metallurgy**, eds. R.W. Cahn and P. Haasen, North-Holland, Amsterdam, 1983, p. 650.
117. L.J. Schowalter, E.L. Hall, N. Lewis and S. Hashimoto, MRS Symp. Proc. 130, 171(1989).

118. T.A. Wagner, Thesis (Dr-Ing.), Low Temperature Silicon Epitaxy: Defects and Electronic Properties, University of Stuttgart, Institute of Physical Electronics, 2003.
119. C. Busse et al., Phys. Rev. Lett. 91, 056103(2003).
120. C. Busse et al., Phys. Rev. B68, 201401(2003).
121. M. Giesen and H. Ibach, Surf. Sci. 529, 135(2003).
122. S. Walter et al., J. Phys. Condens. Matter 14, 3085(2002).
123. A. Ohtake et al., Phys. Rev. B64, 045318(2001).
124. C. Busse and T. Michely, Surf. Sci. Lett. (2004) submitted.
125. G.B. Thompson, R. Banerjee and J.L. Fraser, Appl. Phys. Lett. 84, 1082(2004).
126. O. Gurdel et al,, J. Appl. Phys. 83, 162(1998); H.P.L. de Guevara et al., Appl. Phys. Lett. 83, 4942(2003); M.R. Bauer et al. Appl. Phys. Lett. 83, 3489(2003).
127. P.F. Lyman and M.J. Bedzyk, Appl. Phys. Lett. 69, 978(1996).

Appendix 1

DLTS, photoluminescence and temperature dependent quantum efficiency measurements[A1] have revealed that the point defect densities in Si films formed by ion-assisted homoepitaxial deposition onto Si(100) decrease with increasing deposition temperature. At 550°C this density is $10^{13}/cm^3$. Further, decrease in this density is revealed by increase in the minority carrier diffusion length, as shown in Figure 4.A1 Even at a deposition temperature of 650°C the minority carrier lifetime indicates that it has not yet reached its maximum value with increase in the deposition temperature. In the range of temperature shown in this figure the extended defect density remains constant with deposition temperature.

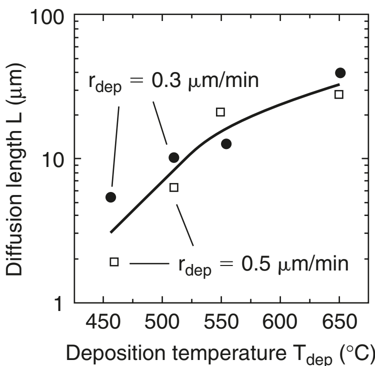

Figure 4.A1. Minority carrier diffusion length versus deposition temperature in a film produced using MBE with ion-assisted deposition. Reproduced with permission from T.A. Wagner, Thesis (Dr-Ing.), University of Stuttgart, Institute of Physical Electronics, 2003.

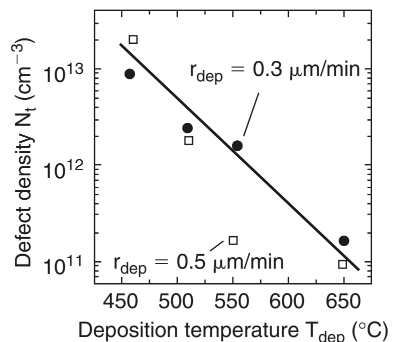

Figure 4.A2. Defect density evaluated from the data in Figure 4.A1. Reproduced with permission from T.A. Wagner, Thesis (Dr-Ing.), University of Stuttgart, Institute of Physical Electronics, 2003.

Thus, the minority carrier lifetime is a function here only of the point defect density. These point defects are a consequence of the production of Frenkel defects by the hyperthermal Si ions used in the ion-assisted deposition mode of forming these films. Such point defects are not present to the same densities in normal high temperature MBE deposition on Si(100). Indeed, in MBE deposition on Si(100) in the absence of a hyperthermal beam it is known that surface vacancies in the adatom layers anneal out before being buried at and above about 600°C and that no interstitials are formed.

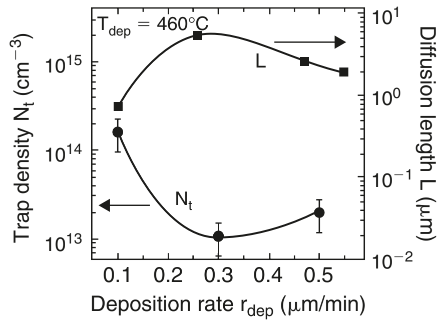

Figure 4.A3. Showing point defect density and minority carrier diffusion length as a function of deposition rate. Reproduced with permission from T.A. Wagner, Thesis (Dr-Ing.), University of Stuttgart, Institute of Physical Electronics, 2003.

Figure 4.A2 shows the point defect density calculated using the data in Figure 4.A1. There is no hint that a minimum is being approached with increasing deposition temperature. For deposition at 460°C a minimum is reached with increasing rate of deposition as shown in Figure 4.A3. These data were obtained from films deposited for solar cell application. One possible explanation for the behavior shown in this figure is that the shorter the time between deposition of successive layers fewer defects are created in the adatom clusters by energetic ions before they are buried but beyond a critical time period the fewer is the number of defects removed from these clusters by surface diffusion.

A1. T.A. Wagner, Thesis (Dr-Ing.), Low Temperature Silicon Epitaxy: Defects and Electronic Properties, University of Stuttgart, Institute of Physical Electronics, 2003.

Appendix 2

For less than one monolayer coverage such that adatom clusters do not contact each other, the criteria governing the presence of clusters centered over hcp sites (fault islands) and over fcc sites (non-fault islands) are that mobile clusters are distributed on the surface sites according to a Boltzmann distribution (i.e. the cluster ensemble is in thermal equilibrium), and that the largest mobile cluster of size i is mobile if the time t_i it needs to exchange between fcc and hcp is smaller than the time t_{+1} needed to add an additional atom to it. (The addition of one adatom to the largest mobile cluster decreases its mobility and causes the cluster one adatom larger than the largest mobile cluster to become stuck.) Thus, clusters larger than the largest mobile cluster will have a distribution identical to that for the largest mobile cluster. If $P_{hcp,i}$ is the population of i size clusters that occupy hcp sites and $P_{fcc,i}$ is the population of i size clusters that occupy fcc sites then $P_{hcp,i}/P_{fcc},i = \exp[(F_{i,fcc} - F_{i,\,hcp})/kT]$. It is this ratio that is measured in the STM observations. The data used to evaluate the free energies is described in detail in Ref. [A2]. Figure 4.A4 shows a comparison between the experimental data, closed square points; with this atomic model, full line. The

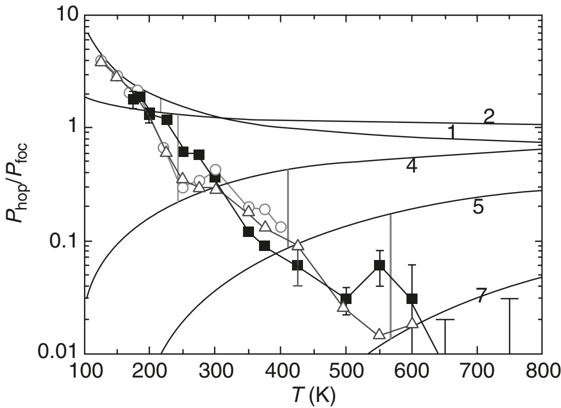

Figure 4.A4. Probability of fault islands versus absolute temperature. Reproduced with permission from C. Busse et al., Phys. Rev. Lett. 91, 056103(2003). © 2003 by the American Physical Society.

authors of Ref. [A2] also used two other theoretical models: one based on the well-established rate equations of island nucleation (Ref. [A3]); the other kinetic Monte Carlo simulation of Ir deposition onto Ir(111). The results for these models are shown as open triangles and open circles, respectively, in Figure 4.A4.

A2. C. Busse et al., Phys. Rev. Lett. 91, 056103(2003).
A3. J.A. Venables, Phil. Mag. 27, 697(1973); J.A. Venables, G.D.T. Spiller and M. Hanbrucken, Rep. Prog. Phys. 47, 399(1984).

C. Detavernier et al., Nature 426, 641(2003) have observed another type of epitaxy denoted “axiotaxy” by them. In axiotaxy a plane in the film is parallel to one in the substrate and the d spacings corresponding to these planes have the same value. The authors note that for this situation the interface between film and substrate can be curved without interference with the commonality of rows at the interface.

This page intentionally left blank

CHAPTER V

Structure of Amorphous Films

Amorphous materials are not homogeneous on a microscopic scale. They may well be described as solid solutions of defects and atoms. Because there is a spectrum of defects, it is very difficult to assign a structure to correspond to measured structural parameters. Further, the processing variables can markedly affect the measured structural parameters and one can find in the literature what appear to be contradictory results for apparently the same experiments. Hence, the reader is warned to maintain a critical attitude to what will be described as “facts” in the remainder of this chapter. Because both of the complexity of α-Si:H and its applicability to industrial products, its defects are probably the most studied to date.

1. Amorphous covalently bonded semiconductors.

1.1. Non-hydrogenated and hydrogenated Group IV elements.

The major factor limiting the properties of amorphous semiconductors is the density of defects in the energy gap. Usually, the lower this density the better are the properties. For example, the dark conductivity in amorphous silicon is reduced from 10^{-7} S/cm to about 10^{-11} S/cm by hydrogenating amorphous silicon while the dangling bond density correspondingly decreases from $10^{19}/cm^3$ to $10^{15}/cm^3$.

There is good evidence for the belief that the main defect adversely affecting properties is the dangling bond (a three-coordinated Group IV atom). The other main class of defects consists of distorted bonds involving both length and bond angle distortions. The latter are believed to affect the number density of dangling bonds in hydrogenated amorphous Group IV semiconductors as a consequence of the distribution of hydrogen atoms between these two types of hydrogen traps under the constraint of partial equilibrium. Hydrogenated films have additional defects associated with hydrogen, their clusters, and with multi-hydrogen bonding to single atoms. Also, there may be other coordination defects. Finally, impurities are defects and also affect the population of the other defects described above.

The main techniques for measuring the density of defect states are electron spin resonance (ESR), photothermal deflection spectroscopy (PDS), and constant photocurrent measurement (CPM). ESR measures the total density of neutral dangling bonds (D^0) from surface and bulk states, PDS measures not only D^0 but

also charged states from surface and bulk and CPM is relatively insensitive to surface states for thicknesses >1 μm. The mean bond angle distortion is related to the half-width of the transverse optic Raman mode, at about 480/cm^{-1} for α-Si. Bonded hydrogen content is revealed by infra-red transmittance spectroscopy and nuclear magnetic resonance (NMR) while hydrogen clustering is detected by NMR. Voids, their volume fraction and sizes are deduced from small angle X-ray scattering data. Other specialized techniques (e.g. positron annihilation, etc.) have been called upon to enlarge the pot of knowledge about hydrogenated amorphous silicon.

1.1.1. α-Si and α-Si:H.

We will first consider the significant facts we need to know in order to be able to examine the relationship between processing and structure. Obviously, one of this group of facts relates to structure and another relates to processing. The former group will be discussed before the other.

Device quality α-Si:H films have an ESR density of neutral dangling bond states below about $10^{16}/cm^3$. In α-Si, as noted, this density is not less than about $10^{19}/cm^3$. This dependence of ESR spin density on the hydrogen content is revealed in Figure 5.1. However, hydrogen not only passivates dangling bonds, but it also bonds to silicon, replacing Si–Si bonds in the form of atomically dispersed Si–H bonds, at a level of 4 at.%, as revealed by NMR measurements,[92] i.e. the bonded hydrogen content is more than the $10^{19}/cm^3$ of dangling bonds in α-Si films. The remainder of the hydrogen is in the form of H_2, about 1 at.% in interstitial positions and voids, in the form of clusters of Si–H at the surfaces of vacancy clusters, and in various complexes with Si.

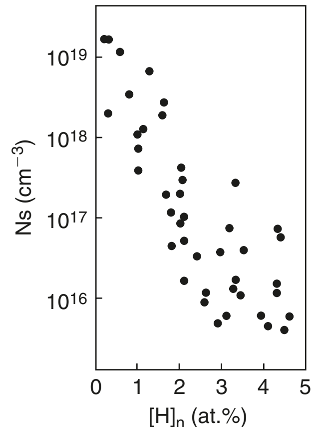

Figure 5.1. ESR spin density versus at.% hydrogen. Reproduced with permission from T. Shimizu and M. Kumeda, in **Amorphous Silicon and Related Materials, Advances in Disordered Semiconductors**, Vol. I, ed. H. Fritzsche, World Scientific, Singapore, 1988, p. 633.

A significant feature of α-Si:H is the density of electron states as a function of energy. These data are revealed semi-quantitatively in Figure 5.2 after Stutzmann.[93] The tail states correspond to weak bonds. The density of states at E_C and E_V is about $10^{21}/eV/cm^3$. Their logarithmic slopes are 0.05 and 0.025 eV, respectively. Hence, there are about $10^{19}/cm^{-3}$ weak bonds.

The electron density of states versus energy function is capable of being altered thermally and by hydrogen content. For example, Raman measurements yield the result that the full width at

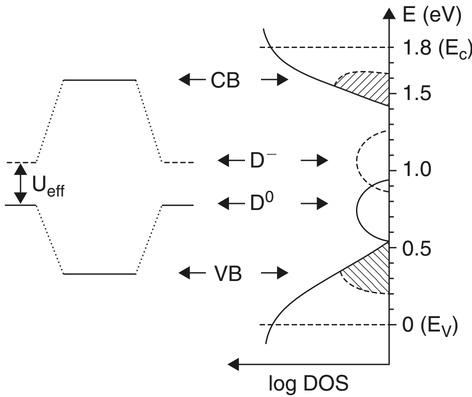

Figure 5.2. Electronic density of states dependence on energy. E_c and E_V are the conduction band and valence band mobility edges, respectively. Localized valence band tail states (VB) are associated with the bonding levels. Conduction band (CB) tail states are associated with the anti-bonding levels (see left-hand side).

half maximum of the $480/cm^{-1}$ transverse optic peak is significantly smaller in as-deposited hydrogenated amorphous silicon than it is in as-deposited amorphous silicon.[4] This Raman parameter measures the mean bond angle disorder. The fraction of bonds that have such disorder in unhydrogenated amorphous silicon is large enough (over 50%)[5] to accommodate the bonded hydrogen content in α-Si:H films, which may contain from 6–8% such strained bonds.[6] Another result[7] that is in agreement with the analysis just given is shown in Figure 5.3. The half-width of the Raman peak upon annealing freshly amorphized α-Si films at 500°C decreases to the level present in device-grade α-Si:H films, $35/cm^{-1}$. The process by which hydrogen accomplishes the same result as obtained by thermal annealing has been termed chemical annealing in the literature. We will examine this concept in the book that follows this one in the series.[104]

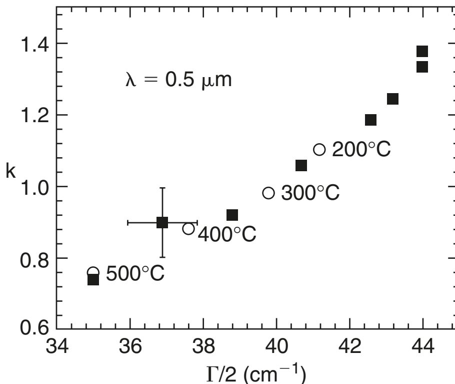

Figure 5.3. This figure is shown to indicate the dependence of the TO Raman peak half-width, Γ/2, on the annealing temperature. Open circles refer to the annealed samples. Reproduced with permission from Reitano et al., J. Appl. Phys. 74, 2850(1993).

This ability to alter the weak bond density of states–energy relation is important because it implies that processing may also be a means of changing this relation for the better (or the worse). We will recall this concept later in this chapter.

For reasons to be developed later, it is desired to deposit at as low a temperature as possible. From Chapter II we know that low temperature deposition involving shadowing will develop void ribbons. For a long time it was believed that such void surfaces deleteriously affected the properties of α-Si:H, as

they do for α-Si. However, after much research it is now believed that for state of the art deposited α-Si:H films such deleterious voids are not present or if they are present they are not harmful to properties. In support of this statement consider the following.

X-ray small angle scattering measurements reveal a microvoid area per unit volume ranging from $1.75 \cdot 10^5$ to $2.4 \cdot 10^5 \, cm^2/cm^3$ in device-grade α-Si:H films.[12] If these microvoid surfaces were to have the same dangling bond concentrations as exist on the external surface of device-grade α-Si:H films[8] (i.e. greater than $3 \cdot 10^{11}/cm^2$), then these device-grade films would contain more than 10^{17} dangling bonds per cm^3 of film. Fortunately, the dangling bond densities in device-grade α-Si:H films are smaller than $10^{16}/cm^3$. Thus, in such films, the surface density of dangling bonds along microvoids must be less than at the external surface and it appears that we may neglect the contribution of such heterogeneity to the total bulk dangling bond density. The reason for this situation, as will be developed later, is that H, if able, facilitates the approach to a metastable equilibrium state in α-Si:H, whereas this capability in α-Si is severely hampered by the existence of too high activation energies. Since most of the dangling bonds in α-Si are found on internal void surfaces[10,11] and the ability of these dangling bonds to rebond is hindered because of their immobility the road to metastable equilibrium is blocked by tall activation barriers in this material.

If the dangling bond density is not determined by the void surface area, as it is in non-hydrogenated amorphous films, what does determine this defect population? Before we answer this question we need to develop the basis for the assertion that at temperatures between about 250°C and 400°C it is possible for α-Si:H to develop a metastable state on being held at temperature for sufficient time. However, before this is done it is useful to develop some background information relative to measures of dangling bond and weak bond densities.

A significant empirical correlation was made by Stutzmann,[13] which is shown in Figure 5.4. The neutral dangling bond density, D^0, as measured by ESR, is a monotonic increasing function of the Urbach tail slope, E_0, where

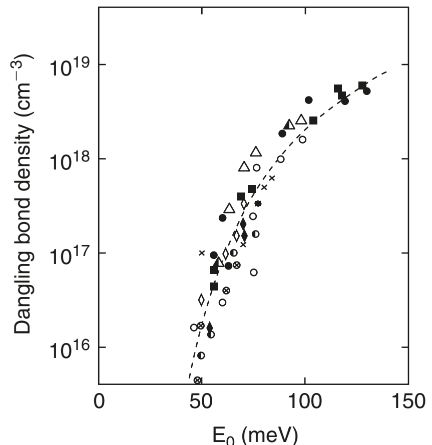

Figure 5.4. Correlation between the dangling bond defect density and the Urbach tail slope in various α-Si:H films. Reproduced with permission from M. Stutzmann, Phil. Mag. B60, 531(1989).

the latter parameter is obtained from measurements of the optical absorption coefficient, α, and the relation

$$\alpha = \alpha_o \exp[-(E\text{-}hv)/E_0]$$

where α is the absorption coefficient for incident photons of energy hν corresponding to the energy E in the energy gap. It is important to note that at a given value of E_0 the uncertainty in the neutral dangling bond density is about one order of magnitude, whereas the correlation between D^0 and E_0 holds over a variation of nearly four orders of magnitude in D_0, regardless of the processing history of the samples. By way of further explanation, the Urbach tail slope is the slope of the density of states in the valence band tail such that the density of states in this tail is given by

$$N_{tail}(E) = N^* \exp[-(E - E^*)/E_0].$$

Now let us consider the evidence for the assertion that metastable equilibrium can be reached in α-Si:H between about 200°C and 450°C. This evidence stems mainly from the work of Street and his collaborators. Figure 5.5 shows a plot of dangling bond density versus temperature in the equilibrating range of temperature. What is significant about this plot is that the values are reversibly attainable.

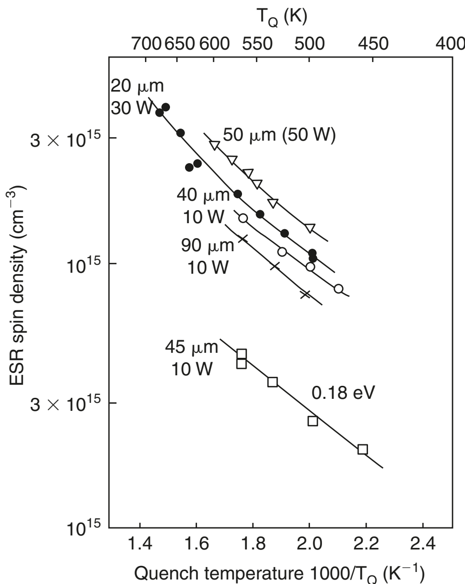

Figure 5.5. Reversible dangling bond density as a function of annealing temperature for samples deposited under different conditions. Reproduced with permission from R.A. Street and K. Winer, Phys. Rev. B40, 6236(1989).

That is, heating from a state on the plot corresponding to a given film to another temperature and then cooling and holding at the original temperature will reproduce the state and vice versa (reversing the words heating and cooling in the above statement). As noted, in the figure different films have their own plot which signifies that this is a metastable equilibrium and that each metastable state differs from another.* The bounds on the equilibrating temperature range are determined by two facts. One is that hydrogen evolves from α-Si:H films in significant amounts above about 375°C (see Figure 5.6). The other is determined by the freezing-in temperature of a species that facilitates the approach to equilibrium. This species is hydrogen. From separate experiments it has been ascertained that in undoped α-Si:H that hydrogen diffuses with an activation energy of 1.5 eV. However, when hydrogen is in the mobile state it has a jump (hopping) activation energy of about 0.3 eV. The latter is the height of the saddle point energy in the energy surface for hydrogen to move from one well to another. However, there are deep wells, corresponding to traps for hydrogen, that are further separated from each other than one unit cell spacing. Both activation energies have been measured. The activation energies depend upon the position of the Fermi level.[95] The fact that the time constant for changes in dangling bond densities in α-Si, in the absence of hydrogen, is much longer than those measured in α-Si:H, in the presence of hydrogen, for similar changes in dangling bond densities, further supports the assertion that hydrogen migration is involved in achieving these changes in α-Si:H films.

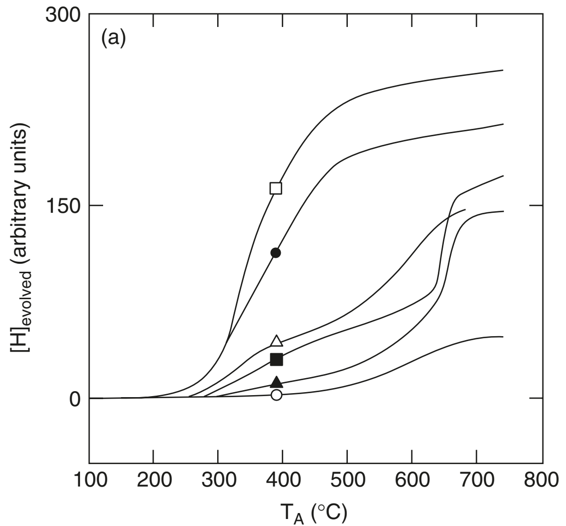

Figure 5.6. H evolved (normalized to sample volume) from α-Si:H as a function of temperature in a temperature ramp of 20°C/min. Reproduced with permission from Phys. Rev. B20, 4839(1979).

We will now consider a very simplified model which in the detail of accounting for electrons involved in reactions is wrong. Nevertheless, it will provide

* The possibility exists that there are defects with very deep traps for hydrogen (much larger than 1.5 eV activation energy) that are frozen-in and have no means of participating in the metastable equilibrium. We naturally exclude these defects from the discussion.

the broad concepts that we need to obtain a grasp of the factors involved in this complex problem. Let us now consider the energy levels associated with electrons and also with hydrogen in α-Si:H. (For the interested reader we provide references to more exact treatments of the statistical mechanics of the defect-pool model,[98] which we simplify here.) Figure 5.2 shows that the dangling bond in a simplified model of undoped α-Si:H has a formation energy of 0.8 eV. We can provide a very simple justification for this value. The energy to remove one Si atom from the bulk silicon lattice is 4.82 eV (i.e. the sublimation energy per atom). There are 2 bonds per Si atom. Hence, to break one bond requires 4.82/2 = 2.42 eV. But two dangling bonds are formed from one bond. Hence, the simple bond energy calculation of chemistry yields a dangling bond formation energy of 1.2 eV. The strain energy released with the introduction of a dangling bond into a weak bond of the α-Si:H network may account for the 0.4 eV decrement.

Let us consider first the equilibrium between weak bonds and dangling bonds. This reaction is

$$\mathrm{Si{\wedge}Si} = 2\mathrm{Si}\text{—} \quad (5.1)$$

This relation defines the concentration of [Si—] dangling bonds in terms of the concentration of weak bonds [Si^Si] by

$$[\mathrm{Si}\text{—}]^2/[\mathrm{Si{\wedge}Si}] = e^{-(E\{\mathrm{Si}\text{—}\}-E\{\mathrm{Si{\wedge}Si}\})/kT} = K_3 \quad (5.2)$$

This energy difference is just twice the difference in the energies between the D^0 level and the valence band (VB) weak bond level in the energy diagram in Figure 5.2. Thus, the concentration of dangling bonds at equilibrium is just

$$[\mathrm{Si}\text{—}] = [\mathrm{Si{\wedge}Si}]^{1/2} e^{-0.5\mathrm{eV}/kT} \quad (5.3)$$

which at 200°C equals 10^{-7}, since [Si^Si] = $10^{19}/10^{23}$. Hence, in terms of density [Si—] = 10^{16}/cm^{-3} at 200°C at equilibrium. This value is close enough to the experimental values found to be considered in agreement with experiment. Thus, the simple model has provided a reasonable explanation for the fact that dangling bond densities are much smaller than the density of hydrogen bonds or weak bonds and that changes in the densities of these bonds at equilibrium are not governed by the one-to-one changes indicated by the equations but by the ratios of the concentrations defined by the equilibrium constants associated with these equations.

If a reader objects to the above perhaps a modification of the above in terms of current defect models will be satisfactory. The equivalent reaction is that of Powell et al.[96] as follows.

$$\mathrm{SiHHSi} + \mathrm{Si{\wedge}Si} = 2\mathrm{SiHdb} \quad (5.4)$$

where SiHHSi is the doubly hydrogenated weak bond, which in crystalline Si is denoted as H_2^*, Si^Si is a weak bond and SiHdb is a SiH bond and dangling bond at next nearest neighbor positions as shown in Figure 5.7. The difference in energy for relation (5.4) should be nearly the same as for relation (5.1) and relations (5.2) and (5.3) should hold for it as well.

The only possible objections to either of the above reactions is that they place dangling bonds too close to each other. However, the diffusion of H or H_2 from isolated SiH bonds to the dangling bond will result in a transfer in position of the dangling bond. Models for this have been proposed in the literature.[97]

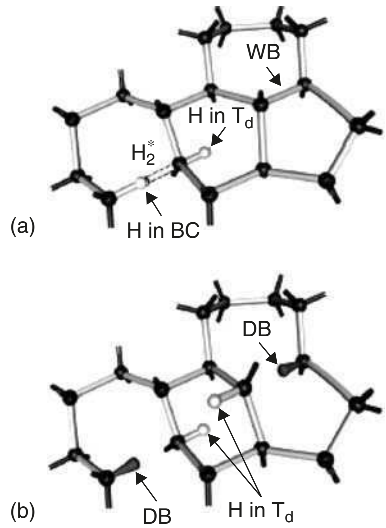

Figure 5.7. Stick model showing defects (a) before and (b) after reaction (5.4). Reproduced with permission from J. Non-Cryst. Sol. 299–302, 556(2002).

We now have the reason to examine possible relationships between processing and weak bond population density. We may consider deposition modes of processing and modes of processing subsequent to deposition. The latter will be discussed first. We may note that in doped α-Si:H the activation energy for diffusion varies from that in undoped films. Thus, in n-type α-Si:H it is possible to obtain mobility at lower temperatures for the unit that acts to equilibrate defects as shown in Figure 5.8. The diffusing unit is H^- and with a smaller activation energy. Is this helpful for processing to reduce dangling bond densities? Unfortunately, no. The reason is that now the predominant defect is negatively charged dangling bonds which in electron doped films require a smaller formation energy than the neutral dangling bonds. Thus, the dangling bond density at a given temperature increases above that in the undoped films from the contribution due to the negatively charged ones, as verified by the data in Figure 5.9 due to Winer, the author of the original defect-pool model paper. The astute reader may be perturbed by the lack of any temperature dependence for the open circle points since by the simple model above one would expect there to be a finite value for this formation energy. However, the matter is more complicated than can be treated by the simple model and the reader is referred to Ref. [98].

Thus, at this writing there is no hope of an equilibrium-based post-deposition processing treatment of improving structure beyond that already reached in state of the art α-Si:H films. Let us consider therefore deposition processing modes. First, physical modes of deposition of α-Si:H films yielded poorer

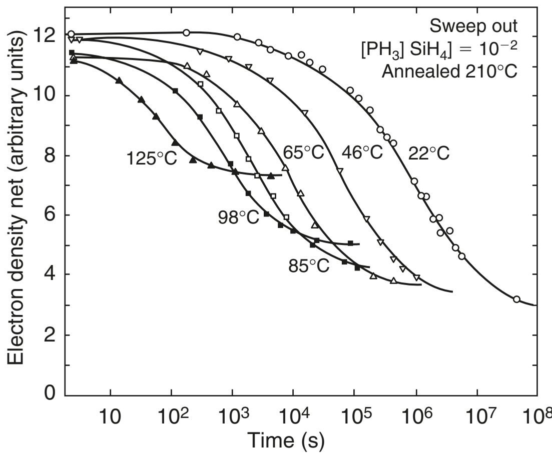

Figure 5.8. Electron density (doping density – dangling bond density) after annealing at 210°C and quenching to temperatures shown as function of time. Reproduced with permission from Phys. Rev. B37, 4209(1988).

properties than chemical vapor deposition (CVD) based methods of deposition of these films until the industry stabilized production using CVD methods. Now, it is possible to prepare films via a PVD mode with the same properties as found in CVD films.[102] We will consider the problems originally associated with PVD of α-Si:H in the Appendix. Most hydrogenated amorphous silicon films are produced via some plasma modified CVD in a silane-containing atmosphere. When the only radical product of the silane decomposition is SiH_3 then it is possible to deposit silicon films that are free of columnar structure. It is believed that this result is a consequence of a large value for the diffusion length of this radical along the surface between impingement and attachment to the film. Contrariwise, when the radical products include SiH_2 and SiH then attachment of the radical to the film can occur upon impingement thus promoting the phenomenon of shadowing and the consequent columnar structure. The latter behavior is a typical result of PVD processes when deposition is at low temperature, as we have shown in Chapter II. In the glow discharge apparatus, the latter radical products become more numerous the higher is the radio frequency (RF) power in the plasma. However, it should be noted that the latter effect occurs when the silane pressure is high enough to involve numerous collisions between the gas

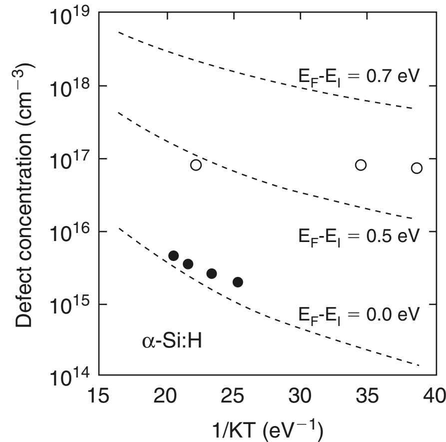

Figure 5.9. Defect concentration versus reciprocal temperature. Open circles are P doped; filled circles are undoped α-Si:H films. Reproduced with permission from K. Winer, Phys. Rev. B41, 12150(1990).

atoms prior to their contact with the film surface and/or when the silane input rate is in the order of or smaller than the silane consumption rate in the plasma. The conditions corresponding to the depositions carried out to produce Figure 5.10 were such that few gas collisions occurred between gas molecules prior to deposition (i.e. the gas pressure was 30 mTorr, and the input rate of silane was increased proportional to the RF power. The latter conditions yielded a dangling bond density at a substrate temperature of 250°C that is independent of the growth rate, as shown in Figure 5.10, whereas the former conditions yield an increasing dangling bond density with increase in the growth rate for the same substrate temperature when the source is monosilane[22] and the inverse effect (i.e. a decrease in defect density with increasing power or growth rate) when the source is disilane.[23] These variations can be all correlated to the effect of the deposition rate or power on the SiH_2 radical concentration in the plasma and the corresponding dihydride concentration in the films in these series of experiments.[24–26] This correlation suggests another, namely, that dangling bond density correlates to dihydride concentration. This is a controversial correlation.

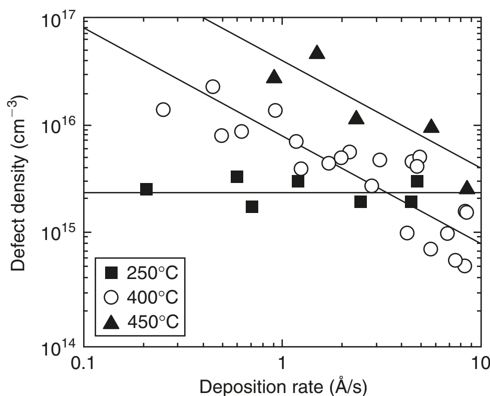

Figure 5.10. Defect densities versus growth rate in α-Si:H films. Reproduced with permission from G. Ganguly and A. Matsuda, Phys. Rev. B47, 3661(1993).

Figure 5.11 based on an independent study[99] confirms the result shown in Figure 5.10 at the growth rate of about 4 Å/s, namely that this same growth rate is independent of temperature. However, the study revealed another fact, namely, the reaction probability for SiH_3 with α-Si:H is 0.3.

There are various radical reaction products that impinge on the surface of a growing α-Si:H film. In particular, we are concerned with SiH, SiH_2, SiH_3 and H. Molecular dynamic simulations reveal that SiH_2 is the dominating reactive species at 230°C, while SiH becomes the dominating species reacting with the film at higher temperature and SiH_3 dominates at lower temperature. When SiH penetrates the surface it can decompose to yield under and over-coordinated Si network atoms, as well as dangling bonds.[100] SiH_2 species are less stable than SiH species in a reaction liberating H to form dangling bonds. Hence, one may well expect the dangling bond population of films containing dihydride bonds to be large. The least dangling bond population is produced at temperatures less than

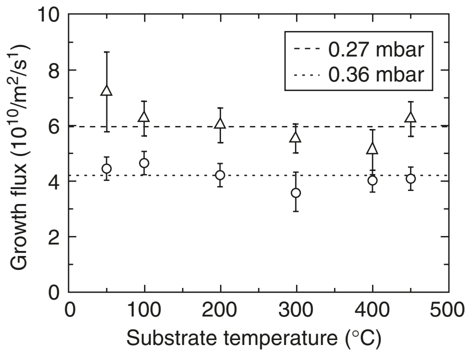

Figure 5.11. Growth flux versus substrate temperature in PECVD. Reproduced with permission from J.P.M. Hoefnagels et al., J. Appl. Phys. 96, 4094(2004).

230°C when SiH_3 is the dominant species reacting to grow the film.

Ganguly and Matsuda[18] have provided a model for surface reactions that relate deposition parameters to dangling bond density. We have not recapitulated their model here, but instead we limit our discussion relating to deposition parameters and defects to experimental facts. Ganguly and Matsuda[18] have shown empirically also that providing that the growth atmosphere consists of the SiH_3 radical to the exclusion of the SiH_2 radical and other components that promote PVD type growth then increasing the growth rate at a substrate temperature of 400°C decreases both the Urbach tail slope and the dangling bond density of as-deposited films. Further, in some more recent work[27] they have shown that increase of the kinetic energy of the SiH_3 radicals impinging the growth surface can result in a further decrease of the dangling bond density.

Figure 5.12 presents a plot of dangling bond densities obtained from independent sources. The points are for as-deposited samples.[28,80] This plot has been made to show that the points imply an activated process with an activation energy of about 0.7 eV. Stutzman noted this possible relationship earlier.[28] Matsuda provided a possible and reasonable explanation for these data. He noted that roughly the dangling bond density is the result of a steady-state induced by the equality between annihilation rates due to SiH_3 forming a hydrogen bond at a surface dangling bond and a generation rate caused by SiH_3 reacting with a bonded hydrogen atom at the surface to form SiH_4 that then joins the vapor state. He noted that at low substrate temperature the dangling bond annihilation rate becomes slow due to the slow diffusion of SiH_3 on the surface while the formation rate remains constant. Hence, there is a build-up in the dangling bond density at low substrate temperature as shown in Figure 5.12. The fact is that the activation energy for SiH_3 diffusion on α-Si:H has been evaluated[83] to be 0.75 eV, a result that acts to support Matsuda's model.

It is interesting to note that deposition, at 300°C, of Si onto a {100} crystalline substrate produces a crystalline film, whereas such deposition onto an amorphous substrate, such as glass, produces an amorphous film. Thus, the substrate determines, via epitaxy or the lack of epitaxy, the structure of the resultant covalently bonded film at a substrate temperature of 300°C. Since the defect structure

of amorphous films can vary markedly, one might expect to be able to affect this defect structure through control of the structure of the substrate. In fact, Schubert and Bauer[31] found an effect of the substrate on the transverse optical Raman peak width for thin films, as shown in Figure 5.13, which disappears beyond a film thickness of about 70 nm. This is an interesting result for it provides supporting evidence that events at the film/substrate interface affect the defect structure of the film and that this effect is diminished by the effect of the events that occur at the film/vapor interface. Apparently the deposition conditions influence the structure in each layer deposited until in thick films the original influence of the substrate is overwhelmed by the integrated influence of the deposition conditions and the latter prevails. It is unfortunate that despite much work our knowledge of the reactions that occur at the surface during deposition is insufficient to allow prediction of deposition methods and conditions for improvement of the properties of α-Si:H. Whatever progress that has been made in achieving improvement in these properties to date has been accomplished by empirical means.

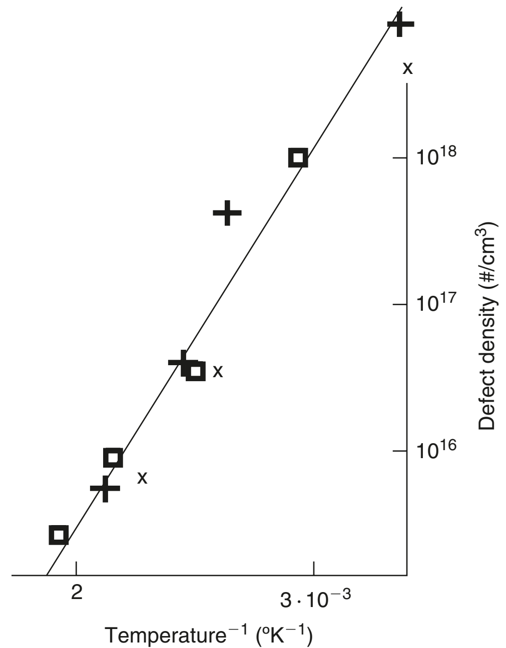

Figure 5.12. Dangling bond density as a function of reciprocal temperature in device-grade α-Si:H films. The full line is only an aid to the eye.

Summarizing, we have extracted from the complex and abundant database regarding the plasma enhanced CVD processing of α-Si:H films the essence concerning the conditions that need to be satisfied in order to deposit films having the lowest possible density of dangling bond defects. CVD conditions are necessary to produce device-grade films. Only empirical knowledge is available to guide the development of techniques to lower the dangling bond density below the values presently attainable. Model-based prescriptions for improvements in deposition procedures are inadequate.

There is another subject, the Staebler–Wronski (S–W) effect, which should be discussed here in view of its practical importance. This effect refers to the reversible increase of dangling bond defects with photoillumination. This result

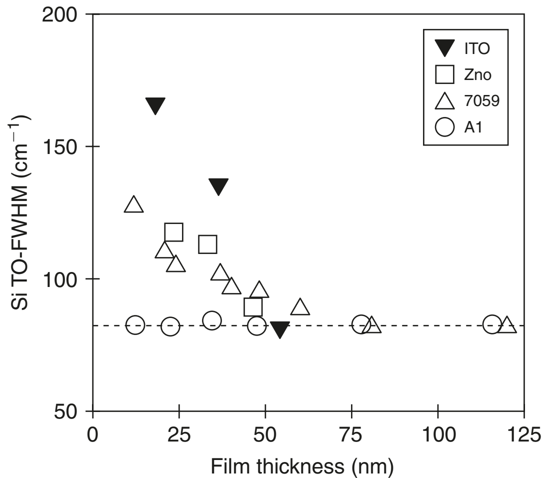

Figure 5.13. Raman TO peak full width at half maximum versus film thickness for various substrates. Reproduced with permission from M.H. Schubert and G.H. Bauer, 21st IEEE Photovoltaic Specialists Conf., Vol. II, 1595(1990). © 1990 IEEE.

detrimentally affects the properties of α-Si:H as solar cell material. It is said that the α-Si:H film is not stable with respect to a change in its properties due to photoillumination. The structural origin of this effect is not really known although it has been studied for decades. (The reversibility refers to the recovery of properties upon appropriate annealing of the film.) However, since the first edition of this book it is believed by many that at least another structural parameter affects the S–W stability of α-Si:H, but the identity of this structural parameter still puzzles investigators, i.e. the same dangling bond density has been found in both stable and unstable films. Despite this ignorance a significant advance has been made since the first edition of this book. A way has been found to bring about an appreciable diminution of the S–W instability with respect to light exposure. The processing advance is the use of appropriate hydrogen dilution during deposition.

The main structural characteristics that were observed to be affected by the appropriate hydrogen dilution processing are the order in the amorphous network as measured by the average deviation of bond angles from the sp_3 configuration (short-range order), medium-range order, as measured by the ratio of the intensity of the Raman TA peak to that of the TO peak and the nucleation of crystalline grains, albeit too small to be detected in a Raman spectrum.

As noted previously the width of the TO peak at about 480/cm is a measure of the deviation of bond angles from their stable crystal value. The change in frequency of this peak also depends upon this bond angle deviation. Increasing

frequency denotes decrease in the bond angle deviation. Recent molecular dynamics (MD) studies have been able to quantify these relationships.[76] In particular, one set of these relationships is given by

$$\Gamma = 18.4 + 6.6\Delta\theta \quad \text{and} \quad \omega = -2.5\Delta\theta + 503.5$$

where $\Delta\theta$ is the average bond angle deviation from that for the sp_3 state, Γ is the FWHM of the 480/cm Raman peak and ω is the frequency of this peak in cm^{-1}.

A processing parameter that correlates to Γ is the hydrogen dilution ratio in the environment of the film surface. As the hydrogen dilution ratio increases from zero Γ decreases, as illustrated in Figure 5.14. This increase in short- and medium-range order of α-Si:H with increase in hydrogen dilution has been observed in many investigations.[75] Not only does the short-range order increase, but the tendency to nucleate and grow crystallites in the α-Si:H network increases also. At this writing (revised edition), it is believed that the optimum microstructure for S–W stability is that produced by hydrogen dilution type deposition at a dilution level just before the level corresponding to the appearance of a peak in the Raman spectrum from crystalline Si at 515 cm^{-1}. For device quality α-Si:H films the TO peak has a FWHM value of about 70 cm^{-1}. The state of the amorphous film just before the onset of crystallization, as revealed in the Raman spectrum, is denoted the protocrystalline state in the literature. Normally, in films produced via plasma enhanced CVD (PECVD) this protocrystalline state occurs at a hydrogen dilution of 2 for a substrate temperature between 240°C and 250°C and 3 for T_S = 200°C.[74] The typical processing that produces this protocrystalline state is described in Ref. [78].

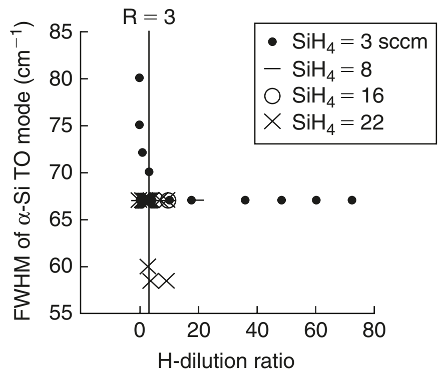

Figure 5.14. The decrease in FWHM for the α-Si peak for the filled circle group all occurred as the amount of crystalline Si increased from 0% to about 80%. Reproduced with permission from D. Han, J.D. Lorentzen, J. Weinberg-Wolf, L.E. McNeil and Q. Wang, J. Appl. Phys. 94, 2930(2003).

With hydrogen dilution such that conditions are just prior to the onset of crystallization, film thickness is found to affect structure as follows. The film during deposition starts with an all amorphous structure, which may or may not contain some porosity depending upon deposition conditions. Upon increase in thickness the order of the α-Si:H network increases and also the volume fraction of c-Si in

the film increases from zero at some finite thickness. Also, it is found that the compressive stress in the film increases with increasing film thickness.[72,77] All this occurs at constant H content versus thickness.

Although defect density as measured by CPM shows no change with hydrogen dilution, drive-level capacitance profiling (DLCP) does reveal a decrease in defect density with hydrogen dilution.[79] CPM measures the defect density along the film surface whereas DLCP measures it in the direction normal to the film surface. The DLCP defect density was found to decrease as the thickness of the film increased at the conditions corresponding to the protocrystalline film. However, ESR measurements reveal that spin density, as shown in Figure 5.15, is at a minimum in the amorphous region adjacent to the amorphous–crystalline transition and then increases with increasing crystalline content.

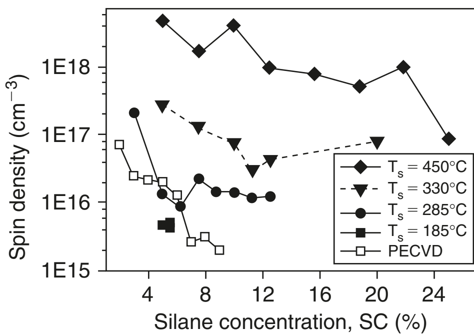

Figure 5.15. Spin density for hot wire and PECVD microcrystalline Si films from onset of crystallinity. Reproduced with permission from F. Finger et al., MRS Symp. Proc. 715, A16.3.1(2002).

The heterogeneous nucleation of crystals in the amorphous matrix will occur first at regions where the excess free energy relative to the average free energy for the amorphous matrix is highest. *Thus, the act of formation of a crystalline nucleus may well remove the defects responsible for the long-time light soaking S–W degradation.* The crystal nucleus in amorphous silicon contains about 110 atoms. Hence, a distribution of crystal nuclei is likely to exist in films deposited with appropriate hydrogen dilution procedure at the stage before the onset of crystallization is indicated in rough observables, such as the Raman or even photoluminescence spectra, i.e. the protocrystalline stage.

Figure 5.16 provides a schematic illustration of the microstructure produced with various hydrogen dilutions, which in the figure increases from right to left. (SC in this figure is the ratio of silane to the sum of the silane and hydrogen concentrations). The features of the microstructure illustrated in this figure are void content (decreasing from right to left), amorphous structure, columnar structure, crystalline structure, amorphous regions along crystalline grain boundaries, ribbon-like voids between grains at grain boundaries and intercolumnar regions, and isolated small crystalline regions within amorphous matrix. This view of the microstructure is based on one study,[101] and, hence one group's processing procedure.

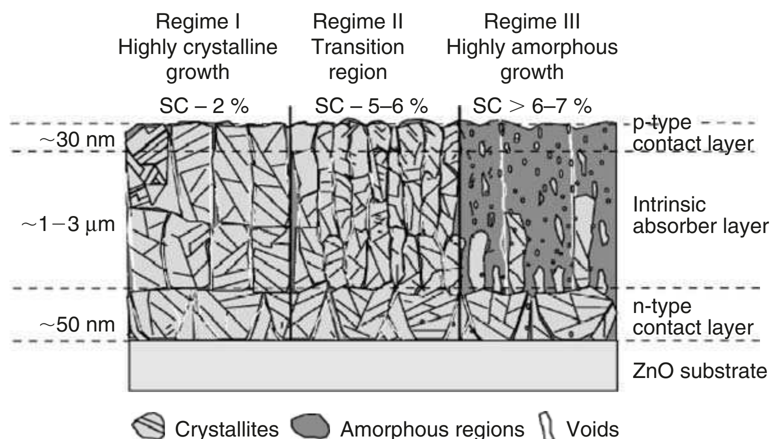

Figure 5.16. Schematic illustration of microstructure as function of silane concentration. Reproduced with permission from F. Finger et al., MRS Symp. Proc. 715, A16.3.1(2002).

Summarizing, to produce the highest quality hydrogenated amorphous silicon for electronic applications it is necessary to deposit films having the minimum dangling bond density possible. For solar cell application where stability to light exposure is important it appears that the microstructure of the film should be that found in the so-called protocrystalline film.

1.1.2. α-Ge and α-Ge:H.

α-Ge:H films are of interest because they have a smaller band gap than α-Si:H films. The optimum process parameters for depositing device-grade α-Si:H are not likely to produce device-grade α-Ge:H if only because Ge bonds are weaker than Si bonds. Thus, it comes as no surprise that device-grade α-Ge:H cannot be produced with the device-grade α-Si:H processing parameters. In contrast with the conditions applicable to the deposition of α-Si:H it is found that high power in the glow discharge is beneficial in the deposition of device-grade α-Ge:H.[39] Indeed, as shown by Paul[40] at the same deposition conditions that produce a "homogeneous", non-columnar film of α-Si:H, a columnar film of α-Ge:H is formed. This result implies that under these conditions deposition has CVD character for α-Si:H, but has physical vapor deposition (PVD) character for α-Ge:H. Paul et al.[41] have further shown that elimination of the intercolumnar void network in α-Ge:H leads to a 100-fold improvement in photoelectronic properties, as might be expected from the experience with α-Si:H. However, the best properties still do not match those for α-Si:H. Also, exposure of the film during deposition to atomic

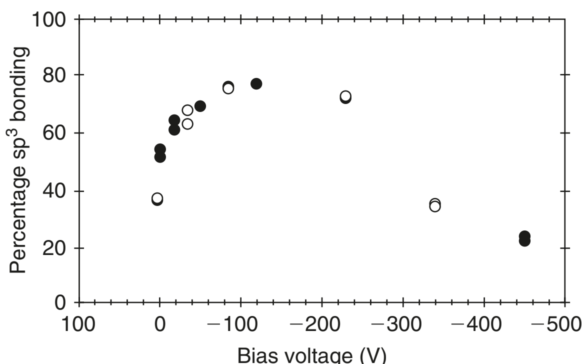

Figure 5.17. Percentage sp^3 content of amorphous carbon film as a function of the bias voltage. The film is formed by deposition of a filtered C ion beam having 20 eV plus bias voltage energy. Reproduced with permission from P.J. Fallon et al., Phys. Rev. B48, 4777(1993).

hydrogen has a beneficial effect on properties.[42] This result is attributed to a reduction in the probability of incorporation of germane radicals into the film via the passivation of Ge dangling bonds at the growing surface by hydrogen atoms. Also, contrary to its behavior with Si, hydrogen does not etch α-Ge:H.

1.1.3. α-C and α-C:H.

Amorphous carbon has one additional type of defect not present in the amorphous silicon and germanium materials. This defect is of course the degree of non-tetrahedral bonding, as measured by the sp^2/sp^3 ratio. Ab initio molecular dynamic simulation of amorphous carbon[43] reveals that the percentage of sp^3 bonds present is small, i.e. about 15%. The structure although three-dimensional appears to be arranged into a succession of "thick planes".

Contrary to the other amorphous covalently bonded materials, hydrogenated amorphous carbon is valued not only because of its electronic properties, but because of its hardness and low coefficient of friction. It has a higher band gap than hydrogenated amorphous silicon. Hydrogen acts to increase the percentage of tetrahedral bonding thereby enhancing the hardness of hydrogenated amorphous carbon films relative to those that are produced in the absence of hydrogen. The tetrahedral bonded fraction of amorphous carbon can be increased also by the use of incident energetic carbon atoms (10–150 eV).[44] Figure 5.17 illustrates the dependence of the sp^3 fraction in a film deposited using an incident magnetically filtered C^+ beam as a function of the incident ion energy.

It is possible to understand the result shown in Figure 5.17 on the basis of some results from another molecular dynamics simulation due to Tersoff.[45] He

found that amorphous carbon films formed in the simulation by quenching from the liquid state, with or without applied external pressure, or by condensation all had about the same energy, 0.4 eV above that of crystalline diamond. However, the sample formed by quenching under 1 Mbar of pressure exhibited a density 14% less than that of diamond with almost half of the atoms being 4-fold coordinated (sp^3 bonded) while the sample formed in the same way, but in the absence of pressure, had a density 32% less than that of diamond and only 9% of the atoms were 4-fold coordinated. This result implies first that the energy difference between the sp^2 and sp^3 bonded amorphous states is small compared to the energy difference between the amorphous and crystalline states. This implication is consistent with the measured difference in energy between the amorphous and crystalline states for silicon, 0.2 eV, and the difference between crystalline graphite and diamond, 0.02 eV. The second implication is that pressure is sufficient to stabilize sp^3 bonds relative to sp^2 bonds in the amorphous state. The 18% increase in density upon application of 1 Mbar pressure is equivalent to 0.64 eV/atom of work expended upon the change in state at this pressure. Thus, it seems reasonable to conclude that pressure acts to stabilize the sp^3 bond relative to the sp^2 bond in the amorphous state. In agreement with this conclusion the measurements of Fallon et al. show (see Figure 5.18) that the compressive stress in the film plane also exhibits a maximum as a function of the incident ion energy, mirroring the dependence of the percentage sp^3 bonding on this variable shown in Figure 5.17.

Not only pressure can affect the sp^3 content, but also hydrogen can increase this content in amorphous hydrogenated carbon films. However, the increment achieved in the sp^3 content by the addition of hydrogen does not equal that which can be produced by self ion bombardment during deposition. For example, the introduction of 40 at. % H merely increases the sp^3 content to at most about 60%. Also, the dangling bond density in the latter film is about $10^{20}/cm^3$, which exceeds the defect

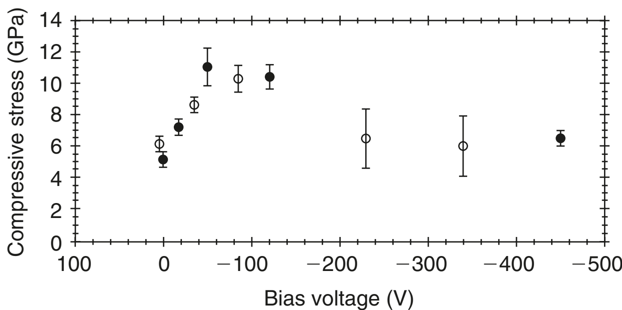

Figure 5.18. Compressive stress in plane of film as a function of bias voltage for same films shown in Figure 5.16. Reproduced with permission from P.J. Fallon et al., Phys. Rev B48, 4777(1993).

density present in α-Si in the absence of hydrogen by an order of magnitude. A likely source of this exceedingly high dangling bond density is the presence of bounded sp^2 bonded thick planes (clusters) with dangling bonds at the circumference of these bounded planes in a matrix of an sp^3 network. When the sp^3 bonded network is continuous, at hydrogen contents less than about 40%, the film is hard. When it is not continuous, at hydrogen concentrations greater than about 40%, the film is soft despite the presence of a higher sp^3 content, greater than about 50% and possibly approaching 80%, in the film.

Robertson[46] has provided a quantitative model for the elastic modulus and hardness of amorphous carbons based upon Phillips'[47] concept of the relation between average coordination number, the number of constraints per atom and the number of degrees of freedom per atom, and upon Thorpe's[48] use of this relation for covalent amorphous networks to obtain their elastic modulus. The number of constraints per atom is obtained as follows. Each bond contributes one constraint, while a bond is shared between two atoms. Hence, the number of constraints per atom contributed by bonds equals $z/2$, where z is the coordination number of bonds to other atoms in the network. The covalent nature of the bonding also contributes constraints via the constraints due to the bond angles. The latter equals $2z - 3$, for $z \leqslant 4$.[40] Thus, the total constraints per atom equals $5z/2 - 3$. In three-dimensional space the number of degrees of freedom per atom is 3. Setting the latter equal to the total number of constraints yields $z_c = 2.4$. Above this average coordination number the network is over-coordinated, rigid, and strained. Below this value it can be deformed at no expenditure of energy. The effect of hydrogen on the average coordination number can be included by considering any bonded hydrogen about a network atom as a reduction in the coordination of that atom. Thus, $z = (1 - X_H)z_0 + X_H(z_0 - 1) = z_0 - X_H$. Robertson[46] has considered the effect of sp^2 bonded graphite clusters and polymeric bonded carbon in an sp^3 bonded matrix on the Young's modulus and hardness of amorphous carbon films using the relation between Young's modulus, E, and average coordination number developed by He and Thorpe[49] given by

$$E/E_0 = (z - 2.4)^{1.5}/(z_0 - 2.4)^{1.5}$$

and found agreement with experimental values of E using experimental values of the sp^3 and H concentrations to calculate z.

1.2. Amorphous semiconductor alloys and compounds.

1.2.1. α-Si,Ge:H and other alloys of α-Si.

Most of the interest in producing alloys of α-Si stems from the desire to increase the efficiency of solar cells based on α-Si:H. The latter has an optical

band gap of 1.75 eV. Combination of a film with this band gap and an underlayer of a lower band gap material, such as α-Si,Ge:H, with a band gap of 1.5 eV and an overlayer with a higher band gap, such as α-Si,C:H, would in principle improve the conversion efficiency of the solar cell. However, this improvement is based on the assumption that all the films have good photoelectronic properties. The search for acceptable alloy films has an empirical basis to date, involving systematic examination of the effects of various deposition parameters on properties. This examination has not yet yielded an understanding of the deposition process sufficient to allow prediction of the processing required to obtain improved properties. However, some improvement in the conversion efficiency of a multi-junction cell has been obtained with the use of a layer of α-Si,Ge:H.[50] These investigators also found that the normal level of impurities affect the photosensitivity in both α-Si:H and α-Si,Ge:H. Finally, it should be mentioned that the most stable α-Si,Ge:H with respect to the S–W effect is that produced via hydrogen dilution just before the onset of microcrystallinity as revealed in a Raman spectrum.

A review of hydrogenated amorphous silicon alloys[1] provides a summary of what is known to early 1993 about these and other alloys with silicon.

1.2.2. Chalcogenides.

Chalcogenides are materials containing the elements sulfur, selenium and tellurium, such as As_2Se_3, which are in the form of glasses and materials in this class were the first used in the xerographic process of copying. They also exhibit a variety of photo-induced effects including structural changes, darkening, phase changes, birefringence, etc. many of which have potential applications. Despite the great research effort devoted to an understanding of these materials, an understanding of their defects, and the relation between processing and structure is largely still not known. An interpretation of their properties in terms of defect models is provided in a recent book[51] and will not be repeated here.

2. Amorphous metals and alloys.

Amorphous films have not yet been produced for those metals for which the covalent character in their bonding is negligible. Only those metals which exhibit some covalent character in their bonding, such as Ga and Bi, have been able to be deposited in the amorphous state. The reason for this behavior has been discussed already in Chapter II.

It is much easier to deposit films of alloys in the amorphous state for a variety of reasons, some of which have been discussed in Chapter II as well. One of the conditions necessary to produce amorphous alloys requires rapid quenching of the

kinetic energy of the impinging atoms and, hence, a very small adatom diffusion distance during such deposition. This condition, as discussed in Chapter II, leads to the formation of columnar structure in the deposited films via the process of shadowing. Such structure may or may not affect properties, as we will discuss below.

Because the main applications for amorphous alloy films involves their magnetic properties, we will focus our attention on the relation between the deposition process and these properties. Very recently the puzzle regarding the origin of the perpendicular magnetic anisotropy in amorphous rare earth transition metal alloys was solved.[52] Up until this work single ion anisotropy,[53] anisotropy in local short-range order,[54] atomic bond angle anisotropy,[55] and film stress,[56] had been proposed as the source of the perpendicular magnetic anisotropy. Harris et al.[52] eliminated film stress and single ion anisotropy as the primary source of the magnetic anisotropy simply by determining that such anisotropy was absent in TbFe amorphous films deposited at a substrate temperature of 77 K although the intrinsic stress in these films was compressive and of the same magnitude as found in films deposited at room temperature and which did have perpendicular magnetic anisotropy. Further, using polarized synchrotron radiation and EXAFS, they found that when these films were annealed or deposited at room and higher temperature, the number of Fe–Fe nearest-neighbor pairs in the plane of the film exceeded the number out of the plane, while the number of Fe–Tb nearest-neighbor pairs out of the plane exceeded the number in plane. (The importance of using polarized synchrotron radiation is that it allows the possibility of distinguishing in-plane from out-of-plane configurations.) Also, they found that the excess number of such pairs correlated to the magnetic anisotropy energy and to the substrate temperature. Although these observations do not eliminate atomic bond angle anisotropy as a possible origin of the magnetic anisotropy, they firmly support local short-range order as the viable candidate for this origin. The fact that annealing the films deposited at 77°K produced both perpendicular magnetic anisotropy and short-range order in films that did not have these anisotropies, without crystallization of the films, implies that the intrinsic compressive stress acts as a driving force for the inception of short-range order and hence acts as a secondary source of the perpendicular magnetic anisotropy. The fact that there are more in-plane Fe–Fe and fewer in-plane Fe–Tb pairs than random in the annealed films is consistent with a compressive stress driving force for this reorientation of nearest-neighbor atom pairs because just these reorientations will bring about a decrease of the in-plane stress-free film area and hence a decrease in the internal film strain energy.

We have seen in the previous chapter in the discussion relating to the long-range order found in III–V compound films, that not only can stress induce reordering of atoms in the surface region during deposition, but also surface energy can also provide such a driving force. These concepts are so new to this field of research at this writing that investigations inspired by them have yet to be performed or reported.

The effect of sputtering deposition conditions on perpendicular magnetic anisotropy and microstructure have been investigated for rare earth transition metals amorphous alloys. It has been found[57] that increase in the argon pressure increases the anisotropy at the same time as the microstructure remains devoid of columnar character up to a pressure of 11.5 mTorr. Above this pressure, further increase in pressure leads to the development of columnar structure, voids and to the loss of perpendicular magnetic anisotropy. These results are explicable in terms of the effect of increasing pressure in reducing the energy of the particles incident on the film surface and their concomitant effects in changing the film stress from compressive to tensile in nature (see Chapter VI). As noted above, just this change in sign of the internal stress will act to reverse the orientations of the excess atom pairs produced under compressive stress and thereby to remove the perpendicular magnetic anisotropy in these amorphous alloys. Similarly, an increase in the incident particle energy as achieved by increasing the substrate bias results in an increase in the perpendicular magnetic anisotropy[58] up to a maximum voltage beyond which it decreases. Again just this trend brings about a change in the sign of the internal stress from tension to compression in agreement again with the expected effect of stress on the magnetic anisotropy. Incidentally, the maximum in the latter with increasing bias voltage is because further increase in voltage again induces columnar structure, porosity[59] and crystallization.[57]

The amorphous state has some further advantages besides the possibility of yielding perpendicular magnetic anisotropy for magnetic applications. These are associated with the lack of grain boundaries, which allows easy migration of domain wall boundaries, and with the uniformity of the magnetic properties, which acts to reduce noise-to-signal ratio. However, few practical applications that take advantage of these properties have emerged.

3. Amorphous oxides.

3.1. Amorphous silicon oxide.

One of the main uses of thin film oxides is as gate insulators. Currently amorphous silicon oxide is the oxide of choice for this application. Such films are produced by a variety of methods, i.e. PECVD,[85] RF sputtering,[86] secondary ion deposition,[87] and ion beam deposition[88]. The structural factors that are known are the density, film stress, rings in amorphous network, and the interface composition (excess Si atoms). Aside from measured parameters, such as density and stress, most of the useful information is deduced from simulation studies. The structural aspect that is primarily responsible for the density is the void population in the film. A Monte Carlo simulation[89] of amorphous SiO_2 in which the number of sites on the substrate surface acting as heterogeneous nucleation sites for the formation

of the α-SiO_2 film was varied showed that the population density of the voids was dependent upon the density of nucleation sites. However, a minimum volume fraction of voids (4–6%) was approached with increasing nucleation site density. It is believed that the pores exist with a high oxygen concentration at the pore surface as a more stable configuration than one without pores but with an enhanced defect density. When pores are present the film stress is tensile in sign.

Deposition using ion beams to provide some energy to the film surface during deposition may reduce stress volume and increase the density. A result of a MD simulation of ion beam assisted deposition[90] concluded that ion beam deposition with an energy of about 10 eV per condensing SiO_2 particle should produce a desirable dense, low-stress film. Apparently, the mechanism of enhancing the density is not only elimination of the void fraction but also enhancement of the medium-range order via replacement of high number membered rings by smaller ones. The basic $Si(O_{1\backslash 2})_4$ tetrahedron in the amorphous structure is unaffected by the processing.

3.2. High dielectric constant amorphous oxides.

References to other amorphous oxide films may be found in Ref. [92], which itself is a study of amorphous ZrO_2 films. RF magnetron sputtering is a standard technique to produce such films although pulsed laser evaporation is another possible one for these materials. Little has been published about the structure of these films or about the relation between processing and structure for them. Most of these amorphous oxides are not network structures as is the case for the SiO_2 films.

4. Amorphous ↔ crystalline transition.

The amorphous to crystalline transition has been studied intensively in silicon,[60] in part because it is used as a means of achieving epitaxy for an overlayer, such as in silicon on insulator (SOI) technology, or for an amorphous buried layer, as induced in ion implantation. These studies have provided data to characterize the velocity of the α/c interface as a function of temperature and of the nucleation of crystalline regions in the amorphous matrix. In this section we are concerned with the latter process since it is a competing process in many of the methods of depositing an amorphous film. Because the crystalline state is more stable than the amorphous state sufficient local fluctuations in energy may nucleate crystalline regions. The likelihood of such nucleation depends upon the free energy of nucleation, which in amorphous silicon equals about 5.5 eV/atom. The critical nucleus in amorphous silicon contains about 110 atoms. How may the energy required for nucleation be supplied to this volume in the deposition process? There are two possibilities. One is via the heat released from an exothermic reaction. Another is via the energy deposited by an incident particle. Let us consider these possibilities.

There are several reactions involving atomic hydrogen that are exothermic. Further, since a microcrystal of silicon will not contain as much bonded hydrogen as the same volume of α-Si:H, the reaction involving the removal of bonded hydrogen by atomic hydrogen would seem to be a prime candidate for the exothermic reaction possibly involved in the nucleation of μc-Si (microcrystalline silicon). It should come as no surprise therefore to learn that nanocrystalline silicon can be induced to form during deposition under conditions that otherwise are optimum for the production of amorphous silicon simply by increasing the concentration of atomic hydrogen available at the growth surface sufficiently.[61] It should be remarked that in a dense matrix the heat released would normally dissipate by conduction in an interval less than 10^{-11} s and this process would not be able to bring about the number of activated processes required to produce a crystal nucleus. However, in the less dense, porous region of the amorphous film adjacent to the deposition surface thermal conduction may be hindered sufficiently to produce the temperature pulses needed for the nucleation to occur. It must be mentioned that the mechanism of nucleation (or formation) of μc-Si is controversial at this writing. One school assumes the presence of μc-Si nuclei in any α-Si:H matrix and ascribes the preferential growth of the former to a more rapid etching away of the latter in the hydrogen-rich atmosphere required to produce μc-Si in plasma reactors. However, evidence has been presented[62] to prove that μc-Si can form below the surface during deposition while the film surface itself is amorphous.

It is also an empirical fact that energetic particle bombardment of amorphous covalently bonded films can induce crystallization either during deposition[63] or subsequent to deposition.[64] In the latter case, both the production and motion of defects within a displacement spike and the increase in temperature in the temperature spike can act to enhance the nucleation of crystals in the amorphous matrix. The onset of crystallization in an amorphous matrix subsequent to deposition at low substrate temperature requires a minimum value of the energy density transmitted to the amorphous solid to be exceeded.[64c] It proceeds by nucleation and growth of crystals in the amorphous matrix.[64d] During deposition, since energetic particle bombardment lowers the temperature at which epitaxial deposition can occur relative to the epitaxial temperature in the absence of energetic particles, either the energetic particles prevent the formation of the amorphous phase or they act to increase the amorphous/crystal interface velocity so that it equals the deposition velocity. Incidentally, crystallization has been detected also in amorphous alloys subject to particle bombardment during deposition,[57,58] but not in pure metals.

Not only does particle bombardment induce crystallization of amorphous solids, but at higher normalized momenta or transmitted energy density particle bombardment can amorphize crystalline materials. The transmitted energy density is the correlating parameter in the amorphization of crystalline silicon at low temperatures and the critical value of this parameter in this case is 12 eV/atom within the range of the bombarding particles.[65]

It may seem to be a paradox that particle bombardment can induce crystallization of an amorphous material and amorphization of the same crystalline material. However, crystallization occurs because particle bombardment of an amorphous material, via the production of mobile defects, can induce nucleation to the more stable, defect-free, crystalline material. Amorphization occurs because particle bombardment of a crystalline material, again via the production of sufficient defects, either produces the amorphous state directly, or by raising the free energy of the crystal, so that it exceeds that for the amorphous state of the material, allows nucleation and growth of a more stable amorphous state. Indeed, the theory[66] governing the effect of energetic particle penetration of the amorphous/crystalline interface on the direction and velocity of this interface, takes into account both the amorphizing effect on the crystal side of the interface and the crystallizing effect on the amorphous side of the interface.

The field considered in this subsection has not been investigated in any depth, although the amorphization of crystalline solids already formed by ion bombardment has a history extending back to the 1960s. From the knowledge that surfaces are preferential sites for the nucleation of the crystalline to amorphous transition[67] or for the nucleation of any transformation,[68] it is most likely that the site of nucleation of transformations during deposition is the surface itself. However, this remains to be demonstrated experimentally. Indeed, particle bombardment of amorphous films induces nucleation in both the volume and at the surface of the film.[69] Also, many more studies delineating the crystalline and amorphous regions need to be carried out. For example, one interesting case would be that for SiO_2, where it has been shown that neutral inert gas atom bombardment subsequent to deposition can transform amorphous silica to crystalline α-quartz.[64c] It would be interesting to determine the parameters governing this transition in particle bombardment assisted deposition of this material.

References

1. W. Luft and Y.S. Tsuo, **Hydrogenated Amorphous Silicon Alloy Deposition Processes**, Marcel Dekker, NY, 1993, p. 14.
2. I. An, Y.M. Li, C.R. Wronski and R.W. Collins, Phys. Rev. B48, 4464(1993).
3. T. Shimizu and M. Kumeda, in **Amorphous Silicon and Related Materials, Advances in Disordered Semiconductors**, Vol. I, ed. H. Fritzsche, World Scientific, Singapore, 1988, p. 633.
4. A.P. Sokolov, A.P. Shebanin, O.A. Golikova and M.M. Mezdrogina, J. Non-Cryst. Sol. 137/138, 99(1991).
5. a) P.A. Fedders, Y. Fu, and D.A. Drabold, MRS Symp. Proc. 258, 335(1992); b) P.A. Fedders and D.D. Drabold, MRS Symp. Proc. 219, 247(1991).
6. R.W. Collins and J.M. Cavese, MRS Symp. Proc. 118, 19(1988).
7. R. Reitano, M.G. Grimaldi, P. Baeri, E. Bellandi, S. Borghesi and G. Baratta, J. Appl. Phys. 74, 2850(1993).

8. K. Winer, I. Hirabayashi and L. Ley, Phys. Rev. B38, 7680(1988); K. Winer and L. Ley, **Advances in Disordered Semiconductors**, Vol. I, ed. H. Fritzsche, World Scientific, Singapore, 1989, p. 405.
9. P.C. Kelires and J. Tersoff, Phys. Rev. Lett. 61, 562(1988).
10. M. Brodsky, D. Kaplan and J.F. Zeigler, Appl. Phys. Lett. 21, 305(1972).
11. N.J. Shevchik and W. Paul, J. Non-Cryst. Sol. 16, 55(1974).
12. A.H. Mahan, Y. Chen, D.L. Williamson and G.D. Mooney, J. Non-Cryst. Sol. 137/138, 65(1991).
13. M. Stutzmann, Phil. Mag. B60, 531(1989).
14. D.K. Biegelsen, R.A. Street, C.C. Tsai and J.C. Knights, Phys. Rev. B20, 4839(1979); M. Stutzmann and D.K. Biegelsen, Phys. Rev. B28, 6256(1983).
15. R.A. Street, **Hydrogenated Amorphous Silicon**, Cambridge University Press, Cambridge, England, 1991, p. 108.
16. R.A. Street and K. Winer, Phys. Rev. B40, 6236(1989).
17. A.H. Mahan, E.J. Johnson and J.D. Webb, MRS Symp. Proc. 297, 103(1993).
18. G. Ganguly and A. Matsuda, Phys. Rev. B47, 3661(1993).
19. A.H. Mahan, J. Carapella, B.P. Nelson, R.S. Crandall and I. Balberg, J. Appl. Phys. 69, 6728(1991).
20. K. Winer, Phys. Rev. B41, 12150(1990).
21. R.A. Street, Phys. Rev. B43, 2454(1991); B44, 10610(1991).
22. J.C. Knights, G. Lucovsky and R.J. Nemanich, J. Non-Cryst. Sol. 32, 393(1979).
23. M. Kumeda, H. Komatsu, T. Shimizu, N. Fukeda and N. Kitagawa, Jpn. J. Appl. Phys. 24, L495(1985).
24. J.C. Knights, Jpn. J. Appl. Phys. 18, Suppl. 18-1, 101(1979).
25. R.C. Ross and J. Jaklik, J. Appl. Phys. 55, 3785(1984).
26. H. Wiesmann, J. Dolan, G. Fricano and V. Danginis, STR-211-3097m Solar Energy Research Inst., January 1987.
27. H. Nishio, G. Ganguly and A. Matsuda, MRS Symp. Proc. 297, 91(1993).
28. J.C. Knights and G. Lucovsky, CRC Crit. Rev. in Solid State and Mat. Sci. 21, 211(1980); M. Vanacek, B.P. Nelson, A.H. Mahan and R.S. Crandall, J. Non-Cryst. Sol. 137/138, 191(1991).
29. T.J. McMahon, Sol. Cells 30, 235(1991).
30. M.K. Cheung and M.A. Petrich, MRS Symp. Proc. 258, 191(1992).
31. M.B. Schubert and G.H. Bauer, 21st IEEE Photovoltaic Specialists Conf., Vol. II, 1595(1990).
32. Ref. [15], p. 192.
33. N. Hata and S. Wagner, J. Appl. Phys. 72, 2857(1992).
34. M. Stutzmann, W.B. Jackson and C.C. Tsai, Phys. Rev. B32, 23(1985); D. Redfield, Appl. Phys. Lett. 52, 492(1988).
35. G. Schumm, Phys. Rev. B49, 2427(1994).
36. J.-H. Yoon, J. Appl. Phys. 74, 1838(1993).
37. J.K. Lee and E.A. Schiff, MRS Symp. Proc. 258, 185(1992).
38. U. Kroll, F. Finger, J. Dutta, H. Keppner, A. Shah. A. Howling. J.-L. Dorier and C. Hollenstein, MRS Symp. Proc. 258, 135(1992).
39. W. Kasper, R. Plattner and J. Eichmeier, J. Non-Cryst. Sol. 137/138, 799(1991).
40. W. Paul, J. Non-Cryst. Sol. 137/138, 803(1991).

41. W. Paul, S.J. Jones, F.C. Marques, D. Pang, W.A. Turner, A.E. Wetsel, P. Wickboldt and J.H. Chen, MRS Symp. Proc. 219, 211(1991).
42. J.H. Chen, P. Wickboldt, D. Pang, A.E. Wetsel and W. Paul, MRS Symp. Proc. 258, 547(1992).
43. G. Galli, R.M. Martin, R. Car and M. Parrinello, Phys. Rev. B42, 7474(1990).
44. P.J. Fallon, V.S. Veerasamy, C.A. Davis, J. Robertson, G.A.J. Amaratunga, W.I. Milne and J. Koskinen, Phys. Rev. B48, 4777(1993); R. Lossy et al., J. Appl. Phys. 77, 4750(1995); Y. Lifshitz, Diamond Rel. Mater. 5, 388(1996); S.R.P. Silva et al., Appl. Phys. Lett. 69, 491(1996).
45. J. Tersoff, Phys. Rev. Lett. 61, 2879(1988).
46. J. Robertson, Diamond Rel. Mater. 1, 397(1992).
47. J.C. Phillips, J. Non-Cryst. Sol. 34, 153(1979).
48. M.F. Thorpe, J. Non-Cryst. Sol. 57, 355(1983).
49. H. He and M.F. Thorpe, Phys. Rev. Lett. 54, 2107(1985).
50. K. Sayama, H. Haku, H. Dohjoh, M. Isomura, N. Nakamura, S. Tsuda, Y. Kishi, S. Nakano and Y. Kuwano, MRS Symp. Proc. 219, 691(1991).
51. H. Fritzche in Insulating and Semiconducting Glasses, ed. P. Boolchand, World Scientific Press, Ltd, Singapore, 2000, p. 653.
52. V.G. Harris, K.D. Aylesworth, B.N. Das, W.T. Elam and N.C. Koon, J. Alloy Compd. 181, 431(1992); IEEE Trans. Magn. 28, 2958(1992); Phys. Rev. Lett. 69, 1939(1992); V.G. Harris, F. Hellman, W.T. Elam, N.C. Koon, J. Appl. Phys. 73, 5785(1993).
53. R. Sato, N. Saito and Y. Togami, Jpn. J. Appl. Phys. 24, L266(1985); Y. Suzuki, S. Takayama, F. Kirino and N. Ohta, IEEE Trans. Magn. 23, (1987).
54. R.J. Gambino, P. Chaudhari and J.J. Cuomo, AIP Conf. Proc. 18, 578(1973); R.J. Gambino and J.J. Cuomo, J. Vac. Sci. Tech. 15, 296(1978).
55. Y. Suzuki, J. Haimovich and T. Egami, Phys. Rev. B35, 2162(1987); T. Egami, C.D. Graham Jr, W. Dmowski, P. Zhou, P.J. Flanders, E.E. Marinero, H. Notarys and C. Robinson, IEEE Trans. Magn. 23, 2269(1987).
56. S. Tsunashima, H. Takagi, K. Kamegaki, T. Fujii and S. Uchiyama, IEEE Trans. Magn. 14, 844(1978); H. Takagi, S. Tsunashima, S. Uchiyama and T. Fujii, J. Appl. Phys. 50, 1642(1979); S. Yoshino, H. Takagi, S. Tsunashima, M. Masuda and S. Uchiyama, Jpn. J. Appl. Phys. 23, 188(1984).
57. J.-W. Lee, S.-C.N. Cheng, M.H. Kryder and D.E. Laughlin, MRS Symp. Proc. 150, 159(1989).
58. M.H. Kryder, MRS Symp. Proc. 150, 3(1989).
59. H.-P.D. Shieh, M. Hong and S. Nakahara, J. Appl. Phys. 63, 3627(1988).
60. G.L. Olson and R.A. Roth, Mater. Sci. Rep. 3, 1(1988).
61. Ref. [1], p. 221.
62. S. Aljishi, S. Jin, M. Stutzmann and L. Ley, MRS Symp. Proc. 164, 51(1990).
63. a) H. Windischmann, J.M. Cavese, R.W. Collins, R.D. Harris, J. Gonzalez-Hernandez, MRS Symp. Proc. 47, 187(1985); b) K. Ogata, Y. Andoh and E. Kamijo, Nucl. Instrum. Meth. B33, 685(1988).
64. a) R.L. Jacobson and G.K. Wehner, J. Appl. Phys. 36, 2674(1965); b) J.R. Parsons and R.W. Baluffi, J. Phys. Chem. Sol. 25, 263(1964); c) T. Mizutani, MRS Symp. Proc. 284, 265(1993); d) J.S. Im and H.A. Atwater, MRS Symp. Proc. 187, 113(1990).

65. F.L. Vook, in **Radiation Damage and Defects in Semiconductors**, ed. J.E. Whitehouse, The Institute of Physics, London, 1973, p. 60.
66. K.A. Jackson, J. Mater. Res. 3, 1218(1988).
67. R.G. Elliman, J.S. Williams, W.L. Brown, A. Leiberich, D.A. Maher and R.V. Knoell, Nucl. Instrum. Meth. B19/20, 435(1987).
68. E.S. Machlin, **An Introduction to the Thermodynamics and Kinetics Relevant to Materials Science**, Giro Press, Croton-on-Hudson, NY, 1991.
69. D.A. Smith, P.V. Evans and S.R. Koppikar, MRS Symp. Proc. 321, 271(1994).
70. Kim Sung-ki, Ph.D Thesis, Kyung Hee University, Korea.
71. H. Fujiwara, M. Kondo and A. Matsuda, J. Appl. Phys. 91, 4181(2002).
72. P. Danesh et al., J. Phys. D Appl. Phys. 37, 249(2004).
73. J.Y. Ahn et al., Appl. Phys. Lett. 82, 1718(2003).
74. D. Han, J.D. Lorentzen, J. Weinberg-Wolf, L.E. McNeil and Q. Wang, J. Appl. Phys. 94, 2930(2003).
75. D.V. Tsu et al., Appl. Phys. Lett. 71, 1317(1997); J. Koh et al., ibid 73, 1526(1998); S. Guha et al., ibid 74, 1860(1999); J. Koh et al., ibid 75, 2286(1999).
76. R.L.C. Vink, G.T. Barkema and W.F. van der Weg, Phys. Rev. B63, 115210(2001).
77. P. Danesh et al., Appl. Phys. Lett. 80, 2463(2002).
78. G. Yue, J.M. Owens, J. Weinberg-Wolf and D. Han, MRS Symp. Proc. 664, A9.7.1(2001).
79. S.Guha et al., Appl. Phys. Lett. 74, 1860(1999).
80. A. Matsuda, M. Takai, T. Nishimoto and M. Kondo, Solar Energy Mat. and Sol. Cells 78, 3 (2003).
81. S. Miyazaki et al., Sol. Energ. Mat. Sol. Cells 49, 45(1997); H. Fujiwara et al., Phys. Rev. B60, 13598(1999).
82. M. Bennett, K. Rajan and K. Kritikson, Conf. Record of 23rd IEEE PVSC, 845(1994); J. Yang, X. Xu and S. Guha, Mat. Res. Soc. Symp. Proc. 336, 687(1994); Y. Lee, L. Jiao, H. Liu, Z. Lu, R.W. Collins and C.R. Wronski, Conf. Record of 25th IEEE PVSEC, 1165(1996).
83. P. Vigneron, P.W. Peacock, K. Xiong and J. Robertson, MRS Symp. Proc 762, A9.2.1(2003).
84. Private communication from A. Matsuda.
85. M.V. Bazylenko, M. Gross and D. Moss, J. Appl. Phys. 81, 7497(1997).
86. A.J. Forty et al., J. Phys. C8, 857(1986).
87. C.F. George and P. D'Antonio, J. Non-Cryst. Sol. 34, 323(1979).
88. A.H. Al-Vayati et al., J. Vac. Sci. Technol. B13, 1639(1995).
89. V.M. Burlakov et al., Phys. Rev. Lett. 86, 3052(2001).
90. A. Lefevre et al., Phys. Rev. B64, 115429(2001).
91. J.P. Chang, Y.-S. Lin, Appl. Phys. Lett. 79, 3666(2001); J. Lee, S.S. Kim and S. Im, J. Vac. Sci. Technol. B21, 953(2003).
92. J.A. Reimer, J.C. Knights and R. Vaughan, Phys. Rev. B24, 3360(1981); P.C. Taylor, in **Semiconductors and Semimetals**, ed. J.L. Pankove, 21C, 99(1984), Academic, New York ; T. Su et al., J. Non-Cryst. Sol. 266–269, 195(2000); K.K. Gleason, M.A. Petrich, J.A. Reimer, Phys. Rev. B36, 3259(1987).
93. M. Stutzmann, in **Amorphous and Microcrystalline Semiconductor Devices: Materials and Device Physics**, ed. J. Kanicki, Artech House, Norwood, MA, 1992, p. 189.

94. R.A. Street, M. Hack and W.B. Jackson, Phys. Rev. B37, 4209(1988).
95. H.M. Branz et al., J. Non-Cryst. Sol. 227–230, 191(2002); W. Beyer, in **Semiconductors and Semimetals**, 61, eds. R.K. Wielardson and E.R. Weber, Academic Press, San Diego, 1999; W. Beyer and U. Zastrow, MRS Symp. Proc. 609, A20.4(2001).
96. M.J. Powell, S.C. Deane and R.B. Wehrspohn, Phys. Rev. B66, 155212(2002).
97. P.A. Fedders, Phys. Rev. B61, 15797(2000); Phys. Rev. B66, 195308(2002); D.T. Britton et al., Phys. Rev. B64, 075403(2001).
98. Z. Smith and S. Wagner, in **Amorphous Silicon and Related Materials**, ed. H. Fritzsche, World Scientific, Singapore, 1988, p. 409; K. Winer, Phys. Rev. B41, 12150(1990); M.J. Powell and S.C. Deane, Phys. Rev. B48, 10815(1993).
99. J.P.M. Hoefnagels et al., J. Appl. Phys. 96, 4094(2004).
100. S. Ramalingam et al., J. Appl. Phys. 84, 3895(1998).
101. F. Finger et al., MRS Symp. Proc. 715, A16.3.1(2002).
102. Y.H. Liang, N. Maley and J.R. Abelson, J. Appl. Phys. 75, 3704(1994); M. Pinarbasi et al., Thin Solid Films 171, 217(1989).
103. M. Shindo et al., J. Non-Cryst. Sol. 59–60, 747(1983).
104. E.S. Machlin, **The Effects of Structure on Properties of Thin Films**, Elsevier, Oxford, 2005.

Appendix

The inadequacy of physical vapor deposition in the production of α-Si:H for the period prior to about 1988 deserves examination. Perhaps we may learn how to overcome whatever is responsible for the resulting structure that provides poor properties. First, the obvious result that follows from low temperature deposition with thermal beams. From Chapter II we know that the structure will consist of voids and void ribbons. Figure 5.A1 bears this expectation out in that it shows that thermal PVD produces a heterogeneous α-Si:H film full of voids. These voids have dihydride species associated with them. But, the significant fact is that in amorphous silicon (and amorphous germanium) a correlation has been found between the number of sites at void surfaces and the number of dangling bonds[A1,A2], i.e. these numbers are equal. In thermal PVD of α-Si:H there is the high probability that many of these voids may not be in contact with atomic hydrogen due to shadowing effects. Hence, any PVD process mode of depositing α-Si:H must use hyperthermal beams to close up such voids before they extend to depth levels further than a H diffusion distance corresponding to the substrate temperature and the trap density.

Suppose the trap (dangling bond) density is $10^{18}/\text{cm}^{-3}$, a number sometimes produced in CVD, then this H diffusion distance will not be larger than $10^{-6}/\text{cm}$. Hopefully, a Si ion beam of 10–20 eV will allow amorphous deposition at a substrate temperature of 250°C without crystallization and should be sufficient to remove voids. We do not want a higher incident ion energy because it would generate more defects at a depth below the surface further than the trap limited H diffusion distance. During this ion beam deposition one would want to supply atomic hydrogen as well and simultaneously. There will be no less than 10^{11} dangling bonds on the surface. These will need to be passivated by the incident atomic hydrogen. A supply of 10^{13}/s of atomic hydrogen should suffice.

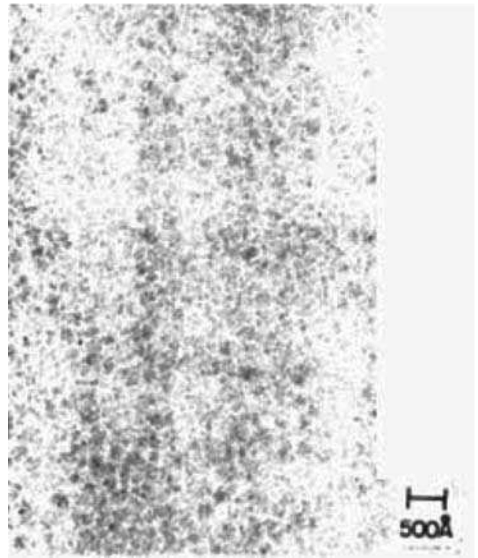

Figure 5.A1. TEM micrograph of α-Si:H film 500 Å thick. Reproduced with permission from W. Paul, in Amorphous Silicon and Related Materials, ed. H. Fritzsche (World Scientific, Singapore, 1989) p. 63.

The only aspect of these criteria that was violated by the various modes of sputtering after it was recognized that the substrate temperature had to be maintained close to 230°C is that of not providing too energetic incident particles to the surface of the film. The predominant PVD mode of deposition α-Si:H at that time involved sputtering. This factor was recognized by some researchers who supplied Si by e-beam-induced evaporation and hydrogen by an ion gun. However, as shown in Figure 5.A2 this deposition mode still was unable to provide the device quality level spin density.[A3] Given our present knowledge it is likely that the films produced via this process had a greater density of weak bonds than the films produced by CVD methods. The subsurface insertion of H_2 by the ion gun is one possible source of the additional weak bonds (i.e. 50% of the ion gun current consisted of H_2^+ ions).

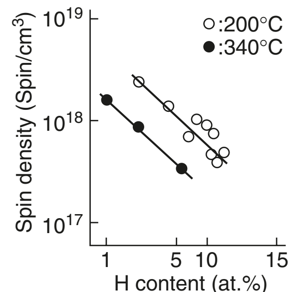

Figure 5.A2. Spin density in Si evaporated and H ion beam produced α-Si:H films. Reproduced with permission from M. Shindo et al., J. Non-Cryst. Sol. 59–60, 747(1983).

Apparently, this problem was also recognized by those who developed the DC reactive magnetron sputtering technique. This method of deposition involves a plasma which is confined by a magnetic loop to the vicinity of the target. This feature greatly reduces the bombardment of the substrate by energetic ions and electrons as compared to the normal techniques previously used. In a sense, if the substrate surface consists of a gaseous film of various reactive species it is similar to the substrate surface in various CVD methods. In any case, the elimination of energetic incident particles

Table 5.A1. Activation energy, E_a/E_g ratio, photoconductivity, density of states (DOS) in the band gap and the refractive index are shown for representative samples with hydrogen content varying from 12 to 38 at.%

Sample number	C_H (at.%)	E_a (eV)	E_a/E_g	σ_{ph} $((\Omega cm)^{-1})$	DOS (cm^{-3})	n (850 nm)
1239	12.5	0.73	0.45	1.0×10^{-5}	8.5×10^{15}	3.62
1237	15.5	0.79	0.47	1.4×10^{-5}	5.0×10^{15}	3.52
1232	20.5	0.89	0.50	1.3×10^{-5}	1.1×10^{15}	3.36
1229	24.0	0.89	0.50	9.9×10^{-6}	1.8×10^{15}	3.34
1130	32.0	0.73	0.37	4.3×10^{-7}	4.6×10^{15}	3.24
1134	38.0	0.68	0.35	3.5×10^{-7}	3.4×10^{16}	3.32

seems to be the crucial factor that enables this technique to produce device-grade α-Si:H films. Table 5.A1 taken from Ref. [A4] shows the low levels of defect density achieved in the films deposited by this procedure as measured by subgap absorption photoconductivity and CPM. A telling comment in the referenced paper is that the surface appearance of the films is smooth and the microstructure is devoid of columnar structure and not characteristic of PVD techniques where the depositing species stick where they hit. The latter observation suggests that this deposition process provides depositing species with high surface diffusivity, in view of the absence of energetic incident particles. Thus, it is not really a PVD process despite the use of sputtering to provide the Si atoms that enter the magnetron-induced plasma.

To this author it appears that the problem of depositing α-Si:H with optimum properties reduces to that of reducing the weak bond maximum energies and densities to the minimum possible while reacting the silicon with hydrogen to form species that can annihilate dangling bonds. Thus, no energetic species that can be inserted subsurface must be incident upon the growing surface. Given this constraint and the lack of adequate surface diffusion to prevent intercolumnar voids one solution is to use incident particles consisting of large inert atoms (e.g. Xe) of low incident energy to provide for the formation of a dense product lacking columnar microstructure with a more benevolent weak bond spectrum.

Another possible mode of ameliorating the weak bond spectrum has occurred to the author based on an analogy in crystalline materials with which he is familiar. It is well known that grain boundary Gibbs adsorption occurs because the adsorbing species lowers the interface energy. In structural terms this means that the Gibbs adsorbing solute replaces more energetic bonds with less energetic bonds. This is accomplished in metallic materials mainly by replacing a strained bond with one that is less strained, i.e. by inserting a larger atom in a bond that is stretched above its equilibrium length. Thus, by inserting quadrivalent atoms such as C, Ge, Sn and perhaps Pb in small amounts to adsorb at the most energetic weak bonds it may be possible to reduce their energies. Since there are 10^{19} weak bonds per cm^3 not more than 10^{19} adsorbant atoms need to be introduced into the α-Si:H network for each adsorbant species, i.e. no more than 0.01 at.%. One needs to be aware of the complication of H reaction with these adsorbant species that may act to prevent the desired result. Similarly, the introduction of tri- and pentavalent adsorbant atoms

may enable bond angle strain to be relieved. The trick will be to have these species enter the weak bonds.

A1. M. Brodsky, D. Kaplan and J.F. Zeigler, Appl. Phys. Lett. 21, 305(1972).
A2. N.J. Shevchik and W. Paul, J. Non-Cryst. Sol. 16, 55(1974).
A3. Y.H. Liang, N. Maley and J.R. Abelson, J. Appl. Phys. 75, 3704(1994); M. Pinarbasi et al., Thin Solid Films 171, 217(1989).
A4. M. Shindo et al., J. Non-Cryst. Sol. 59–60, 747(1983).

CHAPTER VI

Stresses in Thin Films

1. Intrinsic stress.

1.1. Non-energetic deposition.

1.1.1. *Zone a* temperatures (nil mobility).

In the original edition of this book attention was focussed on the fact that in the *zone a* range of temperature, where deposited atoms stick where they hit, the existence of porosity in the films must lead to a modification of prior theories for the origin of the intrinsic tensile stress. This porosity exists, as noted in Chapter II, between the columns or columnar grains formed in the deposition process. The origin of the tensile stress in the Hoffman[1] and subsequent models is the decrease in free energy that occurs when the energy associated with the tensile stress and grain boundary energy is less than the surface energy removed on formation of the grain boundaries. Since porosity is observed in films in the *zone a* regime it is apparent that there still exists internal surface area and energy in the film. To the extent that voids exist (that there is space between columns not filled by cohering atoms), the magnitude of the average tensile stress in the films must be less than that deduced from the Hoffman analysis. If all the voids in the intercolumnar space were to disappear either to form grain boundaries between crystal grains or to produce a continuous bonded network between amorphous columns then the intrinsic tensile stress would not exceed the value given by

$$\sigma_M = [M(2\gamma - \gamma_{gb})/r]^{1/2}$$

where M is the biaxial elastic modulus, γ is the specific surface energy, γ_{gb} is the specific grain boundary energy, and 2r is the column diameter for the case where the joining together of the columns yields grain boundaries and the same relation with the specific grain boundary energy missing for the amorphous columns.

Table 6.1 provides values of the intrinsic tensile stress given by Hoffman's relation compared to experimental values in the *zone a* temperature range and to values of the low temperature yield strength. It is apparent that the values based on the Hoffman theory are too large compared to the experimental values of the intrinsic tensile stress, whereas those for the yield strength roughly compare to the

latter. Doerner and Nix[2] were the first to make the connection between yield strength and internal tensile stress.

The question has arisen as to whether adjacent column surfaces can come close enough so that relaxation (the build-up of intrinsic stress inside the columns) can occur in the *zone a* temperature regime. For this relaxation to occur the surfaces must be closer than that corresponding to the maximum possible stress, i.e. the stress at which the second derivative of the energy with respect to spacing between the column surfaces is zero. This spacing for most metals is in the order of no more than twice the equilibrium interatomic spacing. Indeed, according to a calculation presented in Appendix 1, it is no more than 1.7 Å. This space is too small for an atom to penetrate in depth in line-of-sight deposition. Consequently, high intrinsic tensile stresses approaching the yield strength can only develop under deposition conditions that negate the formation of intercolumnar voids thicker than one interatomic spacing, minimize the void volume fraction while maximizing the cold-welded bridge area. (The cold-welded bridges are obviously areas where the intercolumnar distance is smaller than about 1.7 Å.) Comparison of Figure 6.1 to Figure 2.1 suggests that void volume fraction is minimized in the *zone a* regime when the incident beam of atoms being deposited makes a zero angle with the normal to the film surface.

Table 6.1

Film material	**Intrinsic tensile stress** (GPa)**	**Hoffman stress (GPa)**	**Yield strength* (GPa)**
Pt	1.2	7.5	>0.45
Ni	1.0	6.6	1.0
Co	0.84	8.1	0.76
Cu	0.8	4.4	0.5
Pd	0.6		0.32
Au	0.26	4.3	0.21
Al	0.2	3.4	0.11

* As severely cold worked, from Ref. [7].
** From Ref. [6].

What is troubling about the measured values of the intrinsic tensile stress in the *zone a* temperature regime is that many molecular dynamics (MD) simulations indicate regions of extended and connected porosity in vapor-deposited films, such as illustrated in Figures 2.1 and 2.3. One would expect that the intrinsic tensile stress developed in these films due to intercolumn cohesion would be negligible. However, more modern two-dimensional MD simulations, such as those shown in Figure 6.1, reveal extensive cohesion between columns deposited with a zero angle between incident beam direction and normal to the film plane, and somewhat less area of cohesion for a 45° incident angle, but still greater than that revealed in the one-dimensional simulations of Figures 2.1 and 2.3. But other two-dimensional MD simulations, such as those shown in Figures 6.2 and 6.3a, still reveal appreciable area between columns that lack bonding across them. In Figure 6.3b the incident energy was enough to close up the pores, but not high enough to introduce interstitialcies.

The intrinsic tensile stress in the film of Figure 6.3a was evaluated and equals 0.5 GPa. This value seems high for the low value of interconnected area in

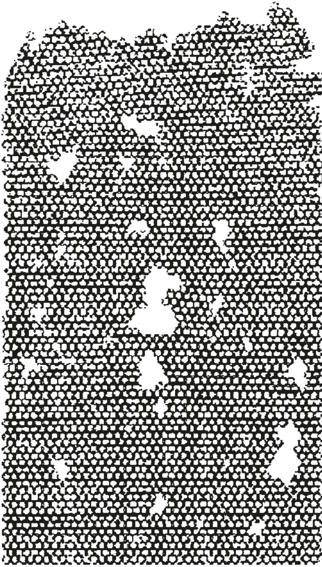

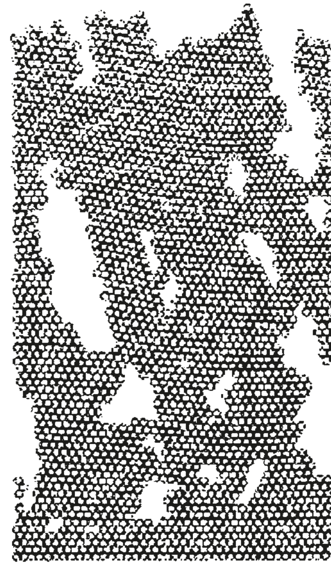

Figure 6.1. Results of a two-dimensional MD simulation using a Lennard-Jones interatomic potential with substrate at 0°K and a high-temperature incident energy. Left snapshot with incident beam normal to surface. Right snapshot with beam 45° to surface. Reproduced with permission from L. Dong et al., J. Appl. Phys. 80, 5682(1996).

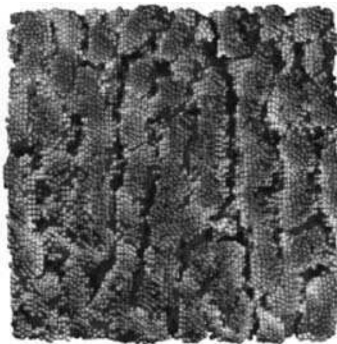

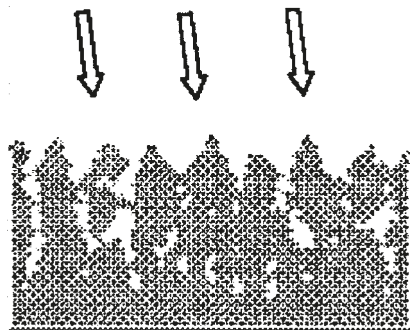

Figure 6.2. Two-dimensional MD simulation using embedded atom potential for Mo. Substrate had 110 orientation and was at room temperature. Low incident energy of 0.17 eV. Top view (a) and side view (b). Tendency to form 100 facets leads to roughness and void formation. Reproduced with permission from E.F.C. Haddeman, B.S. Bunick and B.J. Thijsse, MRS Symp. Proc. 594 (1999).

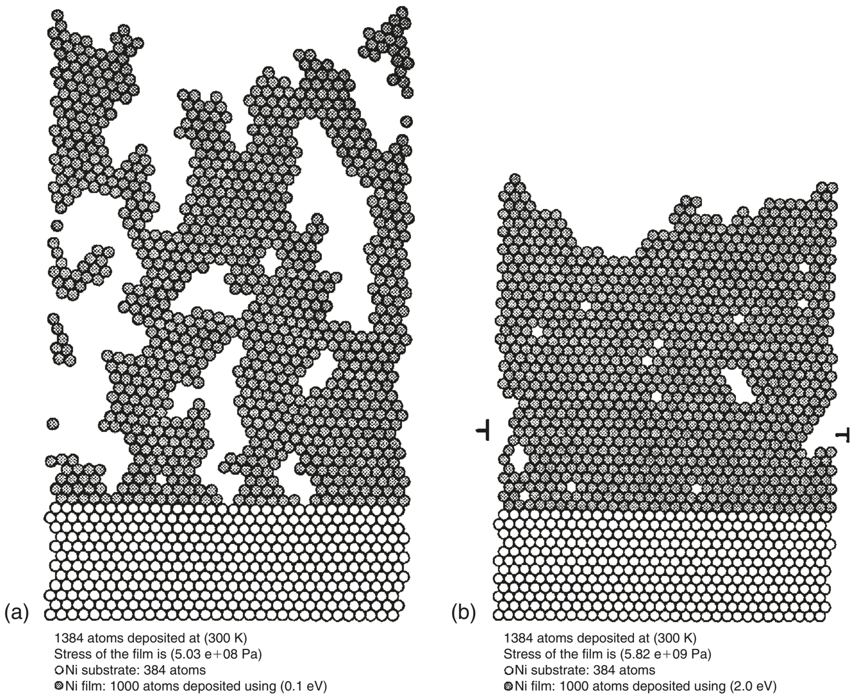

Figure 6.3. Two-dimensional MD simulation snapshot of ion beam deposition. Incident energy: (a) 0.1 eV, (b) 2 eV. Substrate at 300 K. Reproduced with permission from C. Fang, Ph.D. Thesis, Columbia University, 1992.

the film. However, several factors contribute to the tensile stress in this film. One is the long-range interaction of the assumed interatomic potential which spans voids of shorter width. Another is the contribution of the surface tension of the enclosed cylindrical void surfaces, a possibility first suggested by Heavens and Smith.[4] The stress increment due to this source is proportional to $f/(1 - f)$, where f is the void volume fraction, void surface energy, and is inversely proportional to the pore radius. The proportionality constant depends upon void morphology and its magnitude is on the order of unity. Since the average radius of the cylindrical pores in Figure 6.3a is about 1 nm and the volume fraction of voids is about 0.4, then the contribution to the internal tensile stress is expected to be about 0.7 GPa for a surface energy of 1 J/m^2. The apparent agreement with the evaluated stress in the MD simulation of Figure 6.3a is not necessarily significant. In contrast, the measured tensile stress for a real porous amorphous Ge film is shown in Figure 6.4. As shown in the figure the stress remains roughly constant, while the void fraction increases by an order of magnitude. Hence, in this case the intrinsic

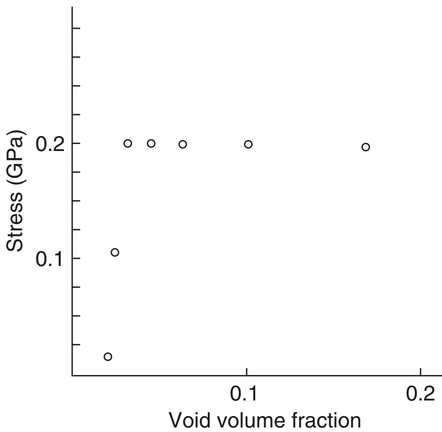

Figure 6.4. Intrinsic stress versus void fraction. Replotted with data taken from D. Fahnline et al., MRS Symp. Proc. 130, 355(1989) with permission.

tensile stress of about 0.2 GPa must have another origin, which is likely to be the strain due to cold welding across bridges between adjacent columns. Further, in these films the average void radius must be larger than about 10 nm for the surface tension contribution to the intrinsic stress to be negligible. Incidentally, what is significant in Figure 6.3 is the fact that for Figure 6.3b the intrinsic tensile stress was calculated to be 5.82 and 0.50 GPa for Figure 6.3a. The difference in porosity or bridging area between these two films accounts for the difference in intrinsic tensile stress. The reason the stress in Figure 6.3b is able to approach the Hoffman value is that the continuous film is so thin that the corresponding yield strength is on the order of the Hoffman stress.

From the above analysis one might expect that observed tensile stresses in film vapor deposited in the *zone a* regime may vary from zero up to the yield strength depending upon the intercolumnar void volume fraction and its morphology. Indeed, values from zero[5] to the yield strength[6a–c] have been reported. The void volume, void morphology, and dimensions in *zone a* deposition depend upon deposition parameters. As shown, on comparison of Figures 6.1 and 2.1, one of these parameters is the incident particle (atom) direction relative to the film normal. Another might be the impurity content in the deposition atmosphere. Still another is some violation of *zone a* regime conditions, e.g. energetic particles, deposition of high sublimation energy per atom on low-thermal conductivity surface, anisotropic surface plane preference producing surface roughness, etc.

Given the likelihood of significant non-bonding area in films deposited in the *zone a* temperature regime the intrinsic stresses that may be calculated from models for the magnitude of the intrinsic tensile stress, such as the zipping models of various types[4] must be considered to be maximum limiting values. In this regard, we may note that the measured intrinsic tensile stresses given in Table 6.1 are a factor, greater than 5, smaller than the maximum corresponding to the Hoffman model, yet are no smaller than the estimated yield strength. Most zipping models predict smaller values of the intrinsic tensile stress. Given these facts, it is reasonable to conclude that in the *zone a* temperature regime the zipping type of cold welding does not occur, the cold welding that occurs across bridge areas proceeds

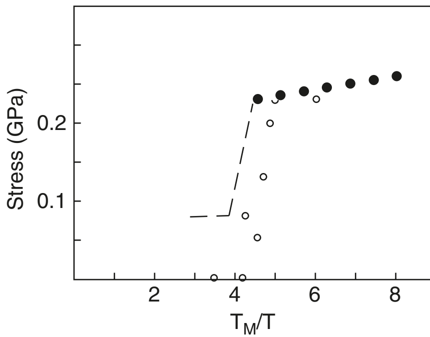

Figure 6.5. Intrinsic tensile stress dependence on temperature for Al. Reproduced with permission from E. Klokholm, J. Vac. Sci. Tech. 6, 138(1969).

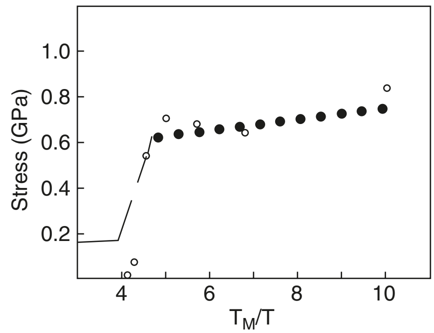

Figure 6.6. Intrinsic tensile stress dependence on temperature for Cu. Reproduced with permission from E. Klokholm, J. Vac. Sci. Tech. 6, 138(1969).

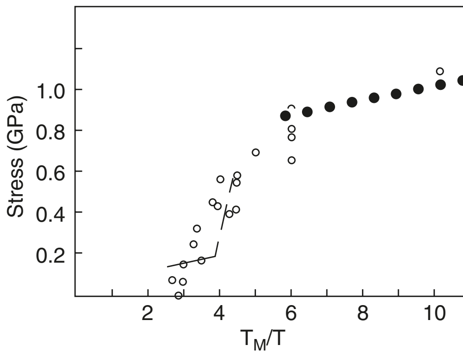

Figure 6.7. Intrinsic stress dependence on temperature for Ni. Reproduced with permission from E. Klokholm, J. Vac. Sci. Tech. 6, 138(1969).

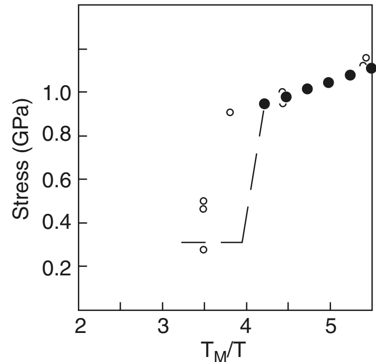

Figure 6.8. Intrinsic stress dependence on temperature for Pt. Reproduced with permission from R.E. Rottmayer and R.W. Hoffman, J. Vac. Sci. Tech. 8, 151(1971).

at the rate of film thickness increase during deposition, and the cold-welded bridge area for the films corresponding to the data in Table 6.1 is a fraction of the total area between columns that is greater than the ratio of the intrinsic tensile stress to the Hoffman value.

1.1.2. *Zone b* temperatures.

In the *zone b* temperature regime surface diffusion of adatoms and some grain boundary motion can occur. This is the temperature regime in which porosity

is minimized although not absent, the interfaces can approach equilibrium configuration and intercolumnar cold welding occurs efficiently during deposition. It is unlikely in this regime for porosity to occupy a major fraction of the intercolumnar area after cohesion of the columns. The question still exists as to the degree of strain introduced into the columns by the cold welding together of the adjacent columns of grains formed in the deposition process. An answer to this question will now be attempted using experimental data.

The temperature dependence of the intrinsic tensile stress for several metals is reproduced as the open data points in Figures 6.5–6.8 from the literature. Superimposed on these figures are the experimental temperature dependence of the yield strength (at constant grain size), scaled to match at the lowest value of the line of filled dots representing this dependence, and the grain size dependence of the yield strength, represented by the dashed line, that occurs as a result of the sudden increase in grain size at a T_M/T value of about 4 (see Figure 3.2). The latter dependence is deduced from the Petch relation, i.e. $YS_1/YS_2 = (D_2/D_1)^{1/2}$, where YS denotes the yield strength. The dashed line is the same in all four figures and as just noted stems from the sudden average increment in grain size shown in Figure 3.2 at $4 \leqslant T_M/T \leqslant 4.5$. The coincidence of the sudden decrease in both the intrinsic tensile stress and the yield strength that occurs about $T_M/T = 4.5$ is not likely to be accidental nor is the coincidence between the temperature dependence of both the yield strength and the intrinsic tensile stress for $T_M/T \geqslant 4.5$ accidental either. In the previous subsection we obtained numerical agreement between the intrinsic tensile stress for metals and the yield strength in the cold-worked state at *zone a* substrate temperatures. Doerner and Nix[2] in addition to noting the similarity between a measured yield strength in thick Ni films and the measured intrinsic tensile stress at the same substrate temperature, also noted a similarity between the dependence of flow strength and the dependence of the tensile intrinsic stress on temperature in Ni films formed by evaporation and condensation for $T_M/T \geqslant 6$ and, hence, were the first to make the suggestion that the magnitude of the intrinsic tensile stress is limited by the yield strength.

Let us consider the bases for the sudden increase in grain size at $T_M/T \approx 4.5$ as T increases. $T_M/T = 4$ also roughly defines the transition temperature, T_1, between *zone b* and *zone II* for metals. It corresponds physically to the disappearance of the intercolumnar void network, as noted in Chapters II and III. This occurs because *adatom diffusion becomes sufficiently rapid at $T_M/T \leqslant 4$ to fill in all the incipient intercolumnar voids and/or cracks before they are buried under the next monolayer to deposit.* At $T_M/T = 4.5$ some of the voids are filled by diffusion and some are not. Those voids that remain act to prevent most of the grain boundaries from migrating, while those that have been removed allow some grain boundaries to migrate and produce an array of much larger grains that act to lower the yield strength markedly. Thus, the sudden grain size increase is due to the onset of intercolumnar void density decrement that occurs at about $T_M/T = 4.5$ and that is completed with a resulting zero intercolumnar void fraction at $T > T_1$.

As shown in Figures 6.5–6.8 the intrinsic tensile stress becomes zero above a temperature close to $T_M/T = 4$. Thus, there is no doubt that the absence of intrinsic tensile stress is due to the filling in of voids and cracks via diffusion and conversely, its presence is due to the cold welding of adjacent column surfaces across an intercolumnar void and crack network. Grain boundaries are present both below and above $T_M/T \approx 4$, yet the intrinsic tensile stress becomes nil at $T_M/T < 4$. If there were still an origin of intrinsic tensile stress at *zone II* substrate temperatures, the yield strength is still high enough to reveal its presence. However, the intrinsic tensile stress is not measurable above $T_M/T \approx 4$. Thus, grain boundaries, per se, cannot account for the presence of intrinsic tensile stress. Indeed, all the mechanisms for the origin of the intrinsic tensile stress that do not depend upon the existence of the intercolumnar void and crack network can be eliminated from contention. These include Chaudhari's grain growth mechanism,[11] the mechanism based on shrinkage of grain boundary voids,[2] and the mechanism based on excess vacancy annihilation.[2] The remaining contender for the origin of the intrinsic tensile stress is the Hoffman model, as modified above.

At this point we would like to emphasize again that the origin of the sudden drop in yield strength, as related to the sudden increase in grain size, and the sudden drop in intrinsic tensile stress, which occurs coincidentally with the former phenomena, is the onset of the disappearance of the intercolumnar void and crack network induced by the sufficient surface diffusion of adatoms to fill the void spaces before the adatoms are themselves submerged beneath depositing atoms. The absence of intrinsic tensile stress above T_1 can only be accounted for by the concomitant absence of the cold welding across intercolumnar voids and cracks in films deposited at substrate temperatures above T_1. The cold welding is absent because all density decrements, such as intercolumnar voids and cracks, have been filled in by surface and interface diffusion of atoms. No motion of adjacent columnar surfaces toward each other is possible above $T = T_1$, i.e. the intercolumn space is at nearly the bulk film density.

1.1.2.1. Origin of compressive stress.

As noted above in the *zone b* temperature range adatom diffusion and grain boundary migration have sufficient mobility to exert their effects during film deposition. Thus, one expected outcome in this temperature regime is an approach at surfaces and interfaces to the local equilibrium condition. Chason et al.[13] has noted that the chemical potential of the atoms on the verge of being deposited is higher than that of a similar atom beneath a plane surface of a film at zero stress. Hence, there is a driving force for atoms at the surface not only to deposit on the film surface but also to enter into the film. This entry can be accomplished in the *zone b* temperature range most easily by diffusion into grain boundaries, increasing the number of atoms per unit area of film plane per unit distance normal to the film (increasing the density)

and thereby introducing a biaxial compressive stress into the film. The latter acts to increase the chemical potential of an atom in the film, so that it approaches that of an atom being deposited. Whether the model just given accounts for the observed compressive stresses in films in this temperature regime will become evident upon further testing of the model which will undoubtedly be carried out subsequent to the publication of this edition of this book. The evidence presently available suggests that the compressive stress approaches a constant value with increasing film thickness.

In the original edition of this book, the experimental evidence that existed at that time indicated the presence of compressive stress in films in non-energetic deposition only in covalently bonded elemental films. Since then compressive stress has been found in metallic films in non-energetic deposition.[14] Thus, the explanation suggested in the original edition for the origin of the compressive stress under these circumstances was wrong.

1.1.3. Effect of variables other than substrate temperature.

1.1.3.1. Oxygen.

Oxygen is a surface active molecule which chemically adsorbs on most metal surfaces satisfying the surface dangling bonds and preventing adhesion (or cohesion) between metal surfaces. Given this effect of oxygen it would be expected that its presence in the deposition chamber would act to prevent the build-up of intrinsic tensile stresses. Further, if sufficient oxygen is incorporated as an interstitial impurity, or if an oxide is formed having a volume larger than that originally occupied by its metal content,* then the accompanying increase in specific volume (stress-free length) should induce the intrinsic stress to become compressive. In fact Alexander and Hoffman[12] found the intrinsic tensile stress to decrease with increasing oxygen content in Ni films; Pulker[7] found that increasing ratios of residual chamber pressure to deposition rate were associated with decreasing intrinsic tensile stress in Cr and Al films; Martinez and Aberman[6b] found the tensile stress to decrease with increasing oxygen in Cr films. However, if oxygen acts to increase the yield strength of the film without changing the specific volume appreciably, or if an oxide with Pilling–Bedworth ratio <1 forms, then the intrinsic tensile stress the film can exhibit would increase. An enhancement of the intrinsic tensile stress was found in Cu films deposited in a partial pressure of O_2.[6c] These explanations are speculative, and characterization of the films and further experimentation are necessary to ascertain their validity. It is unfortunate that the need for adequate film characterization in this specific field of interest has not been recognized, as yet. For example, there have been many measurements of the type illustrated by the results shown in Figure 6.9a and b,

* When this occurs it is said that the Pilling–Bedworth ratio is larger than unity.

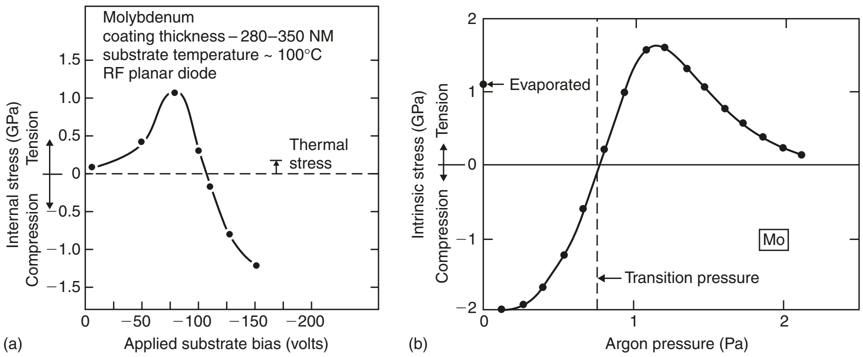

Figure 6.9. (a) Variation of intrinsic stress with substrate bias. Reproduced with permission from J.A. Thornton, **Semiconductor Materials and Process Technology Handbook**, Noyes, Park Ridge, NJ, 1988, p. 329. © 1988 Noyes Publications. (b) Intrinsic stress dependence on argon pressure. Reproduced with permission from D.W. Hoffman and R.C. McCune, **Handbook of Plasma Processing Technology**, Noyes, Park Ridge, NJ, 1990, p. 483. © 1990 Noyes Publications.

which reveal an intrinsic tensile stress increment from a near zero value when either the negative bias voltage is increased from a zero value or the argon pressure is decreased from a value at which the mean free path is a very small fraction of the target to substrate distance. These results can be explained either as a consequence of a concomitant decrease in the oxygen content at the film surface during deposition or as the result of inefficient densification, such as exhibited in the MD simulations described in Figures 6.1 and 6.3. Usually there are no concomitant measurements of the oxygen content in the corresponding films to be able to distinguish between these two alternatives.

1.1.3.2. Other impurities.

Other impurities, such as water vapor, can either induce the intrinsic stress to become tensile or compressive, as was found to be the case for oxygen. Hence, these data cannot be used to distinguish between competing mechanisms for the origin of the intrinsic stress, although, as for oxygen, different explanations can be found to account for the contradictory behavior.

1.2. Intrinsic stress when film surface senses energetic particles.

In Chapter I it was noted that during self-bombardment interstitials are formed either directly by channeling or indirectly via forward sputtering, and in both cases without the concomitant formation of vacancies, or at sufficient incident energy

per particle as a component of a Frenkel defect concomitant with vacancy generation. Thus, particle bombardment of a growing surface creates an excess of interstitial defects over vacancy defects. Because of this excess of interstitial over vacancy type of defect the sign of the intrinsic stress developed in particle bombarded as deposited films will be compressive independent of the substrate temperature. The substrate temperature determines the film volume or length increment per interstitial created and not annihilating at either the film surface or a vacancy. This excess partial molar volume per interstitial depends upon whether the interstitial atom remains at an interstitial site or is captured at a jog along an edge dislocation extending the associated half-plane. The contribution to the compressive intrinsic stress in the latter case depends upon the orientation of the half-plane reaching a maximum when this plane contains the normal to the film plane.

When the growing film is bombarded by energetic inert gas ions or atoms, then the defects, in addition to those described in the previous paragraph, will include inert gas atoms in either interstitial positions or more likely in lattice positions coupled with a self-interstitial defect corresponding to a Frenkel defect formed when the inert gas atom in the interstitial position pushed a neighboring lattice sited atom into an interstitial position and occupied the vacancy it created. The latter process will occur when the excess energy of the inert gas atom in an interstitial position exceeds the sum of the energy to create a Frenkel defect and the excess energy of the inert gas atom at a lattice site. Thus, inert gas atoms that do not escape from the film during deposition will contribute to the film's intrinsic compressive strain, but will not be the sole source of such compressive strain, because of the excess self-interstitials always created during particle bombardment of the growing film.

On the assumption that the compressive strain is proportional to the fractional number of film atoms displaced from equilibrium sites, it has been shown[15,16] that the compressive strain is predicted to be proportional to the product of the relative flux, φ (ion to film atom) and the square root of the particle energy, E_p. This predicted relation has been verified experimentally in a variety of ways. In particular, Hwangbo et al.[17] observed that the stress in ion-assisted evaporated Ag and Al depends linearly upon the product $\varphi \sqrt{E_p}$. Similarly, Nir[18] found a linear relation between the square of the stress and ion energy for diamond-like carbon films bombarded with argon ions during deposition. The increment in packing density in a MD simulation of film densification by energetic particle bombardment was shown[19] to vary linearly with $\varphi \sqrt{E_p}$.

It is possible to vary the stress from tension to compression over some range of stress in films subjected to energetic particle bombardment during deposition as a consequence of two effects. The first stems from the fact that at low enough temperature and in the absence of energetic particle bombardment the intrinsic film stress is in tension at a value usually corresponding to the yield strength. The second is that at a high value of the product $\varphi \sqrt{E_p}$ the maximum value of the compressive stress is again the yield strength, but in compression. Thus, by variation of the

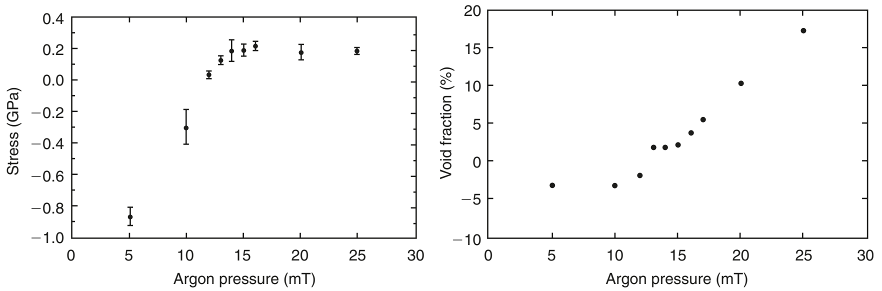

Figure 6.10. Intrinsic stress and void fraction versus argon pressure. Reproduced with permission from D. Fahnline et al., MRS Symp. Proc. 130, 355(1989).

parameter $\varphi \sqrt{E_p}$, within the limits from zero to that corresponding to plastic flow in compression, it should be possible to vary the intrinsic stress from the tensile yield strength to the yield strength in compression. Hence, we are able to account for the ability to observe a functional dependence of the intrinsic stress on $\varphi \sqrt{E_p}$, as discussed in the previous paragraph.

Targrove and Macleod's observation[20] that the packing density depends on the square root of the mass of isoenergetic (500 eV) particles suggests that the parameter that controls the intrinsic stress and related variables should be $\varphi \sqrt{M_p E_p}$. Indeed, the normalized momentum, $2\varphi \sqrt{M_p E_p}$, has been used as a correlating parameter for the intrinsic stress of films subject to energetic particle bombardment during deposition.

The observations that the intrinsic stress depends linearly on the normalized momentum as does the packing density, according to the previous citations, suggests that the stress may depend linearly on the packing density. However, the data in Figure 6.10 reveals that the packing density increases at constant intrinsic stress as the argon pressure decreases for films deposited via sputtering. Indeed, according to the data in this figure the packing density must exceed 98% before there is a compressive decrement to the intrinsic stress. Hence, although both the intrinsic stress and the packing density depend linearly on the normalized momentum they are independent variables. This result is consistent with a physical model in which the number of forward sputtered atoms depends linearly on the normalized momentum and these forward sputtered atoms act to fill the intercolumnar voids without forming interstitial defects. The formation of interstitial defects becomes significant only when these voids are nearly filled and thus the concomitant compressive stress contribution to the intrinsic stress only begins to grow in magnitude after the voids are filled.

The concept just described suggests then that the dependence of intrinsic stress on normalized momentum should be that shown in Figure 6.11. The value of the normalized momentum at which the intrinsic stress begins to decrease toward

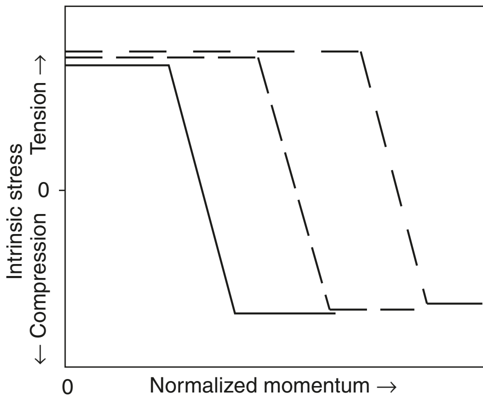

Figure 6.11. Schematic representation of dependence of intrinsic stress on normalized momentum for different initial packing densities. Full line represents highest initial packing density.

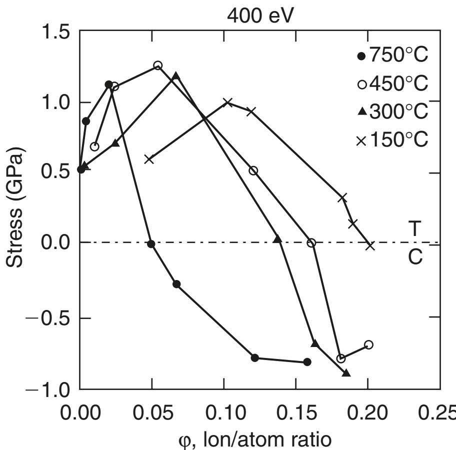

Figure 6.12. Film stress in W as a function of concurrent ion bombardment at 400 eV for films deposited at various temperatures. Reproduced with permission from R.A. Roy, R. Petkie and A. Boulding, J. Mater. Res. 6, 80(1991).

the compressive region should depend upon the packing density in films deposited in the absence of energetic particle bombardment. Tentative support for this concept is provided by the results of Roy et al.[21] given in Figure 6.12 where it is shown that the φ value at which the intrinsic stress starts to decrease itself decreases with increasing substrate temperature for constant energy of concurrent ion bombardment. These data only provide this support based on the assumption that the initial void content decreases (packing density increases) with increase in the substrate temperature for temperatures in *zone 1*. A computer simulation of the deposition process[22] showed that the packing density was found to remain constant up to near the transition temperature T_1 (648°C for W), at which it increased suddenly. If the packing density-substrate temperature function for W is the same as that found in this computer simulation then the films deposited at 750°C would have a higher packing density than those deposited at lower temperatures. It is not known whether the different curves for the 150°C, 300°C and 450°C substrate temperatures represent experimental scatter or variation in the packing density. Thus, while it would be useful to have independent measurements of the packing density as a function of substrate temperature for the deposition conditions used by Roy et al.,[21] it seems reasonable to conclude that the shift of the curve corresponding to a 750°C substrate temperature

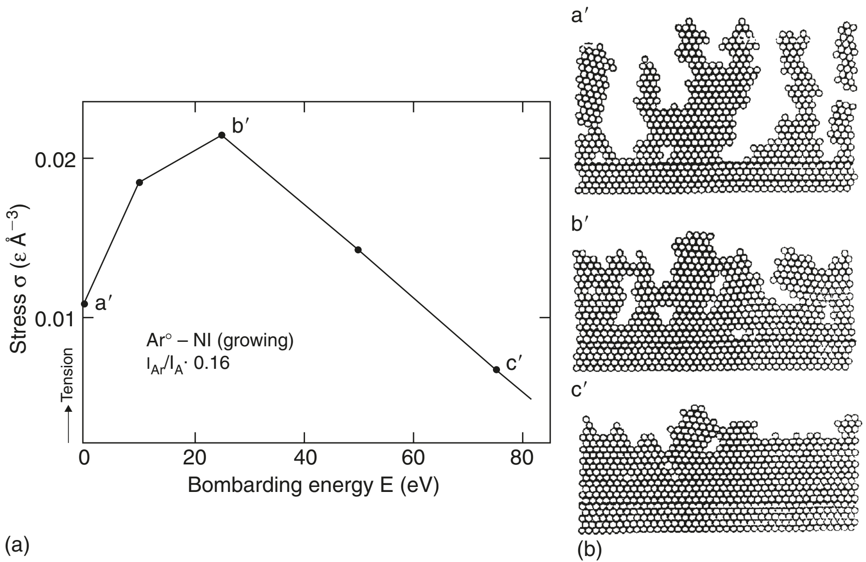

Figure 6.13. (a) Calculated intrinsic stress versus argon bombarding energy for an argon/atom flux ratio of 0.16; (b) MD simulation of microstructure evolution corresponding to the points labeled a′, b′, and c′ in (a). Reproduced with permission from K.-H. Muller, J. Appl. Phys. 62, 1796(1987).

to lower normalized momentum values as compared to the curves for lower substrate temperatures is consistent with the behavior described in Figure 6.11.

There are several aspects of the data given in Figure 6.12 that differ from the idealized representation of Figure 6.11. One is that in Figure 6.12, the tensile stress increases initially with φ instead of remaining as a constant value. Another is that after the φ value at which the sign of the slope of the curve changes to a negative value, the dependence of the stress on φ is not strictly linear. Still another is that the average value of the slope of the decreasing stress segment is not a constant. There are potential explanations for all these deviations from the behavior described in Figure 6.11. It is apparent that there exists a need for experimental determination of the real origins of these deviatory results. In particular: (1) is the initial increase in tensile stress due to the removal of oxygen from surfaces at which cohesion will take place, or is it due to an increase in the yield strength brought about by a hardening effect arising from the defects created by the ion bombardment or does it represent the effect of inefficient densification as in Figures 6.13 and 6.3; (2) does the variability of the slope of the decreasing stress segment stem from a changing volume increment per increment in normalized momentum or from a non-linear dependence of interstitial defects created per unit increment in normalized momentum or from some other source?

It may be of significance that in both MD studies of the effect of ion bombardment on microstructure shown in Figures 6.13 and 6.3, there is an initial increase in intrinsic tensile stress with increase in the normalized momentum. This increment in tensile stress is associated with an imperfect filling of the voids due to the forward sputtering and collapse of unstable arrays that may occur as a consequence of the ion bombardment. For example, in Figure 6.3b the ion bombardment did not generate a perfect stacking of atoms, but did generate one in which the density is less than the equilibrium density for a perfect crystal. Close examination of Figure 6.3b yields the conclusion that there are edge dislocations at the side boundaries centered at the void, as indicated by the symbols for them placed there. Further, measurement of the length corresponding to 32 atoms along a horizontal row and comparison of this length in the deposited region as compared to the substrate region reveals that this length in the substrate region is shorter than in the deposited region. It appears that the collapse of the nearly unstable array of Figure 6.3a produced an imperfect crystal having a lower density than the homoepitaxial substrate. Similarly, Figure 6.13b(b′) reveals that the ion bombardment resulted in the introduction of two dislocations while accomplishing bonding across the void surfaces of Figure 6.13b(a′) and thereby producing intrinsic tensile stress in the upper half of the film of Figure 6.13b(b′). Thus, the initial increment in intrinsic tensile stress may be due to the action of the ion bombardment of bringing the side faces of voids near enough to each other to interact and strain the adjoining columns in the process of bonding. However, the aforesaid explanation of the initial increment in intrinsic tensile stress with increase in the normalized momentum of incident particles during deposition must be considered highly tentative in view of the fact that the tensile stress deduced in these films is based on an interatomic potential that is much longer ranged than those applicable to real materials.[34]

Recently, Davis[23] and Robertson[24] proposed similar models for the dependence of the compressive stress in *initially ideally dense* films produced via ion deposition or ion assisted deposition. Further, this theory predicts that it is not necessary for the compressive stress to rise to the yield strength before it levels off and, hence, modifies the simple model illustrated in Figure 6.11. These models are based on the following hypotheses. First, it is assumed that the rate of increase in number of atoms per unit area implanted in interstitial* sites below the film surface is proportional to the normalized momentum, as first suggested by Windischmann,[16a] based on the knock-on linear cascade theory of forward sputtering of Sigmund.[16b] However, it is recognized that these interstitial defects can relax into positions that do not contribute to the intrinsic stress and can be induced to so relax by the thermal spikes induced by the incident energetic particles. The rate of such relaxation per unit area is taken to be proportional to the number of atoms which acquire more than the excitation energy required for relaxation from each energetic impact, the fraction of these atoms which are in interstitial positions,

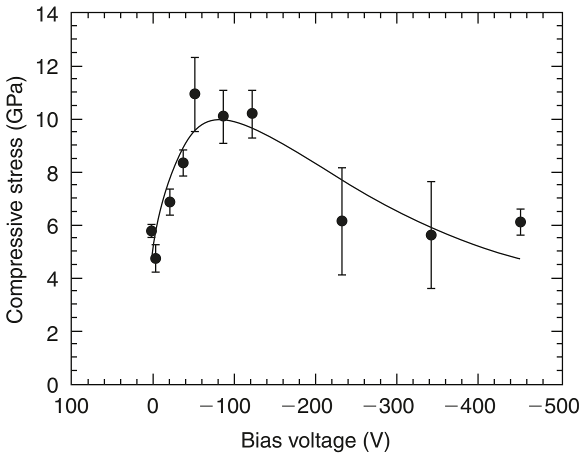

Figure 6.14. Fit of equation (6.1) to data shown in Figure 5.19. Reproduced with permission from P.J. Fallon et al., Phys. Rev. B48, 4777(1993).

and the rate of ion impact. These assumptions lead to a functional relation for the compressive stress given by

$$\sigma = [Y/(1 - \nu)][E^{1/2}/(\tilde{N}/j + kE^{5/3})] \tag{6.1}$$

where Y is Young's modulus, ν is Poisson's ratio, E is the incident particle energy, $\tilde{N}$ is the total deposition rate in number per unit area, j is the energetic particle flux, and k is an adjustable parameter. This functional dependence of $\sigma(E)$ is obeyed in many cases. For example, Figure 6.14 shows such a fit to the data given in Figure 5.19. (Because the strain associated with the $sp^2 \rightarrow sp^3$ transition is not included in equation (6.1), and if the compressive stress does induce this transition, then the significance of this fit must be questioned.) We emphasize again that in the cases being considered the maximum compressive stress is less than the yield strength. Thus, the simple model described in Figure 6.11 must be modified so that the compressive stress obeys equation (6.1) rather than increasing linearly with the normalized momentum to the yield strength in compression.

1.3. Intrinsic stress due to phase transformation.

Under special circumstances it is possible to have a phase transformation occur during deposition of thin films. Three examples come to mind. One is a transformation from the amorphous state to the crystalline state in restricted volumes of the film.[3,25–27] Another is a transformation from an sp^2 to an sp^3 bonded state, both

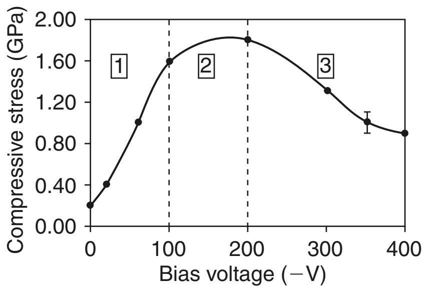

Figure 6.15. Compressive intrinsic stress as a function of bias voltage. Reproduced with permission from P. Catania, R.A. Roy, J.J. Cuomo, J. Appl. Phys. 74, 1008(1993).

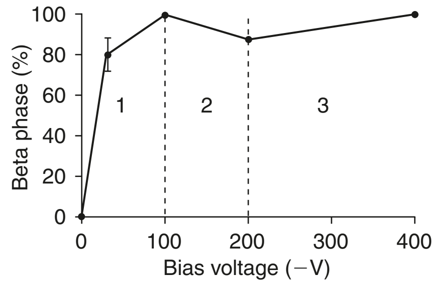

Figure 6.16. Relative amount of β-Ta determined from peak intensities in X-ray diffraction scans. Reproduced with permission from P. Catania, R.A. Roy, J.J. Cuomo, J. Appl. Phys. 74, 1008(1993).

existing in an amorphous arrangement.[28] Still another involves a phase transformation from one crystalline structure to another in restricted volumes of the film.[29,30]

The latter has been found to occur in Ta films deposited from a vapor of thermal origin.[29] Initially, the crystal structure of the deposit is a body-centered-tetragonal (bct) structure, which is believed to form as a consequence of the presence of oxygen atoms which are incorporated to produce an ordered solid solution. When the film thickens, the bct structure transforms to a body-centered-cubic (bcc) structure, which has a smaller molar volume, and thus induces an intrinsic tensile stress increment. Since the transformation acts to increase the elastic strain energy of the film, there must be a greater decrease in the specific free energy between the bct and bcc structures for the transformation to occur spontaneously. Incidentally, the transformation appears to occur via a nucleation and growth mode so that it appears reasonable to assume that the excess specific free energy between the two phases is associated with the oxygen atoms dissolved in the bct structure, which precipitate out of solid solution during the transformation to the bcc structure. The bct structure has been denoted the beta phase by these authors.

However, another view of the beta phase and the transformation is provided in a recent study involving energetic bombardment during the deposition of Ta.[30] These investigators found that, at constant oxygen content ($<0.5\%$) and argon content, as the negative bias increased from 0 to -200 V both the compressive stress and the beta phase fraction in the film increase, as shown in Figures 6.15 and 6.16. (There is a compressive stress at zero bias because even at zero bias the film is bombarded by energetic particles that are primarily argon neutrals reflected from the target.) Based on these results Catania et al.[30] proposed that the transformation is "caused by forward recoil of Ta atoms interstitially or in grain boundaries". These investigators were uncertain from their X-ray diffraction results as to whether the

beta phase is a distorted A15 structure having a theoretical density of 17 g/cm^3 or a beta uranium structure having the theoretical density of 16.33 g/cm^3. Since bcc Ta has a density of 16.6 g/cm^3, it is not possible to conclude whether the transformation is induced by the compressive stress forming the A15 product or directly to the beta uranium product via a forward recoil-induced rearrangement of atoms. The latter possibility can only be rationalized on the basis that the bombardment-induced defects in the bcc tantalum raise its free energy above that for the beta uranium structure thereby allowing the transformation to proceed in the direction of decreasing free energy, otherwise it would be necessary to assume that the bombardment itself induces a transformation "uphill" in free energy. However, it must be noted that beyond a bias voltage of −200 V, the compressive stress decreases, whereas the β-Ta content remains constant, i.e. the fraction of the product phase does not correlate to the compressive stress. Hence, it is not likely that the β-Ta phase is induced directly by the compressive stress.

Transformation from one predominant bond type to another in an amorphous film has been found to occur during deposition of films condensed from thermally induced vapors that are bombarded simultaneously by inert gas ions. In the absence of concurrent bombardment carbon films condensed from carbon vapors having only the thermal spectrum of energies are amorphous with more than 97% of the bonds having sp^2 character. Thus, the initial state of the carbon atoms just deposited and prior to sensing energetic incident inert gas ions must be sp^2. The film after deposition is found to contain a much smaller sp^2 content than the film deposited in the absence of energetic particle bombardment. Thus, the energetic particles have brought about a change in the relative population of sp^2 and sp^3 bond types. Despite this knowledge, what is not known is the change in intrinsic stress due to this change in bond type alone in the corresponding amorphous thin films. If the experimental densities are used to estimate the transformation strain then it becomes apparent that only a very small change in the relative percent of bond types will yield sufficient strain to bring the intrinsic stress to a zero value. However, very large changes in the relative bond concentrations occur so that it becomes apparent that the experimental densities cannot reveal the transformation strain. They neglect the possibility that voids are present and that there may be anisotropy in the density for the sp^2 bonded films. This subject should be an interesting and fertile field for any investigator wishing to increase the sum of knowledge available to us.

Robertson[24] has suggested that the compressive stress is the cause of the sp^2 to sp^3 transformation. Figures 5.18 and 5.19 reveal that although there is a general relation between compressive stress and this transformation, the correspondence is not exact. For example, the maximum in compressive stress is reached at a bias voltage of −50 V, whereas the maximum in the sp^3 content is reached at −110 V. Also, there is only a very small decrease from the maximum sp^3 content at −215 V, whereas the compressive stress relative to the maximum drops by 50% at this bias voltage. Thus, it is apparent that some factor other than compressive stress affects the sp^2 to sp^3 transformation, and vice versa.

The nucleated transformation from an amorphous to a crystalline state during deposition has been investigated for silicon[33] and for amorphous alloys.[31,32] In the absence of concurrent energetic particle bombardment, and at sufficiently low temperature, silicon vapors of thermal origin deposit in the amorphous state. With concurrent particle bombardment during deposition exceeding some minimum normalized momentum, but less than some other maximum value of the normalized momentum, the films formed have crystalline particles embedded in an amorphous matrix. Also, in the absence of concurrent particle bombardment, and in a very narrow substrate temperature range, initially deposited amorphous silicon may transform to polycrystalline silicon during deposition.[26] Thus, the transformation from amorphous to crystalline state occurs during deposition in finite volumes of the film, possibly by a nucleation and growth mechanism.

The crystalline state has a lower specific volume than the amorphous state and consequently the contribution to the intrinsic stress due to the amorphous to crystalline transformation should be tensile in sign. This result has been observed in liquid phase chemical vapor deposition (LPCVD) silicon films deposited at 605°C, in the absence of particle bombardment.[26] No concurrent observations of stress and the amorphous-to-crystalline transformation have been made for carbon films, although as noted above they have been made for the sp^2 to sp^3 transition in such films.

1.4. Intrinsic stress due to epitaxy.

The intrinsic stress in the plane of the film due to epitaxy for the cases where the interface plane is a {001}, {111}, or {110} plane of a cubic crystal for both film and substrate is given by[33]

$$\sigma = B \cdot \varepsilon$$

where

$$B = [(C_{11} + 2C_{12})/2] \cdot \left[3 - \frac{C_{11} + 2C_{12}}{C_{11} + 2(2C_{44} - C_{11} + C_{12})(l^2m^2 + m^2n^2 + n^2l^2)}\right]$$

and where *l, m, n* are the direction cosines of the angle between the normal to the film plane and the cube axes and C_{ij} are the elastic constants. Also,

$$\varepsilon = (a_f - a_s)/a_s$$

where a_f and a_s are the lattice parameters of the film and substrate respectively. If the film is elastically isotropic then $B = 2\mu(1 + \nu)/(1 - \nu) = E/(1 - \nu)$, where μ

is the shear modulus, E is Young's modulus, and ν is Poisson's ratio. The stress normal to the film plane is, of course, equal to zero.

2. Thermal stress.

Little needs to be said here concerning the thermal stress in a film due to the difference in thermal expansion coefficients between film and substrate, and to a difference in substrate temperature between that at deposition and that upon observation. One merely substitutes for ε, in the relation for the stress above, the expression $-\Delta\alpha(T_2 - T_1)$, where $\Delta\alpha$ is the coefficient of thermal expansion of the film minus that of the substrate and T_2 is the film temperature at which the stress is being evaluated after being deposited at temperature T_1.

References

1. R.W. Hoffman, Phys. Thin Films 3, 211(1966); Thin Solid Films 34, 185(1976); F.A. Doljack and R.W. Hoffman, Thin Solid Films 12, 71(1972).
2. M.F. Doerner and W.D. Nix, CRC Crit. Rev. Sol. State Mater. Sci. 14, 225(1988).
3. B.W. Sheldon, A. Lau and A. Rajamani, J. Appl. Phys. 90, 5097(2001).
4. O.S. Heavens and S.D. Smith, J. Opt. Soc. Am. 47, 469(1957).
5. W. Buckel, J. Vac. Sci. Tech. 6, 606(1969).
6. (a) H. Windischmann, CRC Crit. Rev. Sol. State Mater. Sci. 17, 547(1992), Table 7, p. 589; (b) H.P. Martinez and R. Abermann, Thin Solid Films 89, 133(1982); (c) R. Abermann and R. Koch, Thin Solid Films 66, 217(1980).
7. H.K. Pulker, Thin Solid Films 89, 191(1982).
8. R.W. Smith and D.J. Srolovitz, J. Appl. Phys. 79, 1448(1996).
9. E.F.C. Haddeman, B.S. Bunick and B.J. Thijsse, MRS Symp. Proc. 594 (1999).
10. C. Fang, Ph.D. Thesis, Columbia University, 1992.
11. P. Chaudhari, J. Vac. Sci. Tech. 9, 520(1972).
12. P.M. Alexander and R.W. Hoffman, J. Vac. Sci. Tech. 13, 96(1976).
13. E. Chason et al., Phys. Rev. Lett. 88, 156103(2002).
14. J.A. Floro et al., J. Appl. Phys. 89, 4886(2001).
15. H. Windischmann, CRC Crit. Rev. Sol. State Mater. Sci. 17, 547(1992).
16. (a) H. Windischmann, J. Appl. Phys. 62, 1800(1987); (b) P. Sigmund, in **Topics in Applied Physics: Sputtering by Particle Bombardment I**, 47, ed. R. Behrisch, Springer-Verlag, Berlin, 1981, p. 1.
17. C. Hwangbo, L. Lingg, J.P. Lehan, H.A. Macleod, J.L. Makous and S.Y. Kim, Appl. Opt. 28, 2769(1989).
18. D. Nir, Thin Solid Films 146, 27(1987).
19. K.-H. Muller, J. Appl. Phys. 59, 2803(1986).
20. J.D. Targove and H.A. Macleod, Appl. Opt. 27, 3779(1988).
21. R.A. Roy, R. Petkie and A. Boulding, J. Mater. Res. 6, 80(1991).

22. K.-H. Muller, J. Appl. Phys. 58, 2573(1985).
23. C.A. Davis, Thin Solid Films 226, 30(1993).
24. J. Robertson, Diamond Relat. Mater. 2, 984(1993).
25. K. Ogata, Y. Andoh and E. Kamijo, Nucl. Instrum. Meth. Phys. Res. B33, 685(1988).
26. P. Krulevitch, G.C. Johnson and R.T. Howe, MRS Symp. Proc. 239, 13(1992); P. Krulevitch, T.D. Nguyen, G.C. Johnson, R.T. Howe, H.R. Wenk and R. Gronsky, MRS Symp. Proc. 202, 167(1991).
27. T. Mizutani, MRS Symp. Proc. 284, 265(1993).
28. J.J. Cuomo, J.P. Doyle, J. Bruley and J.C. Liu, Appl. Phys. Lett. 58, 466(1991).
29. R.M. Fisher, J.Z. Duan and J.B. Liu, MRS Symp. Proc 188, 257(1990).
30. P. Catania, R.A. Roy and J.J. Cuomo, J. Appl. Phys. 74, 1008(1993).
31. J.-W. Lee, S.-C.N. Cheng, M.H. Kryder and D.E. Laughlin, MRS Symp. Proc. 150, 159(1989).
32. M.H. Kryder, MRS Symp. Proc. 150, 3(1989).
33. J. Cahn, Acta Met. 10, 179(1962).
34. This simulation scenario has been enacted in a real material, Cr: A. Misra and M. Nastasi, J. Mater. Res. 14, 4466(1999).

Appendix 1

For real metals a realistic relation for the energy, E, between two metal blocks whose planar surfaces are separated by the distance a* is that derived by Rose et al.[A1] and described below

$$E = -E_o(1 + 0.9a^*)e^{-0.9a^*} \quad (6.A1)$$

where E_o is the total energy for the two metal blocks at the equilibrium separation a_m between the two surfaces, $a^* = (a - a_m)/\lambda$, where a is the actual separation between these surfaces and $\lambda = (9\pi/4)^{1/3} r_s^{1/2}/3$ a.u. in which $r_s = [3/(4\pi n)]^{1/3}$, where n is the number of outer electrons. We may use this relation to determine the spacing at which the attractive force acting on one surface due to the other block of metal equals the same ratio of the maximum attractive force as the typical tensile intrinsic stress in films is to the theoretical breaking strength, i.e. roughly 0.01. For the specific case of aluminum, using the above relation and the fact that the maximum attractive force occurs when $d^2E/da^2 = 0$, we find that the spacing between surfaces that would yield the observed level of intrinsic stress occurs at a value of 1.7 times the interplanar spacing or a void thickness of 1.67 Å for a typical metal. *Thus, in metals the only voids that can contribute significantly to the intrinsic stress are less one vacancy thick, at the most.* Only voids (cracks) thinner than 1.7 times the interplanar spacing will spontaneously cold weld. It is these regions of 1.7 times the interplanar spacing that form the bridges in films deposited in the *zone a* temperature regime.

A1. J.H. Rose, J. Ferrante and J.R. Smith, Phys. Rev. Lett. 47, 675(1981).

This page intentionally left blank

CHAPTER VII

Reaction-induced Structure

Reactions between separate phases or layers in thin films may be classified as heterogeneous, and those that occur within a single layer or on the surface between adatoms or admolecules may be classified as homogeneous. In integrated circuit technology, the products of these reactions make up elements of circuitry, such as gate oxides, or metallic junction elements, such as silicides. Sometimes the reactions between adjacent thin film layers are undesired, as in superlattices. It is thus useful to attempt to summarize the knowledge that has been gained from studies of these various reactions in thin films.

1. Heterogeneous reactions between thin monocrystalline layers.

1.1. Completely miscible layers.

Given monocrystalline layers having different composition as the elements of the diffusion junction. Usually, even though the two layers have the same crystal structure, given that they are completely miscible, they do not have the same lattice parameter. Thus, there will usually be misfit dislocations in the two layers to minimize the free energy of the two-layer structure. As diffusion proceeds to develop a concentration gradient, the misfit dislocations will move to accommodate the difference in lattice parameters along this gradient. One possible result of such diffusion is the formation of new grains whose lattices are curved to adjust for the difference in lattice parameters that exists along the direction of the concentration gradient.[1,2] The boundaries that separate the curved grains from the matrix are made up of dislocations which once accommodated the misfit in the areas occupied by the curved grains. The tendency to form such curved grains increases with the degree of misfit between the lattice parameters of the layers and with the thickness of the layers.[2]

Usually, lattice diffusion involving two species having different diffusivities and vacancy diffusion as the primary diffusion mode will give rise to another type of defect, namely, voids. However, this effect occurs in bulk diffusion couples and may not occur in thin film diffusion couples if the initial thickness of the fastest component is such that no excess unreacted layer remains at the completion

of the diffusion anneal and this layer is at the composite film surface, rather than at the interface with the substrate.

Thus, in the event it is desired to deposit a void-free, monocrystalline alloy of some specific composition, a preferred strategy is to codeposit the components of the alloy to produce the desired composition onto a monocrystalline substrate that has the desired lattice parameter and crystal structure.*

2. Layers of immiscible components but forming intermediate compounds.

This category is probably the most important of the numerous cases involving reactions between layers of thin films. For example, silicides are often produced via a reaction between a metal layer and the underlying silicon substrate. Given that the product layer forms as an intermediate layer between the two reactants, further reaction requires that at least one of the reactants diffuses through the product layer to combine with the other reactant to form an additional product layer.

2.1. Epitaxial monocrystalline product phase.

If the substrate is monocrystalline then it is possible to form an epitaxial monocrystalline compound via reaction between the polycrystalline reactant layer and the monocrystalline reactant substrate. However, supplementary conditions must be met for the product layer to be epitaxial. There must be coherency across the product layer-substrate interface and the lattice parameter mismatch must be small. Given the latter conditions then the formation of the epitaxial compound is favored over the other possible competing intermediate phases that may exist in the phase diagram of the reactants' system because the surface energy barrier to nucleation of an intermediate phase is at a minimum for the epitaxial compound. An example of this category is $CoSi_2$, which is one of four intermediate phases that exist at equilibrium in the Co–Si binary system. However, since at least one of the reactants must diffuse through the product layer, the diffusion rate of the fastest diffusing component through the product layer varies between the different potential products and thereby can control which product will appear first providing that nucleation does not limit the onset of the reaction. Indeed, in the Co–Si binary system it is possible to have with increasing reaction temperature, Co_2Si, CoSi, and $CoSi_2$ as the products that appear.[3]

* Since the original edition of this book thin film Li batteries have become significant. Since they function as a consequence of a reaction between two thin films a brief summary of this reaction and effect on structure is given in Appendix 1.

$CoSi_2$ has several potential applications in integrated circuit technology. It is being considered as a low-resistivity conducting element in three-dimensional electronic devices since it can be made to be epitaxial with silicon as an overlayer on the latter and silicon can be deposited as an epitaxial overlayer on the silicide. There are three structural aspects of this silicide layer that should be discussed here. One is the surface structure of the silicide, another concerns the island mode of growth of the silicide under certain conditions of growth and the possible related structural defects, and the last relates to the pinholes that may appear in the silicide layer.

Two orientations of the substrate silicon surface are of interest here: (111) and (100). As mentioned in previous chapters, depending upon which of two energetically nearly equal sets of potential wells on the (111) plane is occupied by the contacting monolayer of the epilayer, stacking faults or twins can be introduced. In the case that the epilayer is a different phase, the resulting epitaxial product may have two orientations, which are twin related. $CoSi_2$ belongs to the cubic fluorite structure class. Hence, one of the $CoSi_2$ twins will have its cubic axes parallel to those of the substrate whereas the other twin will be related to the former by a 180° rotation about the $<111>$ axis normal to the substrate surface. These are denoted as the A and B orientations, respectively, in the literature.

The initial stage of growth consists in the formation of separated islands of $CoSi_2$. How then is it possible to produce a single orientation in the epilayer when both A and B oriented islands are formed? It should be mentioned here that a single oriented $CoSi_2$ layer (in the B orientation) is produced only under ultra-high vacuum conditions (or its equivalent). Both orientations are found when oxygen is not removed from the Si substrate surface. An answer is that under ultra-high vacuum conditions the boundaries between the twins are mobile at the growth temperature and move so that the B oriented grains consume the A oriented ones. Apparently, the B oriented grains have a lower free energy than the A oriented ones. (This is a fortunate result since for device considerations it is desirable to have an A/B/A orientation for the Si/$CoSi_2$/Si multilayer assembly.) When oxygen is present the boundaries between the twins become immobilized and both orientations then survive in the epilayer. It must be remarked, however, that the proposed explanation differs from one given in the literature.[4]

Thus, B oriented $CoSi_2$ epilayers can be grown on Si(111). The epilayers contain only a few dislocations in the bulk of the epilayer, but have misfit dislocations at the interface with the substrate. We have not mentioned the growth conditions that yield this desirable product. In fact, to obtain high-quality product it appears to be necessary, after deposition of the Co layer, to anneal at a temperature in excess of 600°C for the formation of the $CoSi_2$ epitaxial layer. Only for anneal temperatures above 600°C does the $CoSi_2$ layer have sufficiently low electrical resistivity for high-speed device application.[5] It is believed that point defects in the $CoSi_2$ layer do not anneal out of the layer below this temperature.[5] (However, it

should be noted that there are methods for producing perfect $CoSi_2$ layers at temperatures lower than 600°C that do not involve point defect diffusion, which will be discussed in a later section.)

$CoSi_2$ layers formed via the interdiffusion of Co and Si layers at temperatures higher than 600°C involve two types of defects. One is a rough surface. The other defect likely to appear in the bulk epilayer is the pinhole, a cylindrical shaped hole that extends from substrate to surface. To understand why pinholes form and how to avoid their formation it may be useful to know that the (111) surface of $CoSi_2$ may be one of two types: C and S. The C type consists of a single monolayer of Si as the termination layer. The S type has three Si layers at the surface. It has been shown that when the S type surface is present on the $CoSi_2$ epilayer,[5] or when there is an excess of Si as an overlayer on the $CoSi_2$ epilayer,[6] from deposition through subsequent annealing, then pinholes are avoided. Also, it is shown that pinholes develop in epilayers that have the C type surface after deposition, but before subsequent annealing, upon being annealed. Further, after annealing, the epilayers have the S type surface. These facts indicate that Si diffuses from the epilayer having the C type surface during annealing to the epilayer surface to convert it to an S type surface. Such diffusion is believed to initiate the formation of the pinholes, i.e. the fastest means of providing Si to the epilayer surface is via the formation of pinholes and surface diffusion along the pinholes. The homogeneous depletion of Si from $CoSi_2$ to provide the two surface monolayers of Si in the S type surface would result in a local increase in free energy in the bulk epilayer, which may provide a much larger barrier to the transport of the required Si than would the heterogeneous formation of a pinhole through the epilayer that could supply the needed Si to make the pinhole surface as well as the epilayer surface S type in character. Apparently, the S type surface has lower energy than the C type surface of $CoSi_2$(111).

The surface roughness problem has been solved by use of a codeposition technique that will be considered in a later section.

The formation of monocrystalline and epitaxial $CoSi_2$ on Si(100) is more desirable from device considerations than on Si(111). Thus, there has been an effort to produce this product. One successful method involves what is now known as the template method, first pioneered in the control of $NiSi_2$ epilayer orientation (A or B) on Si(111).[7] In this method as applied to the production of $CoSi_2$ on Si(100) a layer of Co about 2.6 Å thick is deposited on clean Si at room temperature in ultra-high vacuum, followed by the deposition of several angstroms of Co and Si in stoichiometric ratio and further annealing to 460°C.[8] It has been noted that on Si(100) Co does not react to form $CoSi_2$ at room temperature;[9a] neither does it do so on Si(111).[9b] From an analysis of the results from various surface sensitive techniques it was concluded that at room temperature Co initially diffuses into the Si lattice interstitially, but with an initial Co layer thicker than 2.5 ML there is a change of the Co diffusion mechanism from interstitial to site exchange.[9a] One may speculate that it is the occupancy of lattice sites in Si by Co atoms, as a result of diffusion at

room temperature, that provides the template for the growth of a monocrystalline, epitaxial layer of $CoSi_2$ upon subsequent annealing to 460°C. In the absence of the template procedure, reaction between a Co layer and a monocrystalline Si substrate produces a polycrystalline $CoSi_2$ layer at a temperature above about 600°C, and a polycrystalline CoSi layer at about 375°C. The template scheme demonstrates the extraordinary effect of the state of the interface between two reactants on the subsequent product formed by them.

Much more complicated defect structures are produced in the reaction between rare earth metals and silicon to form $RESi_{2\text{-}X}$ epitaxial silicides on Si(111). One type of defect observed is a vacancy superstructure on the Si sublattice. The other type of defect is the stacking fault with $\{10\bar{1}0\}$ habit planes and 1/6 $<\bar{1}2\bar{1}3>$ displacement vectors.[10] The determination of the origins of these defects requires more research.

An additional structure is manifested in the case of epitaxial PtSi on Si. When stoichiometric quantities of Pt and Si are coevaporated onto clean Si(111) at 500°C in an ultra-high vacuum environment to a total thickness of 200 Å then a monocrystalline and epitaxial film of orthorhombic PtSi is formed on the Si substrate. If now Si is deposited onto the PtSi at a substrate temperature of 400°C, then a double heterostructure of Si(111)/PtSi(010)/Si(111) is produced. If the ultimate Si layer is deposited at a substrate temperature of 600°C instead of at 400°C, then the homogeneous layer of PtSi is disrupted to produce interspersed columns of PtSi and Si in the epitaxial orientations corresponding to those found in the double heterostructure. Figure 7.1 illustrates the microstructure of the interspersed columns. One explanation proposed by the investigators who found this effect[11] is that the driving force to produce the columnar structure is the attempt to minimize PtSi/Si interface area. This explanation is certainly wrong in that formation of the columnar structure must initially increase this interface area, as is apparent from

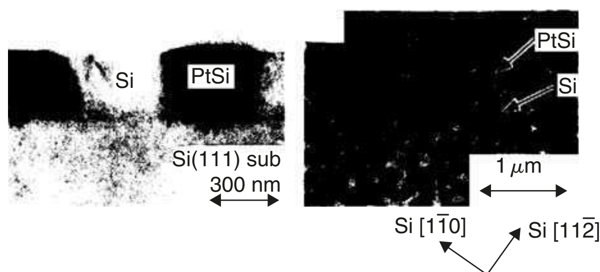

Figure 7.1. Cross-sectional TEM (observed along $(1\bar{1}0)$ azimuth of the Si(111) substrate) and planar SEM photographs observed after 200 Å thick Si deposition at 600°C on a 200 Å thick PtSi layer formed at 500°C. Reproduced with permission from Y. Kumagai et al., J. Appl. Phys. 75, 3211(1994).

Figure 7.1. A more likely explanation is that the columnar morphology decreases the elastic strain energy developed by the misfit between the PtSi and Si structures. Certainly a conclusion of the results cited above is that the Si(111)/PtSi(010)/Si(111) double heterostructure is morphologically unstable and given sufficient mobility will change to produce the columnar structure of Figure 7.1. Thus, in the phenomenon just discussed, it appears that the tendency to reduce the film stress drives the interchange of Pt and Si atoms at the interface between PtSi and Si so as to rearrange the morphology. This rearrangement involves an initial increase in the interface area, although in a later stage the PtSi/Si interface area may be smaller than at the start of this reaction.

2.2. Polycrystalline compound products.

As noted in the previous subsection unclean substrate surfaces can cause the formation of polycrystalline product layers of a substrate-overlayer interaction that are also epitaxial with the substrate. In many cases, the conditions required for epitaxy are not satisfied and sufficient separate non-epitaxial product grains are nucleated so that the final product is polycrystalline. The new and different type of defect found in this case is surface and substrate/product interface roughness on a larger scale. There are several possible reasons to account for this result. Reactions are likely to be diffusion limited and diffusion through a polycrystalline layer for many of the cases belonging to the class of this section is likely to be limited by grain boundary diffusion. The rate of transport along grain boundaries is not the same for all grain boundaries and for a given grain boundary can vary with direction in the grain boundary. Thus, some product grains will grow faster than others. Further, grooves can develop at grain boundary/surface or/substrate intersections in an attempt to achieve local interfacial equilibrium, which contribute to roughness at these interfaces.

One of the polycrystalline phases formed by reaction between a metal layer and a silicon substrate that has found commercial application is $TiSi_2$. This silicide has been used as gate and source/drain conductors in CMOS technology. In the reaction between Ti and Si, the first phase formed is an amorphous TiSi solid solution, then the C49 phase of $TiSi_2$ nucleates and grows at the α-TiSi/c-Si interface, and finally the C49 phase converts to the C54 phase upon further heat treatment. The latter phase is the desired one since it has a resistivity between 12 and 15 $\mu\Omega$-cm and the former has a much higher resistivity. With the trend to smaller dimensions of all circuit elements a problem has arisen with this silicide in that the silicide tends to agglomerate, i.e. it is morphologically unstable as a smooth film. Since the driving force for agglomeration is the reduction of the total free energy associated with the interfaces of the agglomerating phase one possible solution of this problem is modification of the interface energies of the C54 phase. Another

possible solution depends upon the kinetics of the competing processes: the C49 → C54 reaction and the agglomeration process. Because the former is more rapid than the latter, use of rapid thermal processing (RTP) may allow the first process to occur before the latter can change the morphology significantly. However, as the dimension of the C54 $TiSi_2$ phase conducting element decreases the chemical potential gradients of the diffusing species increase. Such increase in chemical potential gradient results in an increase in the rate of agglomeration of the C54 silicide with the result that the difference between the kinetics of the two competing processes becomes smaller. Thus, there may be a limit to the ability to produce adequate $TiSi_2$ conductor elements in submicron CMOS technology via a strategy based on RTP separation of the desired reaction from the undesired agglomeration process. We have in this example another manifestation of the crucial relation between processing and structure.

3. Reactions between adatoms and substrate.

3.1. Silicon dioxide films.

One of the foundations of the silicon-based technology of current microelectronic devices is the ability to form useful oxide insulating layers on silicon by reaction with oxygen via processes that are consistent with wafer integrated circuit technology. Until recently, the method of forming these SiO_2 layers made use of thermal oxidation in a controlled environment. Such oxidation was carried out in furnaces at elevated temperature (800–1050°C). With the current trend to reduce the dimensions of circuit elements, other methods of producing SiO_2 films on Si have been investigated that do not require submitting wafers to these elevated temperatures. The thermally produced oxides represent the reference state relative to which the properties of the oxides produced by these new methods are evaluated.

These SiO_2 films are amorphous and consequently have a complicated defect structure. Although many of these defects have been defined, many more are as yet undefined. Further, the relationships between the defect structure, processing, and properties are also somewhat ambiguous. Thus, the new processing methods have been evaluated empirically by measurement of the significant properties required for use of the oxide films thus produced, such as breakdown field. Although some aspects of defect structure are known to contribute to the breakdown field, others are not known. For example, the roughness of the Si/SiO_2 interface is known to affect the breakdown field, in that increasing roughness decreases the breakdown field. Unfortunately, there seem to be few studies of the effect of processing on this interface roughness, probably conditioned by the fact that characterization of this interface roughness is difficult. Also, recent studies[12] point to the development of

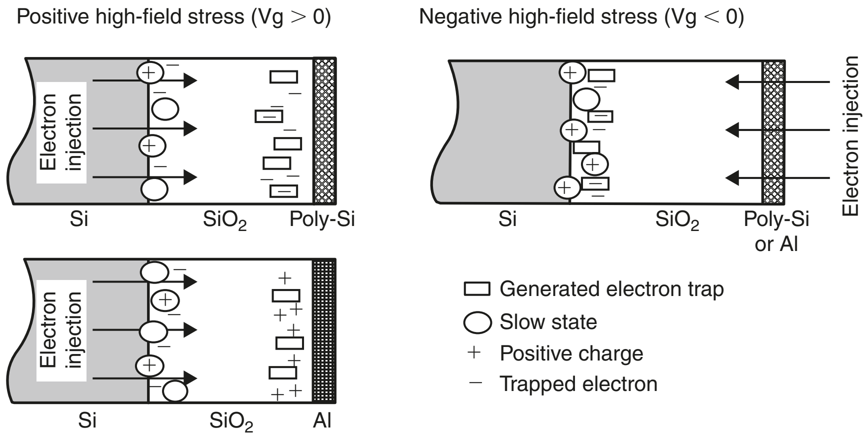

Figure 7.2. Schematic illustration of the charge and defect distribution after negative and positive constant current stressing of MOS capacitors with Al and poly-Si electrodes. Reproduced with permission from M.M. Heys and A. V. Schwerin, **Insulating Films on Semiconductors**, Adam Hilger, IOP Publishing Ltd, Bristol 1991, p. 73.

defects, which are localized at the conductor/SiO_2/Si interfaces, as illustrated schematically in Figure 7.2, that lead to the development of the critical condition that incites the destructive breakdown of the insulator. But, again unfortunately, nothing is known about the origin of these defects. It is known that the nature of the interfaces with the SiO_2 insulating film affects the sign of the charges that build-up at these interfaces, as illustrated in Figure 7.2, i.e. under positive high-field stress positive charge builds up at the Al/SiO_2 interface and negative charge builds up at the poly-Si/SiO_2 interface.

It has been reported that grown oxides have better properties than deposited oxides.[13] This fact may be understood readily with the knowledge that the Si/SiO_2 interface after growth is not the original surface of Si but lies below this original surface, as is illustrated schematically in Figure 7.3, whereas that for the deposited oxide lies at the surface of the Si. Even if this surface is clean, there are foreign atoms in it. Further, the defects likely to exist at the Si/SiO_2 interface will be fewer at the interface produced by diffusion rather than at that produced by deposition thereon. It has already been noted that the most important property of the oxide film, its breakdown voltage, depends upon the quality of the interfaces between the oxide and the contacting conducting layers. Incidentally, this reason for the advantage that a grown oxide has over a deposited one also applies to the silicides used for Schottky junctions with silicon, i.e. the grown silicide has a clean, nascent interface with silicon, whereas the deposited silicide does not.

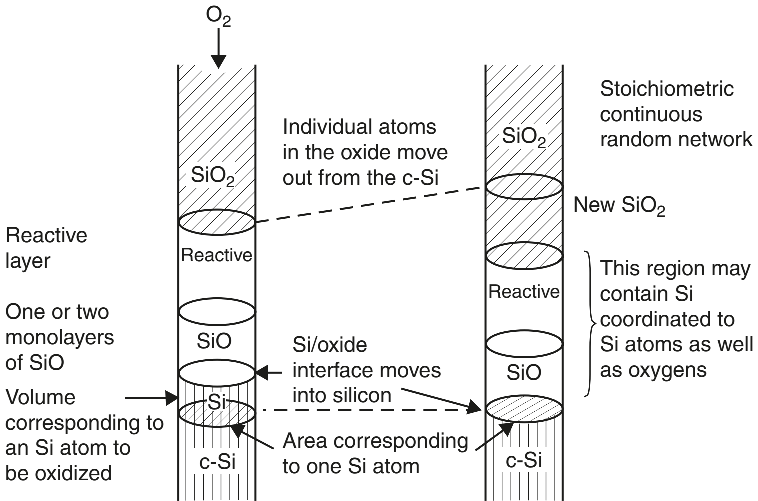

Figure 7.3. The structure before and after oxidation by one oxygen molecule is shown for a column corresponding to one Si atom in the silicon substrate. The reactive layer and SiO layer (if present, since these will depend on conditions) move deeper into the Si, but the outer oxide surface moves further out. Reproduced with permission from A.M. Stoneham, **Insulating Films on Semiconductors,** Adam Hilger, IOP Publishing Ltd, Bristol 1991, p. 19.

Figure 7.3 also indicates that the composition over one or two monolayers of the Si/SiO_2 interface is that of SiO, which may or may not be due to a small-scale surface roughness. The extent of this intermediate layer may be reduced by high-temperature annealing in an oxygen atmosphere.[13] Defects of extrinsic origin, such as Na and H are likely to be present at this interface. These defects may also be removed in high-temperature treatments. Si dangling bonds may also be present in a concentration of one in a hundred Si atoms[14] and may be passivated by combination with H atoms at temperature T obeying $225 < T < 550°C$. The dangling bonds in SiO_2 are not all of one character as in amorphous Si. Rather, although the Si_3Si- dangling bond is the same in both materials, Si_2OSi–, SiO_2Si–, and O_3Si– are dangling bonds that exist in SiO_2 but not in α-Si. Such dangling bonds are believed to make up most of the Si/SiO_2 interface states with the Si_3Si predominating.

When hot electrons or holes enter the oxide over the blocking interfacial energy barrier of 3.1 eV defects may also be generated at this interface, either by electron-hole annihilation or by trap creation via hot electrons. Such defect generation leads to degradation of the oxide in usage. Trap and interface state generation rates are sensitive to the hydrogen content in the oxide and to the annealing atmosphere and do not vary in the same way with variation of this treatment.[15] Methods of preventing

the onset of such damage are currently being researched, such as nitridation of the interface, control over the morphology of source/drain regions and gate oxide, and control over the mechanical stress acting on the gate oxide.*

4. Amorphous to crystalline transitions.

4.1. Silicon.

4.1.1. α-Si → poly-Si.

At this writing the higher electron field effect mobility of poly-Si relative to α-Si:H and the consequent advantage of incorporating such higher mobility in flat-panel displays and the like are driving investigations to discover the factor(s) that limit this higher mobility. Poly-Si can be formed in a variety of ways. It can be produced by a variety of chemical vapor deposition (CVD) techniques at substrate temperatures >600°C; by thermal crystallization of α-Si with the α-Si produced by CVD or by self-implantation and the crystallization carried out by furnace or by rapid thermal annealing, and by laser crystallization of α-Si. The first process produces a columnar array of grains with grain sizes smaller than 100 nm (usually limited to a size about equal to the film thickness). The second process can produce a large grain size array (about 1 μm). The result obtained using the third process depends upon conditions pertaining to the α-Si and the laser crystallization, but in the desirable state consists of an array of grains, that are formed by solidification of the laser melted film under conditions that yield few nuclei and can produce a grain size on the order of 1 μm. However, the mobilities for the products of the three processes range from 1 to 10, 20 to 120, and 10 to 500 cm^2/Vs, respectively.

Apparently, the mode of forming the poly-Si influences the grain size, the structure of the grain boundaries in the poly-Si film and the defect structure within the grains. The grain boundaries and bulk defects are the sites of the traps that affect the electron mobility. Thus, the less is the grain boundary area and the bulk defect density per unit film area the better will be the electronic properties of the poly-Si film. Another possible property that may be significant in this context is the trap density per unit area of grain boundary. We have very little knowledge of the latter phenomenon. We do know theoretically that perfect tilt boundaries do not contain dangling bonds. However, it is by no means an assured fact that the absence of dangling bonds means an absence of traps in the grain boundary. Indeed, bent or weak bonds in such boundaries may act as effective traps.[17] Let us now consider the factors that may affect these parameters.

* Since the first edition of this book progress in miniatiurization has been so rapid that a need to replace SiO_2 by high-dielectric constant insulators has spurred much research. The interface reaction between these high k materials and Si is considered in Appendix 2.

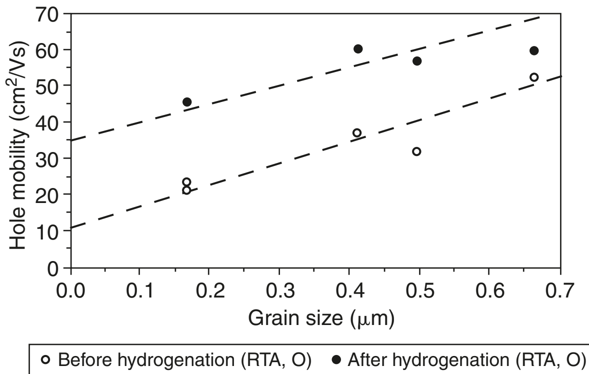

Figure 7.4. Hole mobility versus grain size for rapid thermal processed TFT's. Reproduced with permission from E. Campo, J.J. Pedroviejo, E. Scheid, D. Bielle-Daspet, A.Y. Massaoud, G. Sarrabayrouse and A. Martinez, MRS Symp. Proc. 303, 389(1993).

There is much evidence that for a given technique of producing a poly-Si film the field effect mobility increases as the grain size increases. Figure 7.4 presents one example of this relationship. However, grain size alone does not control the field effect mobility in poly-Si. As indicated in Figure 7.4, passivation as a consequence of annealing in a hydrogen atmosphere also acts to increase this mobility. This process is believed to take place not only by the removal of dangling bonds at grain boundaries, but also by the removal of bent (weak) bonds in the process of converting them to Si-H bonds. However, even for a given grain size and hydrogen passivation, the field effect mobility can vary. For example, poly-Si films of nearly the same grain size (130 versus 145 nm) formed by recrystallization of the same amorphous films in a furnace at 600°C on the one hand and by RTP at 750°C for 80 s on the other hand, and then treated the same way yielded field effect electron mobilities of 30 and 80 cm^2/s, respectively.[18] This observation is readily explained by other observations that show a high density of stacking faults and twins in films crystallized from amorphous films at about 600°C,[19] with the density of such defects decreasing with increasing annealing or crystallization temperature.[20]

One might expect that grains formed by solidification from the melt contain fewer defects than grains formed by crystallization at 600°C of an amorphous matrix. However, this expectation is not borne out by the results of Ready et al.[21] who found that the latter had higher Hall mobility than the former in samples that had about the same grain size. The main advantage of laser melt solidified grains arises from the ability to produce large grains at an appropriate laser pulse power level. This power level coincides with the almost complete, but not quite complete, melting of the film, so that very few grains remain to act as heterogeneous nuclei for the explosive crystallization of large grains of diameter greater than the film

thickness.[22a] These large grains of the order of 1 μm diameter have drift mobilities in excess of 150 cm^2/Vs. The grain size that may be achieved via single pulse laser crystallization appears to be limited by the extent that a heterogeneously nucleated grain can grow laterally before homogeneous nucleation in the supercooled melt pinches off its further grain growth via solidification from the melt. However, it has been found[22b] that multiple laser pulse melting at the intermediate power level corresponding to incomplete melting of the film results in the melting back of grains having other than (111) orientation parallel to the film allowing the (111) oriented grains to grow further on refreezing.* This process leads to the development of films having larger grain size and a stronger (111) texture.

The concept of using sparsely distributed heterogeneous nuclei to control the grain size has also been utilized in both the other methods of producing poly-Si. In particular, in solid phase grain nucleation from an amorphous matrix it has been found that a sufficient fluence of Si^+ ($>1 \cdot 10^{15}/cm^2$) ions of sufficient energy to produce ion mixing at the Si/SiO_2 interface results, upon annealing at 600°C, in a grain size larger than 1 μm in films of thickness on the order of 100 nm. Further annealing at 1050°C and hydrogenation yields field effect mobility higher than 100 cm^2/Vs.[20] The ion mixing results in suppression of heterogeneous nucleation of grains at the α-Si\\SiO_2 interface. It was suggested that this suppression came about either as a result of the distribution of O atoms from the SiO_2 into the Si adjacent to the interface and the consequent effect of O on solid phase growth or by a change in interfacial stress.

The concept of suppression of the natural heterogeneous nucleation and its replacement by artificial heterogeneous nucleation from a controlled periodic distribution of artificial nuclei has been used by Yonehara et al.[23] to produce, via CVD, a poly-Si film having a periodic grain distribution of grain size equal to 200 μm. The field effect hole mobility measured in a p-channel MOSFET made in one such grain was 180 cm^2/Vs. It seems to this writer that the potential of grain size control in poly-Si films via suppression of natural nucleation and use of artificial nuclei still remains to be exploited and offers a promising path for the production of commercially viable poly-Si films for flat-panel display and similar applications. It should be noted that at no time has it been found possible in any poly-Si film to attain the mobility values characteristic of single crystal silicon. This fact indicates that the grains in poly-Si still contain a higher density of trap defects than does the single crystal silicon. Much remains to be learned about the dependence of defects in poly-Si on processing. We will gain some additional knowledge concerning this subject in the next subsection.

* The reason for this behavior is unknown. Since Atwater et al.[41] found that for Si/SiO_2 interfaces, one of the interfaces that exist for these experiments (001), Si exhibited the least energy in contact with SiO_2, the observed result cannot be due to the attempt to minimize interface energies inasmuch as the other interface is the solid/melt interface, which is not likely to vary much with orientation of the solid.

4.1.2. α-Si → epitaxial c-Si transition.

The transition from amorphous to crystalline silicon via the motion of the interface between the two phases to yield an epitaxial Si layer has been studied extensively.[24a, 24b] This transition involves only the growth aspect of the transformation. The nucleation aspect is absent. It has been found that the activation energy for the migration of the amorphous/crystalline interface into the amorphous phase is 2.7 eV. Figure 7.5 provides some data governing the temperature dependence of the velocity of this interface. This velocity is a function of the concentration and type of dopant and of the orientation of the crystal plane parallel to the interface. Energetic particles that penetrate the interface can cause the interface to move in one or the opposite direction,[24b] i.e. enhance the α-Si → c-Si transition or reverse it. Under conditions leading to growth enhancement appreciably more interface migration can be accomplished at much lower temperatures under energetic particle bombardment that can be accomplished thermally, as indicated in Figure 7.6.

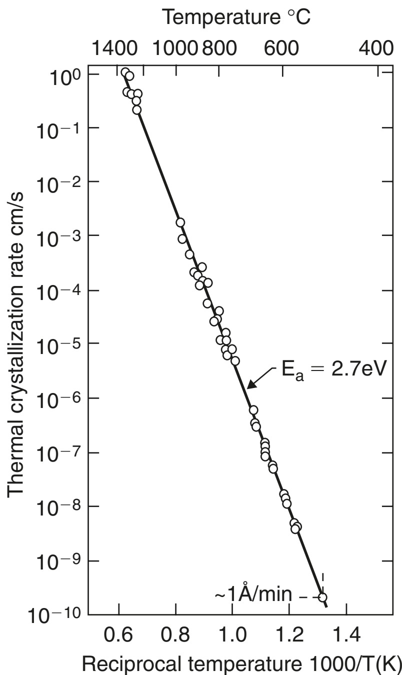

Figure 7.5. Velocity of α/c-Si interface versus temperature. Reproduced with permission from G.L. Olson et al., MRS Symp. Proc. 13, 141(1983).

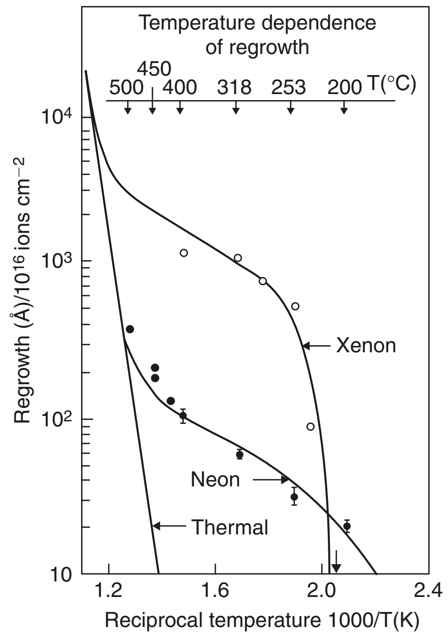

Figure 7.6. Regrowth of c-Si from α-Si due to particle bombardment. Full lines theory due to K.A. Jackson. J. Mater. Res. 3, 1218(1988); data reproduced with permission from R.G. Elliman et al., Nucl. Instrum. Meth. B19/20, 435(1987).

The defect structure "deposited" behind the amorphous/crystal interface is our main interest in this section. Let us gather some facts from the literature to enable us to deduce some tentative conclusions regarding the factor(s) that control the defects arising from this phase transition.

Most information concerning defects present in the recrystallized volume of the original amorphous zone comes from amorphous layers that have been created by energetic particle bombardment. For substrate temperatures at or higher than 100°C during the implantation dense tangles of dislocations are found after annealing that transforms the amorphous region back to the crystalline state independent of the orientation of the original crystal surface.[25a] Dislocation loops and dislocations in the form of a tangle or network have been found. The loops are found at a depth corresponding to the original position of the α/c interface and, thus, may originate in the damage zone in the crystal adjacent to the interface by the condensation of point defects created there by the implantation. The dislocation tangles and network in the region previously occupied by the amorphous layer may originate from loops that intersect the original α/c interface or they may arise from the imperfect impingement of tilted regions of the α/c interface. For implantation at subzero substrate temperatures, microtwins are observed in annealed {111} wafers while dislocation loops only are found in annealed {100} wafers. The origin of this effect of substrate temperature on the character of defects produced after annealing of {111} wafers previously subjected to implantation-induced amorphization is not known. In a more recent study[25b] of the defects found in the recrystallized region of Si–Ge alloys, deposited by MBE on Si(100), amorphized by ion implantation of Si^+ ions at 77 K, and recrystallized at a temperature between 475 and 575°C, it was found that dislocations in the recrystallized zone were produced by the stress due to misfit strain originally present prior to amorphization. In particular, samples which had been annealed at 950°C for 1 h just prior to the ion-implantation-induced amorphization (the latter to a depth smaller than the thickness of the original Si-Ge MBE layer) showed no dislocations to be present except for small loops in the end-of-range damage zone, i.e. no dislocations were promoted into the recrystallized zone above the damage zone by passage of the α/c interface. This result was substantiated by the observation that the dislocations found in the samples subjected to the same treatment, but without the anneal prior to ion implantation to relax the misfit stress, were separated from the damage zone by a dislocation free zone.

A study of the amorphous to crystalline transition in the electron microscope[26a] revealed the presence of twins in the crystalline region behind the amorphous/crystal interface emanating from the interface as it moved into the amorphous phase. However, from evaluation of the activation energy for the interface migration step in this study (3.36 eV) Batstone[26a] concluded that the interface migration was limited by the action of oxygen atoms in the vicinity of the interface. Thus, a further conclusion was that the production of the twins was a consequence of the segregation

of oxygen at the α/c interface. This conclusion is substantiated by the work of Priolo et al.[26b] who found that twins are present in crystals formed by solid state crystallization of amorphous silicon when Au atoms were segregated at the α/c interface. Further, White et al.[26c] and Kennedy et al.[26d] found that oxygen promoted the formation of twins in the α → c transition in Si.

From the above results we may conclude that, for regrown crystal regions of α-Si that have been made amorphous by self-ion implantation, defects (dislocations and twins) in the regrown zone are introduced by impurities and stress. Further, *it is possible that, for self-ion implantation-induced amorphization at 77°K of Si(100), regrowth in the absence of impurities and stress produces defect-free single crystal.*

The amorphous to crystal transition of amorphous phases formed by ion implantation differs in an important characteristic from that of amorphous phases produced by deposition. The α-Si that is produced by self-ion implantation of a pure single crystal of Si, with a fluence that is too small to affect the density significantly, contains the same number of atoms in the volume made amorphous and subsequently recrystallized by the motion of the amorphous/crystal interface as was contained in the original crystal. Hence, in this case it should be possible to recreate a single crystal without defects. However, when the amorphous layer is deposited via CVD or physical vapor deposition (PVD), it has a density smaller than the corresponding single crystal generated by motion of an interface between crystalline and amorphous phases. Hence, it is expected that production of an epitaxial Si layer from a deposited amorphous layer should develop stress and that this stress may result in the production of both misfit dislocations and threading dislocations.

However, epitaxial crystallization of amorphous Si films at temperatures below 600°C, deposited onto clean Si(100) in a vacuum better than 10^{-8} Torr, produced a crystalline layer that contained a density of dislocations too small to have an effect on the electron transport properties.[25c] It is not known whether the paucity of dislocations is due to the stress being too small to induce dislocation multiplication and motion at the annealing temperature or whether no stress is developed contrary to expectation. According to the analysis of Dodson and Tsao[25d] the annealing temperature (600°C) and the expected elastic strain (1.8%) is just on the border separating the region representing coherent (dislocation-free) strained layers from that in which dislocation multiplication and motion can occur in silicon. The results of Ross et al.[27b] are in agreement with this analysis in that stress-induced dislocation density increases in SiGe layers were not observed below 600°C for elastic strains as high as 1%, but were observed above this temperature. Hence, it appears likely that for annealing temperatures below 600°C dislocation multiplication will not occur in solid phase epitaxy of Si(100), whereas it may occur for annealing temperatures higher than 600°C.

The development of tensile stress in films where the poly-Si grains were formed by crystallization from a deposited amorphous matrix has been observed

by Krulevitch et al.[27a] The magnitude of this stress (0.6 GPa) is much higher than that found in deposited α-Si films. At stress levels of 0.18 GPa dislocations have been found to multiply and move above about 600°C in Si.[27b] Kunii et al.[27c] observed dislocations in crystalline layers formed by motion of an α/c interface in CVD Si films. Their amorphous layer was produced by CVD onto a single crystal of Si having a dislocation density $<10^5/\text{cm}^2$. The surface of the latter was cleaned by H_2 etching at 1100°C and protected in situ prior to deposition from silane by HCl etching. Solid phase epitaxy at 600°C yielded a dislocation density of $10^{10}/\text{cm}^2$, which was reduced to $10^8/\text{cm}^2$ after annealing at 1150°C for 4 h. Now in the seeded sequential CVD of epitaxial Si over SiO_2 at temperatures exceeding 1050°C (epitaxy is achieved during deposition in this case without the intervention of an amorphous deposit and subsequent solid phase epitaxy) the dislocation density obtained is less than $10^5/\text{cm}^2$.[27d] Indeed, the production of dislocation free epitaxial Si layers via CVD at such elevated temperatures is normal. Hence, it appears that *solid phase epitaxy of an amorphous Si layer formed by CVD at or above 600°C will yield a high dislocation density in the resultant crystalline Si.*

We now have the basis to account for the fact, noted in the previous subsection, that the highest drift mobilities measured in large grain poly-Si formed by solid state crystallization of amorphous silicon are an order of magnitude smaller than those characteristic of lightly doped pure Si single crystals.

The first thing to note in this regard is that the poly-Si films are all deposited on an oxide substrate. Further, all films that after suitable processing later resulted in large grain poly-Si films were initially deposited via CVD at substrate temperatures lower than about 650°C. Now, Meyerson[28a] has shown that below 700°C it is necessary to maintain a partial pressure of $<10^{-8}$ Torr for both O_2 and H_2O in order to prevent the formation of SiO_2 during the CVD of silicon. Thus, it is likely that these films, which were not formed via ultra-high vacuum CVD or via self-ion implantation of pure single crystal silicon, and which were deposited at temperatures less than 700°C, contain oxygen concentrations above those present in the high-mobility single crystal silicon. As noted above, such excess oxygen can lead to the production of twins in the poly-Si grains produced by crystallization of α-Si. Even in pure α-Si, α/c interfaces parallel to Si{111} will produce twins during their motion. Further, it is highly likely that pure poly-Si films, which are crystallized above 600°C will contain a high density of dislocations. Thus, it may be expected that poly-Si produced by crystallization of α-Si formed by CVD will have lower drift mobility values than wafer grade Si that contains a negligible density of dislocations.

In the above we have not discussed α-Si formed by rapid melting and freezing of the surface of single crystal Si. The solid phase epitaxial (SPE) recrystallization of such α-Si on a (001)Si wafer was found to produce "essentially perfect crystalline Si".[28b] This result indicates that laser melting did not add impurities. The thickness of the α-Si that was induced to undergo the SPE recrystallization

was 250 Å. Hence, it is unlikely that dislocations would have been nucleated or multiplied even if stress had developed in the recrystallized zone. Laser melting and refreezing of single crystal Si at somewhat slower velocities produces a crystalline product. For (001) Si the refrozen product is a homoepitaxial extension of the single crystal Si substrate free of extended defects.[28b] For (111) Si the refrozen product, although it is a homoepitaxial extension of the substrate, contains copious twins and stacking faults for freezing velocities between 6 and 15 m/s and is free of defects for velocities less than 6 m/s.[28b] These results suggest that poly-Si formed by laser melting and refreezing of CVD α-Si films on a SiO_2 substrate may well contain intragranular defects and these defects may be responsible for the fact that the drift mobilities in large grain poly-Si produced by laser melting and refreezing are still much smaller than the corresponding values in pure single crystal Si.

4.1.3. Solid phase epitaxy via diffusion through an intermediate phase.

It has been known for some time that solid phase epitaxy can be accomplished via diffusion from a higher free energy state (α-Si) to a lower energy state (c-Si) through an intermediate phase which may or may not react with the diffusing species.[29] The subject has been reviewed[30] and we will consider here only the essentials governing the process and the structures produced by it.

For homoepitaxial growth of a single crystal via diffusion of the species comprising the crystal through an intermediate phase, which will be called the transport medium, it is only necessary that there be a driving force for this diffusion and that the rate of its transport be sufficient to satisfy the growth requirements. Further, it is also necessary that there be no reaction between the transport medium and the single crystal substrate other than to consume the latter, but not to inject foreign species into it. Consumption of silicon atoms at the substrate surface assures that the new interface between substrate and epitaxial layer is clean. Thus, for the case of the homoepitaxial growth of a silicon single crystal, the transport medium may be an element that forms a eutectic phase diagram with silicon, or it may be a silicide that is in equilibrium with silicon, and in which silicon diffuses rapidly. With Pd_2Si[31a] as the transport medium some metal residue remains in the epitaxial layer. However, use of a monolayer gold as a transport medium[31b] has resulted in a pure and perfect epitaxial film.

Recently, there has been a new twist to the phenomenon discussed in this subsection in that a metal silicide is formed within an α-Si layer by ion implantation of the metal and then annealing at a low temperature. After formation of the silicide it is found that crystalline and epitaxial silicon is deposited on one side of the silicide while the latter moves into the amorphous layer on the opposite side of the silicide.[31c] The interesting aspect of this transition is that it occurs at velocities

of three orders of magnitude larger and at lower temperatures than those associated with the motion of the α/c interface in silicon.*

There are obvious applications of the phenomenon discussed in this subsection to the formation of diamond from amorphous carbon that have not yet been investigated.

4.1.4. Amorphous ↔ crystalline transitions during deposition.

The effects of ion beam assisted deposition and ion beam deposition on the production of epitaxy in semiconductors is of current interest because of the need to lower processing temperatures. It is useful to be aware of certain facts concerning the effects of hyperthermal beams on the production of continuous amorphous layers. Figure 7.7 shows the dependence of the energy density, absorbed in nuclear collision processes in silicon, that is sufficient to produce a continuous amorphous layer, versus temperature.[32] The asymptotic value at low temperatures in the figure corresponds to 12 eV per atom. The low energies used in ion beam assisted deposition or direct ion beam deposition or sputtered deposition are often larger than the displacement energy of the film material. For example, the bulk displacement energy in silicon varies between 18 and 48 eV depending upon the crystal direction that is parallel to the incident beam. The hyperthermal energies used in these deposition processes are often at least 100 eV or more. Thus, there exists a potential for the production of amorphous films in many of the deposition processes involving hyperthermal beams. However, this potential rapidly becomes insignificant as the substrate temperature increases. For example, for Si^+ ions onto Si, energies greater than 75 eV/Si^+ would amorphize a crystalline layer at substrate temperatures below 127°C. For a substrate temperature only about 25°C higher, the Si^+ ion energy would have to exceed 150 eV to bring about such amorphization. (Note that the energies given in Figure 7.7 have to be divided by 0.8 to obtain the energy of the incident Si^+ ion beam since only 0.8 of the incident beam energy is dissipated in nuclear collisions while the remainder is dissipated in electron excitation at these incident energies.)

A complication in any interpretation of the effect of hyperthermal beams during deposition of covalent semiconductors on the production of amorphous films arises from the fact that amorphous films may be produced at low temperatures even during thermal deposition of these materials. For example, deposition of e-beam-evaporated silicon onto a high-temperature vacuum-cleaned Si(100) surface will be epitaxial up to a thickness of several monolayers even at room temperature, whereas deposition onto a hydrogen terminated 1×1 surface will be amorphous.[33] Also deposition onto high-temperature vacuum-cleaned Si(111) will produce a transition from epitaxial to defected crystal to an amorphous layer with increasing thickness. In both cases, there appears to be a thickness of epitaxial

* The advances in this area since 1995 are discussed in Appendix 3.

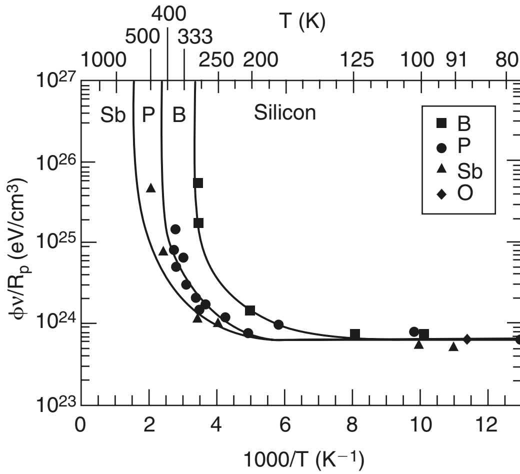

Figure 7.7. Energy density deposited in "nuclear" collision processes by different ions, sufficient to produce a continuous Si layer at different temperatures. Reproduced with permission from F.L. Vook, in **Radiation Damage and Defects in Semiconductors**, ed. J.E. Whitehouse, The Institute of Physics, London, 1973, p. 60.

layer deposited, denoted by h_{epi}, before the film becomes amorphous with continued deposition. The value of h_{epi} depends upon substrate temperature. However, the temperature corresponding to a given thickness of epitaxial layer and for the same deposition rate is about 300°C higher for Si(111) as compared to Si(100).[34]

Let us now consider examples where the energy deposited is insufficient to amorphize the substrate crystal. Consider first deposition onto Si(111) and zero ion energy, i.e. thermal deposition.

It is a fact that the onset of deposition of an amorphous layer onto Si(111) occurs at temperatures about 100–150°C lower than those for the α/c regrowth rate for given values of the growth rate.[24a,34] However, once an amorphous layer is deposited onto Si(111), subsequent annealing will cause regrowth of the crystal at temperatures equal to those for the α/c regrowth phenomenon. Hence, it is apparent that during deposition, conditions at the α/c interface, *at the moment that the amorphous layer forms*, differ from those subsequent to deposition and from those characteristic of the α/c regrowth phenomenon. The factor likely to be different is the concentration of the mobile defects that bring about regrowth. At the regrowth temperature this concentration is approximately equal to the equilibrium concentration of such defects. In the deposition process this concentration exceeds the equilibrium concentration.

We see no reason to assume that the mechanism governing h_{epi}, or the T_{epi} corresponding to a given value of h_{epi}, should be different from that associated

with the epitaxial temperature for solid phase epitaxy of amorphous layers since it is the same for an already deposited amorphous film that is subsequently annealed, but it should be mentioned that others[35b] believe that this phenomenon is controlled by the velocity of annealing out of stacking faults.

Although it is not possible to provide a quantitative prediction of $T_{epi}(111)$ for the case of thermal deposition, because we have no model for the rate of creation of defects during thermal deposition, it is possible to develop such predictions for the case of ion deposition or assisted deposition. We carry out the analysis for such predictions in Appendix 4. Basic assumptions of this analysis are that the concentration of defects is determined by the equality of the rate of creation and rate of annihilation of defects, and that the epitaxial temperature is determined by equating the (α/c) crystal regrowth velocity and the deposition velocity. Jackson's model for the regrowth velocity[35a] is used to produce such quantitative predictions.

The literature contains reference to two different experimental techniques for defining the Si(111) epitaxial temperature. In the work of Weir et al.[34] this temperature is defined by ion channeling measurements as the deposition temperature at which 50% of the atoms in the deposited film are displaced more than 0.1 Å from their crystal lattice sites. In many of the other investigations it is defined as the temperature at which RHEED patterns change in some way. We need to be aware of these definitions of T_{epi} in order to use literature values for this quantity correctly.

Now ion deposition at even 10 eV Si^+ energy involves implantation of most (70%) of the incident ions rather than deposition as adatoms, although the remainder come to rest as adatoms on the surface. The higher the incident energy the smaller is the adatom remnant. The latter may act as normal adatoms, i.e. tend to produce an amorphous surface layer on Si(111) at substrate temperatures below about 350°C since $h_{epi}(111)$ is likely to be smaller than a few monolayers at these temperatures. Further, the implanted ions traverse the α/c interface for amorphous layer thicknesses smaller than the range of the incident ions. Thus, these implanted ions can generate the defects responsible for the regrowth phenomenon, just as they are generated in the ion assisted solid phase epitaxy process. Jackson[35a] has provided a model for the latter. Let us first consider several experimental results for Si^+ deposition onto Si(111) involving the effect of hyperthermal incident beams on the latter transition temperature. In none of these experiments is the ion energy density sufficient to amorphize the crystal surface. This point needs reemphasis. The amorphous arrangement is produced by deposition alone onto the Si(111) surface, which have some adatoms singly bonded to it, and rotation of the other bonds of these adatoms can occur about these single bonds.

Unfortunately, of all the experiments concerned with the effect of ion beams on $T_{epi}(111)$, [36–39] only those of Zalm and Becker provide data for T_{epi} that can be compared with values predicted using Jackson's model and parameters and the condition of setting the deposition velocity equal to the regrowth velocity. The result is a predicted value of 163°C versus an experimental value of 125°C.

Let us now consider deposition onto Si(100). As noted above, it has been shown by Eaglesham et al.[33] that thermal beam deposition onto Si(100) is epitaxial for the first few layers even at room temperature. They found that deposition onto Si(100) is characterized by a critical layer thickness above which the deposit becomes amorphous. They further observed that this critical thickness, denoted by h_{epi}, increases with increasing substrate temperature. Also, they noted that when the amorphous phase was present, above h_{epi}, the film surface was rough, whereas it was smooth for film thicknesses less than h_{epi}. Although they did not make the following assertion, this roughness is sufficient to allow {111} oriented facets to appear. This writer believes that any facet to which adatoms can be singly bonded will develop amorphous layers upon deposition when the substrate temperature is insufficient to allow for bond rotation. Adatoms make two bonds to a {100} surface and bond rotation of these adatoms cannot occur. Thus, in this situation, it should be possible to produce an epitaxial deposit at room temperature onto Si (100) providing: (a) that the surface is maintained sufficiently smooth to prevent the existence of surface area parallel to {111} crystal planes; and (b) that the energy density in any hyperthermal beam directed at the film surface during deposition is less than the critical value required to amorphize the lattice. However, according to the work of Ramana Murty et al.[41] two additional factors affect the ability to produce an epitaxial layer on Si(100): the reconstruction of a dihydride-terminated surface and the hydrogen concentration likely to enter an amorphous layer at a Si(100) surface. In particular, they noted that thermal beam growth onto Si(100) having a dihydride-terminated (1×1) surface resulted in a completely amorphous film, i.e. $h_{epi} = 0$. Further, they observed hydrogen concentrations on the order of $10^{21}/cm^3$ in the amorphous regions of films deposited onto Si(100) at low temperatures in UHV chambers used for MBE. It should also be kept in mind that a Si(100) surface cleaned by heating to about 1100°K or above has a 2×1 reconstructed surface.

For thermal deposition onto thermally cleaned Si(100), the T_{epi} corresponding to $h_{epi} = 300$ Å is 100°C at a deposition rate of 0.3 Å/s and 130°C at a deposition rate of 0.7 Å/s.[34] For a hydrogen-terminated Si(100) surface, with $h_{epi} = 400$ Å the corresponding $T_{epi} = 370$°C at a deposition rate of about 1 Å/s.[42] Thus, in evaluating the effects of hyperthermal energy on the epitaxial temperature corresponding to a given h_{epi} we need to take into account the nature of the surface.

Let us consider deposition with hyperthermal beams onto a thermally cleaned Si(100) surface first. Schwebel et al.[43] have found that sputter deposition yielding a 5000 Å thick film deposited at a rate of 50 Å/min produced polycrystalline films between about 40°C and 250°C, defect containing epitaxial films above the latter substrate temperature, and defect-free epitaxial films above 700°C. The value of h_{epi} expected for thermal beam deposition on this substrate at 250°C is at least an order of magnitude smaller than 5000 Å. Thus, the hyperthermal component of the sputtered beam has increased h_{epi} at 250°C and decreased T_{epi} for this thickness (5000 Å) from about 500°C to at least 250°C, if not 40°C. The beam energy is not

likely to exceed 50 eV/atom deposited. According to Figure 7.7 this energy beam will amorphize a Si crystal surface only below a substrate temperature of about 30°C. The fact that an amorphous film was not formed above 40°C and that the predicted $T_{epi}(111)$ for these conditions is about 190°C implies that the hyperthermal particles incident on the film prevented the formation of a rough surface and the onset of (111) amorphization.

These observations of Schwebel et al. serve to remind us that epitaxial films produced at low temperatures with the aid of hyperthermal beams will probably contain defects. These defects may be entrapped inert gas atoms, frozen-in deposition- or bombardment-induced defects or defect clusters, and grain boundaries.

Wehner et al.[45] sputtered Si onto a Si(100) surface at 2500 Å/h while simultaneously subjecting the surface to a beam of Hg^+ ions at 1 mA/cm^2 at a substrate temperature of 300°C. They found that a 23 eV Hg^+ ion beam produced an epitaxial film 8000 Å thick, whereas such a beam having a 45 eV energy produced an amorphous film. The value of h_{epi} is larger than would have been obtained for a thermal beam. The production of an amorphous film at this temperature may be due to bombardment damage of the crystal lattice because the point corresponding to the conditions associated with the 45 eV Hg beam exceeds the amorphization threshold in Figure 7.7, whereas that for the 23 eV Hg^+ ion beam is just insufficient to amorphize the lattice. Since the expected h_{epi} value at 300°C is about an order of magnitude smaller than the epitaxial film thickness produced in these experiments with the 23 eV beam it must also be concluded that the effect of this bombardment is to maintain a smooth surface during deposition, although since the T_{epi} value is smaller than 300°C it is also possible that the epitaxial film is a result of a (111) crystal regrowth velocity greater than the deposition velocity.

We now consider hyperthermal beams incident upon hydrogen-terminated Si(100) surfaces. Sputter deposition at 210°C of a hydrogen-terminated Si(100) surface produced a 300 nm thick epitaxial layer without defects.[46] At this substrate temperature the value of h_{epi} for the case of thermal deposition onto a hydrogen-terminated Si(100) surface must be less than 40 nm, the value of h_{epi} for such a surface at 370°C. The energy of the incident sputtered Si atoms is no more than a few tens of eV. Hence, the hyperthermal beam energy in this case is insufficient to amorphize the Si lattice whereas it may be sufficient to produce a smooth surface. Further, the sputtering process should act to remove surface bound hydrogen atoms. Also, in the event an amorphous layer forms as the thickness just exceeds h_{epi} the (111) epitaxial temperature is less than the substrate temperature for the conditions of this sputter deposition. Thus, the observation of a greatly increased h_{epi} in these experiments may be a consequence of either the production of a smooth interface, or the removal of hydrogen as it adsorbs, or a (111) epitaxial temperature lower than the substrate temperature.

In an ion assisted deposition study[41] using 50 and 70 eV Ar^+ ions at an ion/atom flux ratio of 0.06 and 0.09, respectively, and at substrate temperatures

between 240 and 380°C it was found that h_{epi} was unaffected relative to the values obtained in purely thermal deposition onto hydrogen-terminated Si(100) in an MBE system. TEM studies showed that the growth front was rough and faceted and in a film deposited at 370°C a high density of twins and platelets were found. Thus, the hyperthermal beam in this case did not achieve any smoothing of the film surface during growth. The observation of rough surfaces and amorphous layers for film thicknesses greater than h_{epi} may be due to $T_{epi}(111)$ being higher than the experimental substrate temperatures. However, the predicted $T_{epi}(111)$ is 245°C for the conditions of this study. Hence, the onset of the formation of amorphous layers in these experiments must be due to another factor. One such factor suggested by these authors is the high concentration of hydrogen found in the amorphous layers. We must recall that in ion assisted deposition there will always be a tendency to form an amorphous layer on Si(111) at low temperatures after some small film thickness. The value of $T_{epi}(111)$, in our view, is then determined by the condition that the crystal regrowth velocity equals the deposition velocity. However, in the presence of appreciable hydrogen in the amorphous layer, the regrowth velocity will be determined by the velocity with which the hydrogen can diffuse away from the α/c interface. Hydrogen does not diffuse appreciably in α-Si until the temperature exceeds about 400°C, as was noted in Chapter V. Thus, the $T_{epi}(111)$ value may well exceed 370°C if the α/c interface velocity is determined by the diffusion rate of hydrogen in α-Si. Indeed, the temperature for hydrogen evolution has been found to equal[47a] or be less than[47b] the temperature for crystallization of α-Si:H.

Ohmi et al.[48] used an RF sputter deposition system in which the bias on the substrate was varied. A particular bias was found at which a 4000 Å thick film was deposited at 1 Å/s onto a hydrogen-terminated Si(100) surface at 300°C. The damage introduced was very sensitive to the substrate bias. This represents a considerable increase in h_{epi} for this substrate temperature relative to thermal deposition.

State of the art plasma enhanced CVD processes are able to deposit films with smooth surfaces at low substrate temperatures as a consequence of a high-surface diffusivity that prevents morphological instability. Further, the active radicals are able to extract hydrogen bonded to the surface and to facilitate the bonding of Si there. Thus, such processes are better suited to the production of epitaxial Si layers on Si(100) at low temperatures than some PVD techniques involving hyperthermal beams. The literature provides support for this view as is developed below.

Epitaxial films 800–1100 Å thick were deposited at a rate of 1–5 Å/min on hydrogen-terminated Si(100) by remote plasma CVD at a substrate temperature of 150°C, which had been pretreated using a remote H_2 plasma clean at 250°C that converted the hydrogen-terminated (1×1) surface to a (3×1) surface.[49]

Plasma enhanced CVD at a substrate temperature of 250°C produced an epitaxial layer 200 nm thick onto a hydrogen-terminated Si(100) when the power

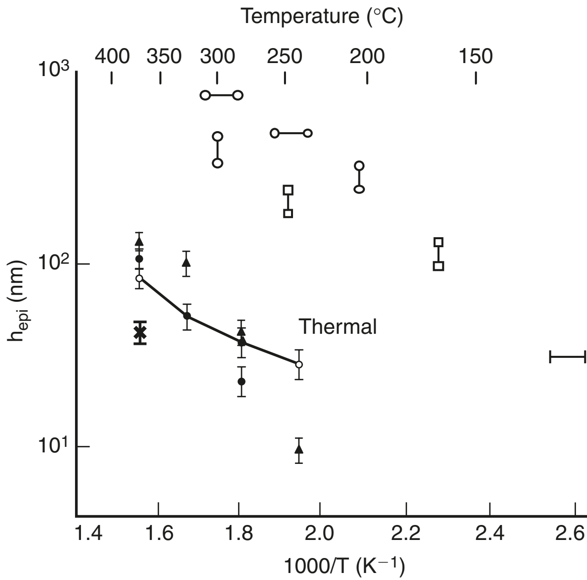

Figure 7.8. Epitaxial thickness for deposition onto Si(100) versus temperature. Points with vertical lines are for deposition onto hydrogen-terminated surfaces. Those with horizontal lines correspond to deposition onto thermally cleaned surfaces. Points with open circles at the ends of lines correspond to sputter deposition; those with open squares involve CVD in plasmas; those with bars involve thermal deposition.

was 90 watts, but an amorphous layer after deposition of an epitaxial layer about 30 nm thick having a rough surface when the power was 10 W.[50]

We have summarized these data in Figure 7.8. From these results it is apparent that deposition onto thermally cleaned Si(100) surfaces yields higher h_{epi} values than onto hydrogen-terminated Si(100) surfaces. (These hydrogen-terminated surfaces must not be (1×1) surfaces since such surfaces give a zero value for h_{epi}.) Further, it is apparent that hyperthermal beam deposition or assisted deposition yield higher h_{epi} values than thermal beam deposition or CVD involved methods. Also, sputtering, at constant other factors, yields somewhat higher h_{epi} values than those involving CVD methods.

Summarizing the above discussion relating to the deposition of epitaxial films on silicon, we found no contradictory evidence to our proposal that the epitaxial temperature for deposition onto Si(111) surfaces or facets is determined by the equality of the α/c crystal regrowth velocity and the deposition velocity, providing that hydrogen is not present in α-Si. If it is present then the equality of the deposition and regrowth velocity as affected by the outdiffusion of hydrogen

becomes the condition determining $T_{epi}(111)$. It is possible to achieve epitaxial deposition on Si(100) in relatively thick films providing that the deposition technique maintains the surface sufficiently smooth so as not to develop {111} facets.*

4.2. Carbon.

4.2.1. Deposition of carbon films using ion beams.

In the above we have considered only the amorphization and solid phase epitaxy of silicon. It may be of interest to apply the same considerations to the case of carbon, for which there is the additional variable of bond type that may be produced in the deposition process.

It is instructive to refer to the work of Ogata et al.[51], which is reproduced in Figure 1.2 and repeated in Figure 7.9 for convenience. If we take the transition between the diamond crystalline region (square symbols) to the start of the mixed amorphous/diamond region (triangles) in the upper right quadrant we obtain a value of about 58 eV transmitted to each Si atom on the substrate surface as the energy density in nuclear collisions required to convert a crystalline lattice to an amorphous one at room temperature. (The incident Ne^+ ion energy has been corrected to obtain the energy density transmitted to the Si atoms in elastic collisions and this value has been multiplied by 0.8 to obtain the energy density in nuclear collisions required to convert a crystalline lattice to an amorphous one.) Comparison of this value with that for silicon in Figure 7.7 shows that it equals the value required to amorphize a silicon crystal at 30°C! This result is not coincidence for the substrate used by Ogata et al.[51] was a hydrogen-terminated Si(100) crystal. Amorphizing the silicon substrate prevents the development of a heteroepitaxial crystalline layer of diamond! Thus, the onset of amorphization in the right-hand quadrant of Figure 7.9 is that for silicon and not for diamond, which must occur at somewhat higher transmitted incident energy.

Another result obtained by Ogata et al.[51] is extremely interesting and will be considered below. It is well known that the assertion that deposited carbon films contain crystalline diamond is questionable unless the assertion is reinforced with Raman evidence showing the presence of the diamond crystal peak at 1331 cm^{-1}. Ogata et al.'s results pass this test in that the films they claim to be crystalline diamond reveal this Raman peak. The fact that they found diamond in films deposited at room temperature in the absence of atomic hydrogen is the result that is interesting. No one else has obtained this result, except perhaps Spencer et al.[56] However, the results of the latter investigators are not reinforced with Raman measurements and, hence, will be discarded.

* Another trick to achieve surface smoothing and larger epitaxial thickness is to deposit onto a vicinal surface having ledge width less than the half-wavelength of surface roughness on a planar surface. (G. Apostolopoulos et al., Appl. Phys. Lett. 79, 3422(2001).

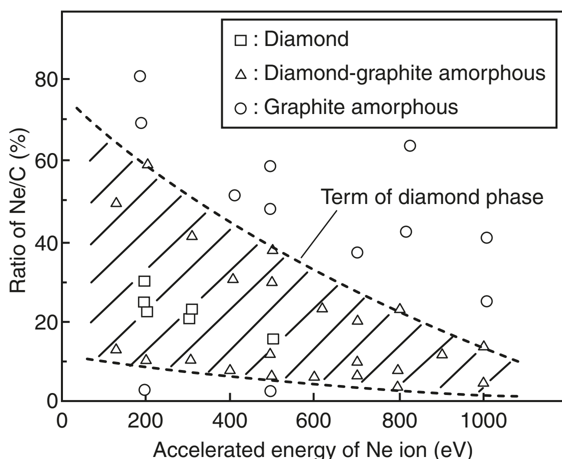

Figure 7.9. Map of nature of carbon film deposit after Ogata et al.[51]

C^+ ion deposition, at energy densities equivalent to those of Ogata et al.[51] yield amorphous films, albeit sp^3 bonded.[57] Examination of Figure 7.9 reveals that the energy density range in which Ogata et al.[51] found a diamond crystalline deposit is narrow: from 45 to 66 eV/atom deposited (36 to 53 eV dissipated in nuclear collisions). Aside from the fact that Ogata et al. used Ne^+ ion assisted deposition and Fallon et al.[57] used C^+ ion beam deposition the main difference in deposition conditions between these investigators appears to be the use of a hydrogen-terminated clean Si(100) surface as a substrate by Ogata et al. and an unclean, oxide covered, Si substrate by Fallon et al. One may conclude from these observations that the diamond crystals are not nucleated in an amorphous film at room temperature, but grow heteroepitaxially from the clean Si substrate in the experiments of Ogata et al. This result is consistent with experience from hyperthermal beam assisted deposition of Si where crystals are not observed below about 300°C in ion beam sputter deposition onto glass substrates.[44]

Robertson et al.[58] first reported finding a crystalline diamond film using a 120 eV C^+ ion beam onto a hydrogen-terminated, clean, Si(100) substrate at room temperature, but later retracted this assertion upon using Raman spectroscopy to examine the film.[59] In fact, according to Figure 7.9, the point corresponding to the deposition conditions of Robertson et al. falls in the region characteristic of an amorphous film! Indeed, a beam of this energy would amorphize the Si substrate surface according to Figure 7.7! Others have reported depositing carbon films onto cleaned Si substrates. In particular, amorphous films were found by Hofsass et al.[60] for C films deposited using monoenergetic C^+ ions ranging in energy from 50–400 eV onto Si cleaned by Ar^+ ions having an energy of 1 keV. The latter cleaning

treatment certainly left the Si surface in an amorphous condition incapable of acting as a substrate for epitaxial deposition. However, these investigators desired to produce amorphous films. Similarly, in the work of He et al.[61] the Si(111) substrate which had been cleaned using a dilute HF etch was then further cleaned in situ using Ar^+ ions of 3 keV energy. Thus, there are two reasons not to expect heteroepitaxial deposition in these experiments and it should not be surprising that amorphous films were deposited in their work. Ullmann et al.[62] deposited C films onto Si(100) using Ne^+ ion assisted deposition, but they also cleaned the surface by in situ sputtering which certainly developed an amorphous surface on the substrate. However, the conditions they used fall outside the window for the deposition of crystalline diamond so they would not have found such films even if they had cleaned the Si(100) surface by etching in dilute HF. Fallon et al.,[63] Martin et al.,[64] and Ishikawa et al.[65] all report depositing C^+ ions onto silicon substrates held in a vacuum of, at best, 10^{-7} Torr and do not mention any cleaning procedure they used on the silicon. Even if they had cleaned the surface so as to leave a hydrogen-terminated clean surface their deposition conditions are outside the window for the production of crystalline diamond.

Given the narrow window for the hyperthermal deposition of crystalline diamond it is not surprising that no one besides Ogata et al. have been able to deposit a diamond film at room temperature using hyperthermal beams during deposition. Further, it is evident that many investigators are not aware of the relation between the state of the substrate surface and the state of the film deposited on this surface. We may remark here that this window may have a wider range at more elevated substrate temperatures. Freeman et al.[66] have succeeded in depositing diamond homoepitaxially using a C^+ ion beam of 900 eV energy at a flux of about $1.48 \cdot 10^{15}/\text{cm}^2/\text{s}$ at a substrate temperature of 700°C on the (111) face of a diamond crystal.

We return now to the result of Ogata et al. which shows a narrow energy window for the hyperthermal beam assisted deposition of diamond on a hydrogen-terminated Si(100) surface at room temperature and speculate on the factors that allow the crystalline diamond to form and grow during deposition or not to grow at lower beam energy densities. One plausible reason for the formation of crystalline diamond on deposition in this window is that the deposited energy is sufficient to allow penetration of the Si(100) and diamond surfaces without amorphizing the crystal surfaces and is also sufficient to remove the hydrogen bonded to the silicon surface to allow the fraction of the beam that comes to rest on the surface to bond to it. However, in view of the experience noted above with respect to homoepitaxial deposition onto Si(100), it would also appear to be necessary for the incident beam to produce sufficient adatom mobility to prevent the development of surface roughness and {111} facets. In an investigation of the effect of ion bombardment on the surface smoothness in ion assisted deposition of Ge at low temperature Chason et al.[67] found that the optimum smoothness was achieved when the rate of deposition is

approximately equal to the rate of production of ion-induced defects. The surface is rough either when the ion current is zero or when there is no concomitant deposition of Ge. Thus, it seems reasonable to conclude that the window of conditions found by Ogata et al. for the deposition of crystalline diamond films coincides with the conditions that produce a sufficiently smooth surface on C(100), i.e. conditions that prevent {111} facets from developing and that thus allow epitaxial deposition to continue without cessation. The presence of amorphous films for conditions outside this window and at lower energies than the critical energies for amorphization of the substrate can then be explained to be the consequence of the development of rough surfaces that permit {111} facets to form when the films are very thin (a few tens of nm) and amorphous films to develop from these facets, analogous to the case of deposition of silicon onto Si(100) when the temperature is less than $T_{epi}(111)$ and the deposition conditions allow rough surfaces to develop.

The results of Ogata et al. for heteroepitaxial deposition of C onto Si(100) and Freeman et al. noted above for the homoepitaxial deposition of a single crystal of diamond are similar to those obtained for homoepitaxial deposition onto Si(100) by Schwebel et al. in that polycrystalline films are produced at low temperatures and a homoepitaxial single crystal at high temperatures. In a photomicrograph of a diamond film surface in Ogata et al.'s paper it is apparent that most of the grains, about 1 μm long, are oriented with a <100> axis normal to the film plane, i.e. the film has a predominantly <100> texture.

Since the publication of the original edition of this work researchers have found ways of heteroepitaxially depositing diamond films. The key has been to use a substrate that has a fairly close lattice match to the diamond lattice. The substrate used was Ir (001), which itself was heteroepitaxially grown on MgO,[80] $SrTiO_3$[81] and sapphire.[82]

4.2.2. Possible solid phase epitaxy of diamond.

The work of Nelson et al.[52] allows us to compare the dependence of the C^+ ion flux which just produces a buried amorphous layer in crystalline diamond on temperature with that for the analogous case of silicon. We plot the points obtained by Nelson et al.[52] with those obtained by Elliman et al.[53] in Figure 7.10. Unfortunately, there is a large uncertainty in the dose and the ion energies are not the same at the two different transition temperatures. We have corrected the experimental values at 350°C (light lines for 100 keV C^+ ions) to normalize these data to the incident energy used to obtain the data corresponding to 620°C (30 keV) using experimental values[54] of the incident energy dependence for this boundary. These values corresponding to the 30 keV incident C^+ ions are shown as heavy lines. The interesting results are that the points for the buried layer in carbon have the same qualitative dependence on temperature as those for the Xe bombardment of silicon. As noted in the theory of Jackson,[35] for the effect of ion bombardment on the α/c

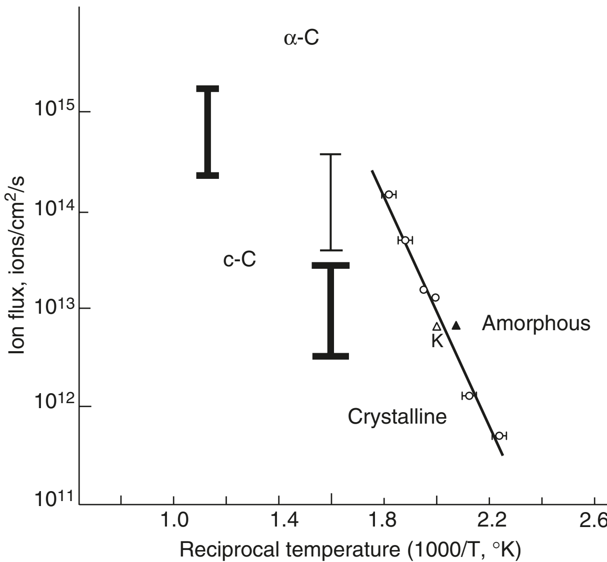

Figure 7.10. Dose rate dependence (for 1.5 MeV Xe^+ ions at $5 \cdot 10^{15}/cm^2$) for zero α/c interface velocity in Si, right-hand line and points;[53] C^+ ion dose rate to just produce an amorphous buried layer in diamond, left hand vertical bars.[52] Light line in the latter corresponds to the experimental data: 100 keV at 320°C. Heavy lines correspond to the values for incident C^+ ions of 30 keV: experimental at 620°C and corrected at 320°C.

interface velocity, this activation energy is that for defect motion in the interface. This is an interesting result for it is the first evidence for the possibility of solid phase epitaxy in diamond.

Summarizing, the outlook for the deposition of crystalline diamond films at low temperature in the absence of atomic hydrogen is promising provided that care is taken to use clean Si(100) substrates, that have not been amorphized by sputter cleaning, and to use deposition conditions within the window suggested by the work of Ogata et al. and the amorphization limit for Si given in Figure 7.7. The effects of hyperthermal beams during deposition on the amorphous/crystalline nature of the deposited film appear to be similar for silicon and carbon films. Much more work needs to be done, however, to characterize such deposition for both materials.

4.3. Amorphous to crystalline transition in other materials.

4.3.1. Amorphous to poly-transition.

Amorphous films may be converted to polycrystalline films by annealing or by ion bombardment at elevated temperature. We have considered this transition

for elemental materials in the previous sections. In this section we consider the effect of more than one component in the amorphous to crystalline transition. It is apparent that this additional degree of freedom implies the possibility of phase separation involving diffusion of one or more species, the possibility of additional defects due to ordering of the species, and the possibility of producing metastable crystalline phases on crystallization of the amorphous phase. Although the latter possibility is also present in elemental films it is less probable in the multicomponent films.

Amorphous silicides may be produced by depositing multilayer stacks of metal and silicon followed by annealing. Additional annealing at higher temperature will crystallize the amorphous phase. A summary of the systems that exhibit such behavior can be found in Ref. [68]. The grain structure that results depends upon the course of the nucleation and growth processes. Both volume and surface nucleation may occur to yield different grain morphologies. Further, depending upon the original composition it is possible to produce a variety of silicides in the same system.

Amorphous silicide films may also be formed by codeposition of the metal and silicon and then crystallized to form a polycide (a fine-grained polycrystalline silicide). For example, in the transformation from amorphous to crystalline $CoSi_2$ it was found[69] that circular grains nucleated randomly in the amorphous film at about 150°C with an activation energy of about 0.8 eV, that these grains had random orientation and that there was no indication of defects in them. Indeed, it has been reported that cobalt and nickel disilicides formed by crystallization of the amorphous phase tend to be free of defects that affect the electrical resistivity, whereas refractory metal disilicides formed in the same manner require elevated temperature annealing to decrease the defect density responsible for excess electrical resistivity.[70–74] It is believed that this phenomenon is a consequence of the different kinetics for these two classes of silicide systems. The noble metal silicides have low-activation energies for their formation whereas the transition metal silicides have high-activation energies, a fact mirrored in the corresponding transition temperatures. The significance of faster kinetics is the corresponding faster annealing out of defects.

$FeSi_2$ films produced by crystallization of the amorphous phase between 380 and 420°C have many defects that can only be removed by annealing above about 550°C.[75] The drift mobility in such films increases with increasing annealing temperature. The nature of these defects is unknown. It is interesting to note that pseudomorphic films of Fe_xSi_{1-x} phases and Si can be formed[75] and that a polymorphic transition can occur between different structures at the $FeSi_2$ composition. It is possible that the defects noted above are associated with the polymorphic transformation. The useful polymorph in this system is the beta phase, which is a direct gap semiconductor with a bandgap applicable in optical communication technology.

The route of forming a crystalline layer via the intermediary amorphous phase is used in semiconductor systems other than silicides. For example, this process is used in reversible phase change optical recording to produce two states of different reflected light intensity.[76] The media need to provide an erase capability

(amorphous to crystalline transition) and a write capability (crystalline to amorphous transition) with a response velocity that satisfies the technical requirements. The latter require that the phase changes occur without changes in composition. For compounds, the isocomposition phase change condition implies that the composition must be strictly stoichiometric since the amorphous phase is produced by melting and rapid refreezing. The undesirable media noise is reduced when the crystalline phase has a cubic structure since the reflectivity in non-cubic materials is a function of orientation. A typical system that is used in this application is the Te-Ge-Sb system where the composition lies along a pseudobinary line or corresponds to a ternary compound composition. Unknown defects which form upon repeated cycling of the reversible phase changes appear to limit applicability of this recording scheme. The theme of defects produced in the amorphous/crystalline transition which we have attempted to describe earlier in this section resonates in many technological applications of this transition and deserves much more intensive study.

Still another example of the application of the amorphous to crystalline transition is in the formation of thin polycrystalline lead zirconate-titanate (PZT) ferroelectric films. Such films have been deposited in the amorphous state onto a Pt coated silicon wafer by excimer laser evaporation of a PZT target in the presence of 100 mTorr of oxygen.[77] Annealing the amorphous film above its glass temperature crystallizes it. There are two crystalline polymorphs: the pyrochlore and perovskite structures. The latter is the desired one and appears at a higher annealing temperature than that at which the former forms. In another study[78] involving the amorphous to crystalline transition of amorphous TiO_2 formed by sputtering, which of two competing polymorphs emerged on annealing was believed to depend upon the technique used in deposition of the amorphous film. The latter work suggests that processing affects the crystal structure that is produced on annealing amorphous films. This theme broadened to include all types of structure deserves much more investigation than it has received to date.

Metallic alloys have also been deposited in the amorphous state and then crystallized to produce polycrystalline films. TiNi, the shape-memory alloy is one example of this category.[79]

4.3.2. Amorphous to epitaxial silicide transition.

Coevaporation of Co and Si in an exactly stoichiometric ratio into clean Si substrates held below 100°C, which forms an amorphous film, to a thickness less than 50 Å, and subsequent annealing, produces an epitaxial film of $CoSi_2$ in the type-B orientation which has a smooth surface and is free of pinholes. Repetition of the codeposition and annealing allows the formation of a thicker film that maintains its monocrystallinity, its smooth surface and absence of pinholes.[9b] The amorphous to epitaxial transition must occur via solid phase epitaxy with local rearrangement of the Co and Si atoms at the amorphous/crystalline interface.

This result suggests that the production of epitaxial layers of compounds and alloys of other systems, but having similar misfits with the substrate, might be accomplished via the same reaction path.

4.4. Summary of section 4.

Summarizing the results of this section, defects are introduced into crystalline semiconductors derived by crystallization of amorphous ones of the same composition by the presence of impurities in supersaturation and by stresses in the amorphous film. In the absence of stress and impurities crystallization of layers that have been made amorphous by ion bombardment yields epitaxial layers devoid of defects. They may also be introduced by stresses that exceed the yield strength brought about by a change in specific volume between the amorphous and crystalline phases, but this possibility needs to be evaluated experimentally. Both stress and oxygen are likely to exist in as-deposited amorphous silicon films which lead to the production of defects in such films crystallized above 600°C. Also, in explosive crystallization of α-Si laser melted films, extended defects are found behind (111) oriented solid/liquid fronts freezing at velocities between 6 and 15 m/s. These defects are absent behind (100) oriented freezing fronts. Similarly, in epitaxial deposition onto (111) and (100) surfaces there is a temperature regime in which stacking faults are frozen-in the deposited film on (111) surfaces, but not on (100) surfaces. Below this temperature regime the deposited films are amorphous on (111) surfaces. No epitaxial temperature exists for deposition onto (100) surfaces. The amorphous/crystalline transition during deposition may control the Si(111) epitaxial temperature and the production of an amorphous film on rough Si(100) surfaces. Low-energy incident ions may amorphize clean crystalline substrates and bring about the deposition of amorphous films instead of epitaxial ones on such substrates. The implications of these considerations in the ion assisted deposition of diamond have been discussed.

References

1. J.W. Matthews and J.L. Crawford, Phil. Mag. 11, 977(1965).
2. J.W. Matthews and W.A. Jesser, J. Vac. Sci. Tech. 6, 641(1969).
3. F.M. d'Heurle and P. Gas, J. Mater. Res. 1, 205(1986).
4. J.M. Gibson, J.C. Bean, J.M. Poate and R.T. Tung, MRS Symp. Proc. 10, 101(1982).
5. R.T. Tung and J.L. Batstone, Appl. Phys. Lett. 52, 648(1988).
6. T.L. Liu, R.W. Fathauer, P.J. Grunthaner, C. d'Anterroches, Appl. Phys. Lett. 52, 804(1988).
7. R.T. Tung, J.M. Gibson and J.M. Poate, Phys. Rev. Lett. 50, 429(1983).
8. S. Yalisove, R. Tung and D. Loretto, J. Vac. Sci. Tech. A7, 1472(1989).
9. a) G. Rangelov, P. Augustin, J. Stober and T. Fauster, Phys. Rev. B49, 7535(1994); b) H. von Kanel, Mat. Sci. Rep. 8, 193(1992).

10. T.L. Lee, W.D. Sue, J.H. Lin, C.H. Luo and L.J. Chen, MRS Symp. Proc. 312, 125(1993).
11. Y. Kumagai, F. Hasegawa and K. Park, J. Appl. Phys. 75, 3211(1994).
12. M.M. Heys and A.v. Schwerin, in **Insulating Films on Semiconductors**, ed. Adam Hilger, IOP Publishing Ltd, Bristol, 1991, p. 73.
13. M. Aslam, IEEE Trans. Electron Dev. ED-34, 2535(1987).
14. A. Stesmans and G. Van Gorp, Appl. Phys. Lett. 57, 2663(1990).
15. D.J. DiMaria, in **Insulating Films on Semiconductors**, ed. Adam Hilger, IOP Publishing Ltd, Bristol, 1991, p. 65.
16. A.M. Stoneham, in **Insulating Films on Semiconductors**, ed. Adam Hilger, IOP Publishing Ltd, Bristol, 1991, p. 19.
17. D. Jousse, S.L. Delage, S.S. Iyer and M. Crowder, MRS Symp. Proc. 106, 359(1988).
18. E. Campo, J.J. Pedroviejo, E. Scheid, D. Bielle-Daspet, A.Y. Massaoud, G. Sarrabayrouse and A. Martinez, MRS Symp. Proc. 303, 389(1993).
19. T. Noguchi, H. Hayashi and T. Ohshima, MRS Symp. Proc. 106, 293(1988).
20. A. Chiang, T.Y. Huang, I.-W. Wu and M.H. Zarzycki. MRS Symp. Proc. 106, 305(1988).
21. S.E. Ready, J.B. Boyce, D.K. Fork, P. Mei, G.B. Anderson and R.I. Johnson. MRS Symp. Proc. 297, 545(1993).
22. a) J.S. Im, H.J. Kim and M.O. Thompson, Appl. Phys. Lett. 63, 1969(1993); b) H.J. Kim and J.S. Im, MRS Symp. Proc. to be published.
23. T. Yonehara, Y. Nishigaki, H. Mizutani, S. Kondoh, K. Yamagata and T. Ichikawa, MRS Symp. Proc. 106, 21(1988).
24. a) G.L. Olson and R.A. Roth, Mat. Sci. Rep. 3, 1(1988); b) F. Priolo and E. Rimini, Mat. Sci. Rep. 5, 319(1990).
25. a) R. Drosd and J. Washburn, J. Appl. Phys. 53, 397(1982); b) Q.Z. Hong, J.G. Zhu, J.W. Mayer, W. Xia and S.S. Lau, J. Appl. Phys. 71, 1768(1992); c) J.A. Roth and C.L. Anderson, Appl. Phys. Lett. 31, 689(1977); d) B.W. Dodson and J.Y. Tsao, Ann. Rev. Mater. Sci. 19, 419(1989).
26. a) J.L. Batstone, Phil. Mag. A67, 62(1993); b) F. Priolo, J.L. Batstone, J.M. Poate, J. Linnros, D.C. Jacobson and M.O. Thompson, Appl. Phys. Lett. 52, 1043(1988); c) A.E. White, K.T. Short, J.L. Batstone, D.C. Jacobson J.M. Poate and K.W. West, Appl. Phys. Lett. 50, 19(1987); d) E. Kennedy, L. Cspregi, J.W. Mayer and T.W. Sigmon, J. Appl. Phys. 48, 4241(1969).
27. a) P. Krulevitch, T.D. Nguyen, G.C. Johnson, R.T. Howe, H.R. Wenk and R. Gronsky, MRS Symp. Proc. 202, 167(1991); b) F.M. Ross, R. Hull, D. Bahnck, J.C. Bean, L.J. Peticolas, R.R. Kola and C.A. King, MRS Symp. Proc. 280, 483(1993); c) Y. Kunii, M. Tabe and K. Kajiyama, J. Appl. Phys. 54, 2847(1983); d) A.S. Yue, S.S. Rhee, and S.W. Oh, in **Semiconductor-Based Heterostructures**, eds. M.L. Green et al., The Metallurgical Society, Warrendale, PA, 1986, p. 301.
28. a) B.S. Meyerson, Proc. IEEE 80, 1592(1992); b) A.G. Cullis, H.C. Webber, N.G. Chew, J.M. Poate, and P. Baeri, Phys. Rev. Lett. 49, 219(1982).
29. M. Komabayashi, K.I. Hijikata, and S. Ido, Jpn. J. Appl. Phys. 30, 563(1991).
30. H.A. Atwater, C.V. Thompson and H.I Smith, J. Mater. Res. 3, 1232(1988).
31. a) G. Ottaviani, D. Sigurd, V. Marrello, J.W. Mayer and J.O. McCaldin, J. Appl. Phys. 45, 1730(1974); b) G.D. Wilk, R.E. Martinez, J.F. Chervinsky, F. Spaepen and

J.A. Golovchenko, Appl. Phys. Lett. 65, 866(1994); c) R.C. Cammarata, C.V. Thompson, C. Hayzelden and K.N. Tu, J. Mater. Res. 5, 2133(1990), C. Hayzelden and J.L. Batstone, MRS Symp. Proc. 321, 579(1994).
32. F.L. Vook, in **Radiation Damage and Defects in Semiconductors**, ed. J.E. Whitehouse, The Institute of Physics, London, 1973, p. 60.
33. D.J. Eaglesham, H.-J. Gossmann and M. Cerullo, Phys. Rev. Lett. 65, 1227(1990).
34. B.E. Weir, B.S. Freer, R.L. Hedrick, D.J. Eaglesham, G.H. Gilmer, J. Bevk, and L.C. Feldman, Appl. Phys. Lett. 59, 204(1991).
35. a) K.A. Jackson, J. Mater. Res. 3, 1218(1988); b) R. Venkatasubramanian, D.L. Dorsey and S.G. Das, MRS Symp. Proc. 280, 179(1993).
36. T. Narusawa, S. Shimizu and S. Komiya, J. Vac. Sci. Tech. 16, 366(1979).
37. P.C. Zalm and L.J. Beckers, Appl. Phys. Lett. 41, 167(1982).
38. T. Itoh, T. Nakamura, M. Muromachi and T. Sugiyama, Jpn. J. Appl. Phys. 16, 553(1977).
39. G.E. Thomas, L.J. Beckers, J.J. Vrakking and B.R. De Koning, J. Cryst. Growth 56, 557(1982).
40. L. Cspregi, E.F. Kennedy, J.W. Mayer and T.W. Sigmon, J. Appl. Phys. 49, 3906(1978); G.H. Gilmer, M.H. Grabow and A.F. Bakker, Mater. Sci. Eng. B6, 101(1990); R. Venkatasubramanian, MRS Symp. Proc. 280, 179(1993).
41. M.V. Ramana Murty, H.A. Atwater, A.J. Kellock and J.E.E. Baglin, Appl. Phys. Lett. 62, 2566(1993).
42. D.J. Eaglesham, G.S. Higashi and M. Cerullo, Appl. Phys. Lett. 59, 685(1991).
43. C. Schwebel, F. Meyer, G. Gautherin and C. Pellet, J. Vac .Sci .Tech. B4, 1153(1986).
44. H. Windischmann, J.M. Cavese, R.W. Collins, R.D. Harris and J. Gonzalez-Hernandez, MRS Symp. Proc. 47, 187(1985).
45. G.K. Wehner, R.M. Warner Jr, P.D. Wang and Y.H. Kim, J. Appl. Phys. 64, 6754(1988).
46. C.-C. Chen, D.L. Smith, G. Anderson and S.B. Hagstrom, MRS Symp. Proc. 259, 443(1992).
47. a) F. Demichaelis, C.F. Pirri, E.Tresso, L. Battezzati, E. Giamello and P. Menna, MRS Symp. Proc. 230, 183(1992); b) N. Sridhar, D.D.L. Chung, W.A. Anderson, W.Y. Fu, L.P. Fu, A. Petrou and J. Coleman, MRS Symp. Proc. 321, 713(1994).
48. T. Ohmi, T. Ichikawa, H. Iwabuchi and T. Shibata, J. Appl. Phys. 66, 4756(1989).
49. T. Hsu, B. Anthony, L. Breaux, R. Qian, S. Banerjee, A. Tasch, C. Magee and W. Harrington, J. Elect. Mater. 19, 1043, 1089(1990).
50. Y.-J. Lin, M.-D. Shieh, C. Lee and T.-R. Yew, MRS Symp. Proc. 235, 807(1992).
51. K. Ogata, Y. Andoh and E. Kamijo, Nucl. Inst. Meth. B33, 685(1988).
52. R.S. Nelson, J.A. Hudson, D.J. Mazey and R.C. Piller, Proc. Roy. Soc. London, A386, 211(1983).
53. R.G. Elliman, J. Linnros and W.L. Brown, MRS Symp. Proc. 100, 863(1988).
54. J.S. Williams, R.G. Elliman, W.L. Brown and T.E. Seidel, Phys. Rev. Lett. 55, 1482(1985).
55. L. Lindhard, M. Scharff and H.E. Schiott, Kgl. Dan. Vid. Selsk. Mat. fys. Medd. 33, 14(1963).
56. E.G. Spencer, P.H. Schmidt, D.C. Joy and F.J. Sansalone, Appl. Phys. Lett. 29, 118(1976) and references therein.
57. P.J. Fallon, V.S. Veerasamy, C.A. Davis, J. Robertson, G.A.J. Amaratunga, W.I. Milne and J. Koskinen, Phys. Rev. B48, 4777(1993).

58. J.L. Robertson, S.C. Moss, Y. Lifshitz, S.R. Kasi, J.W. Rabelais, G.D. Lempert and E. Rapoport, Science 243, R1047 (1989).
59. Authors of previous reference, MRS Symp.Proc. 152, 9(1989).
60. H.C. Hofsass, J. Biegel, C. Ronning, R.G. Downing and G.P. Lamaze, MRS Symp. Proc. 316, 881(1994).
61. X. He, H. Song, W. Li, F. Cui and H. Li, MRS Symp. Proc. 316, 923(1994).
62. J. Ullman, U. Falke, W. Scharff, A. Schroer and G.K. Wolf, Thin Solid Films 232, 154(1993).
63. P.J. Fallon, V.S. Veerasamy, C.A. Davis, J. Robertson, G.A.J. Amaratunga, W.I. Milne and J. Koskinen, Phys. Rev. B48, 4777(1993).
64. P.J. Martin, S.W. Filipczuk, R.P. Netterfield, J.S. Field, D.F. Whitnall and D.T. McKenzie, J. Mater. Sci. Lett. 7, 410(1988).
65. J. Ishikawa, Y. Takeiri, K. Ogawa and T. Takagi, J. Appl. Phys. 61, 2509(1987).
66. J.H. Freeman, W. Temple and G.A. Gard, Vacuum 34, 305(1984).
67. E. Chason, P. Bedrossian, K.M. Horn, J.Y. Tsao and S.T. Picraux, Appl. Phys. Lett. 57, 1793(1990).
68. R. Sinclair and T.J. Konno, MRS Symp. Proc. 311, 3(1993).
69. A. Cros, K.N. Tu, D.A. Smith and B.Z. Weiss, Appl. Phys. Lett. 52, 1311(1988).
70. T. Tien, G. Ottaviani, K.N. Tu, J. Appl. Phys. 54, 7047(1983).
71. F. Nava, P.A. Psaras, H. Takai and K.N. Tu, J. Appl. Phys. 59, 2429(1986).
72. F. Nava, P.A. Psaras, H. Takai, K.N. Tu and O. Bisi, J. Mater. Res. 1, 327(1986).
73. R.D. Thompson, H. Takai, P.A. Psaras and K.N. Tu, J. Appl. Phys. 61, 540(1987).
74. F. Nava, B.Z. Weiss, K.Y. Ahn, D.A. Smith and K.N. Tu, J. Appl. Phys. 64, 354(1988).
75. M. Komabayushi, K. Hijikata and S. Ido, Jpn. J. Appl. Phys. 30, 563(1991).
76. K.A. Rubin, MRS Symp. Proc. 230, 239(1992).
77. C.K. Chiang, W. Wong-Ng, P.K. Schenck, L.P. Cook, M.D. Vaudin, P.S. Brody, B.J. Rod and K.W. Bennett, MRS Symp. Proc. 230, 321(1992).
78. C.Y. She and L.S. Hsu, in **Laser Induced Damage in Optical Materials, 1986**, eds. H.E. Bennett, A.H. Guenther, D. Milam and B.E. Newnam, MRS Sp. Pub. 746, 383(1988).
79. W.J. Moberly, J.D. Busch, A.D. Johnson and M.H. Berkson, MRS Symp. Proc. 230, 85(1992).
80. K. Ohtsuka, H. Fukuda, K. Suzuki and A. Sawabe Jpn. J. Appl. Phys., Part 2, 36, L1214(1997); T. Tsubota et al., Diamond Relat. Mater. 9, 1380(2000).
81. M. Schreck, H. Roll and B. Stritzker, Appl. Phys. Lett. 74, 650(1999); M. Schreck et al., Appl. Phys. Lett. 78, 192(2001); M. Schreck et al., Diamond Relat. Mater. 12, 262(2003).
82. Z. Dai, C. Bednarski-Meinke and B. Golding, Diamond Relat. Mater. to be published (2004).

Appendix 1

Thin film lithium batteries have a thin film anode, a thin film solid electrolyte that can dissolve Li and a thin film cathode that intercalates Li forming a solid solution with some range of solubility. The reaction providing the battery involves reversible delithiation of the cathode. Ideally, the cathode should be a material that dissolves Li from $X_{Li} = 0$ to

some higher value without forming any additional phase. However, this ideal is not usually satisfied. For example, experiment indicates that there is a crystal structure transition between hexagonal and monoclinic at x = 0.45 in Li_xCoO_2. Such structural changes in this application can lead to failure of the battery via the development of induced cracks in the cathode. One role of the materials scientist in this situation is to deduce the identity of the alloying element that will increase the range of Li in a single phase region of Li_xCoO_2. A candidate for this alloying element, Mg, is currently being investigated. (See Abstract 390 of the 206th Meeting of the Electrochemical Society, 2004.)

Appendix 2

The high-dielectric constant insulators have attracted great interest[A1] as a means of decreasing the equivalent oxide thickness without loss of breakdown voltage and leakage current limits and otherwise achieving the desirable properties of a gate insulator but in a miniaturized form. There are at least two classes of such high-k dielectrics.[A2] One involves crystalline oxides grown epitaxially on silicon but with a thin amorphous layer between the two layers. The other class involves crystalline oxides as well but having a crystalline interface with the silicon substrate. An example of the former class is shown in Figure 7.A.1. One problem with this class is that the effective oxide thickness (EOT) is too high. In the case of the sample in Figure 7.A.1, the EOT is 1.5 nm while the desired maximum thickness for this class of high-k oxides is 0.5 nm. Even when the EOT is at a desirable level, the presence of the SiO_2 interlayer with its associated level of defects may not be desirable.[A3] Unless special treatments are followed the Si/SiO_2 defect level is usually higher than for thermally produced SiO_2. The main defects found are Si dangling bonds. Thus, there is reason to expect that treatments can be developed to reduce these defects to acceptable levels, such as H passivation or high-temperature annealing. Because of the additional processing needed to achieve acceptable insulator behavior, the second class of crystalline oxides with crystalline interfaces is being explored. Such assemblies of high-k dielectrics on silicon have been achieved but not with less processing.[A2]

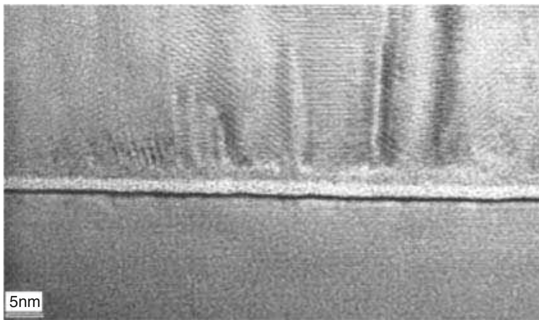

Figure 7.A1. TEM cross section of an Y oxide on Si showing a relatively thick SiO_2 layer between the oxide and the Si substrate. Reproduced with permission from S.Guha et al., Appl. Phys. Lett. 77, 2710(2000).

A1. G.D. Wilk, R.M. Wallace and J.M. Anthony, J. Appl. Phys. 89, 5243(2001).
A2. G.J. Norga et al., MRS Symp. Proc. 786, E 7.3.1(2004).
A3. S.Guha et al., Appl. Phys. Lett. 77, 2710(2000).

Appendix 3

There has been intense research activity studying the effect of metal-induced lateral crystallization and metal-induced crystallization of amorphous Si and other semiconductors since 1995. One objective has been to determine conditions which would yield an absence of grain boundaries along the path of current flow so as to maximize the carrier mobilities. The reason this field has blossomed is the fact that metal-induced crystallization speeds up the crystallization of amorphous films and allows lower crystallization temperatures onto substrates such as glass. Grains larger in diameter than 1 μm and up to 40 μm have been grown.[A4] One mode of processing to achieve this grain size is to deposit on a SiN cap on α-Si an amount of Ni that will form $NiSi_2$ nuclei spaced at least the desired diameter apart. Another mode of processing is to deposit the Ni onto a mask, patterned with holes no less than the desired grain size apart to allow contact between the Ni and α-Si at these holes. An electric field during crystallization enhances the rate of crystallization.[A5] However, the defects within the grains still act to limit the drift-effect mobilities[A6] and subsequent treatments are necessary to attempt to remove these defects. One strategy to minimize intragrain defects is to form narrow strips instead of planar films so as to cut off the extension of extended defect growth. Another is a high-temperature anneal subsequent to crystallization. Still another is to read Section 4.1.2 of this chapter and follow through the obvious implications. Much remains to be done to raise the mobilities to single crystal values.

A4. W.S. Sohn et al., J. Appl. Phys. 94, 4326(2003).
A5. N.A.T. Izmajlowicz et al., J. Appl. Phys. 94, 7535(2003).
A6. J.C. Kim et al., Appl. Phys. Lett. 83, 5068(2003).

Appendix 4

We set the rate of annihilation of defects as given by Jackson to the rate of creation of defects to obtain the average concentration of defects for the steady state which we then substitute into the equation for the crystallization velocity. (This procedure differs from Jackson's procedure in that he integrated the instantaneous value over the interval between successive ion impacts in the same area.) We neglect the contribution from amorphization due to the ion passage through the interface because conditions are below the amorphization threshold in Figure 7.7. We then solve for the epitaxial temperature.

In particular, the average rate of defect annihilation is

$$\langle R_a \rangle = \langle N \rangle^2 \sigma^2 a \nu_o \exp\{-E/kT\}$$

At thermal equilibrium, the defect density is given by

$$N_e = N_e^o \exp[-E_F/kT]$$

Substituting into the equation for the crystallization velocity given by

$$V_i = a\langle N\rangle \Lambda \nu_o \exp\{-E/kT\}$$

yields

$$V_i = a\langle N_e^o\rangle \Lambda \nu_o \exp\{-(E + E_F)/kT\}$$

We assume that the deposition velocity, V_d, equals the crystallization velocity at the epitaxial temperature. Thus, a plot of $\ln V_d$ versus the reciprocal of the epitaxial temperature should yield a straight line and a slope equal to $-(E + E_f)/k$. Indeed, the data of Weir can be used for such a plot and yields the value of 1.85 ± 0.5 for the activation energy. This value differs from 2.7 eV, the value for thermal crystallization via motion of the a/c interface. This suggests that the value of $\langle N\rangle$ in the equation for the crystallization velocity during deposition is not that corresponding to thermodynamic equilibrium but is one characteristic of the deposition process. More data are required to characterize the dependence of $\langle N\rangle$ on the deposition process before these relations can be used to predict the epitaxial temperature dependence on deposition velocity. On the other hand, if during deposition the film surface is subjected to simultaneous particle bombardment then it is likely that the value of $\langle N\rangle$ can be predicted using Jackson's theory as follows.

As applied to this situation the average defect creation rate is

$$\langle R_c\rangle = V_g f(0.8E_i/E_d)/R\Omega$$

Equating the average annihilation rate to the average defect rate yields the corresponding value of $\langle N\rangle$, which is then substituted into the equation for the crystallization velocity above. Again we set $V_i = V_d$, solve for T_{epi} and obtain

$$T_{epi} = \frac{(E/k)}{\ln\left\{\dfrac{0.8f(E_i/E_d)(a/R)\nu_o\Lambda^2}{V_d\sigma^2\Omega}\right\}}$$

We use Jackson's values for the parameters E, ν_o, Λ, σ. The values of V_d, E_i, E_d, a, R and Ω are obtained from the deposition conditions and are deposition velocity, incident particle energy, displacement energy of film lattice, lattice parameter, range of incident particles in film material, and atomic volume of film material, respectively.

CHAPTER VIII

Surface Structure

Roughness, one aspect of surface structure, affects many aspects of thin films. As was discussed in Chapter II, roughness leads to porosity in *zone a* deposition. Roughness affects the magnetic properties of multilayer devices, the crystallographic texture of films, the properties of electronic devices, the effectiveness of gate dielectrics, the optical properties, etc. Hence, a discussion of the relationships between processing and surface roughness of thin films is justified in this chapter. Roughness is not the only characteristic of surface structure. The surface reconstruction of the lattice structure affects catalytic and other surface dependent properties of thin films as well as affecting the bulk defect structure of the deposited film. We have already noted that surface stress can and does affect the ordered arrangement of components of a multicomponent film. The attainment of peculiar configurations at surfaces, such as quantum dots and whiskers, both an expression of surface structure, also is of interest.

1. Surface roughness.

Among the origins of surface roughness of deposited films are a lack of sufficient adatom mobility, highly anisotropic surface energies favoring the formation of facets of low surface energy, highly anisotropic sticking coefficients on polycrystalline substrates, in energetic deposition differential resputtering of polycrystalline film surface, elastic strain energy in deposited film, etc. Thus, among the main processing procedures used to reduce surface roughness are, if possible, deposition or annealing at elevated temperature[1] and use of low energy incident particles to provide adatom lateral displacement without resputtering or the introduction of defects.[2] The effect of substrate temperature on the wavelength and amplitude of the surface roughness is shown in Figure 2.3. Substrate inclination relative to the direction of incident flux also may have an effect on surface roughness dependent upon the film texture, as shown in Figure 2.11.

Figure 2.14 provides a molecular dynamic (MD) simulation of the effect of incident particle energy on the surface roughness under deposition conditions that normally yield columnar growth. As shown, with increase in the incident particle energy up to 18 eV the surface roughness decreases, but at the expense of increased subsurface point defect population.

However, as shown in Figure 8.1, roughness increases for incident particle energy above 20 eV.[3] This is a result of scanning tunneling microscopy (STM) measurements on Cu films grown by ion beam deposition at room temperature and refers to the roughness over a normally planar facet. In a companion MD study[4] of the roughness induced in IBD-MBE a minimum in the surface roughness with increase in incident particle energy is obtained at about 25 eV, as shown in Figure 8.2. The physical basis for this behavior is as follows. At energies less than about 25 eV the incident ions tend to insert themselves into adatom clusters, especially when near to the cluster's edge, thereby extending the area of the cluster without inducing growth in cluster height. Above 25 eV, the incident ions tend to form adatom–vacancy pairs which affect the roughness in an unexpected way. This roughness saturates with growth in thickness of the film. The smoothest surface in this range is obtained at low temperatures and high flux.

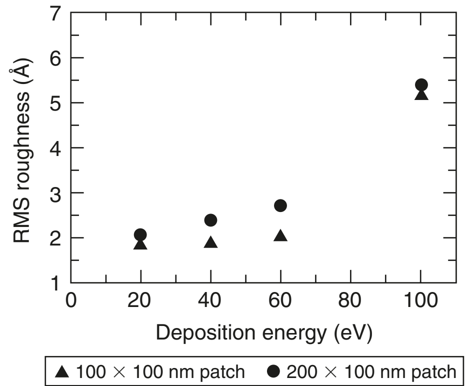

Figure 8.1. RMS roughness versus deposition energy for Cu film in IBD at room temperature, as measured by STM. Reprinted with permission from J.M. Pomeroy et al., MRS Symp. Proc. 647, 7.4.1(2001).

Thus, in other than MBE, in zone 1 temperatures, incident particle energies will tend to reduce the roughness due to columnar growth. In MBE incident particle energies below about 25 eV reduce the roughness but increase it at energies above this level. Above the transition energy the smoothest surfaces are produced at low temperature and high flux.

As noted above, high incident energies in normal physical vapor deposition (PVD) act to produce radiation damage. One response to attempts to

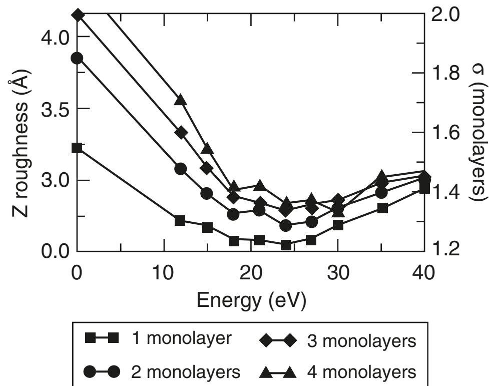

Figure 8.2. RMS roughness versus incident particle energy in an MD simulation of IBD-MBE. Reprinted with permission from J.M. Pomeroy et al., Phys. Rev. B66, 235412(2002). © 2002 The American Physical Society.

eliminate the radiation damage is to use clusters of particles with hyperthermal energy to bombard the film surface.[2a,5] This procedure involves a low energy per incident particle (below the displacement energy) and a high flux of these particles. Because of these characteristics, cluster particle bombardment reduces roughness involving small wavelengths, i.e. the number of atoms in a hill is not more than the cluster bombardment can distribute laterally before it receives atoms from adjacent hills under bombardment acting to make the hill grow. However, cluster

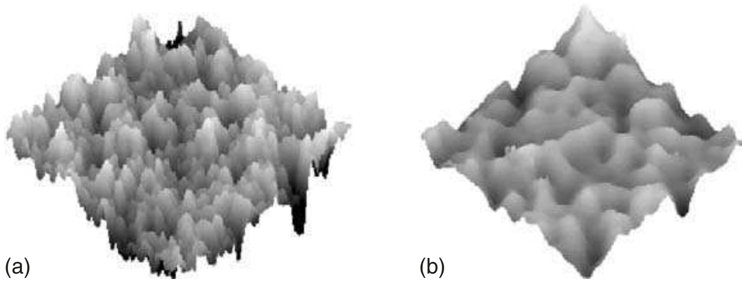

Figure 8.3. AFM images of surface of Si(001) surface (a) before irradiation (RMS: 177.7 nm) (b) after irradiation (1×10^{18} clusters/cm^2 irradiated (RMS: 107.9 nm)) by clusters of Argon ions. Reprinted with permission from T. Aoki et al., MRS Symp. Proc. 749, W17.9.1(2003).

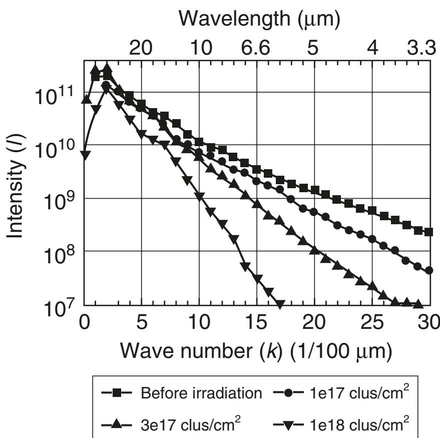

Figure 8.4. Roughness peak intensity as a function of cluster irradiation and wave number of roughness. Reprinted with permission from T. Aoki et al., MRS Symp. Proc. 749, W17.9.1(2003).

bombardment is less efficacious for roughness involving long wavelengths, as is evident from Figures 8.3 and 8.4.

Although the above considerations were evaluated for PVD conditions, they are not limited to them. In particular, in chemical vapor deposition (CVD) there will also be a minimum temperature below which surface diffusion of the molecule carrying the depositing species becomes so small as to encourage the development of surface roughness. The self-bias in PECVD of α-Si:H provides energetic ions that act to smoothen the surface when the substrate is

in the "cathodic" position.[2b] In the CVD of diamond films where appreciable roughness is found, the use of an energetic oxygen ion beam, subsequent to CVD, with oblique incidence and with substrate rotation was found to optimize the surface smoothness.[2c]

Differential laser ablation with more ablation of roughness peaks than hollows has also been used as a smoothing technique.[6] Other modes of laser smoothing have been proposed including surface melting.[7] One, this author suggests, is an in situ chemical polishing procedure which involves selective formation of high vapor pressure products at roughness peaks and then their subsequent laser ablation.

Another source of surface roughness in films deposited by MBE is elastic strain energy in the deposited film. The formation of free surface normal to the principal stresses in the film plane would act to lower the magnitude of these stresses in an appreciable volume fraction of the film. Hence, there is a morphological instability in the presence of in-plane principal stresses that tends to produce a periodic surface morphology presenting free surface normal to the principal stresses. This tendency to develop a periodic wave-like surface morphology with short wavelengths is counteracted by the increase in surface area and energy that occurs with decreasing wavelength of the surface perturbation. Facets may also develop in a further attempt to reduce the overall free energy. This phenomenon has been considered by several investigators.[20] This surface roughness may be useful in the production of quantum dots when the amplitude of the periodic surface equals the thickness of the film.[21]

2. Surface modification for producing ordered arrays.

One of the ordered arrays it is desired to produce on thin film surfaces is a quantum dot array. Although there are techniques for achieving this objective using masking procedures it is still desired to accomplish it by self-assembly. Thus, the periodic variation of a surface property seems to be a necessary condition in this regard. Let us consider various modes of periodic surface property variation.

2.1. Periodic surface reconstruction pattern.

Some surface reconstructed patterns have periodicity on the order of a nanometer or more. It has been found that certain adatoms will assume the periodicity of the underlying reconstructed lattice. One such pattern is the 7×7 reconstructed pattern on the Si(111) surface. Al, In, Mn, Pb, Ag and Tl, are attracted to this 7×7 pattern and can self-assemble into ordered arrays,[8] such as that shown in

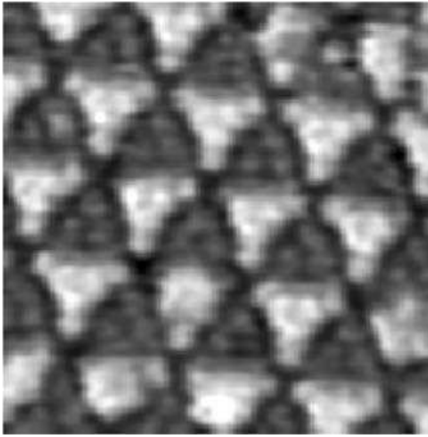

Figure 8.5. An STM showing ordered array formed by 0.1 MI Pb on Si(111)-7 × 7. Image size 8.5 × 8.5 nm^2. Reproduced with permission from www.uam.es/fmc/especifica/Nuevas Microscopies webpage/Index.htm.

Figure 8.5 where Pb is the adatom. As shown, the repeat distance is slightly larger than 1 nm. Effectively, the reconstruction pattern provides a periodic array of potential wells for the adatoms. Thus, for a reconstruction pattern with a suitably larger lattice parameter it may be possible to anchor nanometer sized quantum dots into a two-dimensional periodic pattern. Details relative to the processing needed to achieve these arrays is provided in Ref. [8].

2.2. Periodic surface strain pattern.

One possible means of providing an ordered array of quantum dots is to achieve an ordered array of heterogeneous nucleation sites for these entities. The possibility of using the periodic strain fields due to a periodic array of misfit dislocations has been recognized by several investigators.[10] However, the production of a periodic array of misfit dislocations is not automatic. Indeed, many attempts to achieve this result have not succeeded. Although misfit dislocation arrays are formed often they are not periodic. Figure 8.6 is a sample of such a result. Although the periodicity of the misfit dislocation array is not present, a relation between this array and the nucleated quantum dots does exist. Thus, should a periodic misfit dislocation array be produced it is still possible to use this array to form an ordered array of quantum dots. The question is how to accomplish both goals.

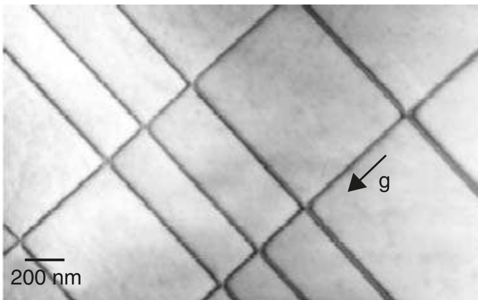

Figure 8.6. Misfit dislocation array. Reprinted with permission from X.W. Liu et al., J. Appl. Phys. 94, 7496(2003).

A tentative conclusion of research governing the nucleation of quantum dots is that they nucleate at positions on the surface of minimum chemical potential for the component forming the quantum dot.[11] How to produce a periodic array of minima

in the chemical potential of the quantum dot's component along the surface on which the quantum dots are to nucleate is the question.

It may be worthwhile to consider some additional information prior to an attempt to answer the foregoing question. Although periodic arrays on surfaces are rare they do sometimes exist. One such array is found under the following circumstances. When a monatomic layer of Au is deposited on Ni(111) at a low temperature (140°K) and allowed to warm slowly to room temperature, a periodic Moire pattern is observed as shown in Figure 8.7. At the Moire circular regions the surface is lower than in between these regions. If the Au is deposited at room temperature a different surface pattern is produced as is evident on comparison of Figures 8.8 and 8.7. In this case, if one looks closely one may see that there is a periodic array of triangles with the circumference of the triangles lower than the remainder of the surface. In the Ni underlayer a partial dislocation surrounds the Ni atoms just below a triangle. From the present point of view the interesting aspect is the periodicity of the Moire and triangle patterns. This periodicity is 9 × 9 Ni versus 8 × 8 Au for both patterns. The triangular pattern differs atomically from the Moire pattern by involving a transfer of 5 Ni atoms from the Ni layer to the Au layer with the transferred Ni atoms randomly distributed in the Au layer.

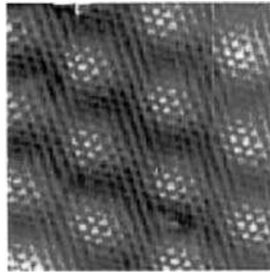

Figure 8.7. STM topograph showing Moire pattern apparent for 1 ML Au on Ni deposited at 170°K. Reprinted with permission from J. Jacobsen et al., Phys. Rev. Lett. 75, 489(1995). © 1995 The American Physical Society.

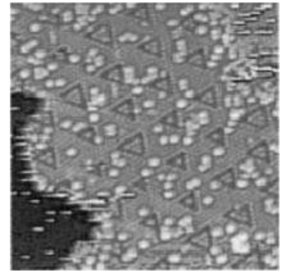

Figure 8.8. STM topograph of Au deposited on Ni(111) at room temperature revealing periodic pattern of triangles. Reprinted with permission from J. Jacobsen et al., Phys. Rev. Lett. 75, 489(1995). © 1995 The American Physical Society.

Additional periodic patterns involving misfit dislocations are found for the same relative heteroepitaxial arrangement of an face-centered-cubic (fcc) (111) plane of the deposited layer either on another fcc (111) face of a crystal having a smaller lattice parameter or on a basal plane of an hexagonal-close-packed (hcp) crystal with smaller atomic diameter compared to that of the layer.

Annealing a 2 ML layer of Ag on Pt(111) at 800 K yields the STM topograph shown in Figure 8.9a. One sees a periodic array of triangles shown

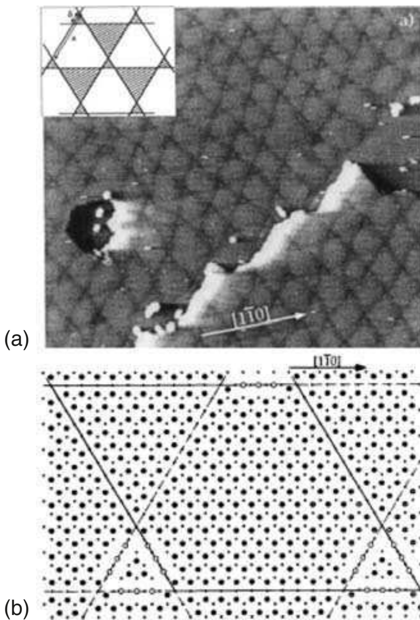

Figure 8.9. (a) STM topograph of 2 ML Ag on Pt(111); (b) Showing misfit dislocation array and atom positions adjacent to interface. Reprinted with permission from H. Brune et al., Phys. Rev. B49, 2997(1994). © 1994 American Physical Society.

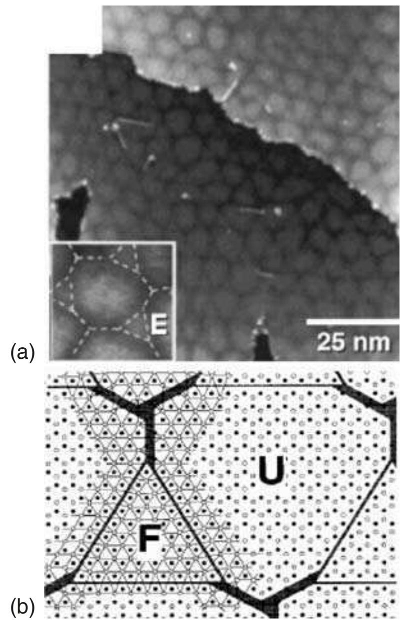

Figure 8.10. (a) 5 ML of InAs on GaAs showing strain fields due to periodic pattern of misfit dislocations where the position of the latter are indicated in detail by the dashed lines in the inset. (b) Schematic figure showing atom positions in faulted, F, and unfaulted, U, regions. Reproduced with permission from H. Yamaguchi et al., Phys. Rev. B55, 1337(1997). © 1997 The American Physical Society.

schematically in the inset. A more detailed view of the misfit dislocation array corresponding to these triangles is shown in the lower figure which also reveals the atom positions in the layers. Black dots represent Ag atoms in the first monolayer. Open and filled circles represent Ag atoms in second layer over fcc and hcp positions, respectively.

Another periodic pattern of misfit dislocations is shown for the case of InAs on GaAs(111) in Figure 8.10a. In this case the STM surface topograph reveals periodic circular blobs. There are small triangles in between some of these blobs which outline misfit dislocations as shown in the inset. The regions separated by these misfit dislocations are shown in greater detail in the schematic figure of Figure 8.10b.

Still another example is that of Ag on Ru(0001). An STM topograph of 1 ML Ag, shown in Figure 8.11, reveals the underlying periodic pattern of misfit dislocations.

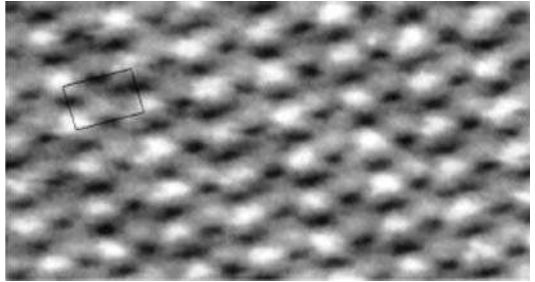

Figure 8.11. STM topograph of 1 ML Ag on Ru(111) showing periodic misfit dislocation array pattern. Reproduced with permission from Sur. Sci. 433–435, 506(1999). © 1999 Elsevier.

It is apparent that in all these examples of periodic misfit dislocation arrays the arrays appear below a few monolayers of the epilayer. If the epilayer contains more than a few monolayers than the periodicity of the misfit dislocation array vanishes.

The potential of these periodic patterns of misfit dislocations for the production of a periodic pattern of quantum dots has excited the interest of several researchers.[10] Brune et al.[12] proposed that when the period of the misfit dislocation array corresponded to the spacing required for one nucleus of a material (a nanodot) deposited on the surface of the epilayer then it should be possible to deposit a periodic array of these material nanodots. Figure 8.12 presents one of their nanodot arrays. The array is that of Fe nanodots on a substrate consisting of 2 ML Cu on Pt(111). However, the application of this particular mode of producing periodic misfit dislocation arrays has not at this writing been used to form a periodic quantum dot array to the best knowledge of the author. Another mode of forming a periodic dislocation array makes use of screw dislocations formed by wafer bonding.[13] The top wafer is thinned sufficiently for the dislocation array to function as the required periodic substrate and then the quantum dots are deposited on the substrate. A subsequent anneal produced the ordered pattern of the quantum dots with 4-fold symmetry shown in Figure 8.13. Another way of using the wafer-bonding mode of forming the periodic array of crossed screw dislocations is to etch the top wafer back

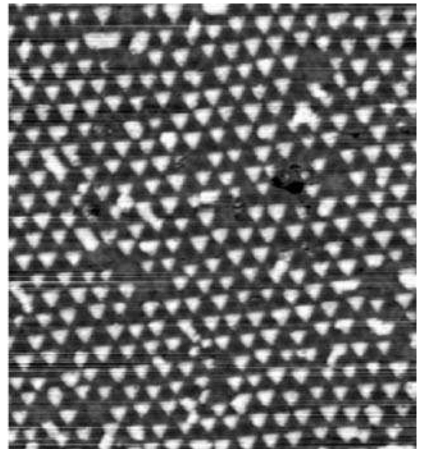

Figure 8.12. STM topograph of Fe islands on 2 ML Cu on Pt(111). Reproduced with permission from Nature 394, 451(1998). © 1998 Macmillan Publishers Ltd.

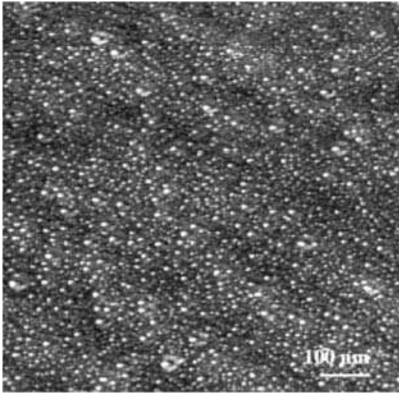

Figure 8.13. Ge quantum dots on wafer bonded Si containing a screw dislocation network close to the substrate surface revealing a 4-fold symmetry pattern. Reprinted with permission from F. LeRoy et al., Appl. Phys. Lett. 80, 3078(2002).

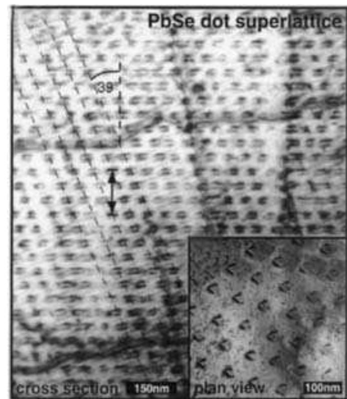

Figure 8.15. XTEM of a 100-period $PbSe/Pb_{1-x}Eu_xTe$ vertical dot stacking. Inset: plan view TEM showing hexagonal lateral ordering within the growth plane. Reproduced with permission from Physica E9, 149(2001).

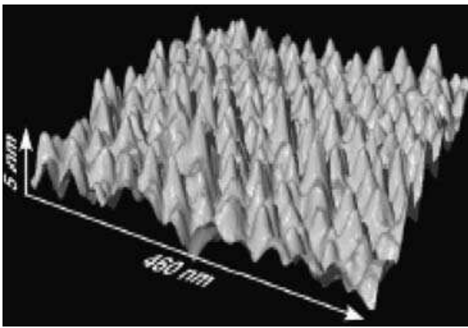

Figure 8.14. Si dots produced by etching a wafer bonded couple twisted relative to each other to produce a square screw dislocation network. Reproduced with permission from NNUN, Abstracts 2002/Chemistry and Biology. p. 12.

to the join. In the final stages of etching the rate of etching is affected by the dislocation array so as to leave the slowest etching material in the form of quantum dots. Figure 8.14 shows an example of the result of this procedure.

Still other ways to achieve a periodic surface structure use either surface composition or morphology modulation or both. Such modulations may form on the surface of a film of a supersaturated solid solution, or a strained heteroepitaxial layer at a temperature where the adatoms may diffuse but the bulk atoms may not. Composition and morphology modulations have been found in film layers which are deposited at the conditions just cited and have been used to produce layers of quantum dot arrays.[14] Figure 8.15 shows a vertical dot array produced by a morphological modulation in a $PbSe/Pb_{1-x}Eu_xTe$ system.

2.3. Periodic ledge pattern.

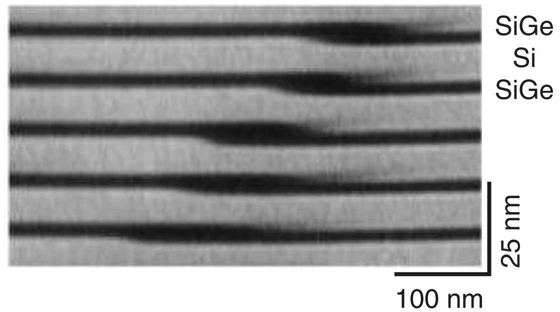

Figure 8.16. TEM cross section of an array of SiGe quantum wires within a Si/SiGe multilayer structure on a vicinal {113}Si substrate. Figure is taken from the annual report of the Walter Schottky Institute on the subject of self-assembled nanostructures.

Elastic relaxation of mismatch strain at the edges of large surface steps drives step-bunching and the accumulation of strained material at the step edges into wire-like structures. The key word here is accumulation implying a build-up of wire-like regions at the bunched steps by transport from regions of higher chemical potential to those of lower chemical potential, i.e. a self-assembly process. Figure 8.16 shows SiGe quantum wires within a Si/ SiGe multiple layer structure on a vicinal (113)Si substrate. A spatial correlation of wires in a direction inclined from the surface normal and a very regular lateral ordering of wires with periods of typically 300 nm is observed. It is caused by self-ordering mediated by the local strain fields extending into the Si host. The structure shown represents an artificial crystal of Si/SiGe wires with a three-dimensional periodic arrangement of wires that was formed by self-assembly and not by patterning. It is possible to form an ordered array of Ge quantum dots on top of these wires by self-assembly of Ge atoms deposited on the total surface. Figure 8.17 shows an AFM image of such Ge islands deposited on top of the wire array. The Ge islands are aligned along the [110] wire direction, the vertical direction in the figure. Although the ordering is not perfect, it is apparent that there is a periodicity to the positioning of the islands. Finally, Ge deposition directly onto a bunched step on Si(111) can yield a regular row of Ge islands as shown in Figure 8.18.

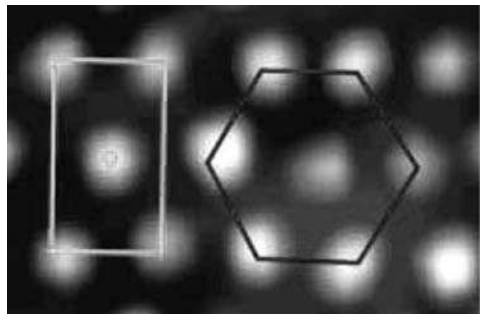

Figure 8.17. Ge islands grown on SiGe quantum wires. The <110> is horizontal. Figure is taken from the annual report of the Walter Schottky Institute on the subject of self-assembled nanostructures.

Figure 8.18. This figure shows a row of Ge islands along a bunched step of a Si(111) surface. Reprinted with permission from N. Motta, A. Sgarlatta, A. Balzarotti and R. Rosei, MRS Symp. Proc. 696, N2.2.1(2002). Vertical scale of image is 75 nm.

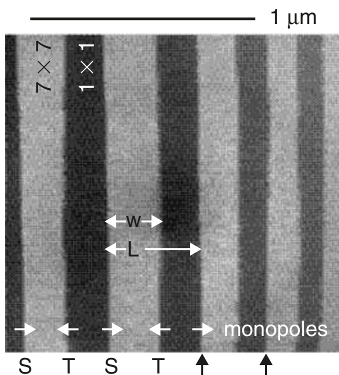

Figure 8.19. Bright-field LEEM image of the Si(111) surface at the phase transition temperature. The (7 × 7) areas appear brighter than the (1 × 1) areas due to the reflectivity difference for 10 eV electrons. Phase boundaries are found alternatively at step edges (S) and on Terraces (T). Dark arrows indicate the terrace analyzed in Figure 2.14. White arrows show the orientation of phase boundary force monopoles. Reproduced with permission from J.B. Hannon et al., Phys. Rev. Lett. 86, 4871(2001).

2.4. Periodic surface phase pattern.

It is known that two surface phases may coexist during a first-order transition[22] because any two surface phases must have different surface stress and the long-range resulting interactions prevent a sharp transition. Hannon et al.[22] have provided quantitative evidence supporting this assertion. In doing so they also provide a new mechanism for the formation of a periodic surface pattern that consists of alternating and coexisting surface phases.

It is well known that the Si(111) surface undergoes a transition from the ordered (7 × 7) structure to a disordered (1 × 1) phase at a temperature $T_C \approx 1135$ K. In one experiment Hannon et al. studied the patterns formed on a surface very slightly misoriented toward the $<1\overline{1}\overline{2}>$ direction. The effect of this slight surface tilt is to produce surface steps parallel to the low-energy phase boundary orientation. Two types of phase boundaries then appear on the surface. One is at the surface step (S) and the other is on the terrace (T). These phase boundaries and phases are shown in a bright-field LEEM image (Figure 8.19) of the Si(111) surface at the phase transition temperature.

The interactions between phase boundaries (and other line defects such as steps) have been studied.[23,24] The boundary between two surface phases that have different surface stress corresponds to a line of force (a "force" monopole). This force, $\mathbf{F} = \nabla \cdot \boldsymbol{\sigma}$, where $\boldsymbol{\sigma}$ is the surface stress tensor (two-dimensional). Also, a localized defect, such as a step, has a "force dipole" as well as higher-order multiple moments (Srolovitz and Hirth[24]). Elasticity theory provides relations for the interactions between these forces.

Hannon et al.[22] have derived a relation for the energy per unit area of a surface

having these coexisting phases and its dependence upon an asymmetry parameter $p = (2\omega/L) - 1$, where ω is the width of the (7×7) domain and L is the terrace width. Five additive terms enter into this energy. One involves the creation energy of steps and phase boundaries. Another corresponds to the difference in surface free energy between the phases, i.e. $\Delta S(T - T_C)p/2$, where ΔS is the difference in entropy per unit area of the surface phases. The third term represents the interaction between elastic and/or electrostatic monopoles at the phase boundaries. The fourth term represents the next longest range interaction in the multipole expansion, i.e. that between the monopoles and the force dipoles at both step and terrace phase boundaries. The fifth term corresponds to a short-range repulsion between the phase boundaries. Minimizing the energy per unit area with respect to p provides the equilibrium distribution of the coexisting phases. Hannon et al.[22] measured the dependence of p on $(T - T_C)$ varying the temperature from both above and below T_C. Their result is shown in Figure 8.20 where the line through the points represents the theoretical dependence. A recent review of LEED based research[25] also provides a review of this subject.

The periodic pattern produced by the coexisting surface phases does not involve long-range diffusion of adatoms. Rather, it involves rearrangement of surface atoms to yield the minimum free energy configuration.

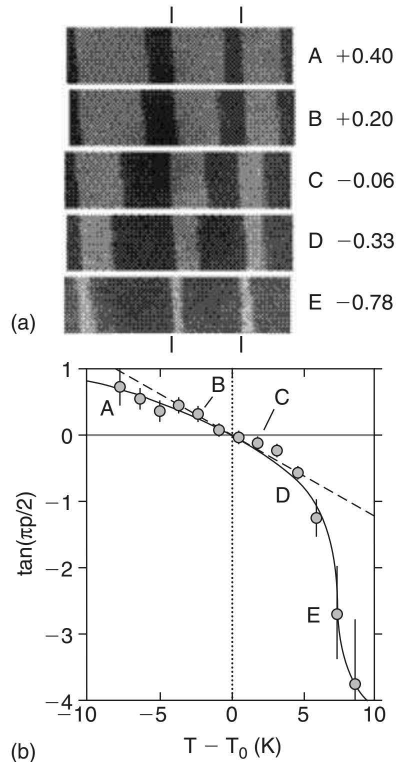

Figure 8.20. (a) LEEM images of the 310 nm wide terrace indicated in Figure 8.19 for selected temperatures near T_C. Each image is labeled by the corresponding value of the asymmetry parameter p. The horizontal dimension of the images is 1.0 micron.
(b) Temperature dependence of $\tan(\pi p/2)$ near T_C for the terrace shown in (a). The slope of the dashed line is $-0.12\ K^{-1}$. The solid curve is a fit to the theory. Reproduced with permission from J.B. Hannon, Phys. Rev. Lett. 86, 4871(2001).

2.5. Periodic nanodots via kinetic control.

An in-depth study of the patterns developed on decomposition of an unstable monolayer solid solution on various substrates has been carried out by

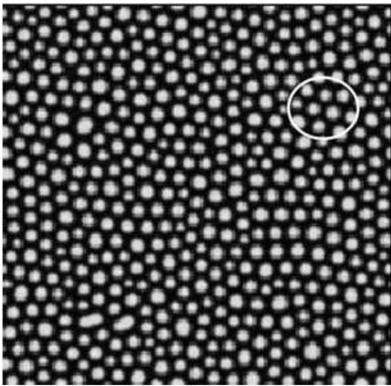

Figure 8.21. Phase field simulation of spinodal decomposition of a supersaturated solid solution monolayer coherent with substrate showing short-range order but no long-range order. Reproduced with permission from W. Lu and Z. Suo, 2001. From a paper prepared for a special issue of Journal of the Mechanics and Physics of Solids dedicated to Professors J.W. Hutchinson and J.R. Rice on the occasion of their 60th birthdays.

Suo and his collaborators.[26] Among the many results was one that indicated the possibility of obtaining a short-ranged ordered structure of nanodots of a minor component phase distributed within a different phase of the major component. Figure 8.21 illustrates one such possible distribution of nanodots. One result of their work was that the time necessary for the long-range ordering (growth of some domains at the expense of other domains) was much longer than that for the nucleation of the small domains. They did note that some means of breaking symmetry could reduce the time to form a long-range ordered array of nanodots. We have already considered one such symmetry breaking mode – that of a periodic misfit dislocation array subsurface, but close, to the monolayer. Here we would like to consider means of achieving long-range ordered arrays of nanodots in the absence of subsurface means of breaking symmetry.

Paraphrasing the result of Suo and Lu it appears that the rate of formation of short-range ordered domains by spinodal decomposition is high relative to the growth rate of these domains. This type of situation has occurred often in nucleation and growth phenomena and solutions of various kinds have been investigated for the means of decreasing the nucleation rate relative to the growth rate. For example, one possible solution to this problem is to deposit the monolayer at a low temperature that quenches in the unstable phase and then use a traveling temperature gradient to nucleate one short-range ordered domain which is then grow out by motion of the temperature gradient without subsequent nucleation. Another possible solution is to search for compositions and temperatures between the spinodal and binodal in order to change the mode of decomposition to one of nucleation and growth rather than of spinodal decomposition and then to find the temperature–composition point that maximizes the ratio of the growth rate of the ordered domain about a nucleus to that of the nucleation rate of such domains. What is desired is a processing condition that allows one ordered domain to form in a reasonable time, with sufficiently rapid growth of this domain so as to engulf the surface area before other domains can nucleate.

The model for decomposition used by Suo and Lu involves the criteria associated with spinodal decomposition, i.e. diffuse interface between the surface phases having the same surface structure – a coherent system. When the phase corresponding to the minor component is not coherent with the major component surface phase the options available for control of the nucleation rate relative to the growth rate are increased because the barrier to nucleation, the interface energy between the two monolayer phases, is not a strong function of temperature in this case. Thus, with the same driving force for the formation of a long-range ordered nanodot array – an effective repulsion between nanodots – temperature can be used to tune the ratio of domain nucleation to growth rate. The effective repulsion between nanodots can be achieved either via a coherent interface between nanodot and substrate with difference in lattice parameters between the two entities or by an effective line tension between minor component and major component phases that induces an elastic strain in the latter phase which is transmitted to adjacent nanodots. In this case the monolayer phases need not be coherent with the substrate. In the Suo–Lu model domains form to minimize the strain energy associated with the repulsion between nanodot precipitates.

In the work of Suo and Lu the pattern produced in long time is determined by thermodynamic stability. This is not the only pattern-determining criterion. As Walgraef[27] has shown, dynamical conditions may control the pattern observed in thin film deposition. In his treatment of this problem there are three dynamic processes to be considered: adsorption, desorption, and surface diffusion. If conditions are such that the desorption rate is negligible relative to the adsorption rate then the tendency towards instability and pattern formation is likewise negligible. However, with a finite desorption rate the Walgraef model yields a region of temperature and surface composition for a single component where instability and pattern formation occurs. This result is a well-known phenomenon in reaction–diffusion dynamics.[28] Figure 8.22 shows schematically the region of dynamically determined patterns produced by this model. Thus, where the binding of adatom to substrate is strong these patterns are not likely to be formed, at least in the first monolayer. Consequently, the chance of obtaining a pattern is increased for substrates that are non-epitaxial relative to the depositing species.

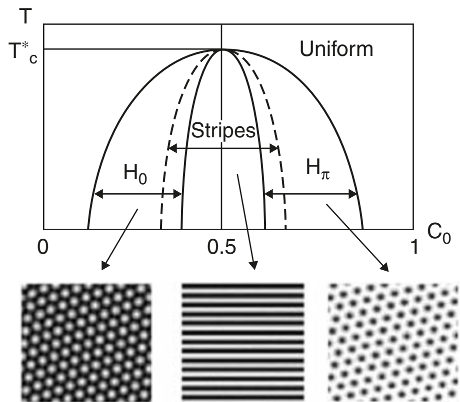

Figure 8.22. Predicted dynamic patterns in temperature, T, atom fraction, C_0, space for Walgraef model. Reprinted with permission from D. Walgraef, Physica 15, 33(2002).

Similarly, pattern formation probability increases with increasing adatom diffusivity, another factor favoring weak bonding between substrate and adatom and with decreasing deposition rate. Walgraef did not comment on the time evolution of the patterns, i.e. whether short-range ordered domains appear in a transient to the final pattern given by the model. However, in a similar treatment, Verdasca et al.[29] noted that in the strong segregation regime where interfaces are sharp and amplitudes saturate at values near to the coexistence curve (i.e. short-range and strong inter-adatom potential) short-range ordered domains do form first and then grow. Only in the weak segregation regime is it implied that one domain occupies the film surface from the start of the reaction–diffusion process.

Obviously, experiment is required to evaluate the predictions of the dynamic models. One possible experiment has been reported in news bulletins only prior to this writing so that the author cannot comment upon its applicability to the above considerations. However, according to the description in Science News 166, 165(2004) the pulsed laser deposition of Ni and Al_2O_3 produces a long-range ordered array of Ni dots in an Al_2O_3 matrix when the temperature and rate at which the target materials vaporize are within small limits. The successful deposition method requires that the ordered pattern be formed first on the deposition of about a monolayer to produce a template for the continued deposition onto the ordered nanodot pattern.

3. Processing and surface reconstruction.

Atoms at surfaces rearrange to lower the free energy. Rearrangement may involve merely relaxations without change in lattice sites or reconstruction with change in lattice sites. Processing can affect the kinetics governing the approach to equilibrium at the surface and by altering the environment of the surface can change the equilibrium state. For example, the equilibium state of a Si(111) surface is a 7×7 reconstruction. However, exposure to atomic hydrogen can bring about a 1×1 reconstruction in which there are no dangling bonds and no strained bonds. Further, in SiC this reconstruction on a Si surface can form a surface metallic layer, which has interesting consequences.[15] The effect of chemical environment on surface reconstruction is an ongoing activity and has a vast literature. Here we will concern ourselves with the effect of physical processing effects on surface reconstruction.

Bombardment of a Si(100) surface with Argon ions of less than 100 eV induces surface damage and the development of a compressive surface stress. The dimers in the 2×1 reconstruction are either bent or cut and also are partially destroyed by this radiation.[16] It was discovered that subsequent irradiation by electrons of energy less than 40 eV removes the compressive stress and recrystallizes

the surface to a slightly paired 1×1 configuration. Evidence was presented that this recrystallization is an athermal process.[17] Electron bombardment with energies higher than about 40 eV introduce surface damage including point defects.[18] Thus, the reverse process of healing by low-energy electron bombardment is unexpected and worthy of further study. Since Si is often deposited in conditions that expose the surface to a plasma it is possible that the latter may affect the deposition process via energetic particles from the plasma that reach the film surface.

Xu et al.[19] found that the surface of Si(100), after removal of the top 2×1 reconstructed atomic layer by exposure to a laser pulse just less than that required to melt the surface, resembled a slightly paired 1×1 surface, closer to the bulk terminated surface arrangement, which is the expected arrangement in the penultimate layer prior to removal of the surface layer. In both of the above studies the 2×1 surface was restorable thermally. These observations suggest that a metastable surface reconstruction can be achieved via appropriate radiation of the surface.

References

1. S. Wei et al., Phys. Rev. B58, 3605(1998).
2. a) N. Toyoda and I. Yamada, MRS Symp. Proc. 749, W17.7.1(2003); b) G.T. Dalakos, J.L. Plawsky and P.D. Persans, Report#2002, GRC159, GE Global Research, Niskayuna, NY, 2002; c) D.-G. Lee, D.R. Gilbert and I.J. Singh, J. Elect. Mat. 26, 1365(1997); d) R. Rabady and I. Avrutsky, J. Opt. Soc. Am. B20, 2174(2003).
3. J.M. Pomeroy et al., MRS Symp. Proc. 647, 7.4.1(2001).
4. J.M. Pomeroy et al., Phys. Rev. B66, 235412(2002).
5. T. Aoki et al., MRS Symp. Proc. 749, W17.9.1(2003).
6. G. Meaden et al., J. Mat. Sci. 32, 3801(1997).
7. Y. Zhong, Y. Ashkenazy, K. Albe and R.S. Averback, J. Appl. Phys. 94, 4432(2003); Z. Kantor, Z. Geretovsky and T. Szorenyi, Appl. Phys. A69, 1107(1999); V.P. Veiko, Proc. SPIE 5147, 95(2003).
8. L. Vitali, M.G. Ramsay and F.P. Netzer, Phys. Rev. Lett. 83, 316(1999); J.-L. Li et al., Phys. Rev. Lett. 88, 0661011(2002).
9. www.uam.es/fmc/especifica/Nuevas Microscopies webpage/Index.htm.
10. A. Yu Sipetov, Low Temp. Phys. 25, 376(1999); R. Leon et al., J. Appl. Phys. 91, 5826(2002); I.A. Ovid'ko and A.G. Sheinerman, J. Phys. Condens. Mat. 16, 2161(2004).
11. B. Yang, F. Liu and M.G. Lagally, Phys. Rev. Lett. 92, 025502(2004).
12. H. Brune, M. Giovannini, K. Bromann and K. Kern, Nature 394, 451(1998).
13. F. LeRoy et al., Appl. Phys. Lett. 80, 3078(2002).
14. J.M. Millunchick and D.J. Srolovitz, "Origins of Lateral Modulations in Lattice-mismatched Films", in **Encyclopedia of Materials: Science and Technology**, Elsevier.
15. V. Derycke et al., Nature Materials 2, 263(2003).
16. T. Narushima, A.N. Itakura, T. Kawabe and M. Kitajima, Appl. Phys. Lett. 79, 605(2001).
17. T. Narushima, M. Kitajima and K. Miki, J. Phys. Condens. Mat. 16, L193(2004).
18. K. Nakayama and J.H. Weaver, Phys. Rev. Lett. 82, 980(1999).
19. J. Xu, S.H. Overbury and J.F. Wendelken, Phys. Rev. B53, R4245(1996).

20. R.J. Asaro and W.A. Tiller, Met. Trans. 3, 1789(1972); M.A. Grinfeld, Dojklady Akademii Nauk SSSR 290, 1358 (1986); D.J. Srolovitz, Acta Met. 37, 621(1989).
21. P. Sutter and M.G. Lagally, Mater. Sci. Eng. B Solid State Mater. Adv. Tech. 89, 45(2002).
22. J.B. Hannon et al., Phys. Rev. Lett. 86, 4871(2001).
23. V.J. Marchenko, JETP Lett. 33, 382(1981).
24. D. Vanderbilt, Surf. Sci. Lett. 268, L300(1992); O.L. Alerhand et al., Phys. Rev. Lett. 61, 1973(1988); E. Pehlke and J. Tersoff, Phys. Rev. Lett. 67, 465(1991); V.L. Marchenko and A. Ya. Parshin, Sov. Phys. JETP 52, 129(1981); D.J. Srolovitz and J.P. Hirth, Surf. Sci. 255, 111(1991).
25. J.B. Hannon and R.M. Tromp, Ann. Rev. Mater. Sci. 33, 263(2003).
26. Z. Suo and W. Lu, J. Nanopart. Res. 2, 333(2000); W. Lu and Z. Suo, Phys. Rev. B65, 085401, 205418(2002); Y.F. Gao, W. Lu and Z. Suo, Acta Mater. 50, 2297(2002).
27. D. Walgraef, Physica 15, 33(2002); 18, 393(2004).
28. D. Walgraef, **Spatio-Temporal Pattern Formation: With Examples from Physics, Chemistry and Materials Science**, Springer-Verlag, 1996.
29. J. Verdasca, P. Borckmans and G. Dewel, Phys. Rev. E52, R4616(1995).

This page intentionally left blank

Index

A

Activation energy 74
 adatom diffusion 6
 grain growth 74
Amorphization 164, 215
 and bond rotation 215
 and dihydride terminated Si(100) 215
 correlating parameter for 164
Amorphization energy in Si 212
Amorphous alloys 161
 origin of perpendicular magnetic anisotropy in 161
Amorphous carbon 157
 effect of hydrogen on bond type 158
 effect of pressure on bond type in 157
 hydrogen and hardness 159
 model for elastic modulus of 159
Amorphous germanium 156
Amorphous hydrogenated silicon 142
 dangling bond density in 142
 microvoid surface area in 144
Amorphous silicon 141
 crystal nucleation in 163
 dark conductivity 141
 defects in 141
Amorphous to crystalline transitions 208
 α-Si to epitaxial Si 208
  defects 208
  effect of amorphization mode 209
 in Ge-Te-Sb system 225
 in PZT films 225
Amorphous/crystalline states 158
 effect of particle bombardment on 164
 energy difference between 158
 in α-Si:H 164
  effect of hydrogen on 164
 in metal alloys 164
Amorphous/crystalline transition 165
 in α-Si:H 164
  effect of hydrogen on 164
  effect of particle bombardment on 164
 in metal alloys 164
 in silica 165
Anisotropic sticking coefficient 77
Atomic peening 10
Axiotaxy 139

B

Background pressure 3
 effect on film's oxygen content 3
Bond angle distortion 142
 effect of hydrogen in α-Si on 143
 effect of annealing of α-Si on 143

C

Carbon films 220
 ion beam deposition of 220
Chamber pressure 3
 impingement rate dependence on 3
Channeling 10
 surface penetration by 10
Chemical annealing 143
Cluster 7
 approach to equilibrium of 7
  effect of condensation event on 7
Cluster mobility 71
 effect on epitaxial temperature 71
Cluster/substrate interface energy 59
 dependence of cluster orientation and texture on 59
Clusters 59
 orientation 59
 size 60
Cohesive energy 193
 between two metal blocks 193
Collision cascade 10
Columnar grains 71
Column diameter 30
 temperature dependence of 30

Column structure 30
small angle neutron scattering by 30
Columnar grains via self-epitaxy 59
Composition fluctuations 110
in semiconductor alloys 110
lack of in SiGe 111
Constant photocurrent measurement (CPM) 141
$CoSi_2$ 196
A and B types 197
defects in 197
types of surface on 198
Critical homologous temperature 58
for adatom diffusion 58
for grain boundary migration 58
Critical temperature 36, 101
effect of deposition rate on 36
RHEED oscillations 101
Critical thickness 116
of pseudomorphic films 116

D

Dangling bond state 142
Dangling bond state density 142
and dihydride concentration 150
and void surface site density 169
effect of deposition condition on 151
in device grade α-Si:H 142
versus hydrogen content 142
Dangling bonds 2
Defects 104, 141, 216
in amorphous Si 141
technique for measuring 141
interfacial 109
Si ion beam deposition induced 216
Sputter deposition induced 216
techniques for measuring 141
{113} planar 104
Density 31
versus film thickness 31
Deposition parameters 1
background pressure 2
deposition rate 14
identification of 1
incident particle energy 4
line-of-sight particle motion 4
other than PVD 18
substrate and its cleanliness 15
substrate temperature 16
Diamond films 219
Ne ion assisted deposition of 219
Diamondlike-films 157
Diffusion-limited aggregation model 35
Dislocation density 85
Dislocation loops 45, 103
produced in plasma deposition 103
Displacement energy 5
Displacement spike 10

E

Eden model 35
Elastic collision 5
energy transferred in 5
Elastic strain energy 67
effect on texture 67
Electron spin resonance (ESR) 141
Energetic particle bombardment 88
on grain morphology and texture 88
summary of effects 88
Energetic particle, effect of 7
of temperature spike 8
on adatom mobility 8
penetration 8
Energy density 13
to produce amorphous layer 13
Epilayer/substrate rotation 126
effect of interface bonding on 127
Epilayer/substrate systems 123
metal/metal 123
Epitaxial deposition 59
onto Si 59
of metals 59
Epitaxial temperature 57, 214, 217
effect of hydrogen diffusion of 217
effect of ion beam on 214
Epitaxial thickness 212, 218
effect of PECVD on 218
Epitaxy 2, 97
definition 15, 97
factors affecting 2

granular 6, 59
texture and 15
unclean substrate on, role of 2, 3
Equiaxed grain structure 59
Equilibrium state 59
approach to 59
Excess volume of interface 121

F

Fanlike mode of column growth 28
Fiber texture 58
on non-epitaxial atomically smooth surface 58
Film stress 68
Forward sputtering 187
theory of 187
Freezing-in temperature 101
for bulk diffusion 101
for stacking faults in metals 107
for vacancy diffusion 102

G

Gibbs adsorption 109
Grain boundary 62
driving force 62
mobility 84
effect of energetic particles on 84
void pinning of 62
Grain morphology 60, 61
columnar 60, 61
in zone a temperature regime 61, 73
in zone b temperature regime 62, 74
in zone II temperature regime 86
zone models of 73
Grain size 60
and cluster size 60
in zone a temperature regime 61, 73
in zone b temperature regime 62, 74
Grain structure 55
Granular epitaxy 37, 59
Graphoepitaxy 15
Growth modes 56
contact angle and 56
island 55
layer-by-layer 55
Stranski–Krastonov 55

H

Heteroepitaxy 121
Homoepitaxial layers
defects in 102
Hydrogen evolution from α-Si:H 146

I

Impingement rate 20
given by kinetic theory of gases 20
Impurity content 71
effect on defect production 209
effect on grain size 64
effect on intrinsic stress 181
effect on transition temperature between zones 71
Intercluster spacing 30
Interface mixing 109
Interfaces 108
diffuse 108
Internal tensile stress 179
temperature dependence of 179
Interphase interfaces 128
Interstitial 10
Interstitials 103
low energy bombardment induced 103
Intrinsic compressive stress 188
theory for 188
Intrinsic stress 183
in films from hyperthermal beams 183
effect of inert gas atoms 183
role of interstitials 183
in films from thermal beams 173
Island mode of growth 99
kinetic origin of 101
inhibition of 99

K

Kirkendall voids 196
prevention of by codeposition 196

L

Layer-by-layer growth mode 55
Long range order 111
  in semiconductor alloys 111

M

Miscibility gap in thin films 110
Misfit dislocations 117
Misfit strain 117
Molecular dynamics simulation 8
  of amorphous carbon 157
  of deposition 33, 39, 102
  of 10eV Si bombardment 103
  of stress in thin film 187
  of temperature spike 8
Momentum, normalized 183
  and packing density 184
  dependence of induced compressive strain on 183
Monocrystalline film 15, 57
  non-epitaxial 15
  on amorphous substrate 15
Morphological instability 34, 200
  and dendrites 34
  in PtSi heterostucture 200
  in titanium disilicide 200

N

Non-epitaxial substrates 57
Normalized momentum 13
Nucleation 93
  dependence of texture on 93
Nucleation theory 14
  comments on application of 14

O

Ostwald's rule 82

P

Packing density 36
  at low temperature 36
Particle energies 4
  in deposition processes 4
Periodic arrays 237
Perpendicular magnetic anisotropy 161
  effect of sputtering conditions on 162
Petch relation 179
Phase separation 113
  by adatom migration 113
Photothermal deflection spectroscopy (PDS) 141
Physical vapor deposition 4
  particle energies in 4
Pinholes 198
  in cobalt disilicide 198
Point defects 10, 46, 197
  in amorphous films 46
  in cobalt disilicide 197
  interstitial 10
  vacancy 10
Poly-Si 204
  defects in 204
  field effect mobility in 205
  methods of forming 204
Pressure spike 12
primary twinning 65

R

Rare earth epitaxial silicides 199
  defects in 199
Reactions
  silicides 197
  oxides 201
Recrystallization 87, 195
  due to diffusion 195
  particle energy for 82
Renucleation 59
  during deposition 59
Rheed oscillations 100
  critical diffusivities for 100
Roughness, surface and interface 200
  diffusion origin of 200

S

S, mode of growth parameter 98
Secondary recrystallization 62
  and zone b texture 64

Semiconductor alloys 110, 111
composition fluctuations in 110
long range order in 111
Si(100) epitaxy 216
Si(111) epitaxy 214
Silane decomposition products 149
mode of film growth and 149
Silicon 212
amorphization energy in 212
displacement energy in 212
Solid phase epitaxy 222
in diamond 222
Spinodal decomposition 110
during deposition 110
Sputter cleaning 81
effect on production of epitaxy 81
Sputtering 10
without surface penetration 10
Stacking faults 104
effect of impurities on 104
in diamond 107
in GaAs 107
in Si 47
Staebler–Wronski effect 152
Step flow 100
critical temperature for onset of 100
Stress 68
film 68
Stresses in Thin Films 180, 186
intrinsic 180, 186
and intercolumnar voids 180
and texture 67
constraint on void origin of 193
critique of models for 180
effect of hyperthermal beams on 186
molecular dynamics derived 193
temperature dependence of 179
Structure zone model 36
Substrate 30, 152
effect of 30
on column structure 30
effect on weak bond density 152
Substrate surface 2
cleanliness 2
effect of chamber pressure 2
penetration depth through 8
template for epitaxy 2
Substrates 57
and Raman peak width 153
Superlattices 101, 112
Surface roughness 67
dependence on
statistical noise in deposition 67
incident particle energy 234
and α-Si 215
wavelength 235
Surface stress 112

T

Tangent law 52
Temperature spike 5
due to bonding 5, 7
to film 5
to cluster 7
due to energetic particle impact 7
range for adatom jump in 6
Template method 125, 198
Texture 61
characteristic of zone a substrate temperatures 61
effect of particle energy on 83
characteristic of zone b substrate temperatures 83
effect of particle energy 83
characteristic of zone II 70
characteristic of zone III 72
critical thickness for transition in 68
dependence on deposition rate 70
dependence on statistical noise in deposition 67
effect of anisotropic sticking coefficient 85
effect of differential sputtering yield on 85
effect of elastic strain energy on 67
effect of ion/atom ratio on 84
effect of particle energy on 83
effect of plastic deformation on 69
effect of stress relaxation on 69
effect of surface roughness on 67

Texture (*contd.*)
kinetic versus thermodynamic origin of 66
of polycrystalline semiconductors 77
dependence on silane pressure 78
possible nucleation origin of 93
thickness dependence of 64, 67
Threading dislocations 119
schemes to prevent formation of 119
Titanium disilicide 200
Transition temperature 107
amorphous/crystalline 107
in silicon 107
Twinning 66
secondary 66
effect of atmosphere on 66
Twins 107
in GaAs 107

U

Urbach tail slope 144, 151

V

Vacancies 11, 102
deposition induced 102, 103
effect of growth mode on 102
observation of 103
migration activation energy 102
in silicon 102
trapped during deposition 11, 21
Void network 82
particle energy to remove 82
Void network stability 39
Void networks 40
effect of energetic incident particle on 40
Voids, intercolumnar 104
in epitaxial flims 104
Void-column structures 30

W

Weak bonds 152
density 152
effect of substrate 152
in α-Si 143

Y

Yield strength and intrinsic stress 174, 179

Z

Zone 1 37
Zone a 60
homologous temperature range 60
Zone b 62
homologous temperature regime 62
Zone II 70
activation energy for grain growth 74
Zone III 72
activation energy for grain growth 74
Zone models 73
interpretation of 75
Zur and McGill hypothesis 121